Changes in cardiomyocyte structure and cAMP/cGMP signalling during heart failure

SOPHIE SCHOBESBERGER

BORN: 27.08.1987

NATIONAL HEART AND LUNG INSTITUTE,

DEPARTMENT OF MEDICINE

IMPERIAL COLLEGE LONDON

Doctoral thesis submitted to Imperial College London for the award of the degree Doctor of Philosophy

London 2015

Abstract:

The contractile function of the heart depends on efficient β adrenergic receptor (βAR) signalling which involves cycling nucleotides as second messengers. Correct secondary messenger signalling is only possible in healthy, well structured cardiac myocytes. Of the three βAR subtypes present in human cardiomyocytes β_1AR and β_2AR classically signal via 3'-5' cyclic adenosine monophosphate (cAMP) to regulate contraction after catecholamine administration, whereby the second isoform may also be cardioprotective. The far less characterised β_3AR has been controversially associated to both increasing contraction through cAMP and protecting the heart through 3'-5' cyclic guanosine monophosphate (cGMP) signalling. During the progression of heart failure following myocardial infarction (MI) both the normal cell structure and the regulation of cAMP and cGMP signalling are changed. This happens in part due to changes in catecholaminergic stimulation of the βARs and in mechanical load, as well as due to a progressive development of hypertrophy. Some of the alterations initially appear to be of a compensatory nature but escalate into HF by worsening cardiomyocyte function and cell survival.

The work presented here (1) investigates the structural integrity of healthy, isolated, single cardiomyocytes by looking at the surface topography via Scanning Ion Conductance Microscopy (SICM) imaging and by examining the internal Transverse Axial Tubule (TAT) network via confocal imaging; (2) elucidates the cyclic nucleotide response to catecholamine stimulation following either global (in the solution) or local (in the SICM pipette) stimulation of either β_2ARs or β_3ARs and measuring either cAMP or cGMP levels via Förster Resonance Energy Transfer (FRET) sensors in a combined FRET/SICM imaging setup; (3) determines how both the structure and β_2AR and β_3AR dependent second messenger signalling change in a progressive rat model of HF 4, 8 and 16 weeks after the induction of chronic MI.

<u>The major findings of the presented work are as follows:</u>

In control cardiomyocytes the structure is highly intricate with regular Z-grooves and crest areas. In MI cells the normal suface topography progressively deteriorates, with the eventual disappearance of Z-grooves by week 16, which correlates with the disorganisation of the cardiomyocyte's internal transverse axial tubule (TAT) network of T-tubules emanating from the cell surface and traversing into the cell centre. This is accompanied by the gradual redistribution of β_2ARs from their normal position inside the T-tubules to the unstructured areas on the cardiomyocyte membrane. The regularity and density of the TAT network is already severely compromised at 4 weeks post MI; at the same time a significant drop in the expression of the structural protein Junctophilin 2 (JPH2) occurs. At 4 and 8 weeks post MI a

potentially compensatory increase in the number of longitudinal elements takes place which was no longer detectable at 16 weeks. The production of cAMP following local stimulation of β_2ARs in the T-tubule openings was already suppressed at 4 weeks post MI and a β_2AR response becomes detectable after local stimulation at the cell crests (areas between Z-grooves) at 8 weeks post MI. At 16 weeks post MI the β_2AR-dependent cAMP level following both global and local stimulations was reduced due to an overall decrease in the adenylate cyclase (AC) activity.

The production of the second cyclic nucleotide, cGMP, following β_3AR stimulation is evident in control cells and to a significantly lesser extent in myocytes isolated from hearts at the end stage of HF. These β_3AR-cGMP levels were degraded mainly by phosphodiesterases (PDE) 2 and 5. Local stimulation through the SICM pipette reveals that functional β_3ARs are primarily localized inside T-tubules in control cells but redistribute equally in between T-tubules and crests in cells isolated from failing hearts.

To improve the accuracy and reliability of local application of agonists via the SICM nanopipette voltage was applied to the pipette, as opposed to previously employed displacement of the liquid in the pipette via air pressure. Mathematical modelling served to determine the correct settings for this voltage driven application. It shows that the SICM nanopipette can reliably and precisely unload the βAR agonist ISO onto the nanoscale structure of cardiomyocytes via voltage.

Publications expected or published from this work:

1. Schobesberger S*, Tokar S*, Wright P, Bhargava A, Glukhov AV, Buzuk A, Monszpart A, Sikkel M, Harding SE, Nikolaev VO, Lyon AR, Gorelik J. Structural Transverse Axial Tubule remodeling precedes maladaptive cardiomyocyte β_2AR signaling during the progression of heart failure (*Under revision for Circulation Heart Failure*)
2. Schobesberger S*, Jönsson P*, Buzuk A, Sigger J, Korchev J, Gorelik J. Precise, nanoscale, voltage-driven application of bio-active substances onto cardiomyocyte surface with organized topography (accepted by the Biophysical Journal on 02/12/15)
3. Schobesberger S, Poulet C, Mansfield C, Wright P, Nikolaev VO, Gorelik J. β3- adrenergic signalling in healthy and failing adult rat cardiomyocytes (*Under preparation for Circulation Research*)
4. Wright P, Schobesberger S, Gorelik J Studying GPCR/cAMP pharmacology from the perspective of cellular structure (*Invited, submitted review for Frontiers in Pharmacology*)
5. Miragoli M, Sanchez-Alonso J, Bhargava A, Wright P, Sikkel MB, Schobesberger S, Diakonov I, Novak P, Castaldi A, Cattaneo P, Lyon AR, Lab MJ. Microtubule-dependent Microdomains as Substrate for Mechanically Induced Ectopic Mitochondrial-dependent Calcium Release in Failing Cardiomyocytes. (*Under revision*)
6. Bhargava A, Sanchez-Alonso JLS, O'Hara T, Glukhov AV, Schobesberger S, Sikkel M, Korchev Y, Lyon AR, Punjabi P, Nikolaev V, Trayanova N, Gorelik J. "Microdomain-Specific Modulation of L-type Calcium Channel Function Triggers Ventricular Arrhythmia in Heart Failure" (Unter Revision für Journal of Clinical Investigation)
7. Glukhov AV*, Balycheva M*, Sanchez-Alonso JLS, Ilkan Z, Alvarez-Laviada A, Bhogal N, Diakonov I, Schobesberger S, Buzuk A, Bhargava A, Faggian G, Houser SR, Gorelik J. "Direct evidence for microdomain–specific localization and regulation of functional L-type calcium channels in rat atrial myocytes." (*Under revision*)
8. Wright PT, Nikolaev VO, O'Hara T, Diakonov I, Bhargava A, Tokar S, Schobesberger S, Shevchuk AI, Sikkel MB, Wilkinson R, Trayanova NA, Lyon AR, Harding SE, Gorelik J "Caveolin-3 regulates compartmentation of cardiomyocyte beta2-adrenergic receptor-mediated cAMP signalling", Journal of Molecular and Cellular Cardiology, Volume 67, February 2014, Pages 38-48, ISSN 0022-2828
9. Potter CM, Schobesberger S, Lundberg MH, Weinberg PD, Mitchell JA, Gorelik J. Shape and compliance of endothelial cells after shear stress in vitro or from different aortic regions: scanning ion conductance microscopy study. PLoS One. 2012;7(2):e31228. doi: 10.1371/journal.pone.0031228. Epub 2012 Feb 16.

(*authors contributed equally to the work)

Presentations:

1. Imperial College London, NHLI postgraduate research day, July 1st 2014, Oral presentation
2. “Altered β_2AR-cAMP signalling in cardiomyocytes is linked to surface and T-tubule structural modifications and not to changes in PDE4 activity during progression of heart failure.” Poster presentation, Gordon Research Conference and Seminar, St. Mount Holyoke, June 2014
3. “β_2AR adrenergic receptor cAMP signalling is altered by structural changes in cardiomyocyte occurring progressively in a rat model of myocardial infarction” Poster presentation, Biochemical Society, London, UK, December 2014
4. "Alterations in ß2-ARs dependent cAMP signaling linked to post infarction remodeling of T-tubules in rat cardiomyocytes" Poster presentation, American Heart Association Conference, Dallas, USA, November 2013
5. "Progressive changes in cardiomyocyte structure and β2–AR cAMP signalling localization during heart failure: mathematical modelling perspective", NHLI postgraduate research day, Imperial College London, June 2013
6. "Progressive changes in cardiomyocyte structure and β2–AR cAMP signalling localization during heart failure: mathematical modelling perspective" Poster presentation, BHF centre symposium, June 2013
7. "Investigation and modelling of differences of cAMP signalling in intact versus failing cardiomyocytes" Oral presentation, NHLI Myocardial Function Symposium, Imperial College London January 2013
8. "Investigation and modelling of cyclic nucleotide signalling in association with structural changes of cardiomyocytes after myocardial infarction” Poster presentation, NHLI/RBHT Paul Wood lecture Imperial College, Royal Brompton, October 2012,
9. "Investigation and modelling of cyclic nucleotide signalling in association with structural changes of cardiomyocytes after myocardial infarction" Poster presentation, BHF centre annual symposium, October 2012
10. “cAMP and cGMP signalling in intact versus diseased cardiomyocytes” Poster presentation, Oxford, UK, Mayneord Phillips Summer School, July 2012

Declaration: I, Sophie Schobesberger, declare that the work represented in this thesis is my own, except if indicated otherwise. If the material I have used was from another investigator then this is stated clearly. This thesis has not been submitted at any other institution than Imperial College London to obtain a degree.

Sophie Schobesberger, Hammersmith Hospital Campus 2015

Copyright:

Dedication:

I dedicate this work to my late mother and dearest friend, who never ceased to try and make things better for her loved ones and for her students. She was a very precious and kind person, a teacher who strove to learn something new herself every day. I will aspire to obtain even a fraction of her wisdom, warmth and knowledge for the rest of my life.

Acknowledgements:

There are a lot of people I am immensely grateful to and whom I wish to acknowledge: First of all I wish to thank my primary supervisor Prof. Julia Gorelik, who cared for me both on a professional and personal level and whose inexhaustible energy and scientific enthusiasm are nothing short of inspirational. Following I thank my second supervisor Dr. Jennifer Siggers for the insights, which she granted me, into the mathematical possibilities to advance natural sciences, as well as for her friendly and motivational demeanour and some fantastic summer get-togethers. I also want to express my immense gratitude to my third supervisor Prof. Sian Harding, who not only is a source of unparalleled, scientific knowledge and whose entire group has been a great help to my doctoral studies, but whose generosity made it possible for me to broaden my horizons at international meetings in America. It is through Prof. Harding that I got to know Dr. Markus Sikkel, Mr. Adam Mills and Mr. Peter O'Gara, three gentleman who kindly contributed their support and technical skills whenever needed. Especially Mr. Peter O'Gara, deserves my utmost gratitude as without him this doctoral thesis would not have been possible and I'd only have laughed half as much during my time in London. Similarly Prof. Viacheslav Nikolaev and his entire group, our collaborateurs from Germany, deserve my thanks for all the amazing ideas, support and effort they contributed to my work.

Without preference but in alphabetical order I also wish to thank the current members of Julia's and my group, Dr. Alexey Glukhov, Ms. Alveera Hasan, Mr. Andrey Buzuk, Dr. Anita Alvarez Laviada, Dr. Carolina Marinho, Ms. Franka Schultz, Dr. Ivan Diakonov, Dr. Jose Alonso Sanches Mardones, Dr. Marina Balycheva, Ms. Marta Mazzolo, Ms. Navneet Bhogal, Mr. Oladipupo Adeyemi, Dr. Peter Wright. I don't wish to appear overly sentimental but as I have grown very fond of each and every single one of them I hope our paths cross again and again in the future and that they won't mind me addressing them all as friends. Similarly I wish to thank Julia's former group members Dr. Anamika Bhargava, Dr. Michele Miragoli and Dr. Sergiy Tokar whom I wish all the best for their families and careers. I furthermore am indebted to Mr. Stephen Rothery from the Imperial College London FILM facility for his kind help in regard to all my concerns with confocal imaging.

Special thanks are also due to my friends Dr. Byambajav Buyandelger, Dr. Catherine Mansfield and Ms. Caroline Roney who helped me during my Phd by being there for me when I needed them. During my time at Imperial I had the privilege to get acquainted and make friends with many more outstanding scientists. I wish I could name them all personally but instead will have to make use of the phrase "You know who you are".

I can not neglect to thank my family starting with my two dearly loved grandmothers Line and Luise followed by my father Hannes, a great story teller, whose children's badinage is their

most sincere homage to him and his kind wife Sonja. I also thank my brothers Stefan, David and Christian and my beloved twin sister Irene. I value all of them too much to put into words. They are my backbone and saw me through the loss of our mother Ilse, who used to calm me and encourage me in such a way as only a loving mother can. Last, but not least, I wish to thank my closest Austrian friends Hanna, Renate, Karin and Roshan for being who they are. Thank you!

Table of Contents

List of figures:

List of tables:

List of Abbreviations and Acronyms:

AC	Adenylate Cyclase
ACE	Angiotensin Converting Enzyme
AKAP	A-Kinase Anchoring Protein
ARB	Angiotensin II receptor blocker
β_1AR	beta1-adrenergic receptor
β_2AR	beta2-adrenergic receptor
β_3AR	beta3-adrenergic receptor
8-Br-2′-O-Me-cAMP-AM	cAMP analogue
CamKII	$Ca^{2+/}$calmodulin-dependent protein kinase
cAMP	3’5’ cyclic adenosine monophosphate
CNGC	cyclic nucleotide-gated channel
CFP	Cyan Fluorescent Protein
CGP20712A	specific β_1AR blocker
CICR	Ca^{2+} induced Ca^{2+} release
DAPI	4',6-diamidino-2-phenylindole
DCM	dilated cardiomyopathy
Di-8-ANEPPS	Di-8-amino-naphthyl-ethenyl-pyridinium
DMSO	Dimethyl Sulfoxide
ECC	Excitation Contraction Coupling
EF	Ejection Fraction
EHNA	erythro-9-2-hydroxy-3-nonyl adenine
eNOS	endothelial Nitric Oxide Synthase
EPAC	Exchange protein directly activated by cAMP
Epac2-camps	cytosolic EPAC2 based cAMP FRET biosensor
ERK	Extracellular signal Regulated Kinase
FEM	Finite element modelling
FILM	Facility for Imaging by Light Microscopy
FRET	Förster Resonance Energy Transfer
GAF	protein binding domain for cGMP
GFP	Green Fluorescent Protein
Gi	inhibitory G-protein
GPCR	G-protein coupled receptor
GRK	G-protein coupled receptor kinase
Gs	stimulatory G-protein
IBMX	3-Isobutyl-1-Methylxanthin

ICI-118,551	selective β_2AR blocker
ICM	Ischemic Cardiomyopathy
iNOS	inducible Nitric Oxide Synthase
ISO	Isoproterenol
L-NAME	*N*-monomethyl-L-arginine
LV	Left Ventricle
LVAD	Left Ventricular Assist Device
M199	cell culture medium 199
MDL 12,330A	AC inhibitor
MI	Myocardial Infarction
M-Mode	Motion Mode in echocardiography
MOI	Multiplicity of Infection
MUMPS	MUltifrontal Massively Parallel sparse direct Solver
NADPH	Nicotine Amid Adenine Dinucleotide Phosphate
NCX	Codium Calcium Exchanger
NKH477	adenylate cyclase activator
nNOS	neuronal Nitric Oxide Synthase
NTA	Nitrilotriacetic Acid
ODQ	1H-[1,2,4] oxadiazolo [4,3-a] quinoxalin-1-one
PA	Polyacrylamid
PBS	Phosphate Buffered Saline
PCC	Pearson's Correlation Coefficient
PDE	Phosphodiesterase
PGE1	Prostaglandine E1
PKA	Protein Kinase A
PKG	Protein Kinase G
PLM	Phospholamban
PTX	Pertussis Toxin
PSF	Point Spread Function
Red cGES-DE5	cytosolic cGMP FRET biosensor
RFP	Red Fluorescent Protein
RIPA	Radioimmunoprecipitation assay
ROLI	Rolipram
ROI	Region of interest
RyR	Ryanodine Receptor
SDS	Sodium Dodecyl Sulphate

SERCA2a	Sarcoendoplasmic reticulum calcium ATPase
SICM	Scanning Ion Conductance Microscopy
SR	Sarcoplasmic Reticulum
SR59230A	selective β_3AR blocker
TAT network	Transverse Axial Tubule network
T-Tubule	Transverse Tubule
T-Sapphire	Flourescent protein T-Sapphire
YFP	Yellow Fluorescent Protein

Chapter 1: General Introduction

1. Introduction:

1.1 Heart failure: definition, progression and current treatment

According to the Office for National Statistics of the U.K. the average life expectancy of UK citizens lies around 78 years for men and 82 years for women and is continually increasing by about 2 years every decade (UK government website: http://www.ons.gov.uk; accessed January 2015). This increase in life expectancy brings with it a rise in age-related cardiomyopathies and chronic heart failure (HF), which our increasingly aging population has to face. In addition to age other known risk factors for the occurrence of HF are hereditary disorders, diabetes, hypertension, smoking and obesity. By definition HF is the inability of the heart to efficiently pump blood throughout the cardiovascular system and is the consequence of various, complex causes including, among others, neuro-hormonal overstimulation and/or mechanical overload of cardiomyocytes (Mudd, Kass 2008). In most cases of HF the clinical symptoms are due to impairment of the left ventricle and can be manifold. As the heart's ability to efficiently pump blood decreases HF patients oftentimes suffer from dyspnea and fatigue, which heavily affects or even inhibits the patient's tolerance to exercise. The kidneys react to a reduction in the blood flow by retaining more fluid and salt. As a consequence the patient may experience pulmonary congestion and or peripheral edema (Dunlay et al. 2014). Though there are exceptions, such as physically-induced heart arrest or stress-induced cardiomyopathies, HF has generally been recognised as a progressive disorder, which at first is asymptomatic before escalating into a symptomatic disease in a time-dependent manner. Depending on the stage of disease progression the risk factors and symptoms require differential treatment (Dickstein et al. 2008). As a consequence patients are classified into 4 different stages of severity. These stages are clinically assessed according to risk factors which might lead a patient to develop HF as well as already developed structural and functional indicators of HF (see table 1). The major contributor to the progression of HF is the irreversible loss of cardiomyocytes. Hence MI is the most troublesome of potential cardiac interferences as it leads to the death of approximately a billion cardiomyocytes and to fibrotic scarring (Laflamme and Murry 2005). MI occurs as a result of interrupted blood flow to a part of the heart and mainly affects the myocardium of the left ventricle (LV). Treatment strategies to deal with the occurrence of HF by slowing it's progression depend on the symptoms of the respective patient but range from angiotensin converting enzyme (ACE) inhibitors and β-blockers to diuretics and mild exercise (Dunlay et al 2014). If the disease has progressed too far the only option to save a patient's life is a heart transplant (Dickstein et al. 2008). Although the advances in cardiovascular science and therapeutic strategies have been manifold the prognosis of HF remains grim with an estimated 65% mortality rate of patients of fewer than 5 years and a significant decrease in their quality of life (McMurray, Stewart 2000).

Table 1 Classification, symptoms and treatment strategies of HF stages adapted from (Dunlay et al. 2014)

HF stage	Risk factors/symptoms	Diagnosis	Treatment strategy
A	Hypertension, obesity, diabetes, atherosclerosis, intake of cardiotoxins, hereditary disorder	At heightened risk, but without structural or functional HF symptoms.	Treatment of hypertension, increased exercise, discouragement of alcohol intake, smoking, drug abuse, treatment of other disorders
B	Remodelling of the LV due to occurrence of MI or valve disease and myopathies	Structural alterations of the heart without HF symptoms	As defined for stage A Additionally: defibrillator, ACE inhibitors, angiotensin II receptor and β-blockers
C	Evident structural heart disease in combination with fatigue and dyspnoea, decreased capacity for exercise	Structural alterations of the heart with past or present HF symptoms	As defined for stages A, B Additionally: salt restriction, diuretics, specialised drugs for specific patients i.e. nitrates
D	Severe HF symptoms even at rest despite medical attention	Evident HF which urgently requires specialised intervention	As defined for stages A, B, C Additionally: heart transplant, permanent mechanical support, experimental surgery

1.2. Ventricular assist devices

In order to counteract the consequences of a weakened heart during cardiomyopathies patients can be outfitted with right (RVAD) or left ventricular assist devices (LVAD). These devices are artificial, mechanical pumps implanted into the patient's chest which help to maintain blood flow and heart function (Giveritz 2011). It has been shown that the introduction of LVADs can re-establish contractility of diseased hearts and lead to reverse structural remodelling of cardiomyocytes via the normalization of microRNA (miR) expression patterns. These miRs, which are small pieces of non-coding RNA, achieve cardiac regulation by binding to mRNAs and marking them for degradation so that the respective protein expression is inhibited (Matkovich et al. 2009).

1.3. Animal models of HF

To look for potential treatment strategies experiments with animal models have proven to be indispensable. Animal models are utilised for testing and optimising cardiac assist devices as well as for elucidating new therapeutical targets or biomarkers, which indicate HF (HF) progression. As the disease itself is highly complex and arises from a number of molecular and physical insults, induction of acute and chronic HF has been achieved in animal models by a variety of means. These include overloading the heart with volume or pressure, administering cardio-toxic drugs or inducing MI. In order to be appropriate for the study of HF an animal model should possess the same pathological features as a human being. MI animal models of HF generated by ligation of the left anterior descending artery (LAD) are fairly reproducible. They generate a localised ischemic insult in the left ventricle and reproduce acute and chronic clinical symptoms of human HF (Monnet, Chachques 2005). In our group we have established an adult rat model of chronic MI via the ligation of the LAD (Lyon et al. 2009), which incorporates the major symptoms of human HF: fibrotic scarring after ischemic myocardial injury, extensive cell death at the site of the injury, a decrease in the left ventricular ejection fraction (LVEF), hypertrophy, adverse remodelling of cardiomyocyte morphology and function and alterations in the sensitivity of βARs to catecholamine stimulation (Lyon et al. 2009; Nikolaev et al. 2010). Most of the work described in this thesis deals with cardiomyocytes isolated from this LAD MI model, for the examination of cardiomyocyte structure and secondary messenger signalling.

1.3. Cardiac regulation via the sympathetic and parasympathetic nerves

The physiological function of the heart depends on its regulation by the sympathetic (SNS) and parasympathetic nervous system (PNS) with their pre.- and postganglionic neurons at separate anatomic positions. As two of the three parts of the autonomic or involuntary nervous system (the third being the enteric nervous system) the SNS and PNS are generally said to fulfil opposing, but complementary functions. For this the SNS and PNS are able to inhibit each other presynaptically (Goldstein 2011). Physically the preganglionic nerves of the SNS emerge from the top and the lower part of the spinal cord and connect via nerve cell clusters, the so called ganglia, to the postganglionic nerves. These nerves then reach out to the target organs, including the heart. The nerves of the PNS emanate from the medial part of the spinal cord and end as postganglionic nerves at the cardiac atria where they modulate cardiac function through neurotransmission via nicotinic receptors (Shaffer et al. 2014). While the preganglionic nerves of both the SNS and the PNS secrete acetylcholine (ACH) for neurotransmission the postganglionic nerves of the SNS and PNS secrete different hormones

at different levels. These include adrenaline (ADR) and noradrenaline (NOR) which are the effectors of the β adrenoreceptors (βAR) (Zipes, Jalife 2009). In healthy individuals the SNS is effectively modulating cardiomyocyte responses such as the increase of the heart rate, cardiac contractility and the constriction of cardiovascular vessels via the βARs. Cardiac modulation is achieved by postsynaptic nerve fibres of the SNS at the sinus atrial node (SAN), the atrioventricular (AV) node and the sub-epicardium of the ventricles. These fibres release negligible amounts of the catecholamine ADR and higher amounts of the catecholamine NOR, which makes NOR the main regulator of the cardiac SNS response (Zipes, Jalife 2009). The main way to inactivate NOR released from nerve fibres is its reuptake into sympathetic nerves and consequent storage in vesicles (Goldstein 2011). In the heart NOR's overall effect is the shortening of the cardiac action potential in the ventricle as well as the shortening of the refractory period of cells, which is the time it takes for cells to be excitable again. NOR and in higher quantities ADR are also released by endocrine cells at the adrenal glands above the kidneys (Lymperopoulos et al. 2007). Both hormones are secreted into the bloodstream and circulate to reach their effector organs and to regulate the "*fight-or-flight"* response. On the other hand the PNS counteracts the effects of the SNS by slowing down the heart rate and by inhibiting responses of the SNS to induce the "*rest-and-digest*" state (Shimizu, Okabe 2007). The vagal nerves of the PNS do so by releasing ACH, which binds to the muscarinic receptors in the heart and increases the threshold for spontaneous, electrical impulse (=action potential) generation in the SAN. The prevalent muscarinic receptor isoform in the heart is M2, which is coupled to inhibitory G (Gi) protein and scales down cAMP production. Hence M2 receptors exercise negative inotropic (decreased contractility) and chronotropic (decreased heart rate) effects via direct or indirect regulation of ion channels like the L-type Ca^{2+} channels (LTCC) (Brodde, Michel 1999). This allocation of regulation allows our organisms to adapt to the specific state they are in. While we are at rest it is the PNS which will maintain most of our functions. If we are however exerting ourselves or have been afflicted by a wound and suffer from blood loss the nervous system will increase cardiac output by a proportional increase in βAR dependent inotropy (increased heart contractility), chronotropy (increased heart rate) and lusitropy (increased heart relaxation) (Nagai and Komuro 2012).

1.3.1. Changes in the nervous system regulation during HF progression

After the occurrence of ischemic injury to the heart, or due to restricted blood flow, the SNS adapts to the decreased cardiac output by elevating its activity. Through heightened catecholamine release as well as increased reuptake into the nervous fibres the SNS tries to compensate for the loss of the heart's contractility (Brum et al. 2006). On the one hand SNS hyperactivity throws the Renin-Angiotensin-Aldosterone system into overdrive, which retains

the organism's fluid and increases the arterial blood pressure. On the other hand it leads to heightened levels of the catecholamines ADR and NOR to be released into the bloodstream and a subsequent increase in heart rate (Kishi 2012). Satisfying the acute need for heightened catecholamine levels however turns into a cardiotoxic, vicious circle if those levels are maintained chronically. One of the consequences of constantly occurring catecholaminergic stimulation is that the sensitivity and the actual number of the β_1 adrenergic receptors (β_1AR), which are the main receptors to translate the catecholaminergic stimuli into cellular responses, decreases (Bristow et al. 1982; Kishi 2012). At the same time the level of Gi proteins, which inhibit positive inotropy, increases (Lohse et al. 2003). Furthermore overstimulation of the β_1 subtype of the βAR family has been shown to induce hypertrophy and expedite cell apoptosis (Zhu et al., 2003). As a result the already injured cardiac structure deteriorates further, while the cardiac function plummets to lethal depths (Tomita et al. 2003). Abnormalities in the regulation of cardiovascular function by the SNS and PNS - especially SNS hyperactivity and excessive hormonal stimulation – have therefore become indicative of MI and HF (Kishi 2012).

1.3.2. Catecholamines

Human plasma contains three catecholamines which serve as chemical messengers and neurotransmitters: dopamine, ADR and NOR. Catecholamine biosynthesis takes place by hydroxylation of tyrosine into dihydroxyphenylalanine ($_L$-DOPA), decarboxylation of $_L$-DOPA to dopamine, hydroxylation of dopamine to NOR and finally methylation of NOR to ADR. The latter conversion takes place mainly in the chromaffin cells in the adrenal glands whereas the preceding conversional steps also occur in nerve fibres (Goldstein 2011). As mentioned earlier catecholamines bind to βARs and thereby mediate the effects of the SNS. Clinical tests allow the measurement of plasma catecholamine levels, in particular increased NOR levels, as a marker of disease progression (Brodde, Michel 1999). Under HF conditions human catecholamine plasma levels of around 80 picogram per ml of ADR and 500 picogram per ml of NOR were observed (Yan et al. 2008).

1.3.3. βAR agonists and antagonists

Though ADR and NOR are full agonists at all 3 βAR subtypes present in the heart it is noteworthy that ADR and NOR possess different affinities for the different βARs. While ADR and NOR bind with same affinity to the β_1AR subtype, ADR is 35 times more potent than NOR at the β_2ARs. The opposite applies to β_3ARs which has a 30 times higher affinity for NOR (Hoffmann et al. 2004). This disparity of catecholamine preference by the β_2ARs and β_3ARs

could be indicative of an intricate regulatory mechanism during heightened stress conditions. Different affinities to the βARs have also been determined for artificial analogues of the catecholamines as well as for βAR blockers. Isoproterenol (ISO), used clinically to treat too slow heart rates (bradycardia), is a full agonist on all 3 βAR subtypes with highest affinity for β_1ARs, about two times lower affinity for β_2ARs and five times lower affinity for β_3ARs. The most efficient, available β_1AR and β_2AR blockers are CGP20712 and ICI118511, respectively (Hoffmann et al. 2004). Human and rat β_3ARs differ from each other both structurally as well as in their regulation (Granneman and Lahners 1994) (this is the only Granneman reference I made, and it wasn't missing in the reference list) and in consequence of these differences the SR59230A serves as a highly selective β_3AR blocker in rodents (Mongillo et al. 2006;Nikolaev et al. 2010) while it exhibits less specificity in human preparations (Candelore et al. 1999).

1.4. The setup and function of the myocardium

In its basic state the human heart is a highly responsive and highly adaptive circulatory, blood pump, which supplies our whole organism with vital nutrients and oxygen and clears away waste products. It is mainly made out of connective tissue and cardiac muscle cells (Weber 1989). The adult cardiac muscle cells are unable to regenerate after injury such as MI which, through substitution of cardiomyocytes with connective tissue, leads to the formation of scar tissue (Laflamme, Murry 2005). The mammalian heart is dividable into four cardiac chambers, two atria and two ventricles. These chambers orchestrate the blood flow in-series via systolic (from the Greek word stello=shortening) and diastolic (from the Greek word diastello=lengthening) movements (Torrent-Guasp et al. 2004) according to electrical impulses, which are spontaneously generated by the cells of the SAN in the right atrium (Shaffer et al. 2014). From outside to inside the tissue of the heart walls can furthermore be divided into three different cell layers: the pericardium, the myocardium and the endocardium (Sanchez-Quitana et al. 1990). The myocardium is the layer responsible for the regulated pumping of the heart and is primarily consisting of cardiomyocytes. Through the rhythmical contraction of the left ventricular (LV) cardiomyocytes the heart efficiently distributes blood throughout the circulatory system and supplies our organism with necessary nutrients and oxygen. When the LV cardiomyocytes contract, starting from the apical tissue to the basal tissue, this leads to a wringing motion of the LV chamber. During the phase of systole this motion increases the pressure inside the chamber and ejects the blood from the LV. The same motion results in a decrease of the pressure during cardiomyocyte relaxation and a filling of the LV chamber during diastole. Only recently the ventricular myocardial fibers have been shown to form one cohesive muscular band which twists twice and then helically folds in on

itself to form the left and right ventricular chambers (Torrent-Guasp et al. 2004). However, despite this unified, anatomical arrangement, the ventricular wall is not a uniformly functioning and aligned structure (Dorri et al. 2010). Due to the heterogeneity of its laminar layers the ventricular wall possesses macroscopically observable differences in its transmural orientation (LeGrice et al. 1995) as well as microscopically determinable variations in force production (Haynes et al. 2014), electrical conductance (Zygmunt et al. 2001) and Ca^{2+} activity (Cordeiro et al. 2004) of single cardiomyocytes. Furthermore differences according to the anatomical position (Wan et al. 2003) as well as due to species affiliation have become evident (Soeller et al. 2007). Therefore it is important to note that the biggest part of this work deals with the structure and function of cardiomyocytes from the basal part of the left ventricle of adult human and rat hearts.

1.5. The cardiac action potential

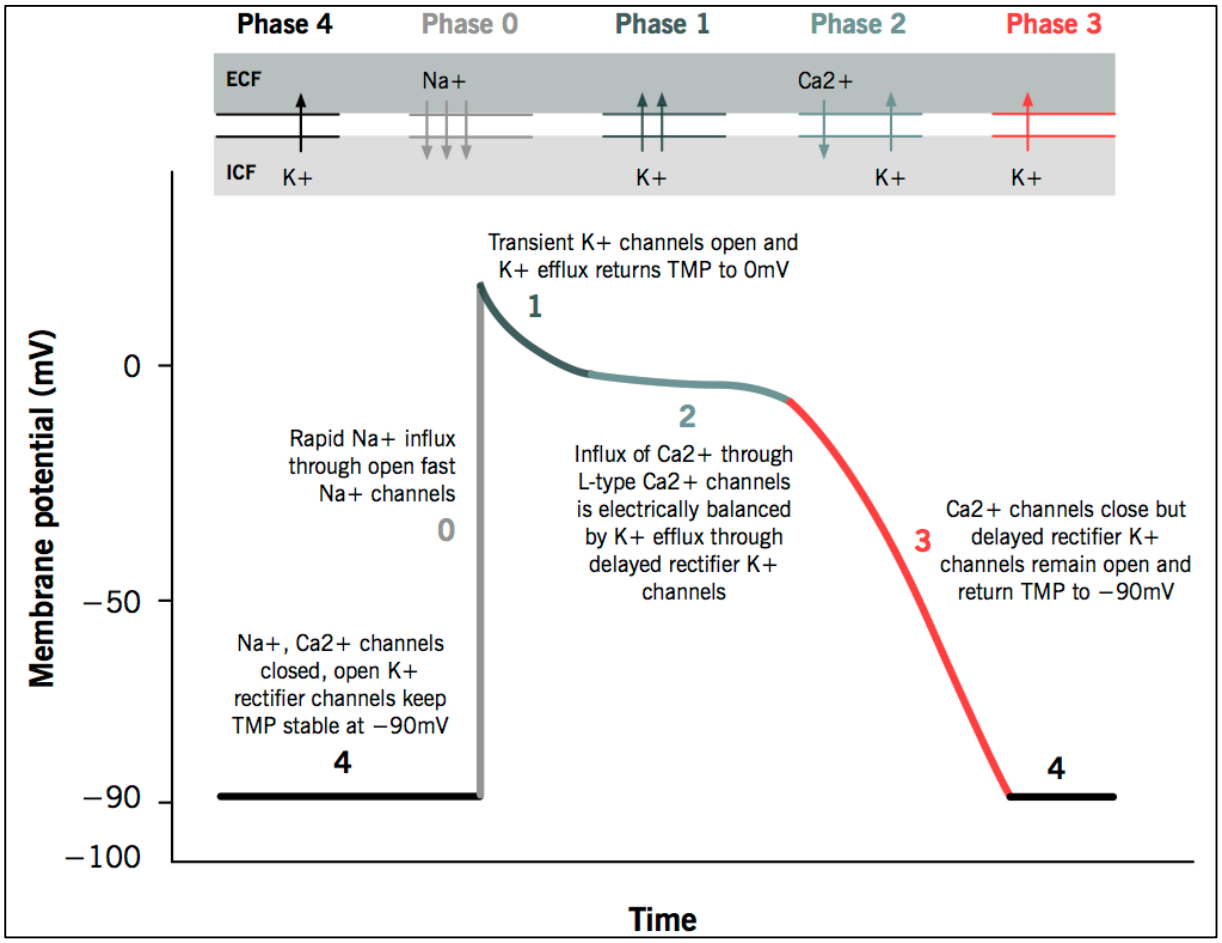

Figure 1 The 4 sequential phases of the action potential of cardiomyocytes. The cardiac action potential depends on ion currents, which set in at specific membrane potential values as indicated in the schematic which was taken directly from Grigoriy Ikonnikov and Eric Wong, Copyright © 2012-2015 McMaster Pathophysiology Review.

The intracellular and extracellular space of cardiac cells possesses disparate levels of ionic constituents, which leads to a disequilibrium of the electrical potential on both sides of the cellular plasma membrane. This disequilibrium is maintained by a distinct ion distribution and steady exchange of Na^+, K^+, Cl^- and Ca^{2+} ions. The cell membrane itself however is only selectively permeable for these ions and regulates the exchange between the extra and intra cellular ion content via specific ion channels. It does so either passively, i.e. through voltage gated channels, or actively through energy expenditure in the form of adenosine triphosphate (ATP). In healthy hearts it takes special pacemaker cells in the SAN of the right atrium to initiate the stepwise opening of these ion channels. The pacemakers generate small depolarizations in surrounding cardiomyocytes through the gap junctions and thereby start the phases of the so called cardiac action potential. As soon as the relative negative membrane potential at rest (-90 mV) inside the adjacent cardiomyocytes reaches the threshold potential (-70 mV) necessary to open the fast voltage gated Na^+ channels, it depolarises even further (to +20 mV) due to the influx of Na^+ ions into the cell cytosol. At this point voltage gated K^+ channels open up and an increased K^+ efflux out of the cell cytosol takes place. This slightly repolarises the cardiomyocytes (back to +5 mV) until the opening of voltage gated Ca^{2+} ion channels and subsequent Ca^{2+} flux into the cells sets in. For a short time the K^+ efflux and the Ca^{2+} influx counterbalance each other and keep the membrane potential at a relative plateau. This ends via a sudden reclosing of the voltage gated Ca^{2+} ion channels. The K^+ efflux however continues until the membrane potential is repolarised back to its resting state (at -90mV) until the next depolarization is initiated (Nerbonne, Kass 2005). The interval between the overall ventricular depolarization and repolarization has been clinically termed as the ST segment according to the position it upholds on a clinical electrocardiogram, which measures the heart's electrical activity. If persistently elevated this ST segment can be indicative of MI (Dickstein et al. 2008).

1.6. Cardiomyocyte excitation-contraction coupling (ECC)

The term excitation-contraction coupling (ECC) is a synonym for how the sequential flux of ions across the surface of excitable, electrically connected cardiomyocytes during the action potential results in intracellular Ca^{2+} cycling processes which lead to linear cell contraction of single cardiomyocytes in-series, in a highly regulated manner (Bers 2002). The opening of LTCCs during the action potential elicits a relatively small increase of the intracellular Ca^{2+} levels which in turn trigger the opening of cardiac Ryanodine receptors (RyR2) on the sarcoplasmic reticulum (SR). The SR is a major, intracellular Ca^{2+} store and subsequently

releases much higher levels of Ca^{2+} into the cytosol. This process is referred to as Ca^{2+} induced Ca^{2+} release (CICR). The now abundantly available Ca^{2+} in the cytosol binds to the myofilament Troponin C in the Troponin complex which, together with Tropomyosin, keeps the actin and myosin filaments from sliding along each other. The binding of Ca^{2+} releases the myosin heads which then use and hydrolyse ATP to ADP to generate energy. Through the consumption of this energy the filaments change their conformation and walk along the actin filaments to produce the energy dependent motion of contraction. For the cardiomyocyte to relax again it is necessary that Ca^{2+} detaches from Troponin C and is removed from the cytosol again. This happens gradually by decreasing the Ca^{2+} concentration through sarcoendoplasmic reticulum Ca^{2+}-ATPase (SERCA2A) driven reuptake into the SR, the sodium calcium exchanger (NCX) and the Ca^{2+}-ATPase in the sarcolemma expelling Ca^{2+} into the extra-cellular space and to a very small degree by Ca^{2+} uptake into the mitochondria via the Ca^{2+} uniporter (Bers 2002; Nerbonne, Kass 2005).

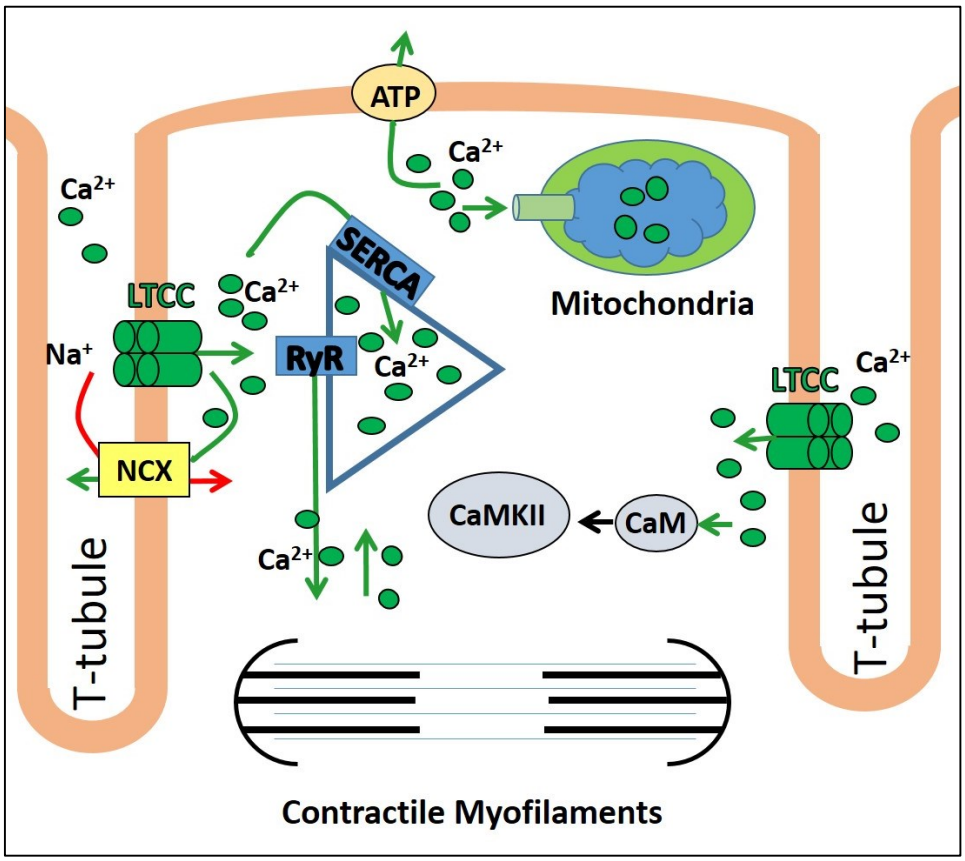

Figure 2. Ca^{2+} cycling and excitation-contraction-coupling related molecules in cardiomyocytes adapted from (Grandi, Herren 2014). Ca^{2+} cycling is indicated by green arrows. LTCC dependent Ca^{2+} cycling regulates CICR from the SR via RyRs. SR released Ca^{2+} facilitates contraction by binding to contractile myofilaments. Extrusion of Ca^{2+} from the cytosol and disassociation from contractile myofilaments is necessary for cardiomyocyte relaxation and is performed by SERCA dependent reuptake into the SR as well as Na^{+} and Ca^{2+} exchanger (NCX) and Ca^{2+} ATPase dependent expulsion into the extracellular space. A small amount of Ca^{2+} is furthermore taken up by the mitochondria for increased ATP production (Brandes, Bers 1997) or binds to Calmodulin (CaM) which goes on to activate Ca2+/calmodulin-dependent protein kinase II (CaMKII). CaMKII phosphorylates a variety of downstream targets and has been implicated in hypertrophy and apoptosis (Zhang, Brown 2004).

1.7. Ventricular cardiomyocyte structure in health

In their healthy state human, ventricular cardiomyocytes are striated, at times branched or rod-shaped and binucleated cells. Cardiomyocytes are furthermore connected to each other via the intercalated disks. This allows intercellular exchange of cytosolic molecules, like Na^+ and Ca^{2+}, between cardiomyocytes via the gap junctions. The gap junctions themselves are small channels, which are made up of the appropriately named connexin proteins (Goodenough and Paul 2009), that reside in the intercalated disk. *In vivo* ventricular cardiomyocytes are arranged in laminar layers of 28 up to 48 microns thickness (2 to 4 individual cells) surrounded by extracellular matrix, collagen and blood vessels (LeGrice et al. 1995). Single, human cardiomyocytes are around 120µm in length and 25µm in width (Severs 2000) and like rat cardiomyocytes they exhibit highly organised and regular surface and internal structures (Lyon et al. 2009). These structures are in part facilitated by the cytoskeleton, whose filaments are composed of actin and desmin while its protein transporting microtubule consists of polymerising α and β tubulin (Hein et al. 2000). The smallest structural and functional units of a cardiomyocyte are the sarcomeres. Sarcomeres contain the contractile myosin and actin filaments, necessary for force production and contraction. Depending on the state of cell contraction the sarcomeres are around 2 microns in length. They are delimited via the Z-lines, which are made out of a vast amount of different proteins (Solaro, Stull 2011). The surface structures of cardiomyocytes can be identified as Z-grooves, crests, transverse tubule (T-tubule) openings, which lead into the Transverse Axial Tubule (TAT) network. As their name indicates the Z-grooves are grooves in the surface sarcolemma of cardiomyocytes and they are separated from each other by intermediate dome-like structures, the crests (Gorelik et al. 2006). T-tubules are invaginations on the sarcolemmal surface of cardiomyocytes (Sperelakis and Rubio 1971), which usually open up to the extracellular space from within the Z-grooves via T-tubule openings. In healthy adult, rat ventricular cardiomyocytes the T-tubules openings the Z-grooves and the crest areas occur at a regular interval of about 2 microns distance (Gorelik et al. 2006). It is noteworthy that all structures mentioned above are also present in the atria, however to a more variable degree, as well as in the right ventricle. However, the major focus of the presented work lies on the investigation and characterisation of left ventricular cardiomyocytes in health and disease.

1.7.1. The cardiomyocyte TAT network

The TAT network is an important structural and functional feature of adult cardiomyocytes in the left ventricle. It stretches in a highly regular constellation throughout the whole body of

ventricular cells in axial and in transverse (T-tubule) directions along the Z-lines (approximately every 2 microns). To a less regular degree the TAT also forms longitudinal elements that connect the T-tubules with each other. In contrast to adult ventricular cardiomyocytes, neonatal cells completely lack a TAT network (Richards et al. 2011). The generation of the TAT network and its maintenance during adulthood is not yet fully understood but an array of various molecules has been implicated. These molecules include caveolin 3 (Cav3), presumably responsible for T-tubule formation and maintenance (Woodman et al. 2002), BIN1 for T-tubule formation through inducing curvature in membranes and for LTCC shuttling (Hong et al. 2010), tropomyosin for T-tubule maintenance (Vlahovich et al. 2009), Tcap for load dependent formation of T-tubules at least in skeletal muscle (Zhang et al. 2009) and junctophilins for correct T-tubule and SR association (Han et al. 2013). Recent studies ascribe junctophilins an additional and important role in the orientation of tubules in the TAT network (Bennett et al. 2013; Pinali et al. 2013). The diameter of fully developed TAT network tubules in ventricular cells is around 20 to 450 nm and many of the proteins necessary for the process of excitation-contraction coupling are concentrated within the TAT network, including β_2ARs at the T-tubule openings as well as Na/Ca^{2+} exchanger (NCX) and LTCCs inside the T-tubules (Ibrahim et al. 2011; Brette, Orchard 2003).This positions the LTCCs directly across from the RyRs on the SR (approximately 10-12nm apart) (Franzini-Armstrong et al. 1999). After electrical excitation this arrangement facilitates fast and homogenous CICR from the SR into the cytosol throughout the whole cardiomyocyte as well as microdomain specific Ca^{2+} removal via NCX. This setup allows for rapid cardiomyocyte contraction and relaxation (Richards et al. 2011). It also allows for microdomain specific formation of β_2AR signalosomes by arranging them in close proximity to their downstream signalling components, which are distinct to β_1AR signalling targets (Nikolaev et al. 2010). The TAT network furthermore limits the diffusion of ions which can enter into them and thereby establishes a microenvironment with relatively constant ion content (Brette et al. 2006). T-tubule disruption in end stage HF in human and animal ventricular cells is well documented (Lyon et al. 2009) and serves as substrate for dysfunctional βAR and Ca^{2+} signalling (Nikolaev et al. 2010). Artificial detubulation by formamide treatment *in vitro* also functionally affects both β_1- and β_2-AR responses and Ca^{2+} signaling in cardiomyocytes (Nikolaev et al. 2010; Brette et al. 2005). As a result the remodelling or partial loss of the TAT network in ventricular cardiomyocytes is heavily implicated in the pathology of HF. Most of the cardiomyocyte structure can satisfactorily be visualised with SICM and parallel confocal imaging of structures visualised via fluorescent molecules, as was done for this study.

1.7.2. Caveolae

Caveolae are cholesterol and glycosphingolipid enriched lipid rafts which form flask or cave-like indentations in the membrane of cells, including left ventricular cardiomyocytes. Though it has been hypothesised that the caveolae might be precursors of the T-tubules they are only found outside of the TAT network (Harvey and Calaghan 2012; Wong et al. 2013). With only 50 to 100 nm width, the caveolae are smaller than other surface structures of cardiomyocytes and the state of the art technique of localising caveolae remains the electron microscope (Wright et al. 2014). Like other lipid rafts the caveolae are able to organize proteins with the necessary affinity, like palmitoylated transmembrane proteins, the β_2ARs, AC 5/6 and the α-subunit of G-proteins in close proximity (Brown and Borutaite 2007; Balijepalli et al., 2006). The caveolae are also the exclusive residence of β_2ARs in neonatal cardiomyocytes (Xiang et al. 2002) and eNOS in adult cardiomyocytes (Petroff et al. 2001). They have been shown to modulate β_2AR signalling (Calaghan and White 2006) and Ca^{2+} signalling complexes in cardiomyocytes (Bossuyt et al. 2002). Caveolae are furthermore reported to gather mechano-sensitive ion channels in their structure, including a subpoulation of LTCC and to be involved in increasing or decreasing their activity depending on mechanical stimuli which the cells receive and the consequent post-translational modifications, like phosphorylation, which occur as a result (Petroff et al. 2001). The flask-like appearance of caveolae, which is assumed to work as an ion reservoir, is due to the structural caveolin coat proteins (Caveolin 1, 2, 3) which they incorporate to varying degrees depending on the tissue. In cardiomyocytes Cav3 is the dominant caveolin form (Song et al. 1996) and is assumed to be involved in a number of cardiomyopathies. Complete knockdown of the protein has been shown to lead to HF (Woodman et al. 2002).

1.7.3. Cardiomyocyte hypertrophy

Hypertrophy is an increase in cell size which cardiomyocytes undergo in order to adept to altered mechanical load i.e. during the progression of HF to compensate for decreased cardiac output. If hypertrophic signalling is maintained at a continuous level it can further the development of dilated cardiomyopathy. The observable increase in cardiac cell size occurs as a result of increased protein expression, altered sarcomere organization and a return to a more fetal phenotype (Yue et al. 2000).

1.8. G-protein coupled receptors

With over 800 known family members, the superfamily of G-protein coupled receptor (GPCR) molecules is one of the biggest protein families present in the mammalian genome (Fredriksson et al. 2003). GPCRs are a key player in translating a huge variety of stimuli, which they receive via extracellular ligand binding, into intracellular signals and physiological reactions (Hill 2006). GPCRs are identifiable by a sequence of seven α helices with high hydrophobicity, which form seven transmembrane (7TM) spanning domains, as well as by their ability to interact with guanine-nucleotide binding proteins (G proteins) (Fredriksson et al. 2003). The heterotrimeric G-proteins with their α, β and γ subunits can influence downstream effector targets like ACs and GCs. In their inactive state the G-proteins are bound to GDP. They are activated through the exchange of this GDP with GTP, which leads to their conformational change and allows their G α subunits to dissociate from β and γ and to initiate a signalling cascade. The different types of G α subunits known to date are: stimulatory (Gs), Gi, the phospholipase C activating (Gq) and $G_{12/13}$ (Audet, Bouvier 2012). βAR coupled Gs increases cAMP. In contrast Gi blocks βAR dependent cAMP production and is implicated in reduced contractility during HF progression. In failing human cardiomyocytes (Brown, Harding 1992) and a model of MI in the rat (Kompa et al. 1999) inactivating of Gi via pertussis toxin partially restored β_1AR-mediated contractility. Interestingly, despite increased Gi expression (El-Armouche et al. 2003) this appears not as the result of increased Gi activity in HF as this has been reported to be unchanged in comparison to healthy hearts (Hussain et al. 2013). It is possible for a GPCR to be coupled to multiple G-proteins as is the case for β_2AR, which are associated to Gs but switch to Gi after phosphorylation by PKA (Zhu et al. 2001). GPCR agonists and antagonists can bind with varying affinity and elicit a variable amount of signal amplification depending on their expression level and the tissue in which they are found (Hill 2006). Also the function and downstream signalling of the GPCRs is regulated by a group of kinases, the G-protein receptor coupled kinases (GRKs), which are also known in context with βARs as the βAR kinases (βARKs) (Ungerer et al. 1993). Owing to the fact that most of the polypeptide chain of the GPCRs is sitting inside the plasma membrane of the respective cell, their detection and the determination of their structure initially posed a big challenge to the scientific community. The first step of cracking this conundrum was achieved through the use of chemical synthesis. By generating radioactive ligands that specifically bind various GPRC receptors Lefkowitz et al. detected the receptors for ADR, the βARs (Lefkowitz et al. 1970). On the basis of the knowledge obtained thus Lefkowitz et al. then proposed that GPCR signal transduction is based on a ternary complex with high and low affinity states that is composed of the extracellular ligand, a transmembrane component and the intracellular G-protein which exists in an equilibrium of 2 states: active or inactive. The ternary complex model had to be

expanded when basal activity of some GPCRs became apparent (De et al. 1980). It required another three decades to find a suitable method to determine the three dimensional structure of GPCRs. The breakthrough was achieved by Okada et al. who determined the three-dimensional structure of inactive rhodopsin via a sophisticated purification process and x-ray crystallography (Okada et al. 1998). Ultimately determining the three-dimensional structure of an active GPCR, namely the β_2AR, was successfully performed by the Kobilka group. This discovery allowed for unprecedented insight into conformational changes occurring from the inactive GPCR to the activated GPCR (Rasmussen 2007). With the newfound insight also came the realisation that the GPCRs adapt to different stimuli by undergoing desensitisation, internalisation and phosphorylation. Due to the multitude of biological processes and pathologies in which the GPCRs are involved, they represent a major target for potential pharmaceutical intervention and therapy (Hill 2006).

1.8.1. Adrenergic receptors (ARs): subtypes and their specific functions

The 9 subtypes (α_1A, α_1B, α_1D, α_2A, α_2B, α_2C, β_1, β_2, and β_3) of ARs that are currently known are all members of the GPCR family. α_1A, α_1B, α_1D are coupled to the phospholipase C (PLC) activating Gq protein and to a very small extent increase cardiac contractility and hypertrophic remodelling while α_2A, α_2B, α_2C are coupled to Gi and might play a role in presynaptic inhibition of NOR release at the atria (Brodde et al. 1999; Hofmann et al. 2006). The role of βARs in the heart is far better understood. βAR are the major translators of catecholamine binding into a cellular response that regulates heart rate and contractility according to the organisms needs. β_1ARs and Gs coupled β_2ARs elicit positive inotropic, chronotropic and lusitropic effects. β_1AR stimulation can furthermore lead to cell apoptosis, while β_2AR in its Gi coupled state exhibits anti-apoptotic signalling characteristics (Xiang 2011). The role and even the actual presence of functional β_3ARs in cardiac cells is still very controversial. This controversy is fuelled by the fact that only some mammals, including humans (Gauthier et al. 1996) and rats (Birenbaum et al. 2008) do express β_3ARs in the ventricle while others, like mice, only express it to a very low extent (Belge et al. 2014). Reports of both cardio-protective (Niu et al. 2012) as well as of potentially cardiotoxic effects via β_3AR signalling have been published (Zaugg 2008).

1.8.2. Cardiac β_1 and β_2 AR signalling in health

cAMP is produced via ACs after the binding of catecholamines to the βARs. In cardiomyocytes there are two β AR subtypes capable of initiating the cAMP signalling cascade: β_1ARs and β_2ARs. In health β_1ARs and β_2ARs are present at an approximate ratio of 70:30 (Wallukat

2002). The cAMP produced by the two βARs is however localised to differential compartments and will elicit different effects depending on its original site of stimulation, its degradation and regulation by PDEs and its concentration (Stangherlin, Zaccolo 2012). In healthy adult cardiomyocytes β_1ARs are detectable throughout the cell surface in caveolar and extracaveolar membrane fractions (Agarwal et al. 2011), while β_2ARs are exclusively localised inside T-tubule openings (Nikolaev et al. 2010) and/or caveolae (Calaghan, White 2006). Once produced cAMP acts by binding and activating spatially segregated targets. These targets include exchange proteins directly activated by cAMP (EPAC), protein phosphatases and cAMP-gated ion channels. But the major cAMP downstream targets are PKAs. In their inactive from PKAs consist of two catalytic (C) subunits with 3 different components (Cα,Cβ,Cγ) and two regulatory (R) subunits with four isoforms (PKA RIα and RIβ or PKA RIIα and RIIβ). They are activated upon cAMP binding and dissociation of the C subunits. PKA RI and RII act in two separate signalling compartments (Stangherlin et al. 2011). βAR-dependent cAMP acts via PKA RII, which phosphorylates and thereby activates various downstream targets including the PKA RII subunit itself (Zakhary et al. 2000), In human hearts autophoshorylation of the RII subunit is pivotal in regulating PKA binding to specific AKAPs and has been shown to be significantly decreased in HF (Zakhary et al. 2000). Furthermore the protein levels of both regulatory subunits, RI and RII, were shown to be decreased in human failing hearts (Zakhary et al. 1999). LTCCs (Keef et al. 2001), the RyRs, Troponin I (Zakhary et al. 1999), Phospolamban (Xiao 2001) and Glycogen Synthase Kinase 3 (GSK3) (Sudgen et al. 2008). PKA also activates cAMP response element-binding (CREB) proteins involved in cardiac hypertrophy (Sudgen et al. 2008). Hence the activation of the cAMP signalling cascade via β_1 and β_2ARs generally leads to positive inotropy and increased contractility of cardiomyocytes (Wallukat 2002). While β_1ARs exclusively signals via Gs proteins and their respective cAMP signals traverse the whole cytosol, β_2ARs can switch between Gs and the Gi and their respective cAMP signals are very confined and localised to small subcellular compartments (Nikolaev et al. 2010). This switch, which is prefaced by PKA and GRK phosphorylation of the β_2ARs, followed by receptor internalization and recycling (Zamah et al. 2002), allows differential signalling via downstream targets. These targets include Akt1 and Akt2 kinases present in cardiomyocytes, which are involved in the regulation of cellular growth, apoptosis and cell metabolism. Both Akt1 and Akt2 phosphorylate GSK3 which acts as a restraint against hypertrophy (Sudgen et al. 2008). Also β_2AR have been associated with Gs independent signalling over the ERKs involved in hypertrophic signalling cascades (Yue et al. 2000). The effects of cardiac β_1AR stimulation seem to be relatively uniform across various species, the function of β_2ARs however appears to underlie species differences. Depending on the species cardiac tissue specific β_2ARs either elicited both increased inotropy and lusitropy or only one of the above (Afzal 2011). β_2ARs in rodents have exhibited either no effect on contractility

(Jiang and Steinberg, 1997) or lead to increased cardiac inotropy without increased relaxation (Xiao et al. 1999).

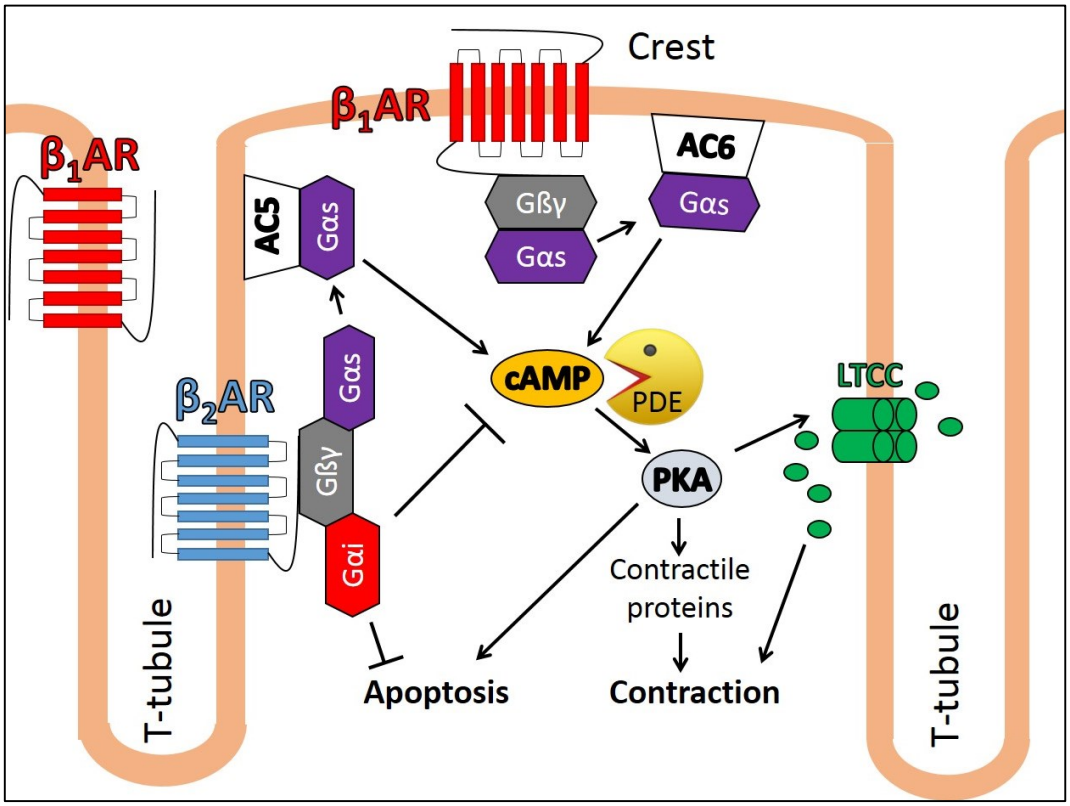

Figure 3 Role of β_1 and β_2 ARs dependent signalling in healthy cardiomyocytes via differential subcellular compartmentation and differential coupling to Gs or Gi protein α subunits. β_1ARs bound to Gs induce cAMP production via AC type 6 and activate PKA which leads to heightened contractile protein as well as LTCCs phosphorylation and hence increased cardiomyocyte contraction, but can also lead to cell apoptosis. β_2ARs activation can also lead to cAMP production via AC type 5 and the activation of the cAMP dependent PKA pathway. Alternative β_2AR coupling to Gi inhibits cAMP signalling and induces anti-hypertrophic signalling pathways.

1.8.3. β_2AR switch from Gs to Gi

As mentioned before the β_2AR is able to switch between the Gs protein, which allows it to function via cAMP production, to the pertussis toxin sensitive, Gi protein, which causes differential cell internal signalling in cardiomyocytes (Xiao et al. 1999). This switch is induced via catecholamine binding to the receptor followed by PKA dependent phosphorylation of the β_2AR, which induces a conformational shift and leads to the activation of the MAP/ERK signalling pathway (Daaka et al. 1997; Kohout and Lefkowitz 2003). Phosphorylation of β_2AR by PKA furthermore initiates the process of receptor desensitisation and internalisation which is described in the following paragraph. The ability of β_2ARs to switch between Gs and Gi also clearly reveals, what is known in pharmacology as “biased agonism” or “functional selectivity”

of receptors. The term “biased agonism” describes the preference of a receptor to signal over specific pathways depending on the bound ligand and the receptors resulting conformational shift. In the case of the β_2AR this means that i.e. in mouse cardiomyocytes NOR leads to full activation of the β_2AR coupled Gs pathway but only ADR can also elicit Gi receptor coupling and signalling (Wang et al. 2008). The biased agonism of the β_2AR in cardiomyocytes might underlie a further regulation namely its compartmentation in caveolae in neonatal cells or, if the caveolae are indeed the precedors of T-tubules, compartmentation via the TAT network (Xiang et al. 2002; Harvey and Calaghan 2012; Wong et al. 2013).

1.8.4. β_2AR desensitization and internalisation

An important mechanism to control cell signalling is the desensitisation process of G-protein coupled receptors (GPCRs). From a functional perspective this desensitization tempers the responsiveness of receptors to hormonal stimulation. The desensitisation process has best been described in β_2ARs and is primarily orchestrated by G protein-coupled receptor (GPCR) kinase (GRK-2 or βARK) and β-arrestins. As soon as β_2ARs are activated and elicit signalling via the G stimulatory (G_s) proteins the counteracting, desensitisation process will set in. As one of PKA’s downstream phosphorylation targets the GRK-2 will be activated and bind to the β and γ subunits of the Gs proteins. From there the GRK-2 will phosphorylate a regulatory site on the active β_2AR, which enables β-arrestins to bind to the receptor and to internalise the receptor via endocytosis into the cytosol to presumably make it sterically impossible for G-proteins to recouple with β_2ARs (Kohout and Lefkowitz 2003). However, despite the assumption that GPCRs can no longer signal over Gs-proteins once internalised, recent findings show that the β_2ARs, at least in HEK293 cells, can still participate in the Gs dependent production of cAMP which sets in slightly later than the response of uninternalised receptors (Irannejad et al. 2013). Also, independently of Gs protein coupled signalling, the internalised β_2AR has been shown to participate in the activation of ERKs (Kaya et al 2012), which has been shown to be involved in cardiac hypertrophy signalling (Yue et al. 2000). The extent of β_2AR desensitisation and internalisation and GRK-2 dependent phosphorylation has furthermore been shown to be sensitive to the concentration and partial agonism of βAR ligands. As a result partial agonists like the sympathomimetic ephedrine lead to a slower desensitisation of about 30 min in comparison to full agonists like ADR who achieved receptor desensitisation in about 1 min (January et al. 1997). A further mechanism to improve the efficiency of β_2AR signalling desensitization is introduced by PDE4 isoform 4D5 enzymes, which are localised close to the receptors. These enzymes have been shown to bind to β-arrestins in order to be recruited to the respective β_2AR and regulate the cAMP pool in the associated, subcellular β_2AR compartment (Lynch et al. 2007). β_3ARs only share about 50%

sequence homology to β_1ARs and β_2ARs and appear to be excluded from desensitization as they lack the necessary PKA or GRK phosphorylation sites (Ligget et al. 1993) but they may exert a further, highly localized suppressing effect on β_1 and β_2AR-dependent cAMP signalling.

1.8.5. MAPK/ERK signalling pathway and its role in hypertrophy

β_2ARs can activate the MAP/ERK pathway via the dissociation of the receptor coupled Gi α-subunit from the β and γ subunits. The latter subunits then go on to activate tyrosine-protein kinase c-Src and signalling over the GTPase protein Ras (Daaka et al. 1997). In a signalling cascade the Ras protein then goes on to activate various Raf proteins, which in turn activate MAPKs, which activate ERKs. The MAPK/ERK kinase pathway has been shown to induce catecholamine dependent hypertrophy via increased gene expression (Yue et al. 2000).

1.8.6. β_1 and β_2 AR signalling in HF

As was alluded to before, SNS system becomes rampant during HF progression. As a result cardiomyocytes and βARs together with their associated signalling pathways undergo drastic modifications. Persistent β_1AR-cAMP signalling leads to aggravated loss of cardiomyocytes and maladaptive cell remodelling. Possibly to counteract these consequences β_1ARs are increasingly desensitized, internalized and degraded during HF progression (Xiang 2011). In parallel β_2ARs abandon their exclusive T-tubular position and are rearranged over the whole sarcolemma. Despite the fact that this redistribution occurs together with proportionally increased coupling to Gi and β_2AR desensitization it has been surmised, that the β_2ARs outside of T-tubules could temporally acquire cardiotoxic β_1AR signalling traits by abruptly reaching β_1AR-cAMP downstream targets (Nikolaev et al. 2010).

1.8.7. ACs and cAMP signalling

ACs are enzymes responsible for converting ATP into cAMP. Once generated the cAMP messenger molecules diffuse at an estimated 700 to 780 μm^2 per second and are involved in several biochemical processes (Heijman et al. 2011; Nikolaev et al. 2004). ACs are activated through the binding of the Gs α-subunit and inhibited by the binding of the Gi α-subunit. In the heart the prevalent AC isoforms responsible for βAR-dependent cAMP production in separate subcellular locations are AC5 and AC6 (Timofeyev et al. 2013). AC5 is situated mainly inside the T-tubule, where it is associated with Cav3 and β_2ARs and potentially a subset of β_1ARs. In contrast the AC6 isoform is bound to the sarcolemmal membrane outside of the T-tubules and carries out β_1AR associated cAMP production (Timofeyev et al. 2013). There are clear

differences in the actual concentration of cAMP pools generated by the ACs in the specific subcellular microdomains present in cardiomyocytes (Iancu et al. 2008). The microdomain specific concentration depends on the level of cAMP production as well as its confined diffusion inside the cytoplasm before being degraded by PDEs or meeting its molecular targets. It appears that β_2AR associated AC5 dependent cAMP pools are much more stringently regulated than those generated by β_1AR associated AC6 (Timofeyev et al. 2013). The expression of AC6 mRNA has been shown to decrease in age (Tobise et al. 1994) and HF (Espinasse et al. 1999)

1.8.8. A-kinase anchoring proteins (AKAPs)

PKAs as well as other protein kinases (protein kinase C) and phosphatases (i.e. calcineurin) are localised to specific compartments and their interaction partners via AKAPs (Mauban et al. 2009; Klauck et al. 1996). Even though the 17 members of the currently identified cardiac AKAP family are structurally quite different from each other they are identifiable by their ability to bind PKA regulatory subunits at nanomolar affinity and to localise them close to their specific downstream targets. This is necessary to facilitate compartmentalised and highly specific cAMP/PKA signalling which leads to distinct physiological cell responses and modulates acute and chronic cardiac function (Soni et al. 2014). The different members of the AKAPs family possess a conserved α helical structure which binds to a hydrophobic pocket at the regulatory (R) subunits of PKAs isoforms PKA-RI and PKA-RII, Most identified AKAPs preferentially bind to RII though there are also AKAPs with dual specificity and preference for RI binding. As a result PKA-RII is localised at multiple, specified sites within cardiomyocytes including to the plasma membrane by AKAP79 or the nuclear membrane by mAKAP (Kapiloff et al. 1999), while PKA-RI is primarily localised to the soluloble cell fractions by AKAPs such as the dual AKAP Ezrin (Di Benedetto et al. 2008; Stangherlin et al. 2011). The crucial role of AKAPs in cardiomyocyte regulation was proven by disrupting AKAP–PKA-RII binding using the anchoring domain of AKAP13 as a blocking peptide (Ht31), which lead to a significant reduction in Troponin I (TnI) and Myosin binding protein C phosphorylation by PKA (Fink et al. 2001). By tethering PKA RI and RII as well as other kinases to differential subcellular locations in the vicinity of specific membrane bound or soluble ACs the AKAPs facilitate highly restricted and functionally separable signal compartments and phosphorylation events. A prime example for this regulation are the different effects elicited by the drugs ISO and prostaglandine E1 in cardiomyocytes. Though both drugs generate comparable levels of cAMP only ISO leads to β_2AR and phospholamban (PLB) phosphorylation and increases contractile force. This disparity arises from AKAP tethering the PKA activated by cAMP to particulate cell fractions whereas PGE1 activated PKA in soluble cell fractions which did not alter cell contractility

(Hayes et al. 1980; Di Bendetto et al. 2008). AKAPs also limit the amount of molecules tethered to specific subcellular domains, as it was shown at the hand of mAKAP. The amount of mAKAP molecule localisation to the cell membrane is not unlimited and overexpression of the AKAP targeting sequence can lead to displacement of the endogenous protein (Kapiloff et al. 1999). Hence AKAPs significantly add to the complexity of cAMP-dependent cell signalling.

1.8.9. cGMP signalling in cardiomyocytes

Like cAMP, cGMP is an ubiquitously present second messenger, which mediates the translation of cell stimuli into physiological responses (see figure 4). In contrast to cAMP however these responses are primarily of a negative inotropic nature in cardiomyocytes (Feil and Kemp-Harper 2006). Elevated levels of cGMP appear to be cardioprotective by preventing hypertrophy and adverse remodelling of ventricular cardiomyocytes (Belge et al. 2014). The how and when cGMP production takes place in cardiomyocytes will be dealt with in the following paragraphs.

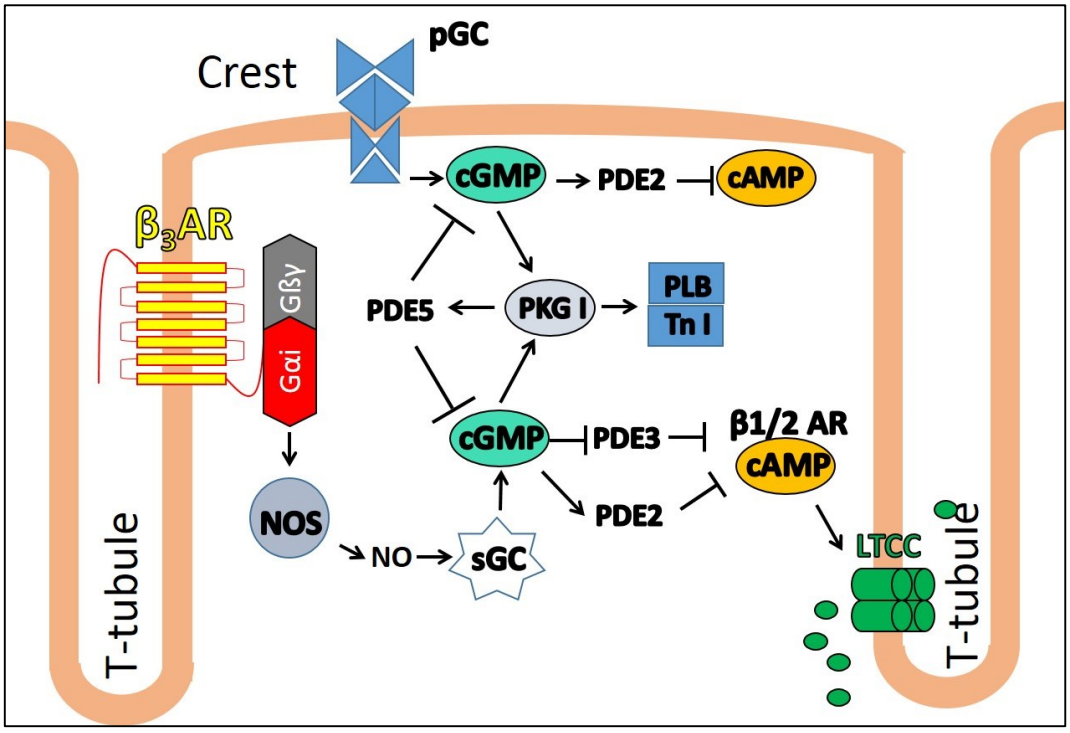

Figure 4 cGMP signalling in cardiomyocytes. cGMP is produced after binding of NPs to pGC and binding of NO to soluble (sGC). NO itself can be endogenously produced via NOS which can be activated by the β_3AR via the Gi α-subunit. Once produced cGMP activates downstream targets, including PDE forms 2,3 and 5 as well as PKGI, which in turn phosphorylates PLB and TnI. Other downstream targets though present are not shown. Only cGMP produced by sGC regulates β_1 and β_2AR dependent cAMP levels via PDE2 and PDE3 and thereby effects βAR regulation of LTCCs.

1.8.10. Secondary messenger signalling of cGMP

The secondary messenger cGMP is generated by GCs. This occurs as a result of NO and controversially also by carbon monoxide (CO) binding to the sGC in the cytoplasm (Pyriochou and Papapetropoulos 2005; Ryter et al. 2006). Alternatiely cGMP is produced via the binding of NPs to the pGC situated on the plasma membranes (Potter et al. 2006). Pools of cGMP will form in distinct cellular compartments depending on which GC is activated (Castro et al. 2010) and can differentially influence cAMP generated by the βARs (Stangherlin et al. 2011). Once cGMP is produced it goes on to bind and activate its downstream targets including PDEs and PKGs (also known as cGKs). Besides the PDEs it is these PKGs which influence cGMP levels strongly by affecting the productivity of the GCs differentially in specific subcellular compartments and by regulating protein phosphatases (Hofmann et al. 2006). In adult rat cardiomyocytes for instance PKG amplifies cGMP depletion when NO is the cause for its production. At the same time PKG allows for higher cGMP accumulation after natriuretic peptide signalling. In adult, rat cardiomyocytes the cGMP generated by the two pGCs stays close to the plasma membrane and is controlled by PDE2. In comparison cGMP, which is produced remote from the plasma membrane in the cytosol appears to be degraded by PDE2 as well as PDE5 (Castro et al. 2010). Mammals possess two types of PKG, which are localised to different subcellular compartments via PKG anchoring proteins (Casteel et al. 2008). These PKGs are PKGI with isoforms Iα and Iβ and PKGII. There are low levels of PKGI in the myocardium and probably no PKGII (Hofmann et al. 2006). Work in transgenic knockout mice showed PKGI to be the primary mediator of cGMP's negative inotropic effects in the myocardium, via inhibition of the LTCCs, as well as a hypertrophy decreasing factor (Kuznetsova et al. 2013).

1.8.11. Particulate guanylyl cyclases and natriuretic peptides

To this day we are aware of three distinct particulate guanylyl cyclases (pGC) and as many natriuretic peptides (NPs) to activate them. In cardiomyocytes the specifically present pGCs are GC-A, which is activated by atrial (ANP) and brain natriuretic peptides (BNP), and GC-B which requires C-type natriuretic peptide (CNP) stimulation. Natriuretic peptides (NP) are important regulators of cardiac contractility (Hofmann et al. 2006). The three types of natriuretic (=urinary Na^+ excretion) peptides (NPs) emerge from separate cellular sources. ANP is generated in/ and secreted from atrial cardiomyocytes. Besides its electrolyte balancing, vasorelaxant and anti-inflammatory roles ANP inhibits the secretion of aldosterone and renin and decreases blood pressure and volume (Pandey 2014). Thus it is vital for maintaing cardiovascular homeostasis. The major source of brain natriuretic peptide (BNP) is provided by the ventricles. In contrast, CNP is produced by endothelial cells in the vasculature.

This conveniently allocates CNP close to the smooth muscle cells, its major target, to cause vasodilation. CNP can also yield positive inotropic effects which are executed via PKG (Pandey 2014). Activation of GC-A and GC-B increases cGMP levels depending on the stimulatory NP and compartment which leads to a decrease in positive inotropic molecules such as cAMP and Ca^{2+} (Pandey 2014). In neonatal rat cells the ANP dependent cGMP pools were shown to specifically affect those cAMP molecules in the respective PKA RII compartment via increasing PDE2 activity but not those in the RI compartment (Stangherlin et al. 2011). Further studies in adult ventricular rat cardiomyocytes revealed that only CNP but not BNP effectively elicited negative inotropy and positive lusitropy despite the fact that both NPs lead to an increase in cGMP levels. CNP conveys this effect by phosphorylation of PLB and Troponin I increasing the speed of Ca^{2+} reuptake into the SR or by increasing Ca^{2+} extrusion into the extracellular space (Moltzau et al. 2014). GC-C, the third GC subtype, is activated by binding of all three NPs but possesses no catalytic GC domain. Interestingly GC-C activation has demonstrated a capacity to lead to raised cAMP, Ca^{2+} and inositol triphosphate (IP3) levels (Pandey 2014).

During the development of various cardiomyopathies a clinically measurable rise of all NPs was reported (Moltzau et al. 2013; Pandey 2014). This rise is detectable early and serves as a diagnostic and prognostic tool of disease progression (Mukoyama et al. 1991; Pandey 2014). Additional administration of NPs as a therapeutical substance (Boerrigter et al. 2009) however has not been proven helpful (Shah et al. 2011).

1.8.12. Soluble guanylyl cyclase (sGC) and nitric oxide synthases (NOS)

sGC is made up of the heterodimeric α and β subunits with catalytic domains. The α1 and β1 isoforms of these subunits are almost ubiquitously expressed. In opposition the α2 subunit is sparser but can be found highly expressed in heart tissue, while the β2 subunit is mainly found in kidney. A splice variant of the α2 subunit can bind with β1 subunits and deactivate sGCs function. As a member of the Heme-Nitric oxide and OXygen binding family (H-NOX) the sGCs possess a heme domain for ligand binding. Though sGC appears to not bind to oxygen it is not yet fully established if its intrinsic H-NOX domain physiologically binds to nitric oxide (NO) only or both NO and carbon dioxide CO_2 (Derbyshire and Marletta 2009). NO releasing drugs have produced beneficial, therapeutic effects in the treatment of HF. Though the role of NO dependent cGMP in physiology is controversial the molecule also exhibits modulatory effects on cardiac contractility and cardiomyocyte remodelling (Hofmann et al. 2006). When NO binds to the sGC protein's heme domain this leads to an extensive 200 fold rise in cGMP production from GTP (Cary et al. 2005). It was furthermore shown, that sGC but not pGC-dependent

cGMP signalling can decrease the βAR-dependent cAMP response in cardiomyocytes. This occurs by sGC dependent cGMP blocking of PDE3 activity in the PKA RI compartment and increasing of PDE2 activity in the PKA RII compartment (Stangherlin and Zaccolo 2012) and by inhibiting LTCCs (Castro et al. 2010). Physiological sources of NO are provided by the NOS. The NOS produce NO via the oxidisation of L-arginine to NG-hydroxy-L-arginine and further to L-citrulline and NO through the utilization of NADPH and oxygen. *In vivo* the NO which stimulates sGCs in cardiomyocytes potentially has autocrine origins from endogenous NOS or is derived from paracrine sources such as the endothelium. As the NO molecule is so small it can easily diffuse through the sarcolemma of cardiomyocytes. There are currently three isotypes of NOS which have been identified: the neuronal (nNOS), the endothelial (eNOS) and the inducible (iNOS) isoform (Derbyshire 2009). eNOS and nNOS are regulated partially by Ca^{2+} and calmodulin and are to a degree constitutively active (Barouch et al. 2002). The activity of eNOS can be increased via its phosphorylation on its Serine residue 1177 and decreased by phosphorylation of Serine 114 (Niu et al. 2012). Similarly nNOS activity will be increased by post translational phosphorylation of Serine 1412 and inhibited by Serine 847 phosphorylation (Watts et al. 2013). iNOS activity however needs to be induced and has been shown to be upregulated in HF. The NOS which are expressed endogenously in cardiomyocytes have different subcellular locations, which are assumed to facilitate their different functions (Barouch et al. 2002). eNOS is localised inside the T-tubules and sarcolemmal caveolae (Zaugg 2008). By contrast nNOS is situated at the SR together with the RyRs (Brown, Borutaite 2007). It has been shown to become translocated from this position to the sarcolemma where it binds to Cav3 in the case of a MI and HF (Kulandavelu, Hare 2012). Detectable iNOS levels only appear in the cytosol of cardiomyocytes after inflammation or due to ischemic injury (Brown et al. 2007). In health eNOS presumably is the most important NOS in relation to cardiomyocyte contractility (Massion et al. 2004). Despite the cGMP/PKG pathway dependent NO effects the gas also elicits cGMP independent effects (Hofmann et al. 2006). Via cardiomyocyte restricted overexpression in mouse it has been shown that eNOS dependent NO signalling not only attenuates βAR dependent cAMP signalling and its inotropic effects but it also increases the negative chronotropic effect on the heart rate of muscarinic receptor signalling and protects against ventricular arrhythmia (Massion et al. 2004). NO dependent cGMP is furthermore able to activate PDE2 to degrade βAR cAMP levels (Mongillo et al. 2006).

1.8.13. Cardiac β_3AR signalling in health and HF

Unlike β_1ARs and β_2ARs the β_3ARs induce negative inotropic effects in cardiomyocytes by NO associated production of cGMP. Another special feature of β_3ARs in contrast to β_1ARs and

β_2ARs is their resistance to receptor desensitization (Nantel et al. 1993) as they do not possess any PKA or GRK phosphorylation sites (Ligget et al. 1993). In healthy hearts the β_3AR is expressed preferentially in the left ventricle but at relatively low levels. It might also be noteworthy that β_3AR are less expressed in female tissue and that NO appears to be differentially regulated in males and females (Zaugg 2008). According to various studies the β_3AR expression increases two- to threefold in aging myocardium (Birenbaum et al. 2008), diabetes (Amour et al. 2007), sepsis (Moniotte et al. 2007) and HF (Moniotte et al. 2001). There are reports of β_3AR coupling to Gs and associated production of cAMP (Xiang 2011; Kohout et al. 2001) but the majority of studies shows cardiac β_3AR coupling to Gi and with it the production of cGMP (Kulandavelu, Hare 2012). At least in rat there appears to be no β_3AR-dependent cAMP production on top of β_1AR and β_2AR as was determined previously by our group (Nikolaev et al. 2010). As cGMP production has been associated with anti-hypertrophic effects and appears to be cardioprotective against adverse remodeling (Lukowski et al. 2014) β_3ARs are likened to a biological “brake” which protects the heart from catecholamine overstimulation (Niu et al. 2012; Belge et al. 2014). Through their coupling to Gi it is speculated that the β_3ARs are involved in blunting the β_1AR dependent cAMP signalling (El-Armouche et al. 2003; Massion et al 2004). β_3ARs can reduce contractility via Gi protein and act via eNOS dependent NO and hence via NO dependent cGMP production via sGCs (Watts et al. 2013). β_3AR-dependent eNOS activity has been linked to Akt kinase (also known as protein kinase B = PKB) dependent signalling and cell survival (Napp et al 2009). Cell survival is induced by Akt binding to SMAD signal transduction proteins. This inhibits SMAD phosphorylation by TGFβ and the TGFβ induced apoptosis pathway (Yuan, Jing 2010). In the case of chronic HF eNOS has been shown to be deactivated by phosphorylation and nNOS becomes the prevalent NOS to generate β_3ARs dependent effects (Niu et al. 2012). It has yet to be determined if this switch and nNOS consecutive translocation to the sarcolemma is detrimental to or protective against HF progression. Presumably it might lead to LTCC blockage and a rise in free O_2^- radicals by nNOS dependent NO no longer inhibiting an oxidoreductase situated at RyR2. O_2^- radicals can lead to irreversible RyR2 activation which in turn would lead to uncontrolled Ca^{2+} leakage from the SR and a reduction in cardiac contractility (Kulandavelu, Hare 2012). Various studies attest β_3ARs beneficial effects though and β_3ARs have been shown to protect against pressure overload (Niu et al. 2012) or neurohormone induced hypertrophy (Belge et al. 2014). β_3ARs also appear to alleviate infarct size and risk of apoptosis and fibrosis of the myocardium during ischemic reperfusion experiments and MI in mouse (Aragon et al. 2011; Niu et al. 2014). Therefore the β_3AR may not be of high relevance at physiological, resting function but could play a crucial role under HF conditions, where an increased amount of Gi α-subunits and βARKs (= G-protein coupled receptor kinase, GRK2) has become evident (El-Armouche et al. 2008). In advanced aging (Birenbaum et al. 2008) or

in HF (Kulandavelu, Hare 2012) an upregulation of β_3ARs together with an upregulation of nNOS and iNOS expression and increased catecholamine plasma levels have been observed while β_1ARs are downregulated (El-Armouche et al. 2003). In the context of aging β_3AR's purely beneficial effects are once more called into question as β_3AR dependent nNOS and iNOS signalling worsens ischemia related myocardial dysfunction in older rats and actually leads to increased infarction size (Zaugg 2008). Another intriguing finding made in β_3AR knockout mice was that β_3AR deletion lead to improved SERCA2a function by increasing its expression and simultaneously increasing PLB phosphorylation (Ziskoven et al. 2007). The exact plasma-membrane location of functional β_3AR in adult ventricular cardiomyocytes is not yet conclusively determined but putatively appears to be the T-tubules or caveolae according to a study that performed myocyte-specific overexpression of the human β_3AR in mouse. Fractionation and western blotting detected colocalisation of the artificially expressed β_3AR with eNOS, nNOS and Cav3 (Belge et al. 2014). The observations regarding β_3AR which are detailed in this thesis were made in adult rat cardiomyocytes after 16 weeks of chronic MI and in age matched control cardiomyocytes.

1.8.14. The interplay of cAMP and cGMP signalling pathways in cardiomyocytes

In cardiomyocytes cAMP and cGMP are able to regulate physiological processes such as cardiac rate and contractility (Beavo and Brunton 2002). In the last few decades evidence has accumulated suggesting that cAMP and cGMP are not distributed homogenously throughout the cytoplasm of myocardial cells (Buxton and Brunton 1983) and that the two signalling pathways are strongly linked to each other via feedback signalling. The interplay of the cAMP and cGMP signalling pathways in cardiomyocytes depends primarily on the compartmentalisation of the secondary messenger molecules by its original site of production, the activity and specificity of PDEs (Stangherlin et al, 2011) as well as the respective secondary messenger concentration (Zaccolo and Movsesian 2007). Hence the compartmentalisation of the second messenger molecules allows for a concentration-dependent processing of multiple stimuli to elicit specific and highly regulated cell reactions (Fischmeister et al. 2006).

1.8.15. Cardiac PDEs

PDEs are a family of hydrolases which catalyse the hydrolysis of the cyclic phosphate bond from the cyclic nucleotides cAMP and cGMP. Hence both cAMP and cGMP are degraded and therefore regulated by PDEs. Out of the 11 mammalian PDE families known today (Conti and Beavo 2007) there are 7 with relevant activity inside cardiomyocytes: PDE1 (Vandeput et al.

2007), PDE2 (Mongillo et al. 2006), PDE3 (Ahmad et al. 2015), PDE4 (Richter et al. 2011), PDE5 (Lee et al. 2010), PDE8 (Gamanuma et al. 2003) and PDE9 (Lee et al. 2015) (see figure 5). These PDEs exhibit different specificity for cAMP or cGMP and are distributed distinctively at various intracellular locations. While some of these PDEs are selective for either cAMP (PDEs 4, 7 and 8) or cGMP (PDEs 5 and 9) others can bind and degrade both cyclic nucleotides (PDEs 1, 2 and 3) (Stangherlin and Zaccolo 2012). In cardiac myocytes the predominant locations of various isoforms are as follows: PDE1 is mainly reported to be cytosolic (Bender and Beavo 2006), PDE2 is associated to the cardiomyocyte sarcolemma together with the LTCCs, PDE3A with PLB and hence the SR, PDE4A1 with the Golgi apparatus, PDE4D5 with the β_2ARs after arrestin binding, PDE4D3 with the RyRs and the nuclei, PDE 5 along the Z-discs together with PKG and with sGCs (Fischmeister et al. 2006; Kass 2012), PDE8 is primarily cytosolic and PDE9 both cytosolic and nuclear (Bender and Beavo 2006). The PDEs themselves are highly regulated via multiple factors like their phosphorylation, their subcellular location due to the presence or absence of specific anchoring proteins and their interaction with regulatory proteins. It is their N terminal and their catalytic units which convey the characteristics of the specific PDE family. The catalytic domain of PDEs consists of 16 alpha helices, which generate a binding pocket for substrates and inhibitors (Conti and Beavo 2007). In some cases the activity of the catalytic domain of PDEs is controlled via the inhibiting or activating binding of the cyclic nucleotides themselves or other proteins to respective N-terminal binding domains. These binding domains include the Ca^{2+}/Calmodulin binding domains present on PDE1 or the cGMP binding domains GAF-A and GAF-B present on PDE2 and PDE5 (Zaccolo and Movsesian 2007; Francis et al. 2011), named after cGMP-activated PDEs, AC and the Fh1A enzymes in which they were first discovered (Conti and Beavo 2007). As a result the cAMP and cGMP signalling pathways interact at multiple points via PDE regulation and can modulate each other by means of their localisation, concentration and the activity of their downstream signalling targets (Stangherlin and Zaccolo 2012). This is clearly demonstrated by cGMP binding to the GAF-A domain of PDE2, which primes the PDE for cAMP degradation (Martinez et al. 2002). Another example for cyclic nucleotide signalling pathway interaction via the PDEs is PDE3. Though PDE3 possesses comparable affinity for both second messengers it degrades cGMP at a slower pace and hence allows for it to temporally block the PDE while cAMP levels increase (Shakur et al. 2001).

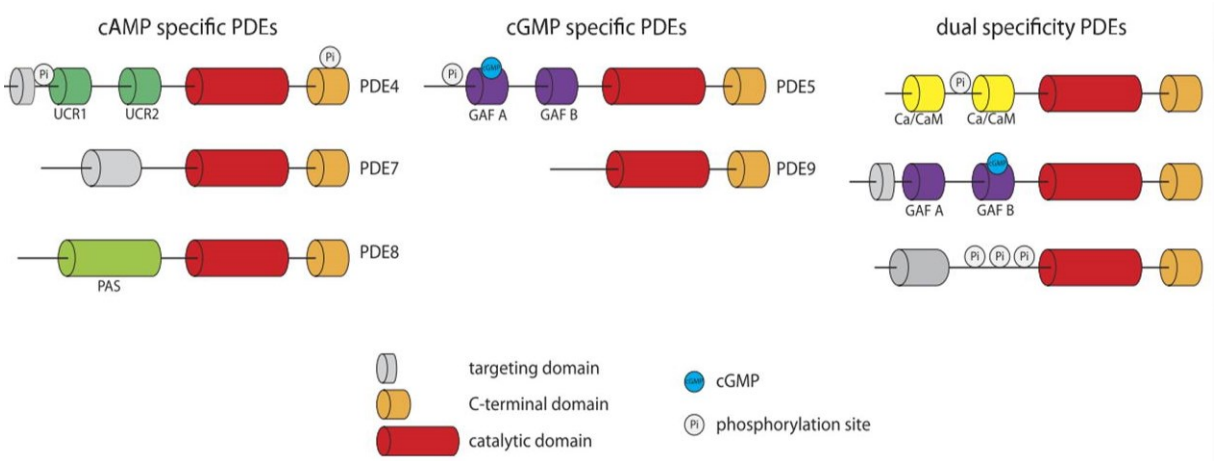

Figure 5 Schematic of cardiovascular PDEs directly taken from (Stangherlin and Zaccolo 2012) to illustrate variable binding and regulating domains and second messenger specificity.

1.8.16. Species differences in cardiac PDEs

Unfortunately the presence and function of PDEs underlies strong species differences and findings in animal models cannot be translated directly to humans (Johnson et al. 2012). For the aim of the present introduction it is important in particular to distinguish between rat and human cardiomyocytes. One example for the differences between species is the presence of the PDE1 variants 1A,1B and 1C which are present in human hearts but appear to be only at very low levels expressed in rats where the PDE1C isoform has a particular activity, namely, it only hydrolyses cGMP but not cAMP (Miller et al. 2009). Similarly, PDE3 isoforms are highly expressed in humans but only marginally present in rat. Still, while PDE3 exhibits higher expression in human than in rat it shows higher cGMP-degrading activity in rat than in humans (Johnson et al. 2012). Another well-studied example is PDE4, which is the predominant degrader of global, catecholamine induced cAMP responses in rodents (Verde et al. 1999), but despite its highly conserved function and expression is less important in humans where PDE1, PDE2 and PDE3 are also highly active (Richter et al. 2011). Under HF conditions PDE4 expression and activity has been shown to be downregulated in both humans and rodents (Richter et al. 2011).

1.9. Mathematical modelling

Though the advancement of microscopic techniques and quantitative, biological methods at the nanoscale level has been vast in the last decades, there are spatiotemporal processes that we are not yet able to resolve. Additionally, progress in microscopy techniques leads to the acquisition of ever larger amounts of data, which cannot be analysed manually (Schindelin

et al. 2012). Hence the introduction of mathematical modelling approaches is required, which combine quantitative and qualitative data in a manner that allows one to predict or test a mechanism for a biological phenomenon, meaning that data can be fitted to the model and trends or phenomena predicted. Mathematical models are generally either strongly specified and highly simplified to solve very specific problems or can be multi-scale to elucidate physiological processes and pathophysiological occurences both at the macroscopical and the microscopical level in the heart (Pullan et al. 2005; Land et al. 2013). Mathematical modelling starts with the identification of a problem and the generation of a hypothesis followed by the development of a mathematical model to test the hypothesis and solving it. The next step is to interpret the solution, and to ascertain whether or not it validates the original hypothesis based on the biological data. If the available data and the model are in agreement then the mathematical model can be used for additional predictions (Pullan et al. 2005).

1.9.1. Investigating the TAT system via modelling

The microscopical structure of the TAT network and its variablity in cardiomyocytes throughout the heart or under disease conditions prompts many questions in regard to its function which are hard to answer sufficiently well via experimental approaches alone. It is known that many proteins seem to specifically home to the T-tubules to form signalosomes in specific subcellular compartments (Scriven et al. 2000) and that the TAT network acts as a reservoir which can maintain a certain level of ionic concentrations (Pasek et al. 2012). But how many proteins and ions are actually situated inside the TAT network in health and disease is unclear (Pasek et al. 2008). It is furthermore well established that the TAT network is an important part of the excitation contraction coupling machinery in ventricular cardiomyocytes and that the network together with efficient excitation contraction coupling is impaired in HF (Sacconi et al. 2012). However it is not completely clear which alterations take place to disrupt both the structure and their associated function. There are so many possible reasons and disruptive alterations that could take place in the various cardiomyopathies that it is almost impossible to pinpoint those changes which are decisive to worsen the respective disease during experimentation (Polakova and Sobie 2013). Mathematical modelling has tried to address these questions in a more controllable way by integrating what is already known about the TAT network and its role in physiological processes, such as Ca^{2+} handling and βAR signalling (Hatano et al. 2012) or the general electrophysiology of cardiomocytes (O'Hara et al. 2011), and then focussing specifically on a subset of potential causes and effects. Our own group recently used advanced mathematical modelling based on a compartmental model of βARs and their electrophysiological effects in cardiomyocytes (Heijman et al. 2011) to better understand the effect of T-tubular loss and disruption of Cav3 dependent signalling domains

on β_2AR-mediated cAMP signaling. We thereby established that Cav3 is important for β_2AR localisation and β_2AR related cAMP signalling levels and that β_2AR signalling complexes inside T-tubules are more prone to be disrupted than β_2AR signalling complexes which are associated to caveolae (Wright et al. 2014).

1.9.2. Modelling to validate experimental methods

Despite explaining biological data that is too intricate and manifold to be easily interpreted mathematical modelling can also help to validate the technical approaches used to obtain biological data. The study presented in this thesis uses a relatively novel scanning technique, namely SICM in hopping mode (Novak et al. 2009) to apply molecules onto the surface of cardiomyocytes via a nanopipette. In the past this relatively slow, but precise, application occurred via pressure unloading of the respective molecules (Nikolaev et al. 2010). However this pressure-driven application is relatively slow and occasionally leads to the unwelcome blockage of the respective pipette in use. Therefore the application mode has been changed to a more reliable, voltage-driven substance unloading from the SICM nanopipette. Though this technical improvement is advantageous, because of its easier and more reliable use it still needed to be validated in regard to the amount and precision of agonist which is applied under differential system settings. The application of a fluorescent marker, though possible, would not yield the correct answer for the application of particles which possess a slight electrical charge like the agonist (ISO) used in this thesis. Hence, the precision of this advanced voltage-driven application mode as well as the averaged concentration of the applied agonist needed to be simulated and determined via mathematical, finite element modelling.

1.10. Aims of the study

The preceding paragraphs tried to show what is already known about the ventricular cardiomyocyte structure and βAR signalling in healthy control conditions and at the end stage of HF. There are studies which have looked at structural alterations during the progression from hypertrophy to decompensated HF in animal models with LAD aorta ligation (Wei et al. 2010; Wagner et al. 2012). However these studies did not look specifically at the effect of these progressive structural alterations on the βAR dependent second messenger signalling alterations. Our own group showed that the β_2ARs might be the βAR subtype which is most important in causing the phenotype of end stage HF by leaving their T-tubular position at some point during HF progression (Nikolaev et al. 2010). But when and why exactly this relocation takes place has not yet been described in a time dependent manner. The β_3AR subtype has

only recently been shown to be present in both human and rat cardiomyocytes (Zaugg et al. 2008; Niu et al. 2012) but its cardiac function and importance in health and disease are still very controversial and a lot of research is still necessary to elucidate it (Kulavandelu et al. 2012). In order to thoroughly study alterations in cardiomyocyte structure and βAR dependent cyclic nucleotide signalling in health and disease, techniques like the SICM microscope, which are available to our group are necessary and their improvement is of high importance. In the past we used pressure-induced displacement of agonists inside the SICM nanopipette onto the cardiomyocyte surface (Nikolaev et al. 2010), but have now changed to voltage-driven application of agonists. This change required us to find out how much and how precise the consecutive application of agonists proceeds out of the SICM nanopipette onto the 3 dimensional structure of cardiomyocytes.

The main objectives of this thesis are therefore as follows:

- Investigate surface and internal TAT network structures in single, left ventricular cardiomyocytes in health and during the progression of HF in an adult rat model of chronic MI. Investigate the aforementioned structures in human ventricular cells obtained from various cardiomyopathies and compare them between the two species.
- Investigate β_2AR dependent cAMP signalling using FRET in health and during the progression of HF.
- Detect if there is functional β_3AR dependent cGMP signalling in adult rat cardiomyocytes in health and HF and study disease dependent alterations.
- Generate a mathematical model to investigate the precision and concentration of agonist unloading onto the cardiomyocyte surface using voltage-driven nanopipette application.

Chapter 2: General Material and Methods

2.1. Materials

Most of the reagents used for this project were obtained from the company (Sigma-Aldrich Company Ltd.Dorset, England) unless otherwise specified or listed in the table below.

Table 2 List of reagents, which were not purchased from Sigma Aldrich

Reagent	Company / Collaborator	Catalogue #
Atrial Natiuretic Peptide (ANP)	Bachem, Germany	# H-2100
β_3AR-GFP	Prof. Nikolaev, Germany	-
Bovine Serum Albumin (BSA)	Fisher Scientific, UK	# BPE9704
8-Br-2´-*O*-Me-cAMP	Biolog Life Science, UK	# B022
CGP 20712	Tocris, UK	# 1024
Cilostamide	Tocris, UK	# 0915
Di-8-amino-naphthyl-ethenyl-pyridinium	Biotium, UK	# 61012
Dulbecco Modified Eagle Medium	Fisher Scientific, UK	# 10567
Fetal Bovine Serum (FBS)	Fisher Scientific, UK	# 10270
Cytosolic Epac2-camps	Prof. Nikolaev, Germany	-
Goat Serum	Fisher Scientific, UK	# 31872
Luminata Forte Western HRP substrate	Millipore, UK	#WBLUF0100
M199 Medium	Invitrogen, UK	#11150
$MgCl_2$	G-Biosciences, USA	# R004
NaCl	Fisher Scientific, UK	# S/3160/63
1H-[1,2,4]oxadiazolo-[4,3-a]quinoxalin-1-one	Abcam, UK	# 120022
Partly frosted coverslides	Thermo Scientific, UK	# 6776108
Plasma-membrane Epac2-camps	Prof. Nikolaev, Germany	-
Polyclonal donkey anti-goat HRP antibody	Abcam, UK	# 97110
SR 59230A hydrochloride	Tocris, UK	# 1511
Tadalafil	Santa Cruz, USA	# sc-208412
Vectashield Mounting Medium	Vector Labs, UK	# H-1200

2.2. Animals and HF model

2.2.1. Animals and animal care

Sprague Dawley rats for research use were obtained from Harlan Laboratories (Wyton, UK). All animals, which were bred and used for the work described hereafter were treated and cared for upholding the standards stated in the Guide for the Care and Use of Laboratory

Animals (NIH publication No. 85–23, revised 1996) as well as the Animals in Scientific Procedures Act of 1986 (ASPA 1986, UK) and its amendments (ASPA1986 Amendments Regulations 2012) including the EU directive *2010/63/EU*. The animals were exposed to a standard 12-hour light-dark cycle at 21°C and obtained standard food at self-regulated periods by the animal facility staff members.

2.2.2. HF model generation

For the study of single cardiomyocytes during their progression towards HF a model of chronic MI in adult Sprague-Dawley rats was generated. This was done via the ligation of the left anterior, descending coronary artery by Dr. Markus Sikkel (Imperial College London) and Mr Adam Mills (Imperial College London) as described previously (Lyon et al. 2009). In short the procedure is as follows: The animal is anaesthetised and has been given antibiotics as well as buprenorphine for pain relief, before both the chest and the pericardium are opened surgically and a suture is bound around the left anterior descending (LAD) artery and tightened to constrict the blood flow. In sham control animals the suture is bound only loosely around the artery so no constriction of the blood flow occurs. After the ligation the animal is closed up again and the *in vivo* ejection fraction volume is determined in sham and age matched control animals as well as at 4, 8 and 16 weeks post the surgical procedure via echocardiography recordings generated in M-mode (Vevo 770 Micro-Imaging System, Visualsonics) to obtain an indicator of wall contractile function (see Figure 6). Subsequently the animals are sacrificed and the ratio of the heart weight to the length of the tibia is determined as a marker of heart hypertrophy. The echocardiography and phenotype measurements were performed by Dr. Markus Sikkel (Imperial College London). In accordance to prior published work and the information gathered in this thesis the chronic MI model undergoes 3 different stages during the progression of HF: a compensated, a decompensated and a failing stage (Monnet and Chachques 2005; Lyon et al. 2009; Nikolaev et al. 2010). For more information about this model please refer to (Lyon et al. 2009).

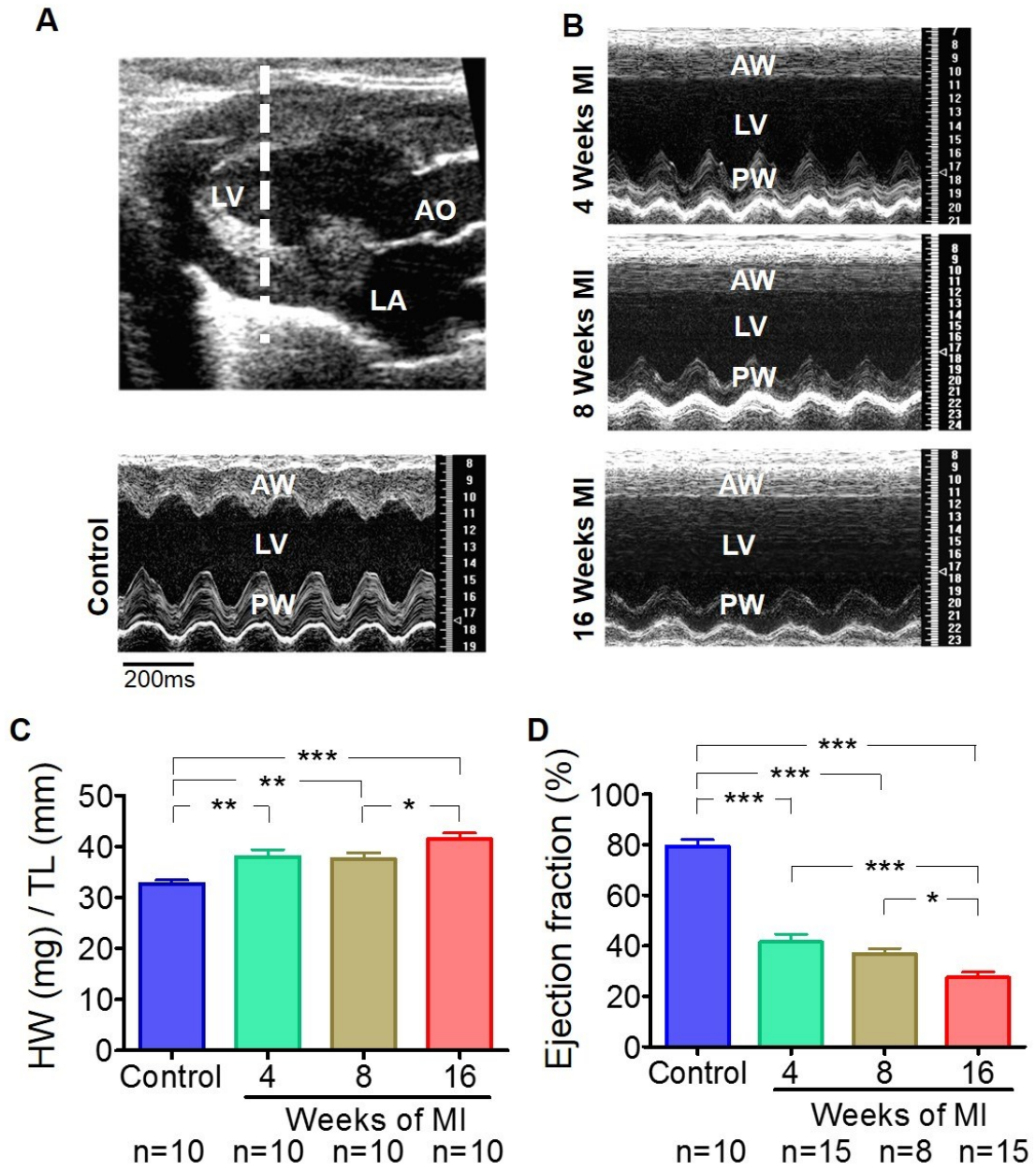

Figure 6 Progressive increase in the rat heart size is accompanied by progressive decrease in contractile function, at different time-points post-MI in comparison to sham-operated control. (A) Echocardiography data; Top panel: Echocardiography image indicating the plane (white punctuated line) in the left ventricle (LV) from which echocardiography data represented in the bottom panel was collected, over time. LA marks the location of the left atrium and AO marks the aorta. Bottom panel: echocardiography data showing the anterior wall (AW) and the posterior wall (PW) function of the left ventricle. (B) Echocardiography data at different time points after MI; (C) Heart weight corrected to tibia length (n=10, p<0.01); (D) Ejection fraction (n>8, p<0.01).

2.3. Cell isolation

2.3.1. Adult rat cardiomyocyte isolation

Adult rat cardiomyocytes isolation: Cells were isolated from the atria and the left ventricle of the aforementioned model of chronic MI by Mr. Peter O'Gara via enzymatic digestion as described previously (Gorelik et al. 2006). For this the rats were anaesthetised and heparinized to stop blood coagulation before being sacrificed by cervical dislocation. Then the chest and the pericardium were opened up to excise the heart and put it into ice cold oxygenated Krebs solution (pH 7.4) containing $MgSO_4$(0.94 mM), KCl (4.7 mM), NaCl (119 mM), $NaHCO_3$ (25mM), Glucose (11.5 mM), KH_2PO_4 (1.2 mM) and CaCl (1mM). The heart was then Langendorff perfused for 5 min using the same Krebs solution, before switching to oxygenated low Ca^{2+} solution (pH 6.95) containing Ca^{2+} (12mM), $MgSO_4$ (5mM), KCl (5.4mM), NaCl (120mM), Glucose (20mM), 4-(2-hydroxyethyl)-1-piperazineethanesulfonic acid (HEPES, 10mM), nitrilotriacetic acid (NTA, 5mM), taurine (20mM) and pyruvate (5mM). After this the heart was perfused for 10 min with a slightly modified low Ca^{2+}/ enzyme solution (pH 6.95) by not adding any NTA (=chelating agent) to the aforementioned list of ingredients but an additional amount of Ca^{2+} (200µM) and the enzymes collagenase (1mg/ml) and hyaluronidase (0.6mg/ml). Now the left ventricle and the atria were separated from the rest of the heart and chopped into bits with scissors before being shaken in oxygenated enzyme solution at 37°C for 5 min. The digested tissue was then filtered through a piece of gauze before repeating the enzyme digest for a further 5 min and filtering through another piece of gauze. The resulting digested tissue solution was spun down at 700 rpm and while the supernatant was discarded the cardiomyocyte pellet was resuspended in buffer without the enzymes. For further investigation a part of the resuspended cells was shock frozen in liquid nitrogen and stored at -80°C.

2.3.2. Human cardiomyocyte isolation

Permission to obtain human heart tissue samples was received from the respective patient and patient anonymity was secured by holding up the criteria of the human tissue act (*Human Tissue Act* 2004, UK). Human ventricular cardiomyocytes were isolated by Dr. Peter Wright and Dr. Jose Sanchez Alonso-Mardones. Human cardiomyocytes were obtained either from mitral valve (MV) surgery from patients with sinus atrial fibrillation or from bypass surgery as well as from dilated (DCM) and ischemic cardiomyopathy (ICM) heart transplant patients (see table 3) with and without LVADs. For reasons of patient anonymity identification data is not available to this thesis but to the respective departmental authority at Imperial College London

(in this case the Royal Brompton database for heart transplants and Dr. Prakesh Punjabi for MV operations). Before the tissue arrived 40ml of low Ca^{2+} solution (pH 6.95) (Ca^{2+} (12mM), $MgSO_4$ (5mM), KCl (5.4mM), NaCl (120mM), Glucose (20mM), 4-(2-hydroxyethyl)-1-piperazineethanesulfonic acid (HEPES, 10mM), nitrilotriacetic acid (NTA, 5mM), taurine (20mM) and pyruvate (5mM)), 10ml of protease solution (0.36mg/ml protease in 100ml Millipore H_2O with 7.5µl of 1M $CaCl_2$) and 20 ml of collagenase solution (1mg/ml collagenase in 100ml Millipore H_2O with 7.5µl of 1M $CaCl_2$) were oxygenated and warmed up to 37°C. Upon its arrival the human tissue was removed from cardioplegia solution and pieces of around 500mg of muscle tissue, which still appeared intact, were separated from adherent fat and connective tissue. Then the tissue was quickly (in under 5min) chopped into smaller pieces and transferred into 10ml of oxygenating low Ca^{2+} solution for 3 min. Afterwards the solution was filtered through gauze retaining the sample and the sample was put into a further 10ml of low Ca^{2+}. This washing step was repeated a further 2 times, before the cleaned sample was transferred into 10ml of protease solution and shaken at 37°C for 30 min. Subsequently the digested sample was filtered through a piece of gauze. Then the solution containing the cardiomyocytes was put into 10 ml of collagenase and shaken for a further 45 min at 37°C before being filtered through a piece of gauze again. Finally the filtrate was spun down at 700 rpm and the supernatant containing human fibroblasts was separated from the pellet containing the cardiomyocytes. The cardiomyocyte pellet was then resuspended in enzyme buffer solution without enzyme for further experimental processing.

Table 3 Details of human cardiomyocyte donors: gender, age and type of cardiomyopathy

Donation Date	Gender	Age	Type of cardiomyopathy
29042014	Female	42	DCM+LVAD, left ventricle
11062014	Male	49	DCM+LVAD, left ventricle
09092014	Male	63	DCM, left ventricle
23092013	Female	26	DCM, left ventricle
24092013	Male	33	DCM, left ventricle
26092013	Male	48	ICM, left ventricle
09062014	Male	58	ICM, left ventricle
12092014	Male	51	ICM, left ventricle
24042014	Female	70	MV
09012014	Female	78	MV
13012014	Male	69	MV

20062014	Female	43	MV

2.4. Cell culture and medium/buffer preparation

2.4.1. HEK293 cell culture

Though most work described here was performed in cardiomyocytes, some work also required the culture of Human Embryonic Kidney 293 (HEK 293) cells. These cells were cultured in Dulbecco's Modified Eagle Medium (DMEM) at 37°C and 5% CO2. The medium was made up of 500ml DMEM with 4.5 mg/ml glucose, FBS 50 mg/ml, 50mg L-glutamine/ml and 10,000 IU Penicillin/mL plus 10,000 µg Streptomycin/mL.

2.4.2. Cardiomyocyte culture

After their isolation both adult rat and human cardiomyocytes were plated onto laminin-coated glass bottom dishes (MatTeK Corporation, Ashland, USA) or laminin-coated glass coverslips (Thermo Scientific, VWR International, # 12392108). All rat cells were immediately incubated at 37°C and 5% CO_2 in modified M199 culture medium and underwent differential treatment after at least 1h to properly attach to the culture dish. Modified M199 culture medium was made up from 500ml M199 medium supplemented with creatine 5mM, taurine 5mM, carnitine 5mM, 1g bovine serum albumin, ascorbate 100mM and penicillin/streptomycin 100mM. Human cells however were first incubated for 1h in recovery medium (M199 with additional fetal bovine serum 10ml/L) before this was also changed to modified M199 medium. The cells were then either designated for immediate investigation or for transduction with adenovirus FRET biosensors for 48h.

2.4.3. Physiological buffer for experimentation

For SICM/FRET imaging and Di-8-ANEPPS staining procedures of live cells physiological solution (pH7.4) was made up from ddH_2O containing NaCl 144 mM, KCl 5mM, HEPES 10mM and $MgCl_2$ 1 mM.

2.4.4. Experimentation temperature and solutions

If not stated otherwise all experiments were performed at room temperature (~22^{o}C) and all solutions were made up with purified Milli-Q water (EMD Millipore, Massachusetts, USA).

2.5. Structural investigation of cardiomyocytes

For the visualisation and structural investigation of single, isolated cardiomyocytes two main techniques were used. The first of which is SICM and the second of which is confocal microscopy.

2.5.1. Scanning Ion Conductance Microscopy

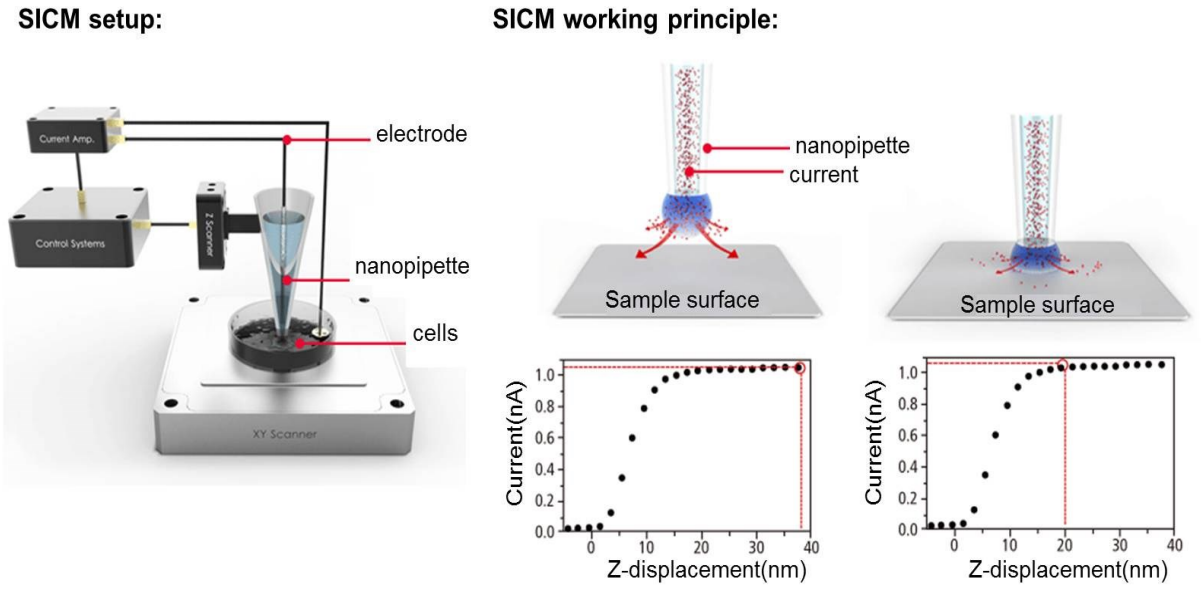

Figure 7 The setup and working principle of SICM. A nanoscale pipette serves as scanning probe to elucidate sample surface structures. A piezo-electrical stage allows for the alignment of the pipette in the x,y and z direction. Two electrodes in the system measure the ionic current that passes through the pipette opening. The pipette remains at a constant distance to the sample surface as determined by the ion current (nA), which is able to pass unrestricted through the pipette opening. Picture taken from: http://www.parkafm.com/index.php/park-afm-technology/park-sicm Copyright © 2015 Atomic Force Microscopy, Park Systems

SICM is a non-invasive, nano-scale resolution scanning modality which was invented by Hansma et al. in 1989. SICM used to be restricted to the scanning of relatively smooth surfaces for risk of colliding with vertical, protruding structures on various cell types. Hopping probe SICM a recent advancement in the field overcame this restriction and enabled the visualization of even highly convoluted, nano-scale cell surface structures (Novak et al. 2009). Hence SICM in hopping mode can be used to visualize the highly structured surfaces of live cardiomyocytes in solution by detecting the inwards and outwards current of ions passing through the opening of a nanopipette which serves as scanning probe. Briefly the scanning process of a cell's surface i.e. a cardiomyocyte with SICM is performed by pulling a borosilicate glass capillary

(IntraCel, BF100-50-7.5) in a laser puller (IntraCel, Sutter Instrument Co, P-2000) to generate a nanopipette with the necessary tip size (with 80-100MΩ resistance) to resolve nano-scale structures like the T-tubule openings and crests on the cardiomyocyte surface. This nanopipette is then outfitted with an electrode and filled with electrolyte solution before being clamped into a pipette holder. The pipette holder can move up and down (in z direction) to lower the nanopipette directly above the sample cells. The sample dish sits on top of a piezoelectric stage, which can move the cells laterally in the x and y direction and is outfitted with a grounding electrode reaching into the physiological buffer with the sample cells. Both the electrode in the nanopipette and the electrode in the culture dish are connected to a feedback system. This system registers the flow of ions between the two electrodes and translates the electrical signal back into computer generated surface scans using the software IonView (IonScope, UK) while keeping the nanopipette at the exact same distance to the respective cell surface throughout all times. While the nanopipette moves along the cell body it is also continuously moved up and down in a "hopping" motion via a piezo-actuator stage to prevent it from colliding with taller cell surface structures (Novak et al. 2009). After obtaining cell surface scans the scanning nanopipette can also apply agonists or antagonists to particular structures on the sample cell surface, given they were added into the pipette solution beforehand, by unloading part of its content. This unloading can either be achieved via pressure application (Nikolaev et al. 2010) or by reversal of the electric polarity of the two electrodes in the system given the respective agonist possesses a net charge in solution. The pressure application was used for the β_2AR localization study, while the polarity reversal method was used for the β_3AR localization studies described in this thesis.

2.5.2. Di-8-ANEPPS staining of the TAT system of adult rat cardiomyocytes

To prepare Di-8-ANEPPS 1.5 ml of DMSO were mixed with 0.5g of pluronic acid and then heated until the pluronic acid had dissolved. Then 630 microlitre of the warm concoction were mixed with 5mg of the Di-8-ANEPPS in powder form and 10 microliter each were aliquoted into Eppendorfs and stored at -20°C until used. For usage to stain cells one of the aliquots was dissolved in 1 ml of FRET solution or any other suitable physiological buffer (i.e. PBS) and put into a sonicator water bath (Fisher Scientific, model FB15047) at 55 degree Celsius under "sweeping" sonication mode for around 5 min. Adult rat cardiomyocytes were then stained with the lipophilic fluorescent dye for 1 min as described before (Lyon et al. 2009) and a Z-stack of optical images at every 0.49 microns was obtained using an inverted confocal microscope (Zeiss LSM-780). Images were processed with the freeware program Fiji (Schindelin et al. 2011) and a custom-made Matlab (The MathWorks, Inc., Natick, MA, USA)

code to assess T-tubule regularity and TAT network density. Longitudinal elements of the TAT network were quantified semi-automatically with a separate custom-made Matlab code which was provided by Mr. Aron Monzspart (University College London) according to my specifications. These specifications included, but were not limited to the following requirements: 1. that the pixel intensity and therefore the position of the stained TAT structures should be taken into account with a suitable threshold, 2. that the axial elements were oriented and hence only picked up as "axial" by the software code if the were not oriented in the direction of the transverse tubules of the TAT system and 3. that imaged structures with a pixel count which equalled more than 1 µm would not be picked up as valid axial tubules.

2.6. Immunocytochemical staining of single cardiomyocytes:

Immunocytochemical staining versus the structural, junctional protein JPH2, the caveolar protein Cav3, the cytoskeletal protein β-tubulin, the sGC molecule was performed as follows:

After cardiomyocyte isolation cells were plated at an approximate number of 5000 into the middle of laminine coated 22mm borosilicate glass coverslips (Thermo Scientific, VWR International, # 12392108). The cells were quickly rinsed with PBS and then fixed for 15 min at room temperature with 40µl PFA/ml diluted in PBS. Then they were washed three times with PBS for 5 min before the application of blocking buffer (50µl donkey serum/ml, 3µl Triton X-100/ml diluted in PBS for JPH2 and β-tubulin and 50µl goat serum/ml, 3 µl Triton X-100/ml diluted in PBS for Cav3 and sGC) for 1h at room temperature. Afterwards the blocking solution was aspirated and without washing the cells the primary antibody was applied (diluted in PBS, 3µl Triton X-100/ml) over night at 4°C. On the following day the samples were washed three times with PBS for 5 min each. Then the secondary antibody was applied (diluted in PBS, 3µl Triton X-100/ml) for 2 hours at room temperature and in the dark. As negative control cells were stained following the same protocol but with the application of the secondary antibody only. After the antibody incubation the coverslips containing the cells were mounted using mounting medium (Vector Labs, Vectashield mounting medium) onto partly frosted coverslides (Thermo Scientific, Shandon™ # 6776108). Finally the coverslips were sealed onto the coverslides with transparent nail polish to make them suitable for long time storage at 4°C and were then ready for imaging.

Table 4 Antibodies for immunocytochemical staining of adult cardiomyocytes

Primary Antibody + concentration	Species	Company and Catalogue #	Secondary Antibody (concentration)
JPH-2 (Y-15) 1:400	polyclonal goat	Santa Cruz # sc-51313	Alexa Fluor 488, Invitrogen, 1:1000
Cav3 1:200	monoclonal mouse	Sigma Aldrich	Alexa Fluor 594, Invitrogen, 1:1000
sGC 1:200	Polyclonal rabbit	Provided by Prof. Nikolaev, Universitätsklinikum Hamburg, Germany	Alexa Fluor 594, Invitrogen, 1:1000
ß-Tubulin 1:100	polyclonal goat	Sigma Aldrich # t5201	Alexa Fluor 546, Abcam, 1:1000

2.7. Confocal imaging of the cardiomyocyte structure or of structural and functional cardiomyocyte proteins

For imaging of the TAT system after Di-8-ANEPPs staining and immunocytochemical staining molecules the Facility for Imaging by Light Microscopy (FILM) of Imperial College London provided the usage of a Zeiss LSM780 Laser Scanning Confocal Microscope (Carl Zeiss, Germany) equipped with a x63 magnification Zeiss DIC Plan-Apochromat oil-immersion objective (numerical aperture 1.4; Carl Zeiss, Germany). An Argon laser was used for specific excitation of the respective fluorophores. Z-stack images were recorded at a distance of 0.4 µm using the microscope associated software ZEN 2011 (Carl Zeiss, Germany). Image processing was however performed with the freeware Fiji (Schindelin et al. 2011).

2.8. Functional investigation of cardiomyocytes

2.8.1. FRET imaging

FRET imaging is a technique based on the naturally occurring, physical phenomenon of partial, non-radiative energy transfer from one excited fluorophore at a higher energy state to another fluorophore at a lower energy state. For this phenomenon to occur the emission spectrum of the donor has to overlap with the excitation spectrum of the acceptor fluorophore. Also the two fluorophores have to be in close enough proximity (usually <10nm) as determined via the sixth power of the Förster radius R_0 (R_0=the distance at which 50% energy transfer takes place between the donor and acceptor fluorophore). Lastly the dipole moment of the fluorophores has to be aligned (Arai, Nagai 2013). To measure FRET in a scientific

environment the usual FRET imaging system consists of a microscope with an excitation light source to elicit fluorescence, a beam splitter to separate and lead the emission light into two separate detection channels, a shutter to restrict the amount and time the fluorophores are excited (as this can lead to their destruction and photo bleaching) as well as a high speed camera to record the signal from the donor and acceptor fluorophores in the two channels simultaneously. The setup used for the experiments described in this thesis was as follows: Our inverted Nikon TE2000 microscope had a 30WDia halogen lamp light source with a 436/20nm excitation filter and a DM455 dichroic mirror. For the work in this thesis the cAMP biosensor Epac2-camps, based on the cyan and yellow fluorescent proteins and the cGMP biosensor Red cGES-DE5 based on a green (GFP) and red fluorescent protein (RFP) were expressed in cardiomoycytes. To record the respective biosensor FRET signals our system used an ORCA-ER CCD camera (Hamamatsu Photonics, Welwyn Garden City, UK). For splitting fluorescent emission our system had a Dual View (Optical Insights) beam splitter with two exchangeable filter cubes: the first cube consisted of BP535/40 and BP480/30 emission filters for cyan (CFP) and yellow (YFP) light detection during cAMP studies and the second cube consisted of BP515/30 and BP590/40 emission filters for green (T-Sapphire) and red (Dimer2) light detection during cGMP studies. The software for recording FRET signals was the 1.4 version of the programme Micro-Manager (Vale Lab, University of California, San Francisco http://www.micro-manager.org/wiki/Micro-Manager; accessed January 2015) and FRET signals were continually recorded at every 5th second. Despite the beam splitter and the light filters a remnant of light from the different fluorophores seeped into the other detection channels. To correct for this “bleed through” the amount of bleed through was determined by Dr. Peter Wright (Imperial College London) after transfection of HEK293 cells with either CFP or T-Sapphire plasmid DNA by establishing the relative intensity of fluorescence in the YFP or the RFP channel respectively (data not shown).

When using FRET measurements to elucidate changes in cyclic nucleotide levels, without prior calibration of the FRET sensor, it is not possible to determine actual, absolute molecule levels but relative molecule levels only. Nor is it possible to detect the actual activity value of specific PDE in FRET experiments. To determine both cyclic nucleotide levels and overall PDE activity in absolute values it is necessary to disrupt the cell membrane and conduct quantitative second messenger and PDE activity assays. This however has the strong disadvantage of also disrupting the highly stringent compartmentation and signalling confinement present in cardiomyocytes. FRET experiments as the ones performed in this thesis do have the great advantage over other techniques of not requiring the disruption and homogenisation of cells. Therefore FRET experiments allow insightful conclusions on compartmentalised cyclic nucleotide levels and associated PDE activity.

2.8.2. SICM/FRET setup for localised detection of functional receptors

Our laboratory is in possession of a custom-made combination of a SICM/FRET microscope (see figure 8). This combination allows for the targeted stimulation and real-time response detection of cyclic nucleotide production after the stimulation of receptors on the surface features of the respective sample after their visualisation by SICM scanning and transduction with a FRET biosensor (Nikolaev et al. 2010). Here the SICM/FRET combination was used to detect functional βARs present at different sites on the cardiomyocyte surface and their second messenger response to catecholaminergic stimulation and PDE inhibition.

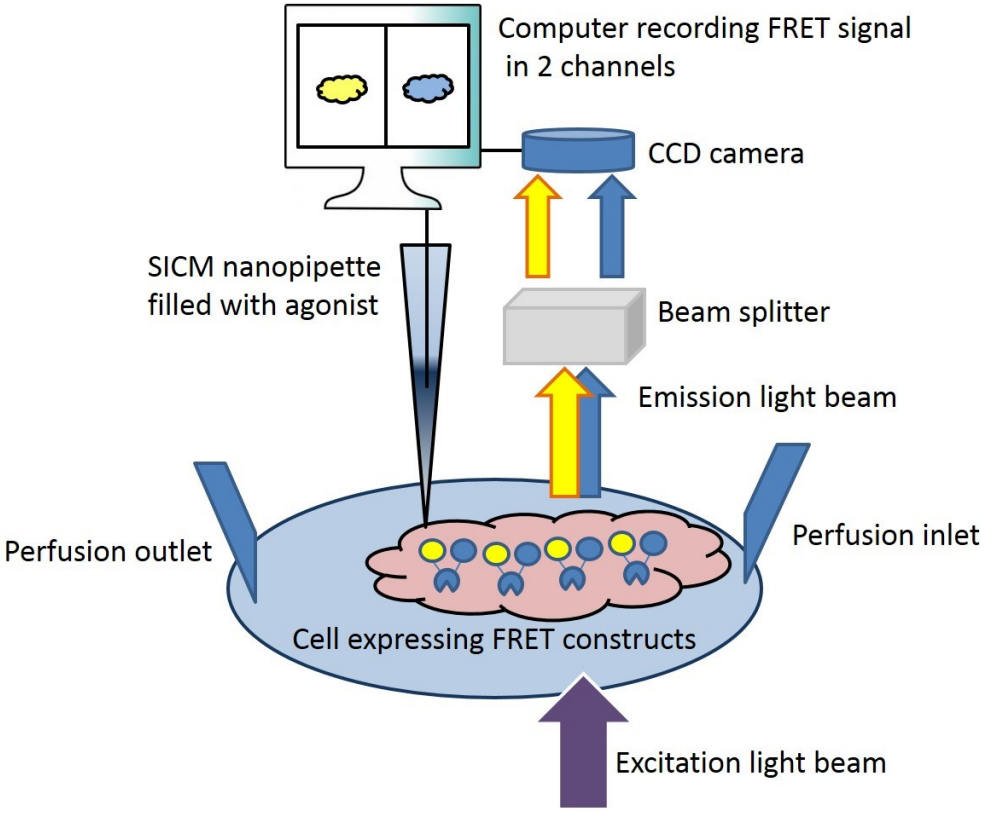

Figure 8 Schematic of the FRET and SICM combination microscopy system showing a cell expressing secondary messenger sensing FRET constructs, the process of fluorescent excitation and emission as well as recording of the respective FRET signal, the arrangement of the perfusion system and the SICM nanopipette.

2.8.3. Cell transduction with cAMP or cGMP FRET biosensors

Adenoviral transduction allows gene transfer into different cell types including human and rodent cardiomyocytes. After their isolation and attachment to a laminine coated dish (MatTeK corporation, Ashland, USA) cells were transduced with adenoviral vector encoding FRET constructs. Depending on the experiment these FRET constructs were either the cytosolic

cAMP biosensor Epac2-camps (Nikolaev et al. 2004), the plasma membrane bound Epac2-camps (Sprenger, Nikolaev 2013) or the cytosolic cGMP biosensor Red cGES-DE5 (Niino et al. 2009). In either case rat cardiomyocytes were transduced at a multiplicity of infection (MOI) of approximately 300-500 virus particles and incubated in M199 media, without media exchange for 48h at 37°C and at 5%CO_2.

Table 5 cAMP and cGMP FRET biosensors used for cardiomyocyte transduction (Sprenger, Nikolaev 2013)

FRET biosensor	half maximal effective concentration	FRET pair
Cytosolic Epac2-camps	cAMP EC_{50}= 0.9 µM	CFP/YFP
Plasma membrane bound Epac2-camps	cAMP EC_{50}= 0.9 µM	CFP/YFP
Cytosolic Red cGES-DE5	cGMP EC_{50}= 40 nM	T-Sapphire/RFP

2.9. Finite element modelling

Finite element modelling (FEM) is a term for one of the most widely used mathematical techniques to solve differential equations describing an engineering or biological problem through the use of a set of algorithms and mathematically stated boundary conditions. “Finite element” refers to the fact that the domain (which can have any number of dimensions) is subdivided into simpler “elements” and that the governing equations in weak form are solved on each one. In this thesis finite element modelling was used to describe the concentration distribution of the agonist ISO after its voltage-driven application onto the 3-dimensional structure of cardiomyocytes via the SICM nanopipette. The FEM was solved for different parameters using the software COMSOL Multiphysics® 4.4 (COMSOL AB, Stockholm, Sweden).

2.10. Statistical analysis

Significant statistical differences of data sets were analysed using OriginPro 8.6 (OriginLab Corporation) and GraphPad Prism 5 (GraphPad Software Inc., La Jolla, California). Normal data distribution was determined by Kolmogorov-Smirnov testing. If the data was normally distributed a two tailed T-test was used for the comparison of two independent groups. If the data had a skewed distribution a Mann-Whitney U test was used instead. If more than two groups were compared with each other a one-way ANOVA with Bonferroni correction testing

was applied. Data was considered significant at a p-value under 0.05. All data are presented as means with standard errors.

2.11. Special remark about the data collected from HF progression samples

The data collection for β2AR-dependent cAMP levels and cardiomyocyte structure during HF progression started well before the PhD project, which is summarised in this thesis commenced. The postdoc who conducted the measurements before the arrival of the student left Imperial College at the beginning of 2013. His records were not made available to the student. Hence the allocation of control cells to hearts from rats which underwent sham operations or rats which were age matched but underwent no operation was not always possible. Whenever data from control cells with uncertain origin is shown in the result sections it is therefore, as far as possible, depicted in scatter blots and/or indicated as “age matched control and sham-operated control cardiomyocytes” in the figure legend.

Chapter 3: The TAT network and surface structure of cardiomyocytes

3.1. Introduction

Chapter 3 focusses exclusively on the structural assessment of single, isolated, mammalian cardiomyocytes. Especially ventricular cardiomyocytes have shown to possess a unique and highly intricate plasma membrane structure consisting of the Z-grooves and sarcolemmal crests (Gorelik et al. 2006) which are more readily in contact with their extracellular environment than the also present Tranverse Axial Tubule (TAT) network (Orchard et al. 2009). This ventricular TAT network provides a framework for coupling the electrical impulse of the action potential at the cardiomyocyte surface to cell internal responses such as the LTCC CICR through RyRs at the SR (Wagner et al. 2012). The highly structured appearance of ventricular cardiomyocytes is in part due to its underlying cytoskeleton, which consists primarily of the microtubuli and actin filaments (Nishimura et al. 2006). These microtubuli home molecules like the LTCC subunits to the T-tubules of cardiomyocytes (Hong et al. 2010). It has been shown in previous studies that the microtubule content in the cytoskeleton of cardiomyocytes increases in hypertrophy and HF (Nishimura et al. 2006). Furthermore the TAT network has been shown to be affected by this increase in microtubuli through the related JPH2 trafficking dysfunction of the disturbed microtubule cytoskeleton (Zhang et al. 2014). Conversely to the increase in microtubuli, the expression of JPH2 has been shown to be decreased in hypertrophy and HF and its knockdown lead to aberrant Ca^{2+} signalling properties of cardiomyocytes (Wei et al. 2010). Treatment with the gout medication colchicine, which binds to the microtubule and thereby prevents their polymerisation, however appeared to prevent microtubule and JPH2 associated adverse cardiac TAT network remodelling and has been linked to a lowered HF risk (Zhang et al. 2014).

It is well established that the TAT network is strongly decreased in end stage HF, in both rat and human cardiomyocytes (Lyon et al. 2009) and its deterioration has been associated with abnormal Ca^{2+} handling (Sacconi et al. 2012) as well as aberrant βAR-dependent cyclic nucleotide signalling (Nikolaev et al. 2010). The abnormal Ca^{2+} handling associated to TAT network alterations is thought to, among other causes, derive from “orphaning” of RyR2 clusters by a disparate configuration of disrupted T-tubules which no longer reach the vicinity of these RyR2 clusters (Song et al. 2006; Wagner et al. 2012). In contrast, aberrant βAR-dependent second messenger signalling associated to TAT network alterations is assumed to derive, among other things, from the physical redistribution of the β_2AR subtype out of the TAT network at the end stage of HF (Nikolaev et al. 2010). Most studies on the TAT network and its role in excitation-contraction coupling concentrate solely on elucidating the differences between control cardiomyocytes and cardiomyocytes at the end stage of HF and miss to test time-dependent progressional changes. Though it has been shown in prior publications that the cardiomyocyte structure undergoes step-wise alterations during the progression from

hypertrophy towards end stage HF (Wagner et al. 2012; Wei et al. 2012) these gradual alterations have not been brought into the context of localised β_2AR-dependent cAMP signalling alterations as was done in this thesis in chapter 3 and 4. Some of the alterations, like the reported increase in longitudinal elements of the TAT network could be of a compensatory nature and could be reflected in maintained βAR signalling despite myocardial injury or they could simply be the return of the cardiomyocyte protein expression profile to a more immature phenotype (Wagner et al. 2012). Therefore it is important to investigate the gradual alterations in the TAT network at the incremental stages of HF progression.

In summary the beginning of chapter 3 deals with the structure of adult, ventricular cardiomyocytes during the progression of HF. For this we studied the progressive alterations in the cardiomyocyte surface and TAT network at 3 different stages post the induction of MI in the rat. We associated these stages with a compensatory phase (4 weeks post-MI), a decompensated stage (8 weeks post-MI) and the end stage of HF (16 weeks post-MI). Furthermore the expression of the structural protein JPH2 was assessed during the progression of HF. Then structural alterations due to chemical manipulation of the cytoskeleton were examined.

Last but not least chapter 3 tries to elucidate potential differences in structural intactness of ventricular cardiomyocytes obtained from human patients. These patients either underwent MV surgery or obtained a heart transplant after ICM or DCM and consented for their cardiac tissue to be used in scientific studies. Some of these ICM or DCM patients were in possession of a LVAD which enabled a structural comparison between LVAD carriers and non-LVAD carriers.

3.2. Materials and Methods

3.2.1. Cardiomyocyte isolation during the progression of HF

To examine the structural integrity of cardiomyocytes in health and during the progression of HF cells were isolated by Mr. Peter O'Gara (Imperial College London) from the left ventricle of age matched control rat hearts and hearts at 4, 8 and 16 weeks post induction of MI via the ligation of the LAD aorta by Dr. Markus Sikkel (Imperial College London).

3.2.2. Cardiomyocytes surface structure assessment

For the investigation of cardiomyocytes surface structures, the SICM was used purely as a scanning tool on the day of the respective cell isolation, to obtain 3D, high resolution topography images. For this 10x10µm cardiomyocyte surface scans were obtained using SICM as described previously (Novak et al. 2009), with nano-pipettes of resistance around 80-100 MΩ. From these SICM surface scans the Z-groove index was calculated. This index quantifies how many Z-grooves are present on the cell surface and allows to detect changes in surface structures (Gorelik et al. 2006). In short it is calculated by measuring the total length of the T-tubules which are actually present in a scan and dividing it by the length of the optimally possible Z-grooves on a surface scan (see figure 9). Given that Z-grooves of the most highly structured cells, the ventricular cardiomyocytes, lie in about 2µm distance to each other the maximally possible length of Z-grooves in a 10x10µm area scan is 50µm, which would correlate to a Z-groove index of 1.

$$Zi = \frac{\text{maximally possible length}}{\text{actually measured length}}$$

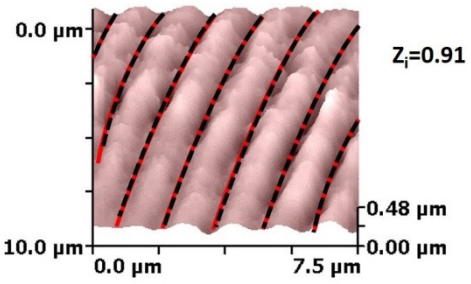

Figure 9 Illustration of the Z-groove index calculation at the hand of a 10x10 SICM surface scan. The Z-groove index value results from dividing the maximally possible amount of the Z-groove length (red) by the actually present Z-groove length (black).

3.2.3. Cell surface topography investigation during HF progression

To study the surface structure integrity of cardiomyocytes during the development of HF, cells were isolated from age matched control rat hearts and after 4, 8 and 16 weeks post-MI. Furthermore the number of T-tubule openings per scan for the ventricular rat cardiomyocytes was determined using the SICM image viewer software (Ionoscope). This was done by processing the scans using the correctional “destripe” and “remove line” options to remove artefacts from the scans and by using its deconvolution option to normalize the height of scans to each other (see Figure 10). Then an automated threshold was run over the SICM scans which made the T-tubule openings visible as red spots (see Figure 10). The width and length of T-tubule openings were determined by drawing profile lines through the T-tubule openings which were visualized in this manner (see Figure 10).

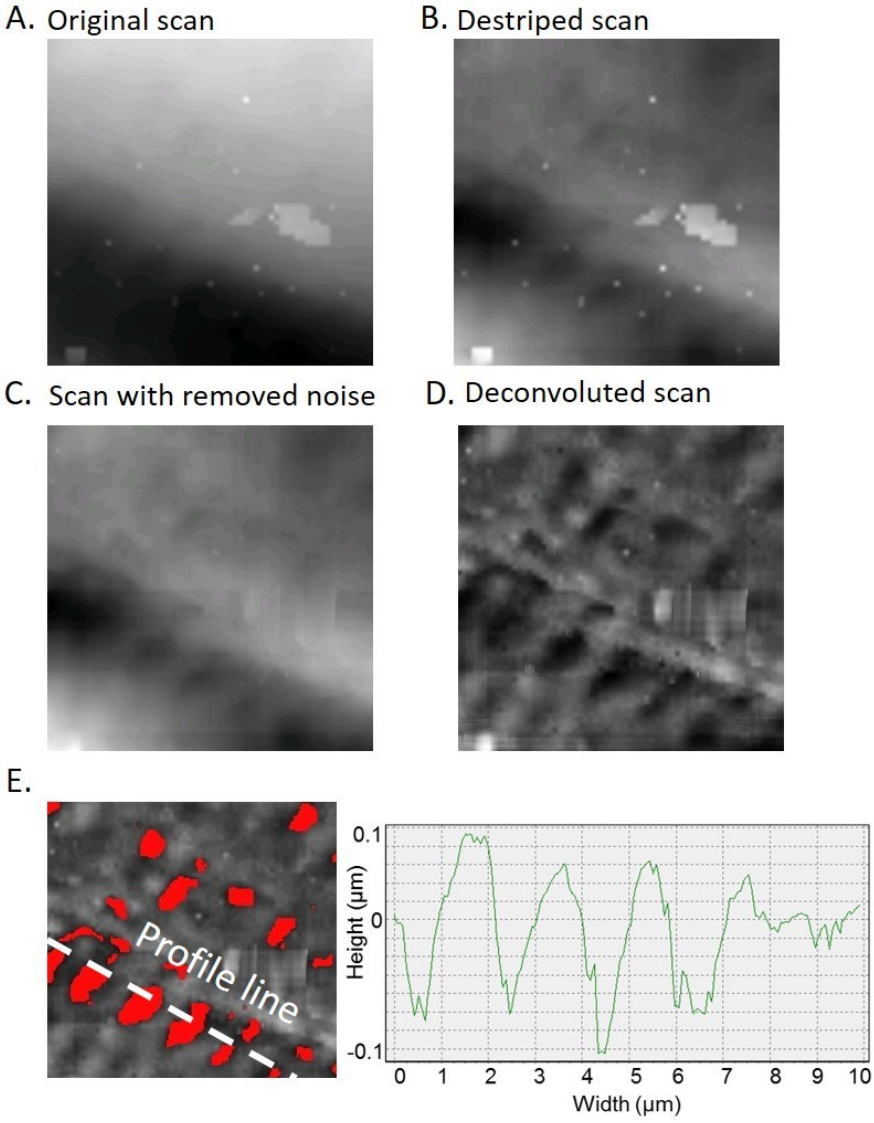

Figure 10 SICM scan processing depiction. Exemplary SICM scan with high noise shown (A.) unprocessed (B.) after destripe processing (C.) after removal of noise (D.) after deconvolution. (E.) Schematic of T-tubule opening investigation steps to determine T-tubule number and size. Left side: Surface scans are consistently processed and thresholded to show T-tubule openings (red spots) before a profile line is laid

through them (white line). Right side: The profile line allows to estimate the dimension of the opening of the T-tubule to the surface.

3.2.4. T-tubule regularity and TAT network density assessment

The TAT network of single cardiomyocytes was stained with the lipophilic dye Di-8-ANEPPS and imaged with confocal microscopy at x63 magnification. For this the Argon laser excited Di-8-ANEPPS at 488nm. The resulting images of the TAT network were analysed using the freeware Fiji (Schindelin et al. 2012) by choosing areas in the middle of Z-images (at least 2µm away from either the top image or the bottom image) and far from the cell nuclei or cell edges (at least 2µm apart). This also allowed to evaluate if the TAT network damage was more likely to occur close or remote from the sarcolemma (see Figure 11). Chosen areas of 40x5 µm were automatically thresholded into binarised images using the default binary threshold from the Fiji software and then plotted into waveforms. The waveforms were converted into power-frequency peaks through a single dimension Fast Fourier transformation (see Figure 12) using a custom-written macro for Matlab (The MathWorks, Inc., Natick, MA, USA) as described before (Ibrahim et al., 2010). The output for each power calculation is an arbitrary number that serves as an indicator of how regular T-tubules appear at a physiological distance of ~2µm as was described before (Wei et al., 2010). The higher the peak the more intact and regular is the structure. Simultaneously 40x5 µm binarised areas of the confocal images were used to define the TAT density by calculating the percentage of black pixels in each chosen area (see Figure 12).

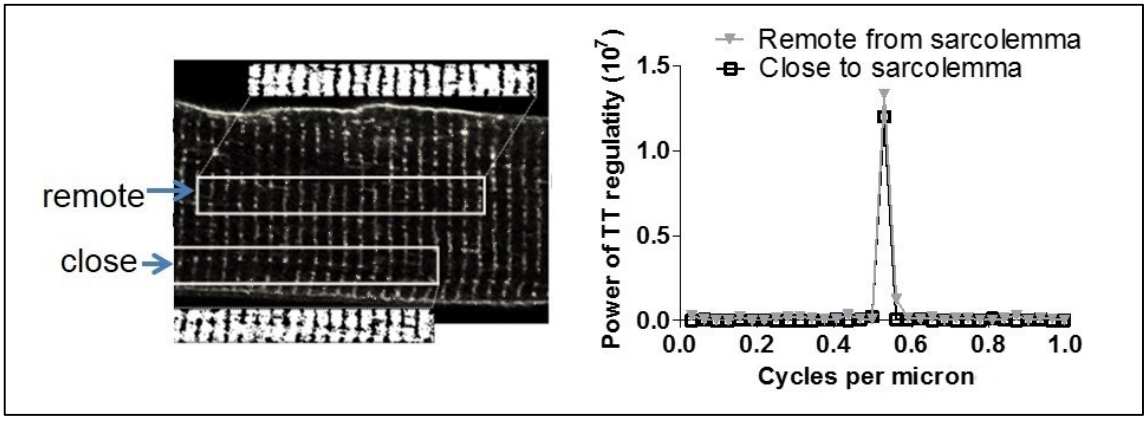

Figure 11 Testing to determine if there is a higher damage proneness of cardiomyocytes close or remote to the sarcolemmal membrane. To the left: representative confocal image of TAT network staining with indicated areas of investigation close or remote from the plasma membrane. To the right: Power peaks of the Transverse Tubule (TT) regularity of the chosen areas close and remote from the plasma membrane after 1dimensional Fast Fourier Transformation.

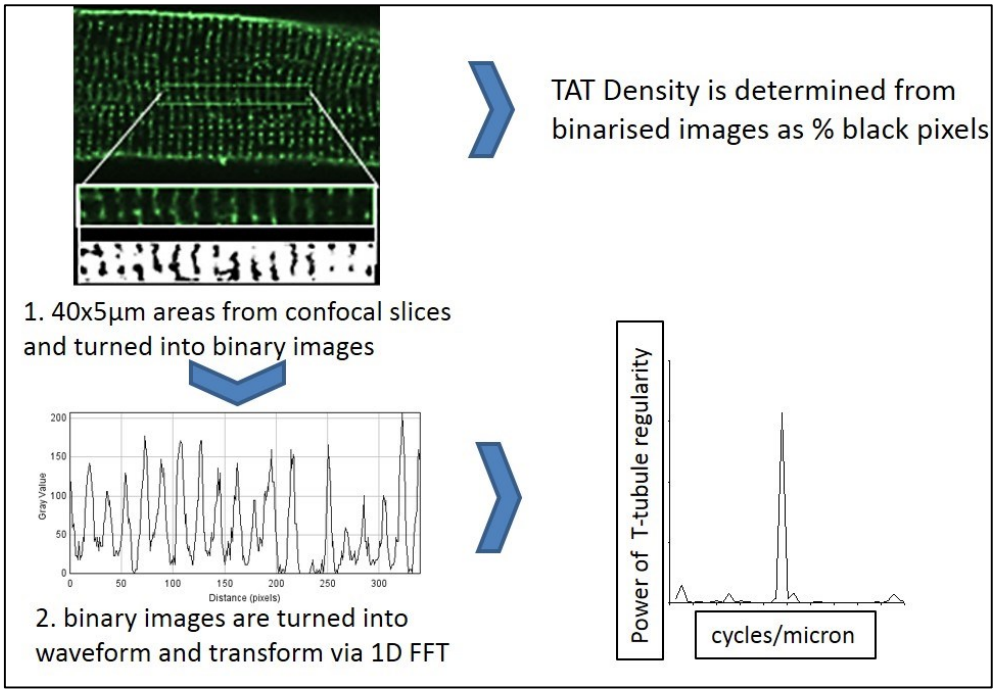

Figure 12 Schematic of TAT System investigation steps to determine TAT density and T-tubule regularity

3.2.5. Number of longitudinal elements:

A less studied and far more irregular feature of cardiomyocytes are the longitudinal elements that connect some T-tubules but not all. After their visualization with confocal microscopy one could go through each consecutive confocal image manually and determine the number of longitudinal elements but that would be a very labor intensive step by step procedure. Due to the variability in the position and occurrence of longitudinal elements it is hard to design a fully-automatic program that will calculate longitudinal elements. Still to avoid the completely manual approach an image processing algorithm was designed for semi-automatic quantification of longitudinal elements. For this confocal Z-stacks were taken of cardiomyocytes stained with Di-8-ANEPPS at various time points post-MI. An area of 40x10 micron was chosen on 10 consecutive confocal Z-stack images with 1µm separation between each of the images. Then the areas were processed as follows: 1) the overall TAT structure was detected using Canny edge detection 2) the detected edges were filled and thinned down to 1 pixel width using low-level, morphological operations 3) transverse oriented tubule candidates were collected by applying adaptive thresholds to the histograms over the 1D projections of the detected structures 4) the detection of spatial regularity/repetition of the transverse tubules was used to make the method more robust towards the errors introduced by the quantization in z-direction 5) all transverse tubule elements were identified and automatically removed from the images 6) the remaining longitudinal elements were verified by eye and quantified. The last step has to be performed by eye since real life TAT structure

proved to be much more curvilinear than the straight elements which were assumed initially for image processing, especially in cardiomyocytes at 16 weeks post-MI. Indeed, in human cardiomyocytes the TAT network layout was too variable to use this semi-automated quantification method.

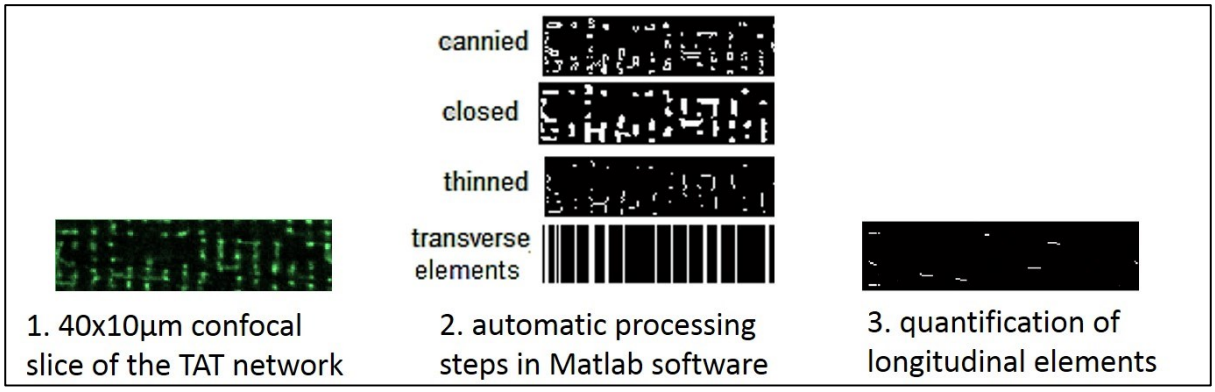

Figure 13 Procedure to determine the number of longitudinal elements in chosen areas of confocal images of the cardiomyocyte TAT network. A 40x10 µm area of a confocal image is chosen and loaded into the Matlab software, which then detects the structural edges by canny edge detection, closes all the edges and thins the structures to 1 pixel thickness before substracting the transverse oriented structures and leaving only the longitudinally directed structures for quantification.

3.2.6. Cardiomyocytes volume determination

Cardiomyocytes experience hypertrophy as an initially compensatory mechanism to counteract the loss of cardiac output tat is experienced by the heart due to myocardial injury (Yue et al. 2000). In order to measure the cellular hypertrophy exhibited at the progressive stages of HF the volume of cardiomyocytes was determined in control cardiomyocytes and 4, 8 and 16 weeks post-MI. For this Z-stack images taken after Di-8-ANEPPS staining were analysed using the imaging software Zen 2012, which automatically translated pixels into microns. The cell volume was measured by determining and multiplying the length, the width and the height of cardiomyocytes.

3.2.7. Culture induced cardiomyocyte structure alterations

It is a well-documented observation that isolated cardiomyocytes lose their structural integrity in culture (Mitcheson et al. 1998). An important part of the experiments listed in this thesis are FRET experiments that are performed after cells have been transfected with adenovirus for up to 48h. To have an insight into how much of the surface and TAT network structure is lost after these 48h and if the application of virus magnifies the loss even further untreated control cardiomyocytes and cells treated with approximately 300 plasma membrane Epac2-camps (pmEpac2) adenoviral particles (provided by Prof. Nikolaev Viacheslav, Universitätsklinikum,

Hamburg-Eppendorf, Germany) were cultured for 48h and investigated using SICM scanning and Di-8-ANEPPS staining as described before (see 2.5.2).

3.2.8. Colchicine and cytochalasin D treatment of cardiomyoctes

For a more in depth study of structure in freshly isolated left ventricular control cardiomyocytes, cells were treated with the cytoskeleton affecting reagents colchicine or cytochalasin D.

Colchicine treatment: Plated control cardiomyocytes were treated with and without 10µM of the microtubule disrupting agent colchicine, dissolved in DMSO, for 1h at 37°C and 5% CO_2. Control cells were also treated with 1µl DMSO/ml only. Control cells and colchicine treated cells were then fixed and immunocytochemically stained with an antibody selective for β-tubulin (see chapter 2, paragraph 2.6.).

Cytochalasin D treatment: It was previously reported, that fungi-derived cytochalasin D, which affects the cytoskeleton via actin filaments, kept both structural and functional features of cardiomyocytes intact for 3 days (Tian et al. 2012).To test if the reagent was indeed able to preserve T-tubule structure control cardiomyocytes were treated with and without 0.5µM cytochalasin D for 48h at 37°C and 5%CO_2..

Cardiomyocytes treated with cytochalasin D, colchicine or DMSO only were stained with Di-8-ANEPPS as described before (see chapter 2, paragraph 2.5.2) and imaged at 63x magnification using the confocal microscope at Imperial College London FILM facility as described before (see chapter 2, paragraph 2.7.). The relative amount of β-tubulin was determined in untreated and colchicine treated control cardiomyocytes after confocal imaging (see chapter 2, paragraph 2.7.) using the freeware Fiji (Schindelin et al. 2012) by choosing 50x10 µm areas of interest in the middle of the cell from 10 confocal images at a distance of 1 µm of each other, followed by binarising the images and measuring the % of black pixels in the images.

3.2.9. Cardiomyocyte structures in human cardiomyopathies

Cardiomyocytes from the human left ventricle from MV surgery patients or from patients with ICM or DCM with or without LVAD were isolated as described before (see chapter 2, paragraph 2.3.3). The cells were cultured for 1h before they were utilized for SICM surface scanning and TAT network investigations after Di-8-ANEPPS staining. Z-stacks of the TAT network were recorded at 63x magnification using the inverted Zeiss LSM780 Laser Scanning

Confocal Microscope at Imperial College London FILM facility as described before (see chapter 2, paragraph 2.7.).

3.2.10. Quantitation of the structural protein JPH2

JPH2 was quantified via Western Blotting both in Prof. Nikolaev's laboratory in Göttingen, Germany as well as at Imperial College London. Therefore about a million isolated control cardiomyocytes and cardiomyocytes from hearts after 4, 8 and 16 weeks of MI were washed in ice-cold PBS and lysed in 100µl ice-cold Radio Immuno Precipitation Assay (RIPA) buffer 30 minutes at 4°C and under constant agitation. The used RIPA buffer consisted of NaCl (150 mM), 1µl Triton X-100/ml, 500µg sodium deoxycholate/ml, 1µg sodium dodecyl sulphate (SDS) /ml diluted in Tris (50 mM), pH 8.0. Afterwards the samples were centrifuged for 20 min at 4°C and 12,000 rpm (in an Eppendorf table top centrifuge, 5417R) before taking off the supernatant and transferring it into pre-cooled Eppendorf tubes for further processing. Next the protein concentration was determined using a standard Bradford assay on a 96 well plate. A concentration curve for normalisation was prepared with BSA as standard: putting ddH_2O blanks only, 0.5 µl of 1mg BSA/ml plus 9.5 µl ddH_2O, 1 µl of 1mg BSA/ml plus 9 µl ddH_2O, 2 µl of 1mg BSA/ml plus 8 µl ddH_2O and 4µl of 1mg BSA/ml plus 6 µl ddH_2O into two consecutive wells each, before setting up duplicates of 0.5 µl sample plus 9.5 ddH_2O and duplicates of 1µl sample plus 9 µl ddH_2O wells. Then the Bradford reagents (Bio-Rad) were added in the following order to each well: 25µl of Bradford Reagent A mixed with 20 µl Bradford Reagent B and 200 µl of Bradford Reagent C. Then the 96 well-plate was spun down gently on a centrifuge and allowed to incubate for 15 min at room temperature. Afterwards the plate was put into the plate reader and the assay was run using a basic endpoint protocol at a wavelength of 750nm. Sample concentrations were calculated automatically and allowed for the samples to be diluted to approximately 50µg of sample per 20µl ddH_2O and put at -80°C until further use. For the electrophoretic separation of proteins a 10% sodium dodecyl sulphate (SDS) polyacrylamide (PA) separating and stacking gel was prepared. For this an ethanol-cleaned glass plate with a spacer was assembled in a gel sandwich holder (Bio-Rad). Then 1µl fresh ammonium persulfate (APS, Sigma, A3678)/ml solution was prepared before mixing 3.3ml of 300 µl acrylamide/ml with 2.5ml of 1.5M Tris-HCl pH 8.8, 4ml ddH_2O, 100µl of 100µg SDS/ml, 80µl of 100µg APS/ml and 1µl Tetramethylethylenediamine (TEMED) /ml and pouring the mixture into the assembled gel sandwich till about 2cm to the top to create the separating gel. To smooth the top of the separating gel ddH_2O was carefully pipetted on top of it. As soon as the separating gel had polymerised the stacking gel consisting of 0.5ml 300 µl acrylamide/ml, 1ml of 0.5M Tris-HCl pH 6.8, 2.4ml ddH_2O, 100µl of 100µg SDS/ml, 80µl of 100µg APS/ml and 1µl TEMED/ml was cast on top of it and equipped with a 10 well gel comb after the ddH_2O

had been removed. Once the stacking gel had polymerised as well the gel was positioned inside a gel sandwich electrode assembly filled with running buffer consisting of 25mM Tris, 192mM Glycine and 1µg SDS/ml. The gel comb was removed and the wells were gently cleaned by pushing through running buffer liquid with a pipette. Subsequently the samples were prepared by retrieving them from -80°C and mixing 20µl sample with 5 µl of 5x premade sample buffer consisting of 0.125M Tris-HCl pH6.8, 200µl glycerol/ml, 40µl SDS/ml, 20µl β-mercaptoethanol (β-ME)/ml and 0.2µl bromphenolblue/ml. Then the samples were put onto a heating block for 5 min at 95°C and loaded onto the gel after a standard protein ladder had been loaded into the first well. Next the gel was attached to the power source and run for about 1h at a voltage of 160mV. After the run had finished the gel was prepared for protein transfer onto a nitrocellulose membrane by building a wedge made up from bottom to top of the negatively poled side of the transfer holder plus 3 images of Whatman paper soaked in transfer buffer plus the gel containing the protein samples plus the nitrocellulose membrane cleaned with ethanol and afterwards also soaked in transfer buffer plus 3 more soaked Whatman paper images and the positively poled side of the transfer holder. Next the holder was put into the transfer apparatus filled with transfer buffer made of 30.2mg Tris base/ml, 144mg glycine/ml and 200ml ethanol in 1.8L Millipore water and the protein transfer was run over night. On the next morning the nitrocellulose membrane with the transferred protein was retrieved from the apparatus and blocked for at least 1h in milk made from 50mg milk powder/ml diluted in 100ml of Tris Buffer Saline Tween20 (TBST) at 4°C and under constant agitation. After the blocking the membrane was quickly washed with TBST before putting on a 1:3000 dilution with TBST of the primary JPH2 antibody overnight at 4°C on a shaker. The following day the membrane was washed 5 times for 10 min with TBST at 4°C on a shaker before putting on a 1:1000 dilution of the secondary horse radish peroxidase (HRP) bound antibody for 1h at 4°C on under constant motion. Following the membrane was again washed 5 times for 10 min with TBST at 4°C on a shaker and then the Western blot was developed using Luminata Forte Western HRP activation substrate.

3.3. Results: Cardiomyocyte structure in HF progression

3.3.1. Cardiomyocyte cell volume in health and progressive HF

The cell size of cardiomyocytes can be used as a marker of hypertrophy. On this occasion the volume of cells (length x width x height) was determined from whole cell, confocal Z-stack images after Di-8-ANEPPS staining taken from control cardiomyocytes and from cardiomyocytes isolated from a progressive HF model at 4, 8 and 16 weeks post-MI. Even

though the whole hearts of the animals, which were sacrificed for this study showed significant increase in size as soon as 4 weeks post-MI (see chapter 2, paragraph 2.2.2., figure 1), the cell volume of viable, single cardiomyocytes after their isolation was not significantly increased until 8 and 16 weeks post-MI (see figure 14) when they were on average 36% larger.

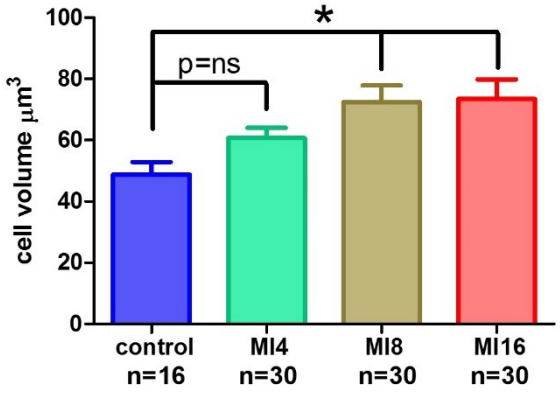

Figure 14 Cardiomyocyte cell volume in health and during the progression of HF. Cell volume (in µm^3) was determined via analysis of confocal Z-stack images in sham operated control cells and cardiomyocytes at 4, 8 and 16 weeks post-MI. n= number of single cells measured. Animals utilised n=4 for each time point. Bars represent mean values ± standard error of the mean. Statistical one-way ANOVA test followed by Bonferroni correction post-hoc testing, p<0.001, p=ns; no significant difference.

3.3.2. Cardiomyocyte surface structure during HF progression

In end stage HF the surface structure of left, ventricular cardiomyocytes is severely disrupted. To study the progressive deterioration from health to end stage HF cells at 4, 8 and 16 weeks post MI were SICM scanned on the day of their isolations and their Z-groove index as well as the number of T-tubule openings was analysed. Topography images of the cardiomyocyte sarcolemma generated by SICM allowed clear distinction of T-tubule openings and the crests between the Z-grooves. Profile measurements of topographical images showed that in adult, healthy ventricular cardiomyocytes spacing between Z-grooves is ≈2µm, corresponding to the sarcomere length (Gorelik et al. 2006). While the Z-groove index as a marker of structural integrity decreased throughout the progression of HF by about 9% the number of T-tubule openings on the surface scans decreased significantly at 4 weeks post-MI and again at the end stage of HF (see figure 15).

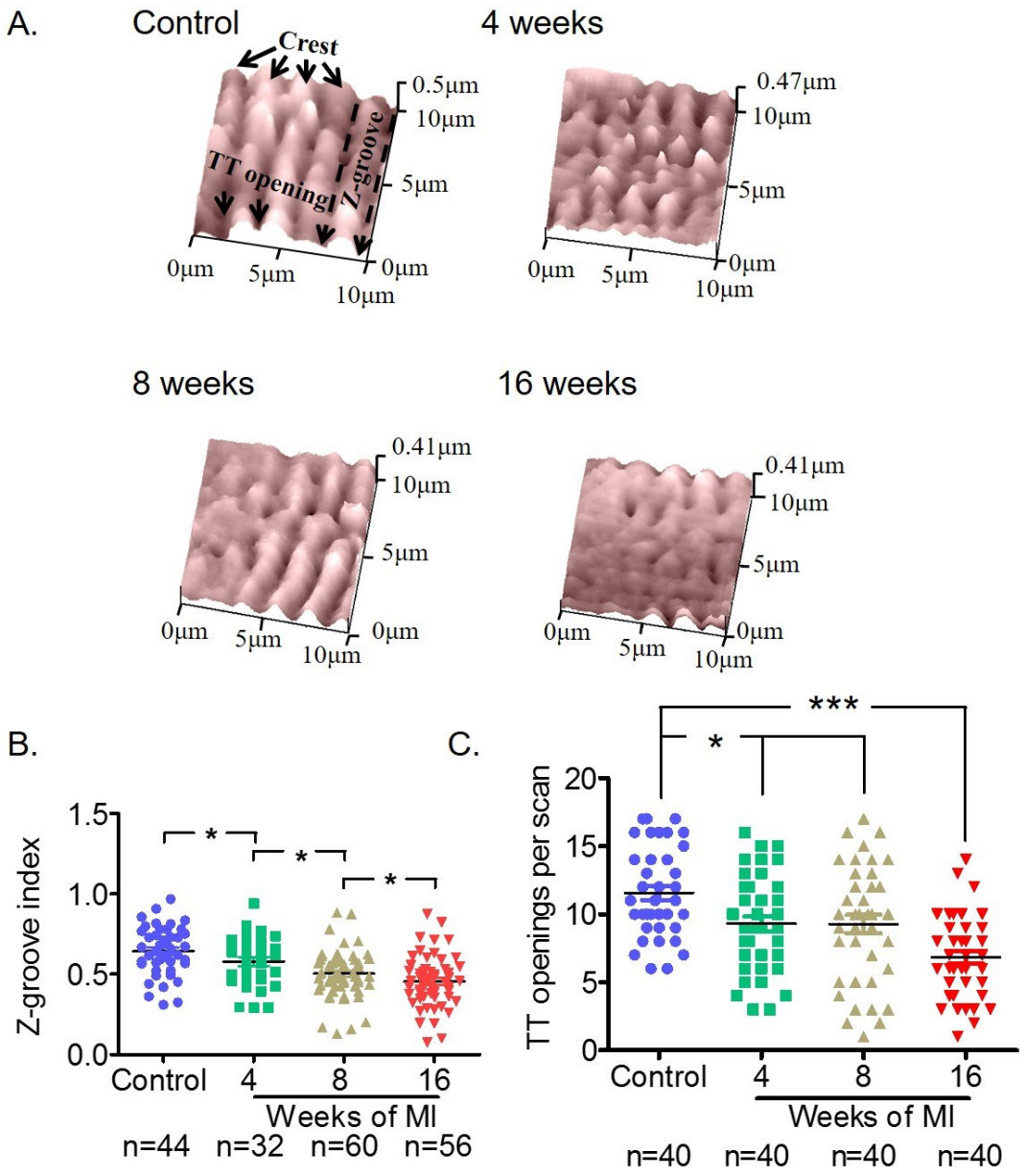

Figure 15 Changes in the surface integrity of cardiomyocytes during the progression of HF. (A.) Representative 10x10µm SICM surface scans of left, ventricular cardiomyocytes from in age matched control and sham-operated control cardiomyocytes control and at 4, 8 and 16 weeks post-MI. (B.) The Z-groove index of cardiomyocytes in control cells and at different time points post-MI. (C.) The number of T-tubule (TT) openings in control cells and at different time points post-MI (to the right). n= number of single cells measured. Animals utilised n≥5 for each time point. Bars represent mean values ± standard error of the mean. Statistical one-way ANOVA test followed by Bonferroni correction post-hoc testing, ***p<0.0001,*p<0.05.

3.3.3. TAT system in rat during HF progression

It is well documented that cardiomocytes from different species at the end stage of HF exhibit a loss of TAT presence and intactness (Ibrahim et al. 2011; Lyon et al. 2009). The gradual changes of the TAT system during the progression towards HF are less well documented (Wagner et al. 2012; Wei et al. 2012) and no one has studied them in the same rat HF model

with chronic MI at the 4 weeks, 8 weeks and 16 weeks post-MI stage. In healthy cardiomyocytes, the TAT network spans the entire cytoplasm and consists of periodically spaced T-tubules and irregular longitudinal elements that connect the T-tubules. Consistent with prior studies by our group (Ibrahim et al. 2010; Lyon et al. 2009) our calculations of T-tubule regularity indicate that they are interspaced highly regularly at ~2μm intervals in healthy cardiomyocytes. The TAT structure assessment at the stages after MI induction shows that the regularity of the Transverse oriented tubules (T-tubules) already decreases significantly by ~47% ($p<0.001$) at 4 weeks post-MI together with T-tubule density (~11%, $p<0.01$) and remains so until end stage HF (see figure 16). However at the 4 and 8 weeks post-MI stages the cardiomyocytes exhibit a significant increase (~41%) in the number of their longitudinally oriented T-tubules (see figure 17). Similar results have been observed in a mouse model of HF (Wagner et al. 2012).

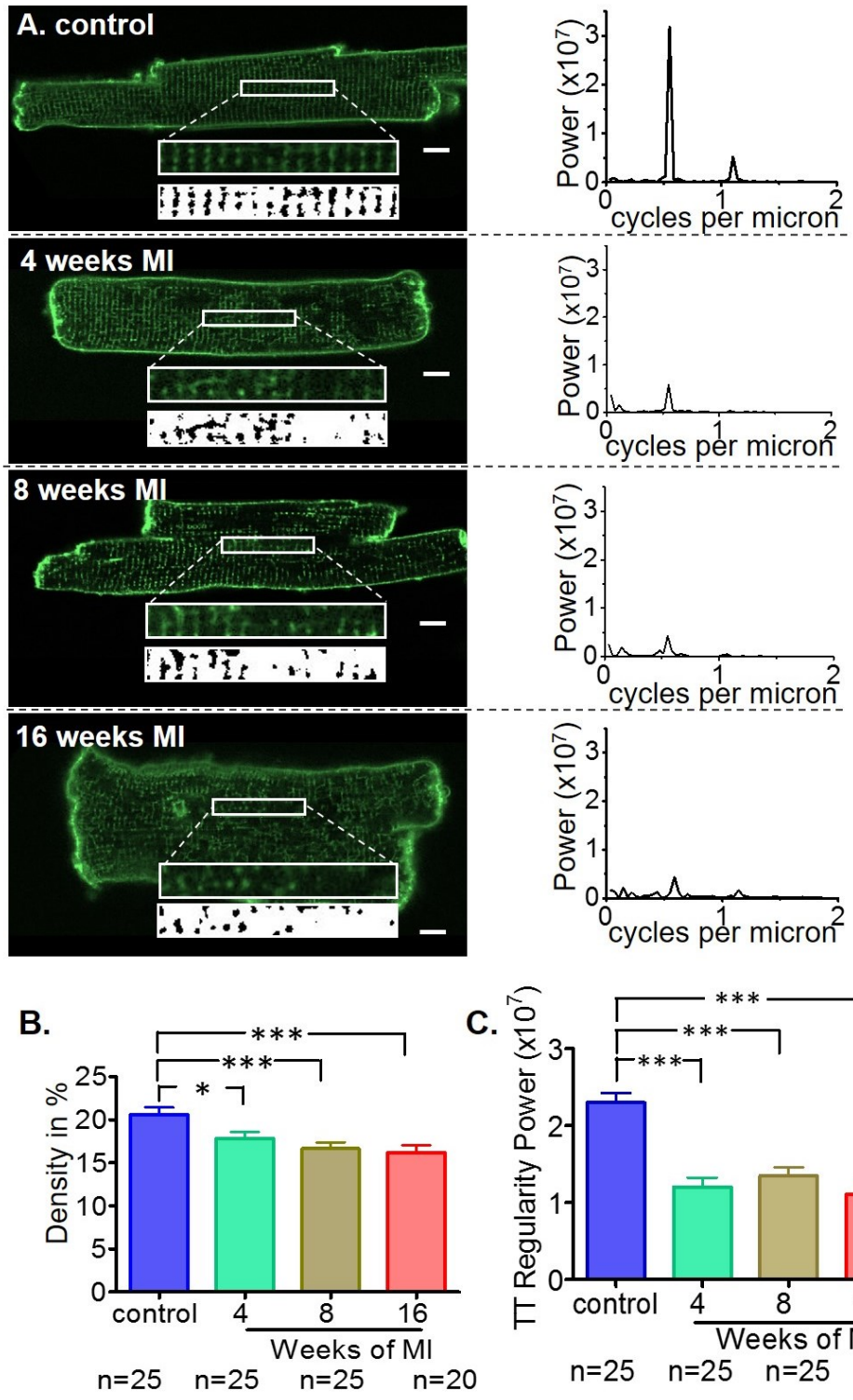

Figure 16 Changes in cardiomyocyte TAT structure during the progression of HF. T-tubule regularity and TAT density in sham-operated control cardiomyocytes and cells at different time points after MI. (A.) To the left: Representative confocal images of the TAT network with 10x5 µm areas of interest blown up 2.65 times together with their binarised counterparts of cardiomyocytes in control and at 4, 8 and 16 weeks post MI; scale bars equal 10µm. To the right: Power peaks of the corresponding T-tubular regularity. (B.) TAT network density in control cells and different time points post-MI. (C.) T-tubule regularity in control cells and different time p Bars represent mean values ± standard error of the mean oints post-MI. n= number of single cells measured. Animals utilised n≥4. Bars represent mean values ± standard error of the mean. Statistical one-way ANOVA test followed by Bonferroni correction post-hoc testing, ***p<0.0001, *p<0.05.

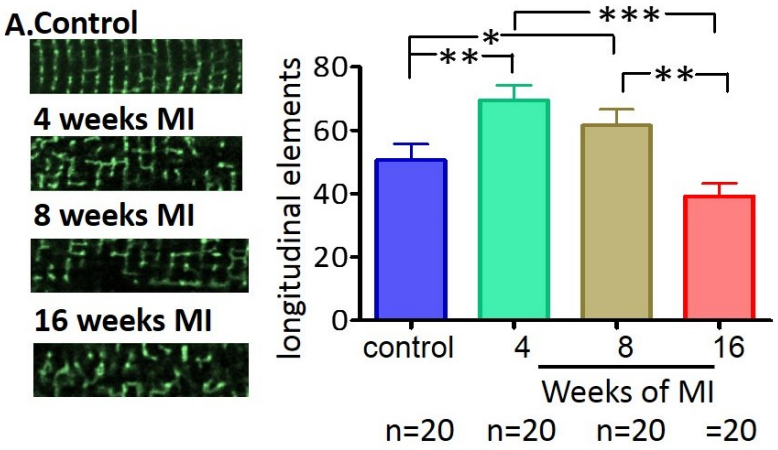

Figure 17 Changes in the number of longitudinal elements of the TAT network during HF progression. A. Representative fragments of 40x10µm of the confocal images of cardiomyocytes in sham-operated control and at 4, 8 and 16 weeks post-MI. (B) Relative number of longitudinal tubules n= number of single cells measured. Animals utilised n=4 for each time point. Bars represent mean values ± standard error of the mean. Statistical one-way ANOVA test followed by Bonferroni correction post-hoc testing, ***p<0.0001, **p<0.001, *p<0.05.

3.3.4. TAT damage occurs with similar frequency throughout the cardiomyocyte

To assess a potential damage proneness of the TAT system close to the plasma membrane or remote from the plasma membrane the TAT network of single cardiomyocytes was quantified by consciously choosing areas close and remote from the plasma membrane for analysis after Di-8-ANEPPS staining and confocal imaging. As our investigation shows damage was not more likely to occur either close or remote from the sarcolemma but appeared equally at both sites in the cardiomyocytes (see figure 18).

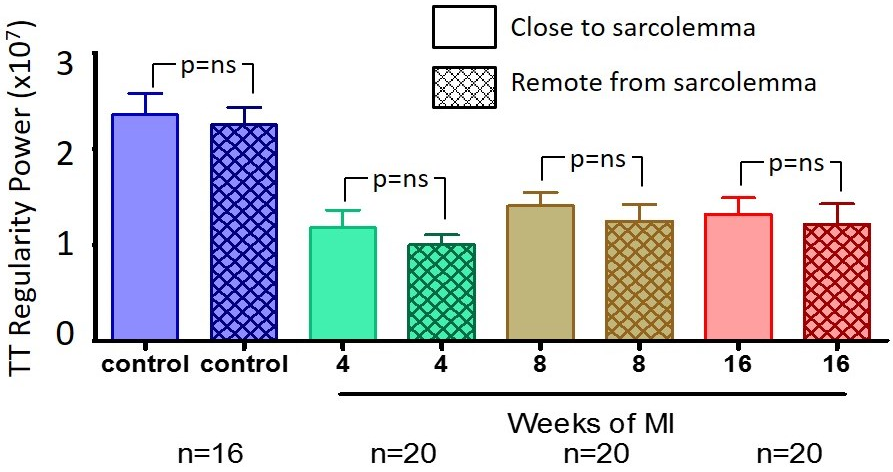

Figure 18 T-tubule (TT) regularity in areas close (plane boxes) and remote (hatched boxes) from the sarcolemma in sham-operated control cardiomyocytes and cardiomyocytes 4, 8 and 16 weeks post-MI. n=number of single cells measured. Animals utilised n=4 for each time point. Bars represent mean values ± standard error of the mean. Statistical two-sided Student's T-test, p= ns; no significant difference.

3.3.5. JPH-2 levels decrease early and drastically in HF progression

Among other proteins JPH2 has been identified as a vital protein for both structural maturation of cardiomyocytes (Seki et al. 2003; Chen et al.2012) as well as for the structural and functional integrity of their TAT network. JPH2 has also been shown to be decreased in hypertrophy and HF (Wei et al. 2010; Lyon et al. 2012). For this reason we measured the expression level of JPH2 during the progression of HF at 4, 8 and 16 weeks post-MI and immunocytochemically stained with an antibody selective for the protein. The results show that JPH2 expression is already strongly reduced at 4 weeks post-MI and remains thus until the end stage of HF (see figure 19).

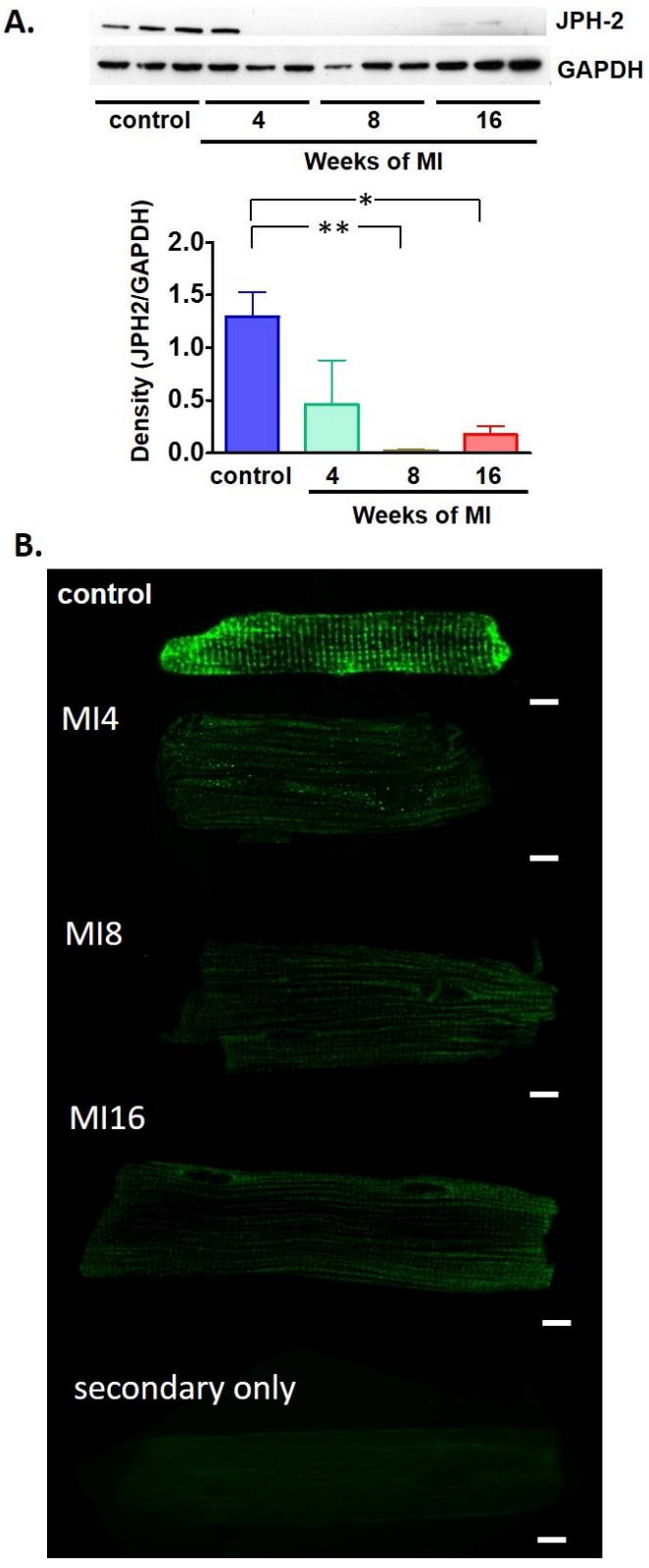

Figure 19 Changes in JPH2 expression and localisation during HF progression. A. Representative Western blot provided by Prof. Nikolaev (Universitätsklinikum, Hamburg Eppendorf, Germany). The density of the respective JPH2 bands is normalized to corresponding house-keeping gene GAPDH bands (n=3-4 animals, 3 replicates). B. Representative, immunocytochemical staining of JPH2 in an age-matched control cardiomyocyte and cardiomyocytes 4, 8 and 16 weeks post-MI as well as a secondary antibody (Alexa Fluor 488) only stain. Staining in cells post-MI showed no JPH2 stain. Scale bars equal 10µm. Statistical one way ANOVA test followed by Bonferroni correction post-hoc testing, **p<0.01, *p<0.05.

3.3.6. Structural dedifferentiation of cardiomyocytes in culture

Cardiomyocytes experience structural dedifferentiation in culture. To assess the extent of this dedifferentiation the TAT system of cells after 48 hours of culture was stained with Di-8-ANEPPS and imaged using confocal microscopy (see figure 20). To furthermore see if adenoviral transduction exacerbates culture induced cell dedifferentiation cardiomyocytes treated with the EPAC2-camps adenovirus for 48h were also stained with Di-8-ANEPPS and their TAT structure was assessed after confocal imaging (see figure 20).

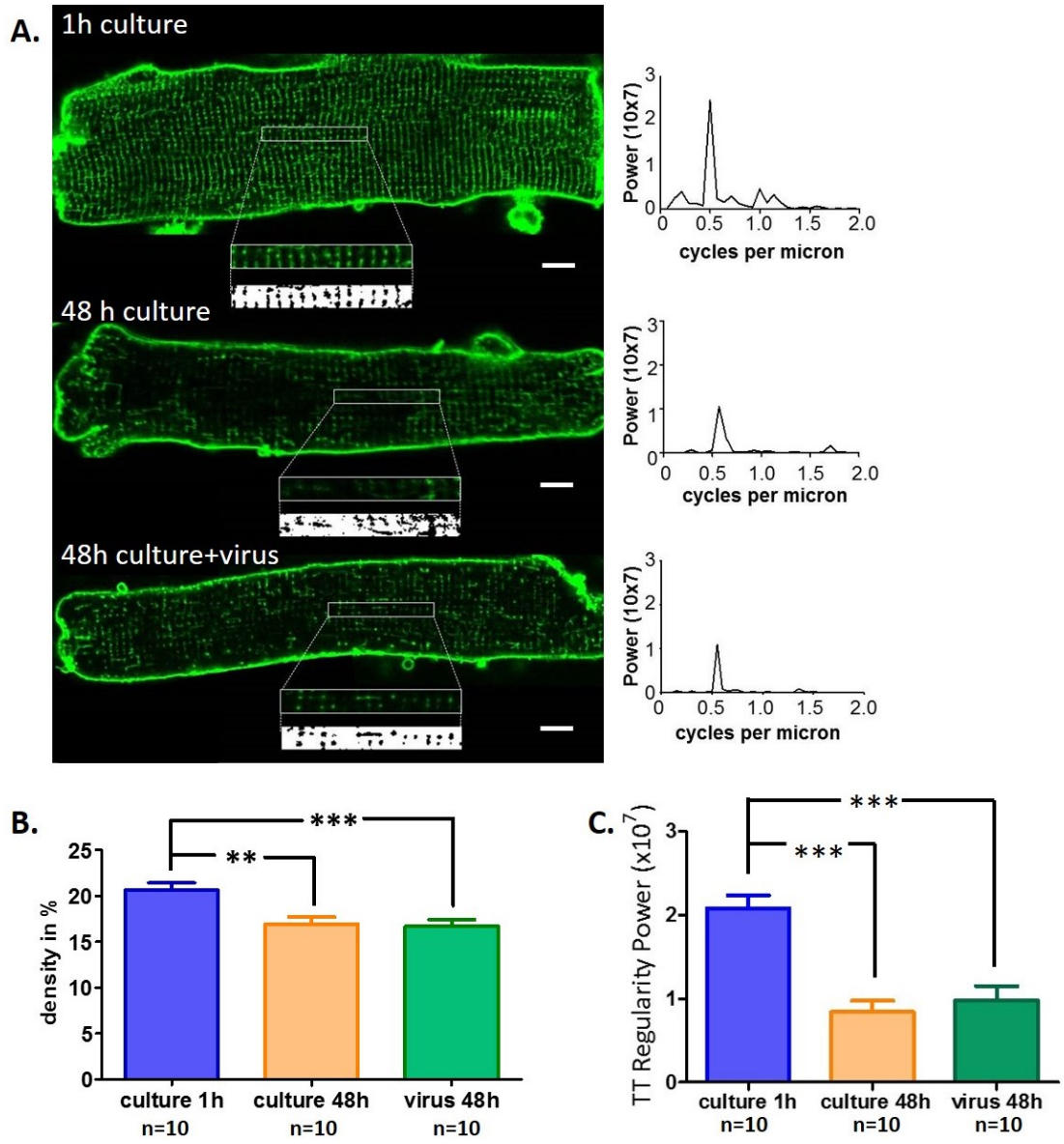

Figure 20 TAT network in freshly isolated cardiomyocytes and myocytes after long term culture with and without addition of adenovirus. (A.) To the left: Representative confocal images of the TAT network with 40x5 µm areas of interest blown up 2.65 times together with their binarised counterparts; scale bars equal 10µm. To the right: Power peaks of the corresponding T-tubular regularity, (B.) density of the TAT network and (C.) regularity of the T-tubules in control cells after 1h in culture and cells with and without adenovirus kept in culture for 48h. n=number of single cells measured. Animals utilised n=2 each. Bars represent mean values ± standard error of the mean. Statistical Student's two sided T-test, ***p < 0.0001, **p < 0.001; p=ns; no significant difference.

3.4. Results: cytochalasin D and colchicine effects on cardiomyocyte structure

3.4.1. Cytochalasin D increases the number of longitudinal elements in culture

Submicromolar levels of the fungal agent cytochalasin D, which acts by inhibiting filamentous actin from forming the microfilaments of the cytoskeleton, were previously reported to stop the structural deterioration of cardiomyocytes in culture (Tian et al. 2012). The application of 0.5 µM of cytochalasin D and its effect on the cardiomyocyte TAT network were assessed after Di-8-ANEPPS staining and confocal imaging. Though the calculated regularity of the T-tubules was significantly decreased by around 29 % after the application of low levels of cytochalasin D the TAT density did not decrease significantly in the cytochalasin D treated cells at 48h of culture (see figure 21). This was due to a rise in longitudinal elements by approximately 55% in comparison to control cardiomyocytes after only 1h of culture (see figure 22).

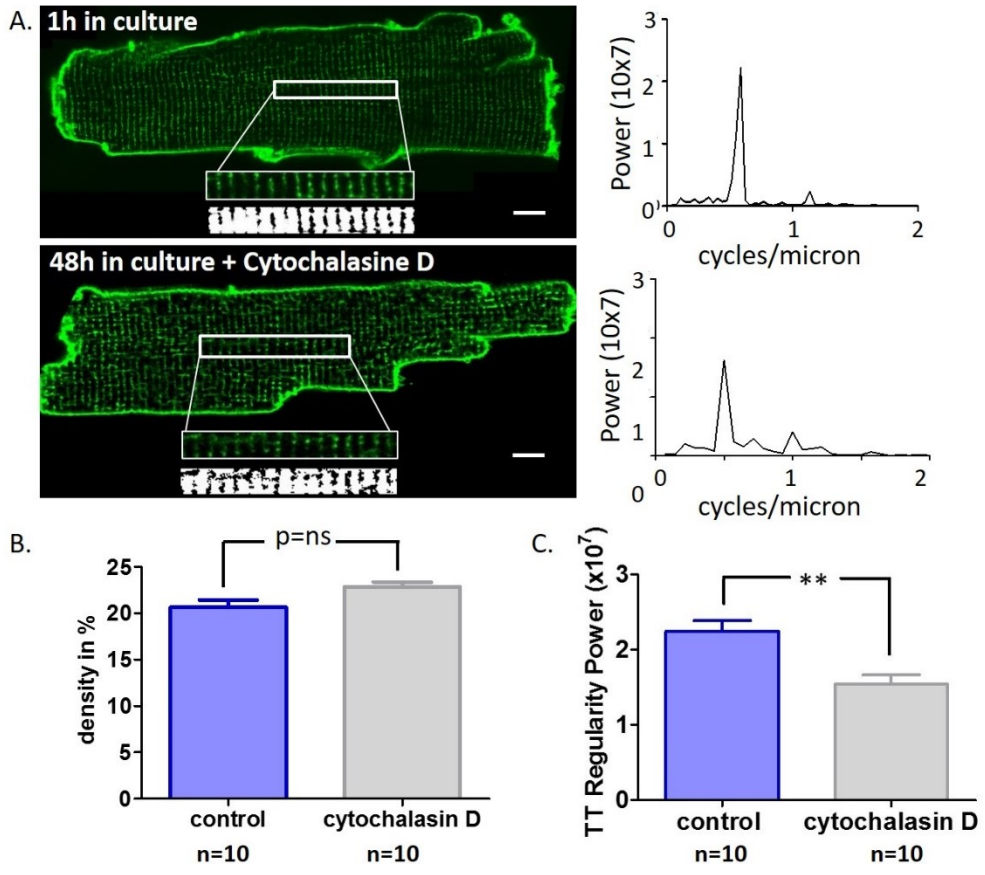

Figure 21 TAT network in freshly isolated cardiomyocytes and myocytes after long term culture treated with cytochalasin D. (A.) To the left: Representative confocal images of the TAT network with 40x5µm areas of interest blown up 2.65 times together with their binarised counterparts; scale bars equal 10µm. To the right: Power peaks of the corresponding T-tubular regularity, (B.) density of the TAT network and (C.) regularity of the T-tubules in control cells after 1h in culture and cells treated with cytochalasine D for 48h in culture. n=number of single cells measured. Animals utilised n=2. Bars represent mean values ± standard error of the mean. Statistical Student's two sided T-test, **p < 0.001; p=ns; no significant difference.

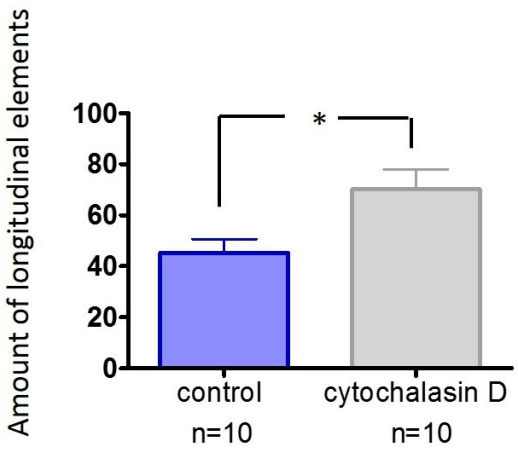

Figure 22 Number of longitudinal elements in the TAT network of control cells after 1h of culture and cells treated with cytochalasin D for 48h. n=number of single cells measured. Animals utilised n=2. Bars represent mean values ± standard error of the mean. Statistical Student's two-sided T-test, *P < 0.05.

3.4.2 Colchicine decreases the TAT network but not the surface structure of cardiomyocytes

The administration of the pharmacological compound colchicine, which acts as a microtubule polymerisation inhibitor in cardiomyocytes, has been shown to have beneficial effects on the myocardium, by preventing cell apoptosis (Saji et al 2007) and excessive T-tubule remodelling in failing cardiomyocytes by stopping increased microtubule polymerisation which occurs in HF (Zhang et al. 2014).

To see how treatment with colchicine affects the microtubule skeleton of control cardiomyocytes and with it the surface structure and the TAT network of cardiomyocytes, cells were treated with colchicine for 1h at 37ºC and 5% CO_2. The cells were then SICM surface scanned and stained with Di-8-ANEPPS and their TAT network was recorded with confocal imaging. Then control and colchicine treated cells were fixed and stained with an antibody selective for β-tubulin a microtubule marker, before being imaged with the confocal microscope again. SICM scanning of control and colchicine treated cardiomyocytes did not reveal any effect of microtubule polymerisation onto the surface membrane of cardiomyocytes (see figure 23). However, cells treated with colchicine exhibited a significantly reduced amount of about 47% of the relative β-tubulin levels as determined from confocal images in comparison to control cardiomyocytes (see figure 24). Cardiomyocyte treatment with colchicine furthermore lead to a significant decrease in the integrity of the TAT network and reduced the TAT density by around 9% respectively while the T-tubule regularity dropped by approximately 28% (see figure 25).

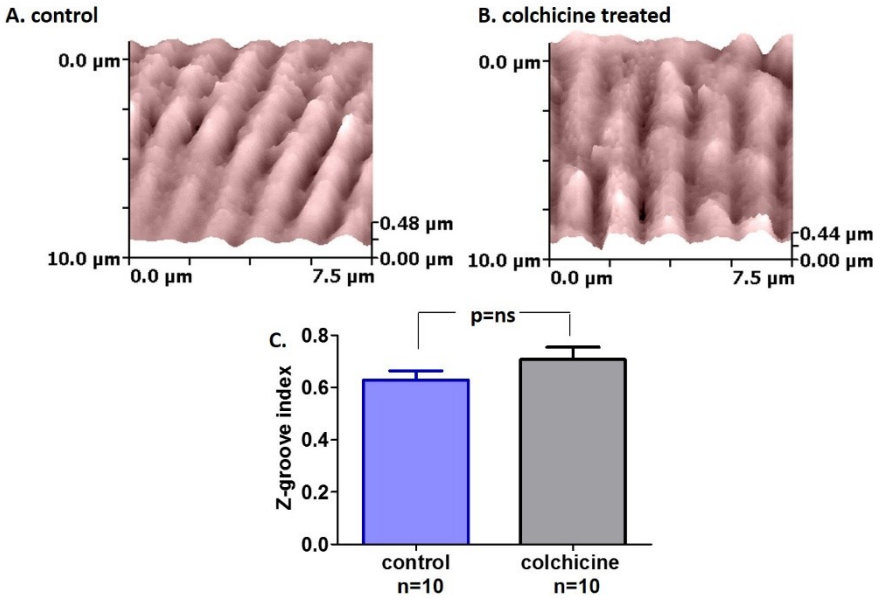

Figure 23 Surface structure of ventricular, rat cardiomyocytes from control cells and cells treated with colchicine. Representative 10x10 SICM surface scans of (A.) a control cardiomyocyte and (B.) a cardiomyocyte treated with the microtubuli polymerisation inhibitor colchicine. (C.) Z-groove index of control cardiomyocytes and cells treated with colchicine. n=number of single cells measured. Animals utilised n=2. Bars represent mean values ± standard error of the mean. Statistical one-way Student's two sided T-test, p=ns; no significant difference.

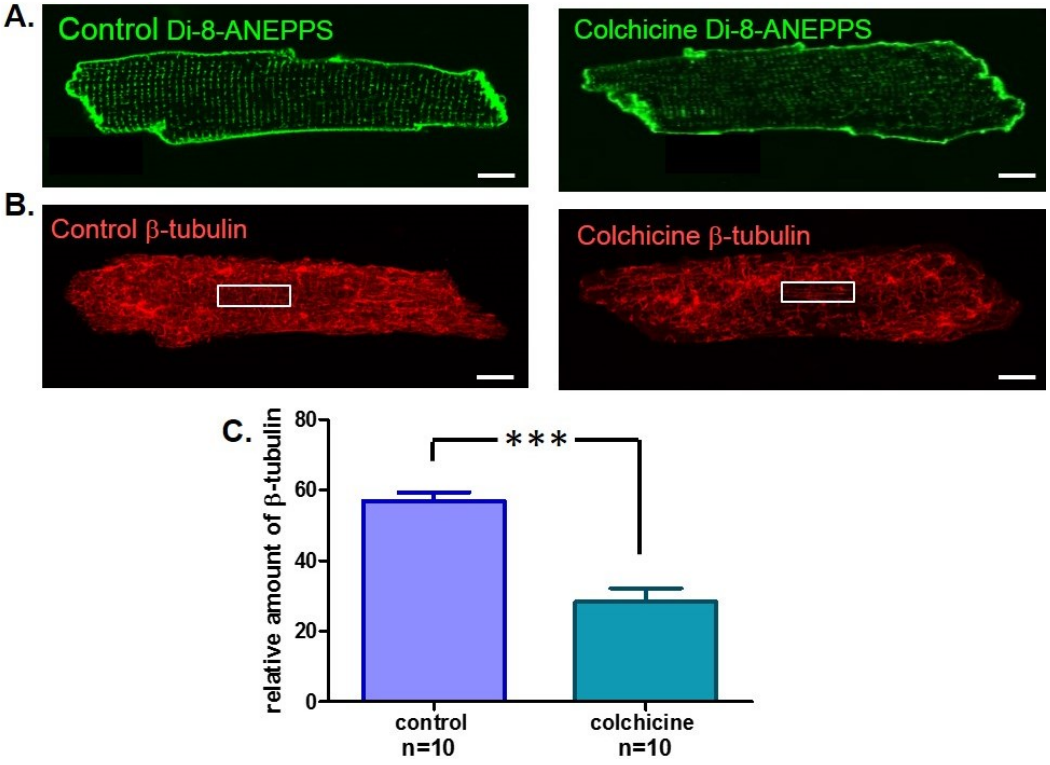

Figure 24 TAT network dependency on the cytoskeleton in cardiomyocytes. (A.) Representative confocal image of Di-8-ANEPPS staining of a untreated control cardiomyocyte (to the left)) and a cardiomyocyte treated with the microtubuli polymerization inhibitor colchicine (to the right). (B.) Representative confocal image of β-tubulin staining in the same control and colchicine treated cardiomyocytes shown above with 40x10 µm areas of interest, which were used to determine relativ β-tubulin levels; scale bars equal 10µm. (C.) Relative β-tubulin protein levels in control and colchicine treated cardiomyocytes. n=number of single cells measured. Animals utilised n=2. Bars represent mean values ± standard error of the mean. Statistical two-sided Student's T-test, ***p<0.0001.

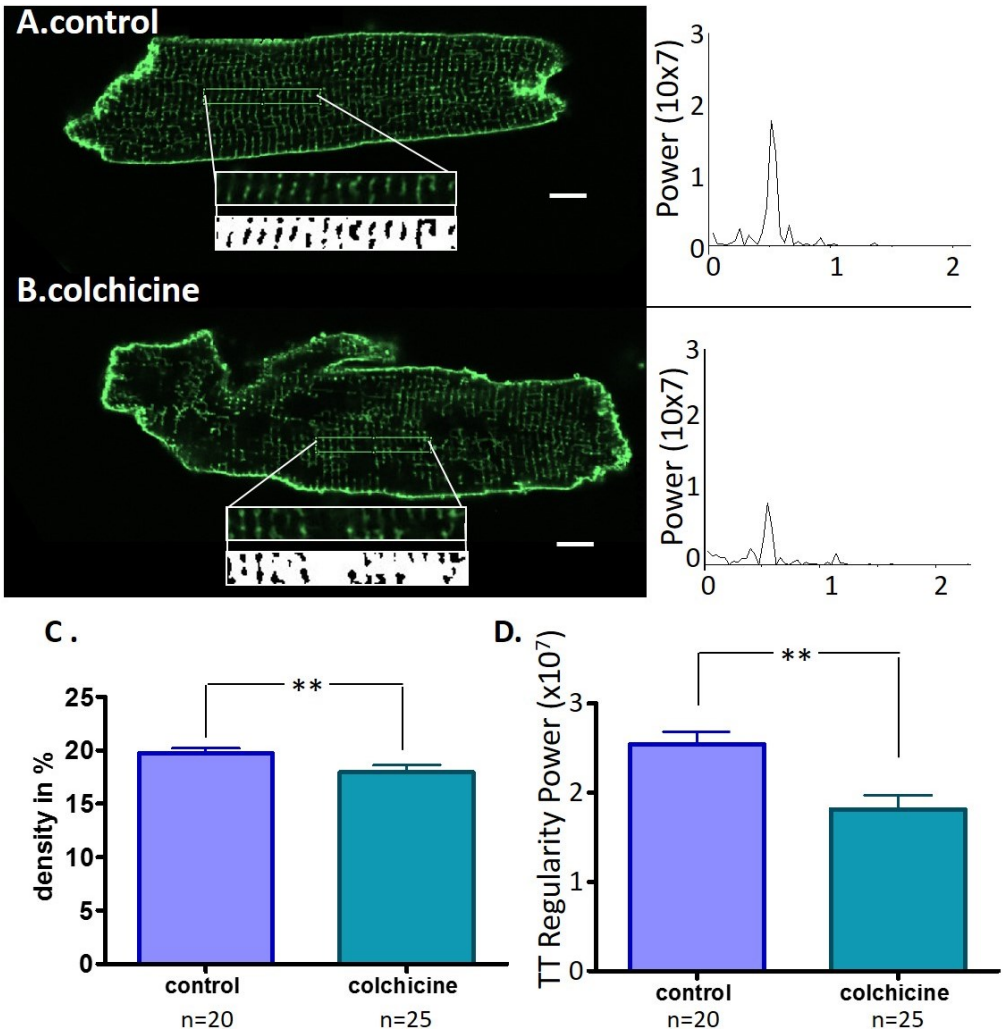

Figure 25. TAT network in untreated control cardiomyocytes and cardiomyocytes treated with the microtubuli polymerization inhibitor colchicine. (A.) To the left: Representative confocal images of the TAT network with 40x5 µm areas of interest blown up 2.65 times together with their binarised counterparts of control cells and cells treated with colchicine; scale bars equal 10µm. To the right: Power peaks of the corresponding T-tubular regularity, (B.) density of the TAT network and (C.) regularity of the T-tubules in control cells and cells treated with colchicine. n=number of single cells measured. Animals utilised n=3. Bars represent mean values ± standard error of the mean. Statistical Student's two sided T-test, **p<0.001.

3.5. Results: Cardiomyocyte structure in humans

3.5.1. Human ventricular cardiomyocyte structure

Human ventricular cardiomyocytes possess structures similar to those observed in rat cardiomyocytes. Just like in rat these structures are severely disrupted in human cardiomyocytes at the end stage of HF (Lyon et al. 2009). Fortunately for this study we are in receipt of cardiac tissue from MV and heart transplant patients. These transplant patients have suffered from DCM and ICM and some of them were given a LVAD. From these hearts we obtained left ventricular cells. Though the MV replacement cells cannot be considered healthy, they are not in end stage HF. We here utilized them as our control case due to their slightly more intact structures. To see the extent of structural disruption in human cardiomyocytes their surface structures were visualised through SICM scanning and analysed together with Dr. Jose Sanchez Alonso-Mardones (Imperial College London) (see figure 26). Simultaneously the cardiomyocyte's TAT network was stained with Di-8-ANEPPS before confocal imaging. The surface of left ventricular cardiomyocytes isolated from control patients possessed a relatively intact surface structure while cardiomyocytes from DCM and ICM patients, though practically at the end stage of HF, still exhibited a degree of visible surface structures. These surface structures were not increased by the presence of LVADs, but showed similar Z-groove index values to the cells from unsupported hearts (see figure 26). Ventricular cells from control patients exhibited the highest presence and order of TAT network structures, while cells from DCM and ICM hearts showed significantly lower TAT density (~51% and ~50% respectively) and regularity (~77% and ~72% respectively) in comparison to control patient hearts (see figure 27). The loss of TAT density and T-tubule regularity was comparable between the two cardiomyopathies without LVADs. It was however surprising to find that the TAT density in human cardiomyocytes from DCM patients who were equipped with a LVAD was actually slightly higher than in MV cardiomyocytes (~30%) whereas the LVAD had no significant effect on the T-tubule regularity nor on cardiomyocytes from ICM patients (see figure 28).

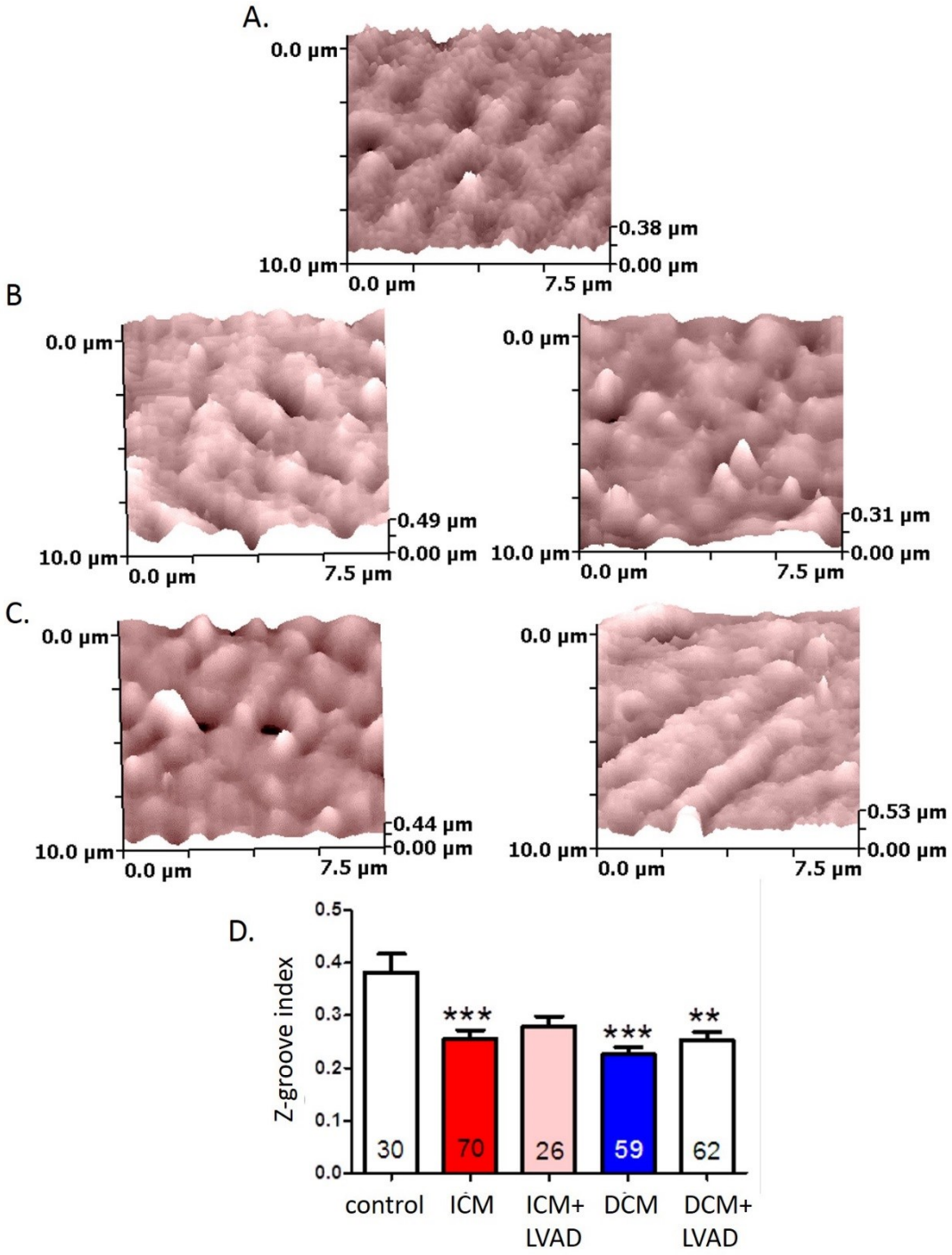

Figure 26 Topography of human, ventricular cardiomyocytes from MV surgery and transplant patients. 10x10 µm SICM surface scans of a ventricular cardiomyocyte isolated from (A.) a patient who underwent MV surgery; (B.) patients with ICM without (to the left) and with (to the right) a LVAD or (C.) from patients with DCM without (to the left) and with (to the right) a LVAD. (D.) Z-groove index of cardiomyocytes isolated from MV surgery patients as well as ICM and DCM patients with and without LVADs. Surface scans of the ICM and DCM cardiomyocytes with LVADs and the Z-groove index histogramm were kindly provided by Dr. Jose Sanchez Alonso-Mardones (Imperial College London). Statistical one way ANOVA test followed by Bonferroni correction post-hoc testing, ***p<0.001, **p<0.01.

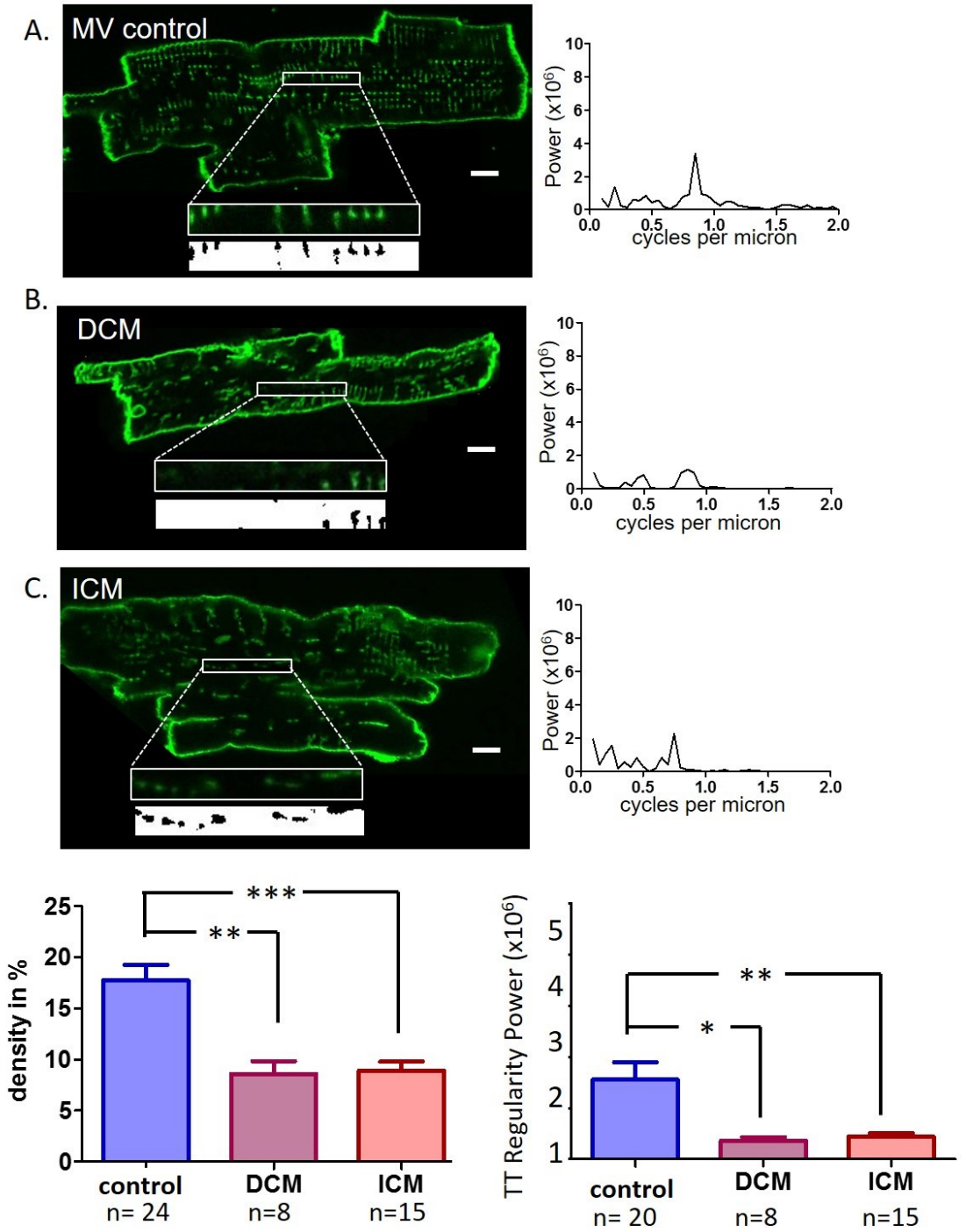

Figure 27 Human TAT structure in ventricular cardiomyocytes. (A.) From top to bottom: Representative confocal images of the TAT network with 40x5 µm areas of interest blown up 2.65 times together with their binarised counterparts of human ventricular cells from MV replacement surgery; a human ventricular cell from a DCM patient; a human ventricular cell from an ICM patient; scale bars equal 10µm. To the right: Power peaks of the corresponding T-tubular regularity. (B.) TAT network density in MV control cells, DCM cells and ICM cells. (C.) T-tubule regularity in MV control cells, DCM cells and ICM cells. n=number of single cells measured, number of donor patients n=2-4. Bars represent mean values ± standard error of the mean. Statistical one-way ANOVA test followed by Bonferroni correction post-hoc testing, ***p<0.0001, **p<0.001, *p<0.05.

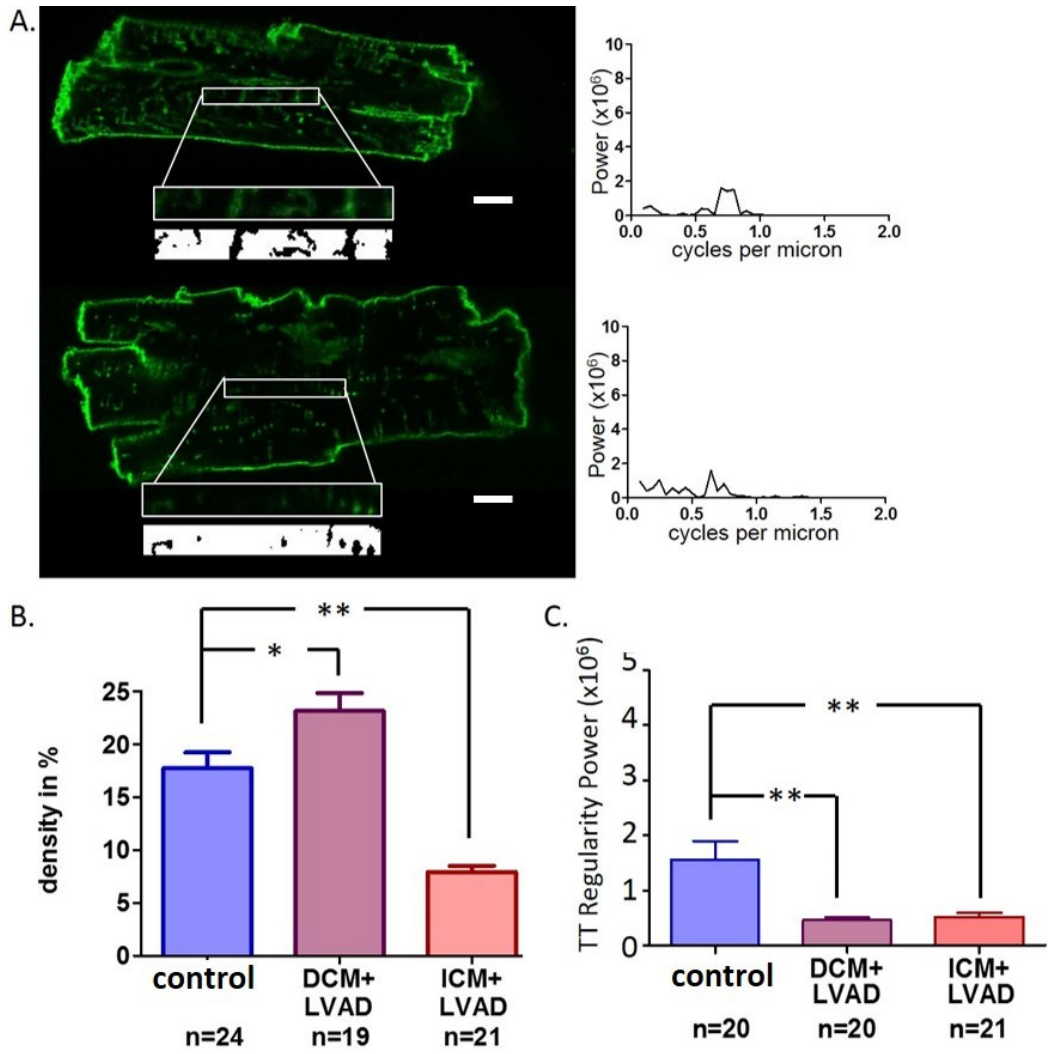

Figure 28 Human TAT structure in ventricular cardiomyocytes from failing hearts with LVADs. (A.) From top to bottom: Representative confocal images of the TAT network with 40x5 µm areas of interest blown up 2.65 times together with their binarised counterparts of human ventricular cells from a DCM patient with a LVAD; from an ICM patient with an LVAD; scale bars equal 10µm. To the right: Power peaks of the corresponding T-tubular regularity. (B.) TAT network density in MV control cells, DCM cells and ICM cells. (C.) T-tubule regularity in MV control cells, DCM cells and ICM cells. n= number of single cells measured, number of donor patients n=2-4. Bars represent mean values ± standard error of the mean. Statistical one-way ANOVA test followed by Bonferroni correction post-hoc testing, **p<0.001, *p<0.05.

3.6. Discussion: Cardiomyocyte structures

3.6.1. Cardiomyocyte structure during HF progression:

HF is generally a progressive disease (Dickstein et al. 2008). However, the majority of studies only concentrate on the TAT network disruption at the end stages of HF and fail to elucidate the progressive alterations in the TAT network, which occur during disease progression (Wagner et al. 2012; Wei et al. 2012). Chapter 3 described the structural alterations taking place in cardiomyocytes in the progression from compensated hypertrophy (at 4 weeks post-MI) to decompensation (at 8 weeks post-MI) and at the end stage of HF (at 16 weeks post-MI) in rat cardiomyocytes after the induction of a chronic MI by left anterior descending artery (LAD) ligation. The concept of an advancing course for HF in our MI model has been corroborated by reports from groups using the same experimental model where the advanced signs of HF were observed after 8 week post-MI in rat e.g. reduction of SERCA2 gene expression (Zarain-Herzberg et al. 1996), sympathetic nerve stimulation (Ganguly et al. 1997) and whole heart morphological and functional changes (Nahrendorf et al. 2001).

In the acute period of cardiac injury, post-MI, cardiomyocytes are exposed to increased wall stress and neuro-hormonal activation (Yan et al. 2008; Clerfond et al. 2015). This instigates hypertrophic signaling and the development of a hypertrophic phenotype such as was observed already at 4 weeks post-MI in whole heart and at 8 weeks post-MI in single cardiomyocyte volume in this thesis. T-tubular structures are able to respond to load via a stretch sensitive complex (Knoll et al. 2002). The MI induced mechanical overload induced in this study via ligation of the left anterior descending aorta could trigger a decrease in T-tubule regularity and density as was also already observed at 4 weeks post-MI in this thesis and persisted until 16 weeks post-MI. Our SICM scans showed that Z-grooves reduced steadily over the 16 week observation period following MI. The formerly clear surface structures on cells were exchanged with areas of a smoother appearance and the gradual disappearance of T-tubule openings. Disruption of the highly ordered cardiomyocyte structure, in particular by disorganisation and partial loss of the TAT network in the LV, has been observed in a variety of MI models and was linked to the impaired contractility observed in HF due to asynchronous Ca^{2+} handling in cardiomyocytes (Heinzel et al. 2008; Wei et al. 2010; Wagner et al. 2012) as well as βAR dysregulation (Nikolaev et al. 2010). However, a recent study of the TAT network using a high resolution stimulated emission depletion microscopy (STED) system also reported a progressive reorganisation and partial elongation of T-tubules at 4 and 8 weeks post arterial ligation in mice (Wagner et al. 2012). Such changes were undetectable by conventional confocal microscopy and hence could not be assessed in this thesis. The

significance of the localisation of βARs inside the TAT network and the consequences of TAT network alterations on βAR-dependent cyclic nucleotide signalling will be expanded upon in the following chapters 4 and 5. One intriguing observation made during the progressional stages of hypertrophy towards HF is the rise in longitudinal elements of the TAT network (Wagner et al. 2012) which was also observed in the study described herein: At 4 and 8 weeks post-MI an increased number of longitudinal TAT elements appeared which may reflect a compensatory alteration. This early increase in the number of longitudinal tubules is lost again at 16 weeks post-MI at the end stage of HF. HF has been shown to be accompanied by cardiomyocyte dedifferentiation and a reactivation of the fetal gene programme (Wagner et al. 2012). Therefore the structural remodelling observed may also reflect a return to a more 'fetal phenotype'. Interestingly, longitudinal elements have been shown to increase together with Cav3 protein expression (Wagner et al. 2012). A recent publication, which in HF shows increased formation of longitudinal depositions of α-actinin, a cytoskeletal protein vital for sarcomere formation might build a substrate along which the longitudinal tubules might form (Lichter et al. 2014). Hence after cardiac injury the TAT network undergoes progressive and complex structural remodelling which at first is compensatory but turns adverse at the later stages of HF. Investigating possible molecular mechanisms underpinning the early structural remodelling of cardiomyocytes, one of the proteins involved in the maintenance of T-tubules, JPH2, decreased dramatically as early as 4 weeks and remained low throughout the progression towards HF. JPH2 maintains the junctions between TAT elements and the SR (Gorelik et al. 2013). Structural proteins like JPH2 and Cav3 have been shown to be downregulated in hypertrophy and HF (Minamisawa et al. 2004). Though JPH2 and Cav3 appear to be associated (Minamisawa et al. 2004), knockdown of JPH2 did not induce any changes in Cav3 (Chen et al. 2013). Recently JPH2 ovexpression was shown to attenuate TAT network damage due to pressure oveload (Guo et al. 2014). In this work JPH2 was already decreased early on and hence remodelling of the TAT network may in part be triggered by down-regulation of JPH2. This suggestion is corroborrated by the finding that junctophilins appear to be partly responsible for the orientation of tubules in the TAT network (Bennett et al. 2013; Pinali et al. 2013). The functional consequences of the observed alterations in the TAT network described in chapter 3 will be elaborated upon in chapters 4 and 5 in regard to cAMP and cGMP second messenger signalling. As was mentioned in the general introduction (see chapter 1, paragraph 1.7.1.) there are more possible candidates which could be crucially altered during HF progression such as tropomyosin, BIN1 and Tcap. Expression of two of these candidates, BIN1 and Tcap, has been shown to be decreased during HF (Lyon et al. 2012). Tcap has been indicated as a regulator of T-tubule formation according to the mechanical load which the respective cells experience (Zhang et al. 2009), whereas BIN1 appears to serve as T-tubule maintainer and membrane curvature inducer (Hong et al. 2010).

Interestingly gene therapy with SERCA2a in HF cells lead to structural reverse remodelling and a return of BIN1 and Tcap levels comparable to control cells but not of JPH2 protein levels (Lyon et al. 2012).

3.6.2. Cardiomyocyte dedifferentiation due to long term culture:

It is well established, that primary cells in culture suffer from dedifferentiation (Mitcheson et al. 1998). Especially the FRET experiments described in this thesis in the following chapters have to be interpreted with this fact in mind. During the structural investigation of cardiomyocytes after only 1h of culture in comparison to cardiomyocytes after 48h of culture with and without viral transfection we revealed TAT network damage similar to that observed in cells freshly isolated from animals with myocardial infarction. This is a big limitation when it comes to the investigation of the physiological role of the cardiomyocyte structure in physiological function. At the same time the surface structures of cardiomyocytes were still intact.

3.6.3. Colchicine and cytochalasin D effects on cardiomyocyte structure

It has been shown repeatedly, that primary cell lines in culture progressively lose their physiological phenotype and dedifferentiate (Tian et al. 2012; Mitcheson et al. 1998). A recent study claimed that submicromolar levels of the filamentous actin polymerisation inhibitor cytochalasin D can counteract culture related cardiomyocyte dedifferentiation. While testing the validity of this claim it was evident, that the T-Tubule regularity of cardiomyocytes still decreased in culture. However at the same time cardiomyocytes treated with cytochalasin D created increased longitudinal elements between their T-tubules, which kept the TAT network density similar to that in control cardiomyocytes.This might explain why prior reports did not see a functional change in cytochalasin D treated cells, as the longitudinal cells could compensate for the observed loss loss in T-tubule regularity (Tian et al. 2012). A similar increase in longitudinal elements can also be observed in cardiomyocytes stemming from hearts during their progression towards HF but not at the end stage of HF. As a consequence the data obtained from the cytochalsin D treatment might be more insightful into the pathophysiology of chronic HF than expected. Interestingly, a recent study showed that α-actin forms increased longitudinal depositions in the cytoskeleton during HF (Lichter et al. 2014). The increased number of longitudinal tubules observed in this thesis after cytochalasin D treatment and in HF cells could therefore form along these α-actin depositions. So if the cytochalasin D used here solely affected the actin filament polymerisation and had indeed no other side effects, then it could be interpreted from the data presented here, that it is disturbed

actin filament polymerisation, which supports the generation of longitudinal elements in between T-tubules. This deduction is based on the assumption that the microtubuli are not the target of the drug cytochalasin D therefore they should be unaffected and potentially should still be able to rearrange the TAT network composition, while the actin filaments are blocked from polymerising. Another study approach in chapter 3 was to test the importance of the microtubule cytoskeleton in regard to the structural integrity of the TAT network by applying the microtubule polymerisation disruptor colchicine. Colchicine treatment of control cardiomyocytes significantly decreased the β-tubulin amount. Colchicine furthermore lead to a decrease in the TAT network density and T-tubule regularity but not of the surface structure of cardiomyocytes. In the case of HF where tubulin is supposedly increased it might not lead to TAT network deterioration but could indeed serve to conserve the cardiomyocyte structure (Nishimura et al. 2006). As colchicine was applied for 1h only before confocal imaging of the cells the colchicine data also implies that the TAT network is under constant reformation which is facilitated by the cytoskeleton. Therefore chapter 3 also demonstrated the importance of the microtubule and filament cytoskeleton in maintaining the TAT network structure. Through the treatment of the cytoskeleton in cardiomyocytes with colchicine and the aforementioned cytochalasin D one can affect the intactness of the TAT network and it can either be chemically deteriorated or to some degree stabilized for cell culture. The aforementioned results and discussion lead to the additional observation that the surface structures of cardiomyocytes do not depend on the internal TAT network structures and vice versa. It therefore should be concluded, that these two structural aspects arise and are maintained by different factors. In case of the TAT network the microtubule and filament cytoskeleton is a likely candidate of such a factor as was shown with the cytochalasin D and colchicine treatment of cardiomyocytes, whereas the surface structure determinants might be of a more mechanical nature. This deduction is based on the observation that surface structures are significantly decreased during HF progression but neither by chemical treatments nor by long term culture (48h) in which the cells are immobilized by the reduced presence of Ca^{2+} needed for contraction.

3.6.4. Human cardiomyocyte TAT network structures from dilated cardiomyopathy patients benefit from LVADs

Human cardiomyocytes from the left ventricle possess similar structures to rat cardiomyocytes. These structures however undergo strong structural deterioration in all types of defined human cardiomyopathies. Like in rat the loss of TAT network structures in humans was previously associated with decreased contractility and Ca^{2+} homogeneity (Lyon et al. 2009). In this thesis it is was hard to determine just how similar healthy human cardiomyocyte

structures are to healthy rat cardiomyocyte structures for lack of healthy, human control samples. In their stead cardiomyocytes from patients undergoing MV replacement surgery were obtained and designated as control. Prior work by our group showed that unfailing human cardiomyocytes possess a Z-groove index of approximately 0.82 (Lyon et al. 2009), which is twice as high as the value obtained in cardiomyocytes from MV patients. Unfortunately the same study did not measure the TAT network density and T-tubule regularity in a similar fashion as was done in this theses, but analogous decreases in the two values would be expected in cardiomyocytes from non-failing versus MV patient hearts. Failing human cardiomyocytes were obtained from patients with DCM or ICM with and without LVADs. Both DCM and ICM cardiomyocytes without an LVAD showed an even further decrease in the Z-groove index and TAT network presence than MV cardiomyocytes. The most surprising finding during the investigation of human cardiomyocyte structures was the observation that DCM patients with LVADs had a slightly increased TAT network density but a decreased T-tubule regularity in comparison to MV patients. This was due to a change in alignment of the T-tubules in the DCM plus LVAD patients. In ICM patients the LVAD showed no such effect on structure. This might be an indication that an LVAD in DCM patients is more beneficial than in patients with ischemic injuries. It would be interesting to observe if these differences can be reiterated to a differential microRNA expression profile between the two cardiomyopathies as it was reported that the LVADs can reinstate a less pathological microRNA profile in humans (Matkovich et al. 2009).

3.6.5. Reverse structural remodelling

As was elaborated upon in chapter 3 and in previous publications from our group (Lyon et al. 2009; Ibrahim et al. 2012) structural deterioration of cardiomyocytes is a commonly observed feature in cardiomyopathies from various species, including human and rat cardiomyocytes. Though it is not yet fully understood if this structural deterioration is cause or effect (or both) of the functional insufficiency observed in HF, ways to reverse remodel the setup of the failing myocardium are thought to potentially remedy HF. Our own group has shown that SERCA2a gene therapy (Lyon et al. 2012) and mechanical unloading (Ibrahim et al. 2012) can rescue the structural phenotype as well as the functional efficiency of cardiomyocytes in regard to Ca^{2+} handling and contractility to some extent. The reason for this reverse structural as well as functional remodelling is thought to be a partial return of β_2ARs, which had emigrated out of the T-tubules, as well as a return in expression of the structural proteins BIN1 and Tcap. Interestingly during the SERCA2a gene therapy study expression of the structural protein JPH2 was not reinstated (Lyon et al. 2012). A recent study in mouse which uses JPH2 overexpression to determine its role in cardiac structure and function (Guo et al. 2014) yields

a complementary insight into our SERCA2a study. In this study JPH2 overexpression lead to a rise in physical bridging of the SR with the T-tubules and a rise in NCX1 protein levels in control cardiomyocytes. This was however not accompanied by a rise in SERCA2a showing that JPH2 and SERCA2a and their associated effects on the TAT network are independent of each other. The same study also showed that JPH2 overexpression is protective against pressure overload induced cardiac injury and damage to the TAT network (Guo et al. 2014). It remains to be determined if JPH2 overexpression in a model of end stage HF could lead to reverse functional and structural remodelling.

3.6.6. Conclusion regarding cardiomyocyte structure

The structural investigation in chapter 3 elucidated the progressional alterations which the surface membrane structures of cardiomyocytes experience during the progression from health towards HF after a MI and identified a drastic decrease in the structural protein JPH2 early after myocardial injury. The potential consequences of the maintained lack in JPH2 levels on β_2AR-dependent cAMP signalling will be reiterated in chapter 4 (see chapter 4, paragraph 4.3.6). Chapter 3 furthermore showed that treatment with cytochalasin D can affect the TAT network via the cytoskeleton and that it is potentially the microtubule cytoskeleton which plays a role in forming longitudinal elements, which are transiently increased during HF progression. Interstingly a recent study showed that microtubule are also important for positioning JPH2 proteins between the T-tubules and the SR (Zhang et al. 2014). The microtubule network has been shown to be increased in HF (Nishimura et al. 2006) and in this study we showed that colchicine treatment of cardiomyocytes can directly affect the TAT network by decreasing the number of microtubules. The focus of chapter 3 was on cardiomyocyte structure, however it only marginally investigated the involvement of various proteins in cardiac structure. Though a list of candidates have been identified (BIN1, Tcap, Cav3, etc.), definite information is still lacking on which proteins are the major factors for structural maturation, maintenance and reformation of the TAT network (Ibrahim et al. 2011). In our experimental animal model as well as in prior publications (Bennet et al. 2013; Zhang et al. 2014) the expression of the structural protein JPH2 decreased early after the induction of myocardial injury and therefore attracted our attention. We believe it is strongly involved in worsening the progression of cardiomyocytes towards HF.

Chapter 4: Cardiomyocte β_2AR dependent cAMP signalling in health and during HF progression

4.1. Introduction

The previous chapter established structural aspects of cardiomyocytes, which are important for the physiological arrangement of βARs on different sites of the sarcolemma and for efficient excitation-contraction coupling of cardiomyocytes. Utilizing SICM and FRET imaging our group recently showed that there is a clear segregation of the β_1AR and β_2AR location on the plasma membrane of healthy cardiomyocytes. While the β_1AR are distributed throughout the sarcolemma β_2ARs solely inhabit the T-tubule openings of cardiomyocytes (Nikolaev et al. 2010). As was shown before these T-tubule structures are severely lost or altered during the progression of HF (Wagner et al. 2012; Wei et al. 2012). In healthy cardiomyocytes, ligand binding to the β_2ARs generates highly localised cAMP pools, which regulate and are regulated by confined, functional compartments, which are different from those of the diffusive β_1AR dependent cAMP pools (Nikolaev et al. 2006). These compartments consist, among other proteins, of PDEs, protein kinases and other downstream targets of cAMP and their arrangement changes drastically at the end stage of HF. This rearrangement is reflected in strongly downregulated β_1AR levels (Lohse et al. 2003) as well as β_2ARs receptor redistribution from the T-tubules to the crests (Nikolaev et al. 2010). Therefore, pathological remodelling of the TAT network at the end stage of HF is strongly associated with dysregulated βAR-dependent cAMP signalling. In addition to the structural aspects of cardiomyocytes, βAR-dependent cAMP compartmentation is achieved by the position and activity of its producing ACs and its degrading PDEs, which are associated with them (Stangherlin and Zaccolo 2012). The spatial loss of β_2AR-dependent cAMP compartmentation in end stage HF leads to the activation of unphysiological downstream signalling targets. When and to what extent β_2AR redistribution and loss of compartmentation of its associated cAMP pools appears during the progression of left ventricular hypertrophy to the end stage of HF has not been investigated before. Therefore chapter 4 highlights the importance of stringently controlled and spatially confined β_2AR dependent cAMP signalling and investigates the pathophysiological changes which occur in cardiomyocyte β_2AR signalling during the progression of HF. As in the preceding chapter a model of progressive MI was used for single cell isolation and the progressive time points after MI were defined as compensatory (4 weeks post-MI), decompensated (8 weeks post-MI) and at the end stage of HF (16 weeks post-MI). The standard way of measuring the ubiquitous, second messenger molecule cAMP used to be biochemical studies such as radioligand binding after cell and tissue lysation. Though these studies proved informative in regard to the levels of total cAMP produced in various

cell and tissue types as well as pathologies they could not reveal the convoluted, spatiotemporal

dynamics of second messenger signalling at specific locations and concentrations in live cells. Fortunately the requirement of second messenger detection approaches in live cells and in real time was increasingly realized by both the artificial introduction of cyclic nucleotide-gated channel (CNGC) based measuring approaches as well as the development of specific FRET biosensors (Sartiani et al. 2002, Nikolaev et al. 2004). For the investigation of the β_2AR dependent cAMP signalling levels in control cardiomyocytes and the changes occurring during the progression of HF the cytosolic or plasma membrane bound FRET sensor Epac2-camps was used. Basal cAMP levels and maximally detectable FRET responses as well as the major cAMP degrading PDEs were assessed in control cardiomyocytes. Ensuing whole cell and localised cAMP FRET measurements were conducted in cardiomyocytes isolated from control hearts and at 4, 8 and 16 weeks post-MI to determine progressive alterations in cAMP levels and diffusion in the cytosol.

4.2. Methods and Materials

4.2.1. Cardiomyocyte transduction with cAMP FRET biosensors

After their attachment to the glass bottom of laminine coated, glass-bottom dishes adult cardiomyocytes from age matched control rats and rats at 4, 8 and 16 weeks post-MI were transduced with virus encoding the cytosolic cAMP FRET sensor Epac2-camps or the plasma membrane bound cAMP FRET sensor Epac2-camps (see figure 29) at a multiplicity of infection of 300-500 virus particles per cell for 48h to determine β_2AR dependent cAMP levels and diffusion after local and global catecholaminergic stimulation.

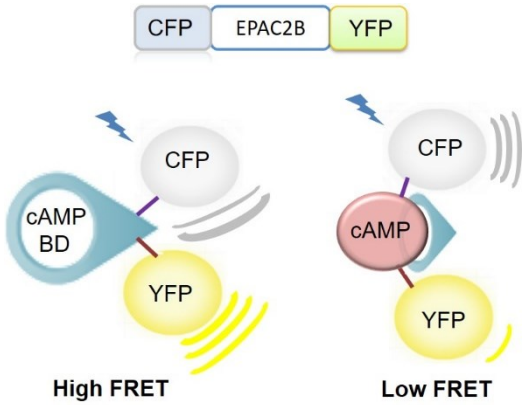

Figure 29. The FRET measurement principle of relative cAMP levels using the FRET construct EPAC2-cAMPs. At the top: The construct is based on a cyan fluorescent protein CFP, the cAMP binding domain of the type 2 exchange protein activated by cAMP (EPAC2) and a yellow fluorescent protein (YFP). Left hand side: In the absence of cAMP the FRET donor CFP gives part of its energy in a non-radiative fashion to the proximal, FRET acceptor YFP. Right hand side: The presence and binding of cAMP leads to a conformational change of the FRET biosensor, which removes YFP from the proximity of CFP, which in turn can no longer transfer any energy onto YFP.

4.2.2. Determining basal and maximally inducible cAMP FRET response

The level of basal cAMP in primary, transgenic mouse cardiomyocytes expressing the cAMP FRET sensor Epac1-camps lies around 1µM (Börner et al. 2011). In order to determine how high the relative, basal cAMP levels are in rat cardiomyocytes after 48h of transduction with the cAMP FRET sensor Epac2-camps, ACs were blocked with 100µM MDL-12,330A hydrochloride while recording the FRET signal. Consecutively the maximally inducible cAMP FRET response of whole cells was measured by applying the non-degradable cAMP analogue 8-Br-2′-*O*-Me-cAMP. Though it has to be mentioned that the affinity of the FRET sensors to cAMP analogues is different to actual cAMP molecules the analogue can still give an approximate indication of how high the FRET amplitude can become in a certain cell type and under certain conditions. It also allows determination of the variability of detectable basal and

maximally inducible cAMP levels in cultured cardiomyocytes, which might be a lot higher in transduced cells than in cells from transgenic animals due to uneven FRET sensor expression (Börner et al. 2011).

4.2.3. Whole cell β_2AR dependent cAMP FRET imaging in cardiomyocytes

Whole cell β_2AR dependent cAMP signals were measured in cardiomyocytes expressing the cytosolic Epac2-camps FRET biosensor. For this a custom-made, gravity based perfusion system was employed to deliver and remove drugs into and from the external solution. During calibrations, complete replacement of extracellular solution was achieved in less than 5 seconds. To avoid cross-stimulation of β_1ARs all FRET experiments were performed with solutions containing 100nM of the β_1AR blocker CGP20712A. Whole-cell β_2AR stimulation was achieved with 100nM ISO; and subsequent whole cell AC stimulation was achieved with 5μM NKH477. Experimental whole cell cAMP signal measurements were conducted together with Dr. Sergiy Tokar (Imperial College London). The analysis of the resulting FRET data was primarily performed by me. The FRET data was corrected for bleed-through of CFP emission into the YFP spectrum and analysed as it was described previously (Nikolaev et al. 2010). In short the Micro-Manager files were opened and regions of interest were drawn around the whole cell. Then the changes in pixel intensity of the recorded FRET images from the YFP and the CFP channel were calculated over the recorded time and their ratio was determined. The FRET signal was recorded using a Hamamatsu ORCA ER camera (Hamamatsu) and Micro-Manager 1.4 with custom-written FRET analysis plugins. The obtained raw data was processed with the use of baseline correction functions using Origin Pro 8.5 (Origin Lab Corporation) and recurring noise was reduced via 3 Median smoothing. The FRET response was calculated by averaging the values of 10 frames of the baseline signal and 10 frames of the response signal and by subtraction of the averaged response from the averaged baseline.

4.2.4. Testing of whole cell PDE4 regulation of β_2AR dependent cAMP levels during HF progression

Measurements of β_2AR-dependent cAMP FRET signals in control cardiomyocytes and cardiomyocytes 4, 8 and 16 weeks post-MI during the application of the PDE4 blocker Rolipram (ROLI) were conducted. For this cells were treated with 100nM of the β_1AR blocker CGP207 12A for at least five minutes before 100nM ISO followed by a bolus of 10μM/L of the specific PDE4 blocker ROLI and 100μM of the non-selctive PDE inhibitor 3-Isobutyl-1-methylxanthine (IBMX) were directly applied into the cell bath while recording the FRET

response. Measurements and analysis were conducted together with Dr. Sergiy Tokar (Imperial College London). Just as before the obtained raw data was processed by applying baseline correction functions from the software Origin Pro 8.5 (Origin Lab Corporation). Recurring noise was reduced via 3 Median smoothing. The FRET response was calculated by averaging the values of 10 frames of the baseline signal and 10 frames of the response signal and by subtraction of the averaged response from the averaged baseline.

4.2.5. FRET/SICM imaging of locally stimulated β_2AR dependent cAMP levels in T-tubule openings and on cell crests.

Topography images of 10x10 µm areas of age matched control cardiomyocytes and cardiomyocytes 4, 8 and 16 weeks post MI were obtained using SICM to elucidate the position of T-tubule openings and crests. After blocking of β_1ARs through the superfusion of 100nM CGP20712A for at least 5 min β_2ARs were stimulated locally for 50 seconds via the SICM nano-pipette containing 50µM ISO and 50µM CGP20712A by applying pressure as described (Nikolaev et al. 2010) or via voltage application by switching the relative electrical potential inside the scanning nano-pipette from negative (-200 mV) to positive (400mV). A gravity based perfusion system continuously replaced the bath solution in less than 5 seconds. The drugs were applied either to the T-tubule openings or to the crest areas, the coordinates of which were determined by observing SICM topography images. All measurements were conducted together with Dr. Sergiy Tokar (Imperial College London) except for additional experiments in control cardiomyocytes and cardiomyocytes at 16 weeks post MI, which were exclusively performed by myself. For these the nano-pipette was lowered to approximately 500 nm above the respective surface structures before applying the agonist via the aforementioned voltage switch. The FRET signal was recorded and analyzed as before by the use of baseline correction functions from the software Origin Pro 8.5 (Origin Lab Corporation) and recurring noise was reduced via 3 Median smoothing. As before the FRET response was calculated by averaging the values of 10 frames of the baseline signal and 10 frames of the response signal and by subtraction of the averaged response from the averaged baseline.

4.2.6. cAMP signal diffusion study

To study cAMP diffusion inside the cytosol cardiomyocytes from age matched control hearts and hearts at 4, 8 and 16 weeks post-MI were transduced with virus encoding the cytosolic FRET sensor Epac2-camps. To ascertain, that the FRET sensor itself did not lead to a further diffusion of the cAMP FRET signal by either its own movement or by helping cAMP to evade

degradation by PDEs seperate control cardiomyocytes were transduced with virus encoding the plasma-membrane bound FRET sensor Epac2-camps. Then propagation of the cAMP signal was studied after localized β_2AR stimulation via the nanopipette at different distances from the original nano-pipette stimulation site. For this FRET data was opened in Micro-Manager 1.4 and regions of interest (ROI) of about 15 microns width were drawn repeatedly at ever more distant areas to the nano-pipette. Then the FRET response amplitude was measured in these ROIs. The response was accounted as local when the amplitude of cAMP dropped by more than 50% when measured at a distance of 15 to 30μM from the pipette. Otherwise the response was considered as diffusing throughout the whole cardiomyocyte. As before the obtained data was processed by using the baseline correction functions in the software Origin Pro 8.5 (Origin Lab Corporation) followed by 3 median smoothing. Additionally data obtained in our group in a study of SERCA2a gene therapy in the same chronic, rat MI model used in this thesis was reanalyzed in regard to cAMP diffusion. In the study SERCA2a induced reverse structural remodeling in cardiomyocytes which lead to a reinstatement of the TAT network and a return of β_2ARs from the crest into the T-tubules (Lyon et al. 2012). Also, in order to test if coupling to Gi is involved in β_2AR-dependent cAMP signal compartmentation, pertussis toxin (PTX) treated control cardiomyocytes from another prior study (Nikolaev et al. 2010) were reanalyzed in regard to cAMP diffusion. PTX adds an ADP-ribose moiety onto the the α subunit of Gi and prevents β_2AR coupling with Gi and has been shown to increase β_2AR-dependent cardiomyocyte contractility (Xiao et al. 1995).

4.3. Results:

4.3.1. Measurable cAMP levels are relatively uniform in transduced cardiomyocytes

Even in an unstimulated state cardiomyocytes *in vivo* and *in vitro* produce basal levels of cAMP. Due to culture conditions these basal secondary messenger levels could presumably be altered and skew cAMP measurements if the FRET sensor is differentially saturated at the beginning of FRET response measurements (Börner et al. 2011). Hence cardiomyocytes were treated with the AC inhibitor MDL-12,330A to deplete cAMP levels as far as possible through PDE degradation. This treatment was followed up with the application of the non-degradable cAMP analogue 8-Br-2′-*O*-Me-cAMP to elicit the maximally detectable FRET ratio response by the cAMP biosensor Epac-cAMPs. Though the sample numbers are quite low, the data shows that basal cAMP levels are low in comparison to maximally inducible cAMP levels (see figure 30).

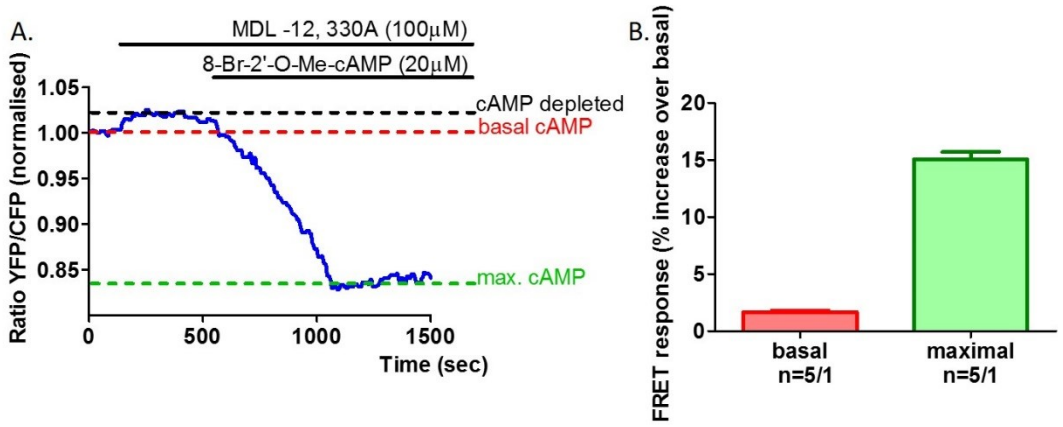

Figure 30 Determination of basal and maximally inducible FRET responses in isolated cardiomyocytes. (A.) Representative FRET signal curve of a cardiomyocyte expressing cytosolic Epac2-camps showing FRET signal under a cAMP depleted state (black dotted line) obtained by blocking all adenlylate cyclases with the inhibitor MDL-12, 330A, the level of basal cAMP (red dotted line) as is measured at the beginning of the recording as the baseline and the maximally inducible cAMP FRET signal (dotted green line) by consecutive cell perfusion with the cell membrane permeable, cAMP analogue 8-Br-2'-O-Me-cAMP. (B.) Basal and maximally inducible Epac2-camps FRET response. n= number of single cells measured / number of animals utilised for testing. Bars represent mean values ± standard error of the mean.

4.3.2. β_2AR-dependent whole cell cAMP levels alter during HF progression

To assess relative, whole cell β_2AR-dependent cAMP levels and their alterations during the progression of HF cardiomyocytes expressing the cytosolic cAMP FRET biosensor Epac2-camps were stimulated with ISO and the AC activator NKH477 after β_1AR inhibition with CGP20712A. The results showed that whole cell β_2AR-dependent cAMP levels were decreased significantly by about 30% as soon as 4 weeks post-MI. Contrary to what might have been expected at 8 weeks post-MI the level of response recovered to the β_2AR-dependent cAMP levels observed in control cardiomyocytes. Ultimately at 16 weeks post-MI a significant decrease in both β_2AR-dependent cAMP levels (~48%) and the overall AC produced cAMP levels (~63%) as compared to control cells was established (see figure 31).

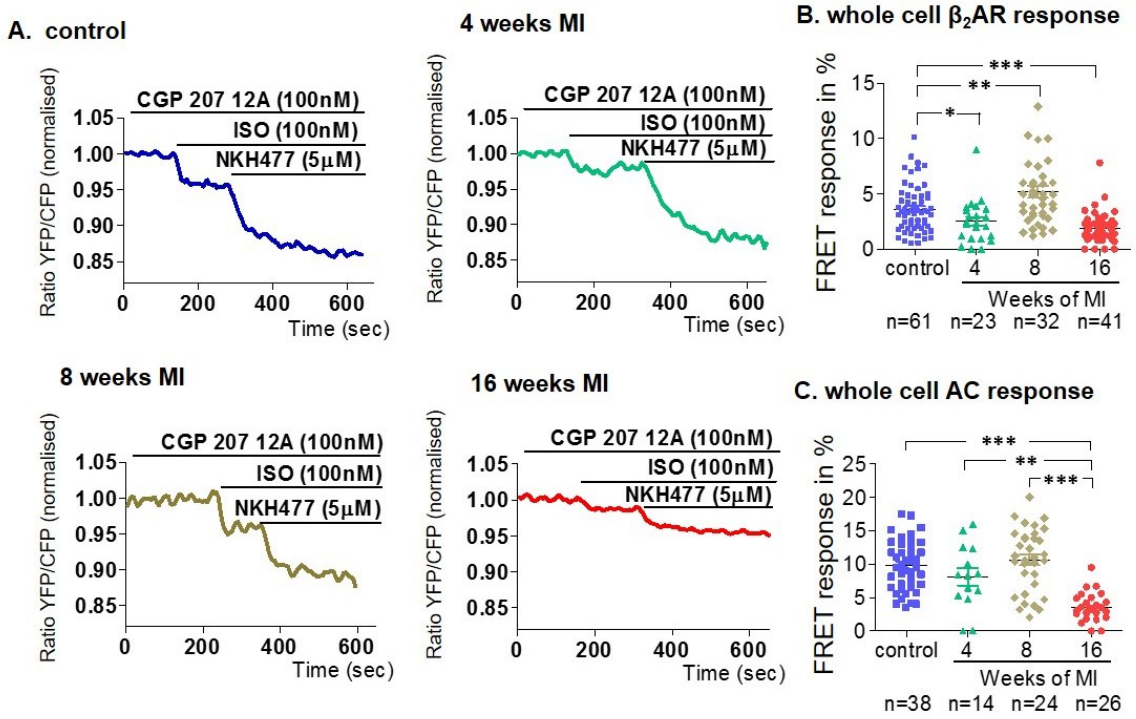

Figure 31 ß$_2$AR dependent and maximally inducible, AC dependent cAMP FRET signal during HF progression in age-matched and sham-operated control cardiomyocytes and at 4, 8 and 16 weeks post MI after whole cell ß$_1$AR inhibition with CGP 20712A and stimulation with ISO and NKH477. n= number of single cells measured. Animals utilised n≥4 for every time point. Scatter-blots with mean values indicated as black line. Statistical one way ANOVA test followed by Bonferroni correction post-hoc testing, ***p < 0.0001; **p < 0.001; *p < 0.05.

4.3.3. PDE4 regulates FRET detectable β_2AR-dependent cAMP levels during HF progression with unaltered activity

The cAMP hydrolysing PDE4 plays an important role in β_2AR-dependent cAMP signalling compartmentation (Lynch et al. 2007; Nikolaev et al. 2010). To uncover if PDE 4 activity in regard to β_2AR-dependent cAMP degradation changes in our model of progressive HF control cells and cells at 4, 8 and 16 weeks post-MI were stimulated with ISO after β_1AR inhibition with CGP20712A and then perfused with the specific PDE 4 inhibitor ROLI, before addition of the non-selective PDE blocker IBMX. According to our results the overall activity of PDE4 on β_2AR-dependent cAMP levels did not falter nor increase during the progression of HF according to the FRET measurements (see figure 32).

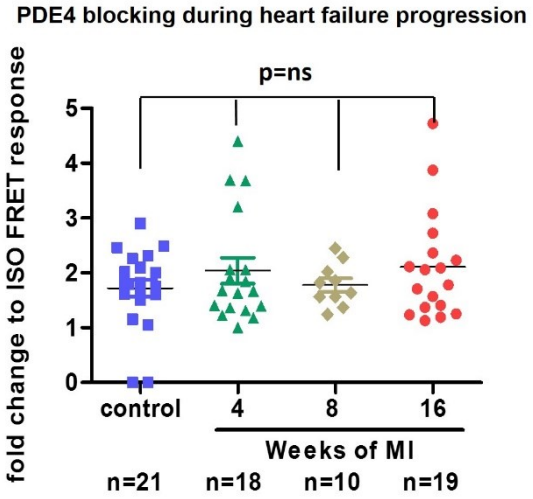

Figure 32 β_2AR-dependent cAMP FRET response stimulated with ISO after β_1AR inhibition followed by selective PDE4 inhibition. Activity of PDE4 determined as fold change increase in the cAMP FRET response induced by β_2AR stimulation with ISO after β_1AR inhibition and addition of the PDE4 inhibitor ROLI in age matched control and sham-operated control cardiomyocytes and cells at 4, 8 and 16 weeks post-MI. n= number of single cells measured. Animals utilised n≥4 for every time point. Bars represent mean values ± standard error of the mean. Statistical one way ANOVA test followed by Bonferroni correction post-hoc testing. p= ns; no significant difference.

4.3.4. Locally stimulated β_2AR-dependent cAMP levels and the position of β_2ARs change during HF progression

In healthy cardiomyocytes the β_2AR does not reside at the sarcolemmal membranes outside of the T-tubules. In end stage HF however this placing changes through the redistribution of a portion of the β_2ARs to the whole sarcolemma (Nikolaev et al. 2010). Presumably this redistribution takes place gradually during the development of end stage HF. Utilizing the same SICM/FRET combination our group utilized in the past to initially reveal the migration of β_2ARs out of the T-tubule openings (Nikolaev et al. 2010) the local β_2AR-dependent cAMP FRET response was measured after local receptor stimulation via the SICM nanopipette in T-tubules

and on crest areas of age matched control cardiomyocytes and cardiomyocytes 4, 8 and 16 weeks post-MI. As in a previous study from our group (Nikolaev et al. 2010) the β_2AR-dependent cAMP response in control cardiomyocytes was 5-fold larger in the T-tubule openings than when stimulated at the crests. At 4 weeks post MI the β_2AR-dependent cAMP in T-tubule openings decreased to approximately 28% of the response observed in control cells while no alteration took place at the crest areas. Consecutively at 8 weeks post-MI β_2AR stimulation at the cardiomyocyte crest elicited a surge of around 3 fold in cAMP levels compared to control cardiomyocytes. This indicates that the redistribution of β_2ARs takes place at the stage of decompensation (8 weeks post-MI). No further significant changes in locally stimulated β_2AR-dependent cAMP levels were observed at 16 weeks post-MI (see figure 33).

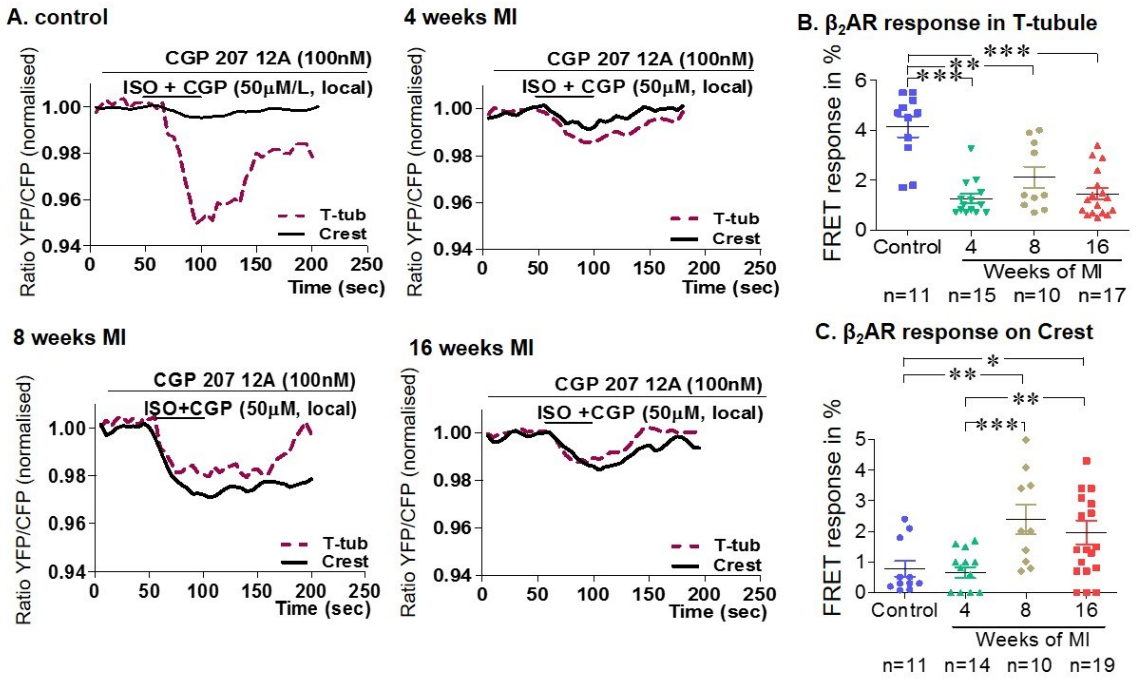

Figure 33 Progressive changes in the β_2AR dependent cAMP response to local stimulation at different time points after MI. (A.) Representative β_2ARs-cAMP FRET response curves after local β_2ARs stimulation either in T-tubule openings (red trace) or on crest areas (black trace) of age-matched and sham-operated control cardiomyocytes and cardiomyocytes 4, 8 and 16 weeks post-MI. Local β_2ARs-cAMP FRET response after agonist application into (B.) T-tubule or (C.) crest. n= number of single cells measured. Animals utilised n≥4 for every time point. Bars represent mean values ± standard error of the mean. Statistical one way ANOVA test followed by Bonferroni correction post-hoc testing, ***p < 0.0001; **p < 0.001; *p < 0.05.

4.3.5. β_2AR-dependent cAMP compartmentation is lost during HF progression

Using the SICM/FRET combination described before (Nikolaev et al. 2010) allows for the determination of β_2AR-dependent cAMP signal diffusion in cardiomyoctes after local stimulation in the T-tubule openings. To determine when β_2AR-dependent cAMP signal confinement is lost during the progression from health towards end stage HF the distance of

cAMP diffusion after local stimulation of β_2AR in cardiomyocytes was assessed in control cells and during the progression of HF after cardiomyocyte transduction with the cytosolic, freely diffusible FRET sensor Epac2-camps. Additionally control cells were transduced with virus encoding the plasma membrane bound cAMP FRET sensor Epac2-camps to ascertain that the freely diffusible cAMP sensor did not carry cAMP molecules farther than would be the case with an immobile sensor. There was no significant difference in the recorded cAMP diffusion distances observed in cardiomyocytes expressing either the cytosolic or plasma membrane bound cAMP FRET sensor (see figure 34). The results furthermore indicate, that while β_2AR dependent cAMP does not diffuse further than 15 up to 30µm after local stimulation in T-tubule openings in control cardiomyocytes the cAMP signal confinement is lost in cardiomyocytes as early as 4 weeks post-MI and remains this way until end stage HF (see figure 35).

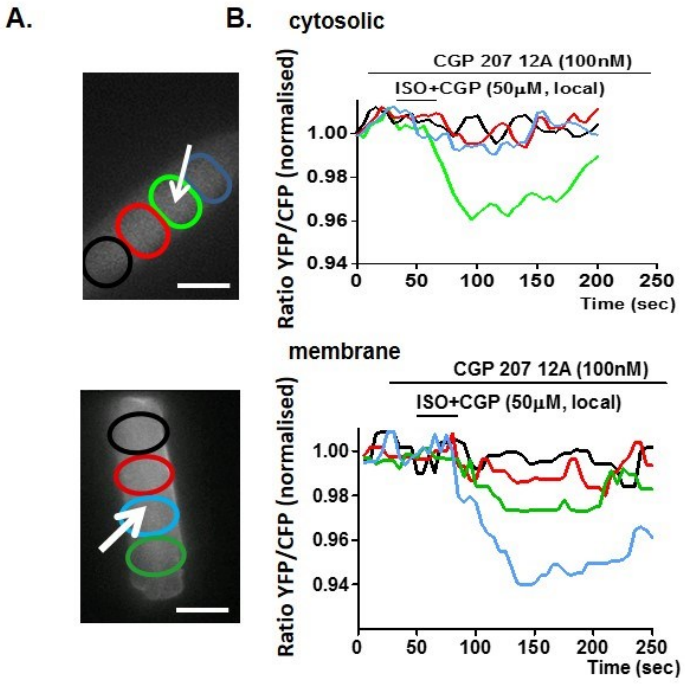

Figure 34 Diffusion of cAMP after local stimulation of β_2ARs in T-tubule opening of a cardiomyocyte expressing the plasma membrane bound cAMP sensor Epac2-camps. (A.) representative, fluorescent image of a cardiomyocytes expressing the plasma mebrane bound Epac2-camps cAMP sensor to indicate areas of interest (coloured ovals) situated at various distances from the point of stimulation (indicated by white arrows) where FRET was measured after local stimulation of β_2ARs; scale bars equal 20µm. (B.) corresponding FRET response curves in the four areas of interest as indicated on FRET cell images (same colours correlate to same areas of measurement) (n=6, from 2 animals).

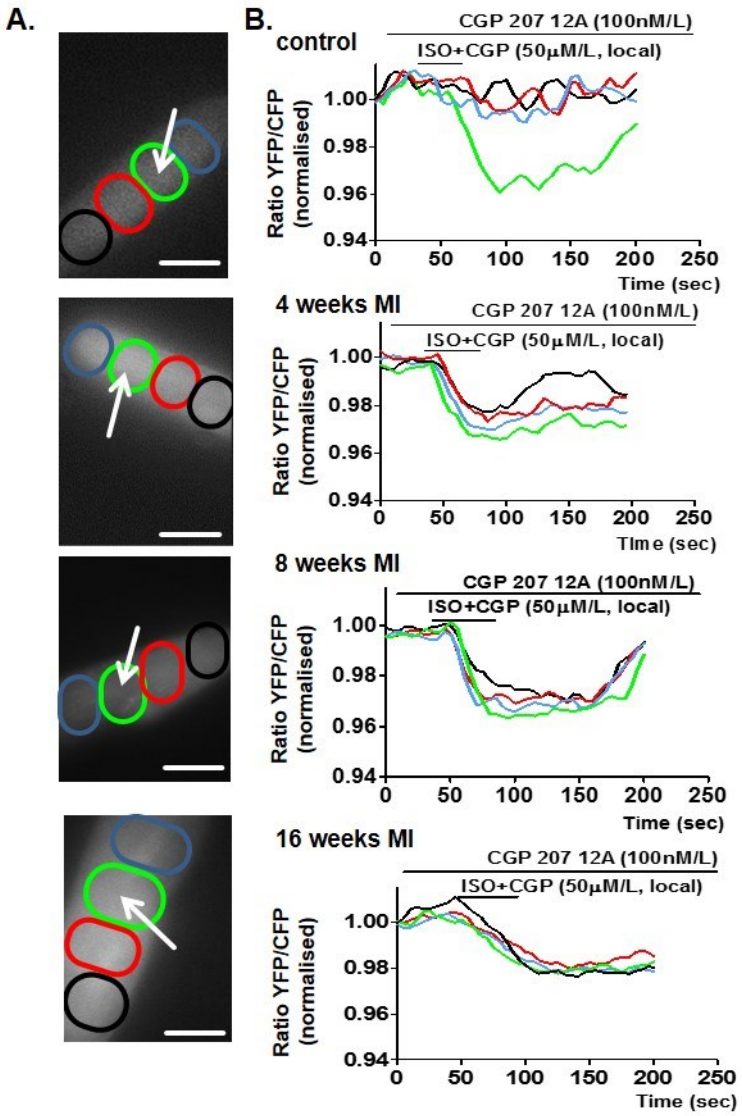

Figure 35 Diffusion of cAMP after local stimulation of β_2ARs in T-tubule openings at different time points after MI. (A.) representative, fluorescent images of cardiomyocytes expressing the cytosolic Epac2-camps cAMP sensor to indicate areas of interest (coloured ovals) situated at various distances from the point of stimulation (indicated by white arrows) where FRET was measured after local stimulation of β_2ARs; Scale bars equal 20 µm. (B.) Corresponding FRET response curves in the four areas of interest as indicated on FRET cell images (same colours correlate to same areas of measurement) (n≥10, from 4-5 animals each).

4.3.6. SERCA2a induced reverse structural remodelling does not confine β_2AR dependent cAMP signalling

Prior work conducted in our group introduced SERCA2a overexpression into the same rat HF model, which was used for this thesis, at 16 weeks post-MI (Lyon et al. 2012). This SERCA2a gene therapy led to reverse structural and functional remodelling, including the full to partial return of β_2AR into the T-tubules. To obtain further insight into β_2AR-dependent cAMP signalling after reverse structural remodelling, data from this prior work was re-examined in regard to cAMP diffusion as this had not been done before. Interestingly β_2AR-dependent

cAMP diffusion was not stopped in SERCA2a gene therapy treated cardiomyocytes but still diffused throughout the whole cytosol (see figure 36).

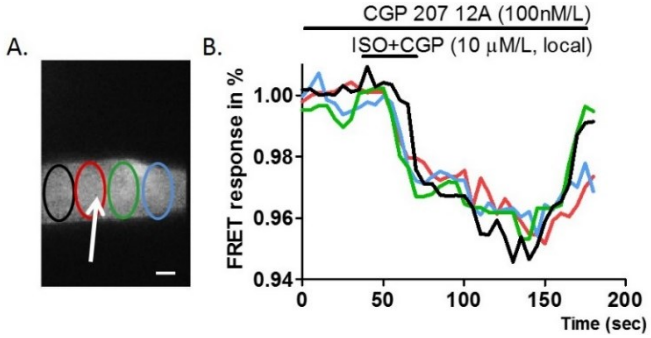

Figure 36 Diffusion of cAMP after local stimulation of β_2ARs in T-tubule opening of a cardiomyocyte expressing the cytosolic cAMP sensor Epac2-camps from a rat with chronic MI after SERCA2a gene therapy. (A.) representative, fluorescent image of a cardiomyocytes expressing the cytosolic Epac2-camps cAMP sensor to indicate areas of interest (coloured ovals) situated at various distances from the point of stimulation (indicated by white arrow) where FRET was measured after local stimulation of β_2ARs; Scale bar equals 5µm. (B.) corresponding FRET response curves in the four areas of interest as indicated on FRET cell images (same colours correlate to same areas of measurement) show no restoration of β_2AR-cAMP confinement to the restored TAT network (sample number n=14, from 4 animals).

4.3.7. PTX induced cAMP signal diffusion in control cardiomyocytes

It was shown that Gi protein is susceptible to receptor uncoupling via pertussis toxin treatment and that Gi uncoupling leads to an increase in β_2AR dependent cardiomyocyte contractility (Xiao et al. 1995). In a prior study our group treated cardiomyocytes with PTX before stimulating β_2AR-dependent cAMP signalling locally (Nikolaev et al. 2010). In order to investigate if Gi uncoupling might lead to the loss of β_2AR-dependent cAMP confinement the data was reanalyzed and showed that cAMP confinement was indeed lost after PTX treatment of cardiomyocytes (see figure 37).

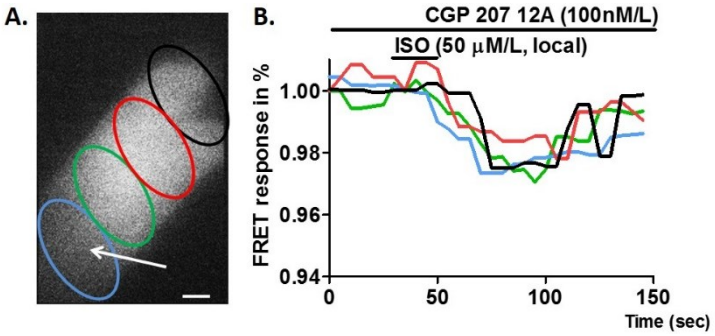

Figure 37 Diffusion of cAMP after local stimulation of β_2ARs in T-tubule opening of a control cardiomyocyte treated with pertussis toxin. (A.) representative, fluorescent image of a cardiomyocytes expressing the cytosolic Epac2-camps cAMP sensor to indicate areas of interest (coloured ovals) situated at various distances from the point of stimulation (indicated by white arrow) where FRET was measured after local stimulation of β_2ARs; scale bar equals 5µm. (B.) corresponding FRET response curves in the four areas of interest as indicated on FRET cell images (same colours correlate to same areas of measurement) show β_2AR-cAMP diffusion throughout the cytosol (n=9, from 3 animals).

4.4. Discussion: β_2AR-dependent cAMP signalling

4.4.1. Whole cell and localised β_2AR-dependent cAMP signalling

In the FRET study of whole cell β_2AR-dependent cAMP levels stimulated by ISO during β_1AR inhibition a drop in cAMP levels was observed at only 4 weeks post-MI. At 8 weeks post-MI this decrease reversed into a slight increase of cAMP levels in comparison to control cardiomyocytes. Finally at 16 weeks post-MI the cAMP signal again receded to cAMP levels below those observed in control cardiomyocytes (see figure 31). According to literature β_1AR expression declines in HF by up to 50% the number of β_2ARs however appears to be stable (Madamanchi 2007). Hence changes in β_2AR-dependent cAMP signalling can't be reduced to a matter of receptor quantity but derives from different sources. Likely candidates to alter β_2AR-dependent cAMP levels are the cAMP phospodiesterases (PDE), the β_2AR position and its connected coupling to the Gs and Gi proteins as well as the receptor associated ACs. As we have shown here it is PDE4 which predominantly degrades the β_2AR-dependent cAMP pools. According to FRET measurements the amount of β_2AR-dependent cAMP being degraded by PDE4 does not change during HF progression (see figure 32). So changes in PDE4 activity are ruled out as the major factor for altering β_2AR-dependent cAMP signalling during HF. The potential involvement of other PDEs in changed β_2AR-dependent cAMP levels during HF progression however still remains to be determined. Next the β_2AR position was determined during HF progression via a combination of FRET imaging and SICM scanning. The β_2AR localisation studies showed that β_2AR change their residence from the T-tubules to the crests at 8 weeks post-MI. This deduction is based on the observed drop of β_2AR-dependent cAMP levels in T-tubules at 4 weeks post-MI followed by an increase in β_2AR-dependent cAMP levels at the crest at 8 weeks post-MI (see figure 33). It is not entirely elucidated why β_2AR-dependent cAMP levels decrease at 4 weeks post-MI but the β_2ARs themselves could still be functional. By predominantly exhibiting G_i coupling at this stage β_2ARs for example could still play a role in cell physiology/pathophysiology by activating ERK dependent signalling and gene expression pathways (Kaya et al 2012). One factor that influences β_2AR-dependent cAMP levels during HF is the relocalisation of PKA which could potentially lead to increased receptor switching to Gi (Nikolaev et al. 2010). Also increased Gi-α subunit levels can decrease cAMP production directly by acting on ACs 5 and/or 6 and sequestration of Gs-α through the β and γ subunits as Gi is in excess of Gs in HF (Xiao et al. 2003). Hence the decrease of β_2AR-dependent cAMP levels at 4 weeks post-MI is assumed to stem from β_2AR uncoupling from Gs and potentially increased signalling over Gi in the T-tubule compartment. In contrast the increased whole cell β_2AR-dependent cAMP levels and local β_2AR-dependent cAMP levels at the cardiomyocte crests at 8 weeks post-MI could derive

from increased Gs binding of β_2ARs in new compartments that were formerly not occupied by β_2ARs. In this thesis the total AC activity stimulated by NKH477 was not significantly affected at the earlier stages of remodelling (4 and 8 weeks post MI). However at 16 weeks post-MI the total AC activity was significantly reduced. According to a study conducted by Hussain et al. G_i protein expression is increased in a rat HF model but its activity is unchanged (Hussain et al. 2001). The depression in β_2AR-dependent cAMP levels at 16 weeks post-MI is therefore assumed to derive from reduced AC activity and not from increased β_2AR signalling over Gi.

The reason why and the mechanism of how β_2AR eventually redistribute from T-tubules to crest areas remain elusive. It has been speculated that β_2AR might relocate in order to substitute for decreased β_1AR activity during HF (Nikolaev et al. 2010). Such substitution has been shown to occur on a cAMP independent level through the activation of phospholipase A2 which can enhance cardiomyocyte Ca^{2+} handling and consequentially cell contraction (Madamanchi 2007). Here in the described FRET study of β_2AR-dependent cAMP signalling β_2ARs also appear to substitute for β_1AR associated loss through their relocation to cardiomyocyte crests and increased cAMP generation at the crest and globally at 8 weeks post-MI. Hence β_2AR relocation from T-tubules onto crests may compensate for the pronounced loss in β_1AR activity at 8 weeks post-MI but ultimately contributes to the hearts decompensation and insufficiency at 16 weeks post-MI. These observations may explain how spatial and functional β_2AR alterations can lead to an advanced HF phenotype and how β_2ARs might be targeted therapeutically at different stages during HF progression.

4.4.2. PDE4 degrades β_2AR-dependent cAMP in health and disease

The members of the cAMP degrading PDE4 family PDE4 A, B, C and D are expressed by 4 different genes, which produce at least 20 different splice variants. PDE4's role under physiological circumstances seems to serve as a fail-safe to keep cAMP pools in specific subcellular compartments (Richter et al. 2011). According to literature the overall PDE4 expression and activity are decreased in hypertrophed rat hearts (Abi-Gerges et al. 2009) but no significant changes are seen in human cardiomyopathies (Richter et al. 2011). Alterations in PDE4D have furthermore been shown to lead to heightened phosphorylation of RyR2 and with it increased Ca^{2+} leak from the SR (Miller and Yan 2010).

The work regarding PDE4 dependent regulation of β_2AR-dependent cAMP levels described herein shows PDE4 activity on β_2AR-dependent cAMP levels remains stable under HF progression, as far as is detectable via FRET measurements. However, ROLI, the drug of our choice used for FRET measurement of cAMP levels after PDE inhibition makes no distinction

between separate PDE4 isoforms or splice variants. Such distinction might be important as the PDE4 subtypes could be differentially affected during HF progression as was indeed shown for the PDE4D isoforms, which translocated to specific positions inside cells (Berthouze-Duquesnes et al. 2013). Hence in future experiments the location and activity of the PDE family members could be addressed, if specific blockers are made available.

4.4.3. β_2AR-dependent cAMP diffusion in control cardiomyocytes and during HF progression

In the past our group has shown, that β_2AR-dependent cAMP is confined in control cardiomyocytes but lost at end stage HF (Nikolaev et al. 2010). The cause for this loss in confinement could derive from multiple sources. In earlier work by our group unhindered cAMP diffusion in healthy, control cardiomyocytes was inducible by the inhibition of PDE4 (Nikolaev et al. 2010). The same study showed that cAMP diffusion throughout the cytosol was inducible via the disruption of PKA RII and AKAP. In the same study cardiomyocytes were furthermore treated with pertussis toxin (PTX) to detect differences in the β_2AR-dependent signal amplitude after localised β_2AR. The study however did not measure the respective cells in regard to β_2AR-dependent cAMP diffusion after the PTX induced uncoupling of β_2AR from Gi. Therefore data from the study was reanalysed and revealed that cAMP confinement was lost. During HF progression cAMP diffusion in the cytosol also became completely unconfined after only 4 weeks post-MI and remained thus until the end stage of HF (16 weeks post-MI). Reverse structural remodelling which was achieved through SERCA2a gene therapy of cardiomyocytes in prior work by our group lead to a physical return of T-tubule structures and of β_2ARs into these T-tubules 16 weeks post-MI (Lyon et al. 2012). However a reanalysis of the data obtained during this SERCA2a study showed that the cAMP signal still diffused freely throughout the whole cytosol. The reason for this could be due to either one or all of the following factors: disrupted AKAP to PKA RII binding, reduced coupling of β_2AR to Gi, reduced efficiency of PDE4 confinement of cAMP and lack of bridging of the SR with the T-tubules due to disrupted expression of the structural protein JPH2, as was described in chapter 3. Given that no changes in FRET measured cAMP levels were observed during HF progression after ISO stimulation and PDE4 inhibition this study concludes that it is probably structural deterioration linked with altered AKAP and PKA binding as well as Gi coupling and JPH2 related changes which lead to unconfined cAMP diffusion in HF progression.

4.4.4. Conclusion in regard to β_2AR dependent cAMP signalling in cardiomyocytes during their progression towards HF

Our observations have potential implications for the optimal selection of treatment strategies to prevent the transition from hypertrophy towards HF. For example, beta-blockers with different β1AR: β2AR selectivity have different actions at progressive stages of HF development (Dunlay et al. 2014). The observations described herein could explain these differential actions and might urge the development of improved HF treatment strategies depending on the stage of disease. Intervening to prevent the structural remodelling of the TAT system early in the disease may maintain the spatial relationship of the TAT network with the SR. This could conceivably maintain or restore β_2AR localization to the T-tubules, as we have shown before (Lyon et al. 2012). The native, spatial restriction of β_2AR-dependent cAMP signalling is lost during HF progression, and may represent a new potential therapeutic avenue. We speculate that this is due to a plethora of factors including structural deterioration of the TAT network, β_2AR-Gi uncoupling, changes in PDE4 dependent cAMP regulation, disruption of PKA RII to AKAP binding and loss of physical contact of the TAT network with the SR due to a lack in JPH2 protein levels. In order to validate the importance of JPH2 in cAMP signal confinement it would be especially interesting to reintroduce JPH2 expression into failing cardiomyocytes and to see if this alone or in conjunction with reverse structural remodelling induced by SERCA2a (Lyon et al. 2012) can lead to restored cAMP confinement and an ameliorated HF phenotype.

Chapter 5: Cardiomyocyte β_3AR cGMP signalling in health and disease

5.1. Introduction

The presence and functionality of β_3AR receptors in cardiomyocytes is a topic of controversy. Discordant reports either confirm or dispute the importance of this βAR subtype in human and animal hearts (Kulandavelu, Hare 2012). Furthermore, if deemed present, reports are not in complete agreement if the β_3AR signals via the second messenger cAMP or cGMP and hence which potential effects it exerts on cells and tissues (Kohout et al. 2001; Kulandavelu, Hare 2012). Using a FRET imaging approach our group did not detect any β_3AR dependent contribution of cAMP in rat cardiomyocytes as tested through catecholaminergic stimulation with or without prior β_3AR blockage (Nikolaev et al. 2010). Hence the possibility of β_3AR dependent cAMP production in the course of the described study was assumed negligible or none existent. The reports linking β_3ARs to cGMP production in the myocardium also link it to Gi and eNOS dependent NO production and hence to NO dependent cGMP production via sGCs (Watts et al. 2013). eNOS is localised inside the T-tubules and sarcolemmal caveolae (Zaugg 2008; Belge et al. 2014) and artificially overexpressed β_3ARs also appear to localize to the T-tubules in mouse cardiomyocytes together with the caveolar protein Cav3 and eNOS (Belge et al. 2014). Reports have shown an increase in β_3AR expression levels during HF (Moniotte et al. 2001). Additionally a switch of β_3AR-dependent cGMP production from eNOS derived NO to nNOS and iNOS derived NO has been observed in HF (Zaugg 2008), which may or may not indicate according changes in associated cGMP levels. So far direct measurements of accurate β_3AR-dependent cGMP levels in live cardiomyocytes and at real time were prevented by the lack of suitable sensors. However the recent development of the high specificity and affinity cGMP FRET sensor Red cGES DE5 makes it possible to detect spatio-temporal changes even in low levels of cGMP (Niino et al. 2009).

Hence chapter 5 concentrates on the detection of cGMP in cardiomyocytes. Besides informative studies of cGMP in cardiomyocytes it initially deals with general pretesting of the Red cGES DE5 FRET sensor. Consecutively it puts particular focus on the investigation of β_3AR dependent cGMP levels by establishing if β_3AR dependent cGMP signalling actually occurs in rat cardiomyocytes and if so which PDEs regulate these β_3AR dependent cGMP levels. Furthermore chapter 5 attempts to elucidate potential signalling alterations taking place between control and end stage HF cardiomyocytes. Additionally it tries to elucidate the subcellular location of functional β_3ARs and of the related signalling molecules eNOS and sGC in adult control and failing cardiomyocytes.

5.2. Methods and Materials

5.2.1. 3′,5′-cyclic guanosine monophosphate (cGMP) FRET sensor

Just like the cAMP response in cardiomyocytes the cGMP response to stimuli is transient and underlies subcellular compartmentation. Thus in order to study it thoroughly it is important to be able to monitor it continuously and in real time in living cells. For the work described in this thesis cGMP was measured with the high affinity red cGES DE5 FRET biosensor, which was recently developed and provided to our laboratory by Prof. Viacheslav Nikolaev (Universitätsklinikum Hamburg-Eppendorf, Germany). This FRET biosensor is based on the cGMP binding domain of PDE5 in conjunction with the GFP T-sapphire and the RFP Dimer2 (see figure 38).

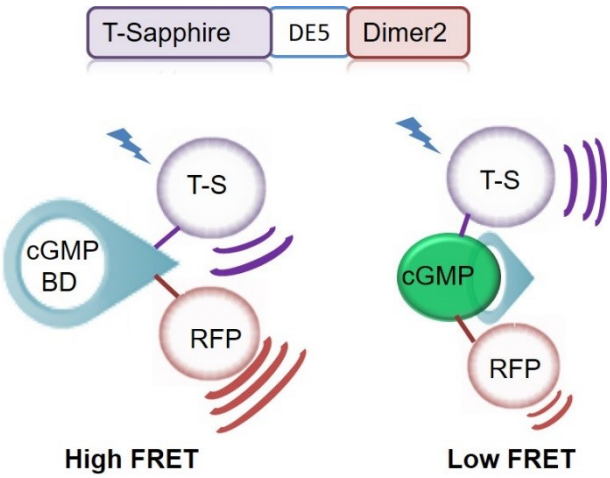

Figure 38. The FRET measurement principle of relative cGMP levels using the FRET construct Red cGES-DE5. At the top: The construct is based on the fluorescent protein T-Sapphire (T-S), the cGMP GAF binding domain of PDE5 (DE5) and the RFP Dimer2. Left hand side: In the absence of cGMP the FRET donor T-S gives part of its energy in a non-radiative fashion to the proximal, FRET acceptor RFP. Right hand side: The presence and binding of cGMP leads to a conformational change of the FRET biosensor, which removes RFP from the proximity of T-S, which in turn can no longer transfer any energy onto RFP.

5.2.2. Testing if perfusion elicits RedDE5 cGMP FRET signals

Endothelial cells are able to release NO in response to increased blood flow *in vivo* (Früh et al. 2013). The technique used for the isolation of primary, rat cardiomyocytes in this thesis should thoroughly remove endothelial cells (see chapter 2, paragraph 2.3.1). To exclude the possibility that the changes in fluid dynamics around the cells might lead to the production of NO and NO-dependent detectable cGMP levels, which could lead to a misinterpretation of the obtained data, cardiomyocytes expressing the cGMP sensor Red DE5 were “mock” perfused

with nothing but FRET solution and volumes of up to 1ml of simple FRET buffer were applied via an Eppendorf pipette. Simultaneously the FRET response was recorded.

5.2.3. Testing if DMSO elicits RedDE5 cGMP FRET signals

DMSO is commonly used as a solvent of non-water soluble compounds. In this study some of the PDE inhibitors (Vinpocetine and Cilostamide) used for FRET experimentation needed to be dissolved in DMSO. Therefore it was important to test if DMSO itself can elicit cGMP levels in the cardiomyocytes, which were used for experimentation. As a result cardiomyocytes were treated with 1µl/ml DMSO while the cGMP FRET signal was recorded.

5.2.4. Whole cell cGMP stimulation with NO donors, NPs and ISO

After successful transduction with the cGMP FRET biosensor Red cGES DE5 adult, rat, control cardiomyocytes were perfused with 20µM of the NO donor sodium nitroprusside (=SNP, dissolved in double distilled water) or with 50µM of S-Nitrosoglutathione (=GSNO, dissolved in double distilled water). Similarly control cardiomyocytes were perfused with 1µM of the natriuretic peptides ANP and CNP (both reagents dissolved in double-distilled water) respectively. Also control cardiomyocytes and cardiomyocytes at 16 weeks post-MI were perfused with 100nM ISO (dissolved in double-distilled water).

5.2.5. Determining relative, basal sGC dependent cGMP levels

After adult cardiomyocyte transduction with the cytosolic cGMP FRET biosensor cGES Red DE5 for 48h, the respective FRET response of whole cells was measured after inhibiting sGC dependent cGMP production with 50µM of 1H-[1,2,4] oxadiazolo [4,3-a] quinoxalin-1-one (=ODQ, dissolved in ethanol). Attempts to measure maximally inducible levels of cGMP in cardiomyocytes by applying the membrane permeable cGMP analogue Br-2′-*O*-Me-cGMP were unsuccessful.

5.2.6. Testing the source of the cGMP signal after ISO stimulation

Against expectation a cGMP FRET signal response was obtained in the aforementioned experiments after ISO stimulation of Red cGES DE5 transduced cardiomyocytes (see paragraph 5.2.4.). In order to establish the source of the measured cGMP cardiomyocytes were preincubated with either 100nM CGP 20712A and 50nM ICI118551 (both reagents

dissolved in double-distilled water) for 5 min to block β_1ARs and β_2ARs or with 100nM SR59230A (dissolved in double-distilled water) to block β_3AR for 5 min or with 300 µM Nω-Nitro-L-arginine methyl ester hydrochloride (=L-NAME, dissolved in double-distilled water) for 10 min before cells were perfused with 100nM ISO and the cGMP FRET signal was recorded.

5.2.7. Whole cell β_3AR dependent cGMP PDE study

cGMP pools generated by the stimulation of β_3ARs are known to derive from sGCs (Watts et al. 2013). Nevertheless they might be subject to degradation by different PDEs than the PDEs already identified as mainly responsible for the degradation of general NO derived cGMP pools. To establish which PDEs are responsible for β_3AR-dependent cGMP cardiomyocytes expressing Red cGES DE5 were treated with 100nM ISO (dissolved in double-distilled water) plus 10µM of one of the specific PDE blockers Vinpocetine (dissolved in DMSO), erythro-9-Amino-β-hexyl--α-methyl-9H-purine-9-ethanol (=EHNA, dissolved in double-distilled water), 10µM Cilostamide (dissolved in DMSO) or 10µM Tadalafil (dissolved in double-distilled water) at a time and 100µM of the non-selective PDE blocker IBMX (dissolved in ethanol) while the cGMP FRET signal was recorded. It is known that cardiomyocytes produce constiutive levels of cGMP via the sGC (Götz et al. 2014). To determine if these cGMP levels are regulated by PDE5 control cardiomyocytes expressing Red cGES DE5 were furthermore treated with 10µM of the PDE5 blocker Tadalafil followed by 100µM of IBMX without prestimulation with ISO.

5.2.8. FRET/SICM imaging of locally stimulated β_3AR dependent cGMP levels in T-tubule openings and on cell crests

10x 10 µm SICM surface scans of age matched control cardiomyocytes and cardiomyocytes at 16 weeks post-MI were taken to reveal T-tubule opening and crest structures. β_1ARs and β_2ARs were blocked through the superfusion of 100nM CGP20712A and 50nM ICI118,551 for at least 5 min. Then the SICM nanopipette was positioned either 500nm above T-tubule openings or crest areas, the coordinates of which were determined through SICM topography images, before β_3ARs were stimulated locally for 50 seconds via the SICM nano-pipette containing 50µM ISO and 50µM CGP20712A and 25µM ICI118,551 by switching the relative electrical potential inside the scanning nano-pipette from negative (-200 mV) to positive (400mV). Throughout the procedure a gravity based perfusion system continuously replaced the bath solution in less than 5 seconds. The FRET response was calculated by averaging the values of 10 frames of the baseline signal and 10 frames of the response signal and by subtraction of the averaged response from the averaged baseline.

5.2.9. cGMP signal diffusion study

To study cGMP diffusion inside the cytosol of cardiomyocytes from age matched control hearts and hearts at 16 weeks post-MI were transduced with virus encoding the cytosolic FRET sensor Red cGES DE5. Then the propagation of the cGMP signal was studied after localized β_3AR stimulation via the nano-pipette at different distances from the original nano-pipette stimulation site. For this FRET data was opened in Micro-Manager 1.4 and regions of interest (ROI) of about 15 microns width were drawn repeatedly at ever more distant areas to the nano-pipette. Then the FRET response amplitude was measured in these ROIs. As before the obtained data was processed by using the baseline correction functions in the software Origin Pro 8.5 (Origin Lab Corporation) followed by 3 median smoothing and baseline plus response averaging over 10 consecutive frames. However the elicited, local cGMP FRET response was too small to correctly analyse diffusion distances.

5.2.10. Cardiomyocyte transduction with β3AR-GFP

Adult, ventricular cardiomyocytes from control rats and rats 16 weeks post-MI were plated and transduced with an adenovirus construct for the expression of β_3ARs fused to GFP (Belge et al. 2014) provided by Prof. Nikolaev Viacheslav (Universitätsklinikum, Hamburg-Eppendorf). The medium used for 24h cell transduction with the β_3AR-GFP construct was prepared from 500ml cell culture grade water, 10,78mg modified eagle medium (MEM) with foetal growth restriction factor/ml, 750µg $NaHCO_3$/ml, 50mg L-glutamine/ml and 10,000 IU Penicillin/mL plus 10,000 ug Streptomycin/mL .

5.2.11. Immunocytochemical staining of Cav3 and sGC

The β_3ARs have been associated with the caveolae and T-tubule structures in cardiomyocytes and are thought to signal over sGC (Belge et al. 2014). In order to investigate the subcellular co-localization of β_3AR and T-tubule associated sGC ventricular cardiomyocytes from control, rat hearts and hearts 16 weeks post-MI were immunocytochemically stained with an antibody selective for the structural protein Cav3 and the sGC (see chapter 2, paragraph 2.6.). Confocal Z-stack images were taken at the Imperial College London FILM facility at 63x magnification using its inverted Zeiss LSM-780 confocal microscope. Dr. Claire Poulet (Imperial College London) provided additional immunocytochemical staining and Z-stack imaging for the aforementioned proteins for increased n-numbers and improved double staining of proteins to detect colocalisation.

5.2.12. Measuring colocalisation of Cav3 and sGC

The extent of colocalisation of Cav3 and sGC was determined using the freeware Fiji (Schindelin et al. 2012). For this analysis areas of interests were drawn manually around the respective cells in the confocal imaging software Zen. Then the colocalisation of the immunocytochemically double-stained proteins was determined automatically throughout each confocal Z-stack with the Zen "colocalisation" plugin. This plugin makes use of automatic thresholding, statistical significance testing, scatterplot creation and analysis of whole Z-stacks to determine the suitability of images for analysis and their respective Pearson's correlation coefficient (PCC). The PCC is a non subjective measure of correlation, which is highly reproducible and can evaluate the overlap of fluorescent signals in images. The output value of the PCC is a number between -1 (negative correlation) and +1 (positive correlation). If the PCC is around 0 then no positive or negative correlation exists. If the PCC value lies between 0.8 and 1 or -1 and -0.8, the correlation is described as strong, whereas values between 0.5 and 0.8 or -0.8 and -0.5 are considered to be moderately correlated and values between 0.2 and 0.5 are said to be of a weak correlation.

5.3. Results

5.3.1. Perfusion does not elicit RedDE5 cGMP FRET signals during FRET measurements

During whole cell FRET studies the investigated cells might experience a transient increase and change in flow conditions of the surrounding fluid when reagents are applied onto them via a pipette. This is increasingly so the case for cells which undergo SICM/FRET combination studies where it is necessary to attach a perfusion system to constantly exchange the surrounding fluid. To assure that no endothelial cells are in culture and produce NO in response to the usage of the perfusion system, cells expressing Red cGES DE5 were perfused while the FRET response was recorded. The perfusion did not elicit any detectable cGMP FRET response.

5.3.2. DMSO can elicit RedDE5 cGMP FRET signals in cardiomyocytes

Dimethyl sulfoxide (DMSO) is a hygroscopic, solvent oftentimes used under laboratory conditions to dissolve water insoluble, lipophilic substances (Capriotti and Capriotti 2012). In this case DMSO was used as a vehicle to dissolve the PDE inhibitors Vinpocetine and

Cilostamide. To determine potential effects of DMSO on the production of cGMP the vehicle itself was applied onto cardiomyocytes expressing the cGMP FRET biosensor Red cGES DE5 and the resulting FRET response was recorded. The application of 1µl DMSO/ml indeed led to an increase in cGMP levels (see figure 39).

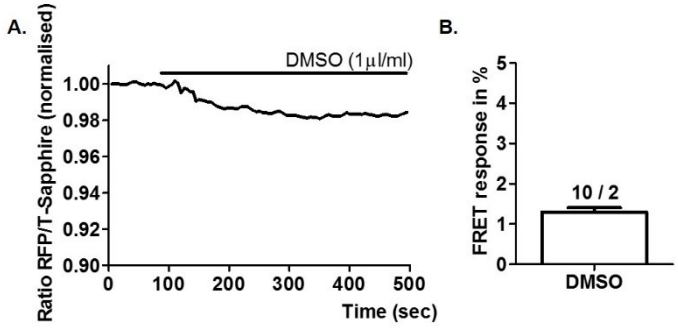

Figure 39 DMSO dependent increase in cGMP FRET response. (A.) Representative cGMP FRET response curve to the application of 0.1% DMSO onto Red cGES DE5 transduced cardiomyocytes. (B.) cGMP FRET response to DMSO. Numbers above bars = number of single cells tested / number of animals utilized. Bar represents mean value ± standard error of the mean.

5.3.3. NO and NP dependent cGMP signals in cardiomyocytes

To test the ability of Red cGES DE5 transduced cardiomyocytes to sense cGMP stimulation with NO donors and natriuretic peptides, cells were stimulated with the NO donors SNP and GSNO or with the NPs ANP and CNP respectively. While the reagent SNP did not elicit a detectable cGMP FRET signal in the investigated cells (data not shown), GSNO and the natriuretic peptides ANP and CNP did. While GSNO and ANP lead to the production of similar amounts of cGMP of around 2% the natriuretic peptide CNP generated the highest levels of cGMP of around 6% (see figure 40). However it is important to draw attention to the relatively low response rate of only 19 out of 142 cells (~13%) to CNP stimulation, which was observed during FRET experimentation.

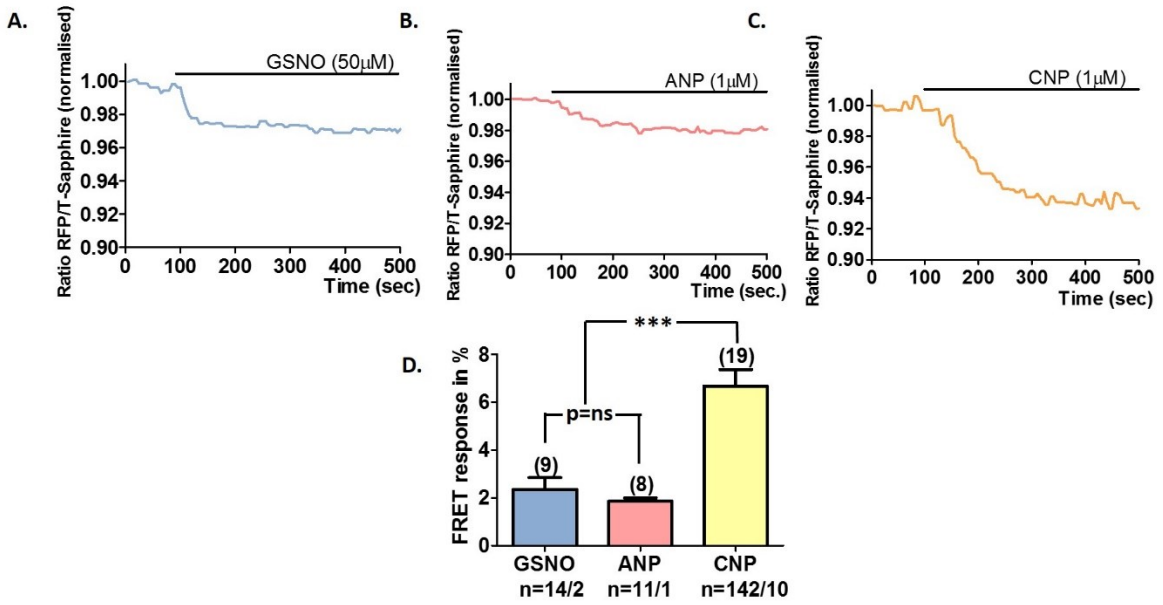

Figure 40 NO donor and NP dependent cGMP FRET response. cGMP FRET response curves to the application of (A.) the NO donor GSNO, (B.) the NP ANP and (C.) the NP CNP onto Red cGES DE5 transduced cardiomyocytes. (D.) cGMP FRET response to GSNO, ANP and CNP. Bars represent mean values ± standard error of the mean. Numbers above bars = number of single cells tested / number of animals utilized. Statistical one way ANOVA test followed by Bonferroni correction post-hoc testing, ***p < 0.0001, p = ns; not significant.

5.3.4. Relative, basal sGC dependent cGMP levels

sGCs continuously generate cGMP (Götz et al. 2014). To establish the levels of basal sGC dependent cGMP production in cardiomyocytes expressing the cytosolic cGMP FRET sensor Red cGES DE5, cells were treated with the sGC blocker 1H-[1,2,4] oxadiazolo [4,3-a] quinoxalin-1-one (ODQ). Tests showed a clear reduction in FRET measured cGMP levels of around 3.5%, revealing the relative, basal cGMP producing activity of sGCs in cardiomyocytes after 48h of culture and transduction (see figure 41).

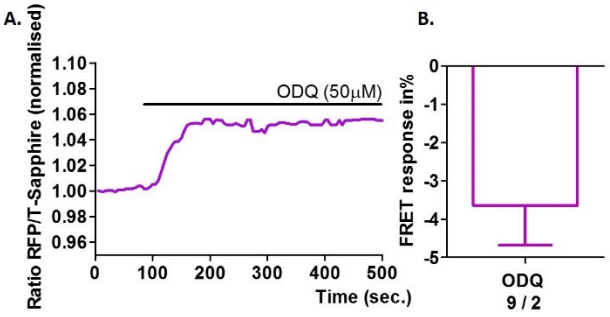

Figure 41 1H-[1,2,4] oxadiazolo [4,3-a] quinoxalin-1-one (ODQ) dependent decrease in cGMP FRET response of control cardiomyocytes. (A.) cGMP FRET response curve to the application of the sGC blocker ODQ onto Red cGES DE5 transduced cardiomyocytes. (B.) cGMP FRET response to 50µM ODQ. Numbers below bar = number of single cells tested / number of animals utilized. Bar represents mean value ± standard error of the mean.

5.3.5. Cardiomyocytes produce β_3AR dependent cGMP levels

To see if the recorded FRET signal of around 4%, which was obtained during Red cGES DE5 transduced cardiomyocyte stimulation with the β adrenergic agonist ISO stems from β_3AR receptors, cells were treated respectively with specific β_1AR and β_2AR blockers (ICI118551 and CGP 20712A) as well as a specific β_3AR blocker (SR59230A) and a NOS blocker (L-NAME) before ISO application. While inhibiting signalling over β_1ARs and β_2ARs did not lead to any significant changes the specific blocking of β_3ARs or eNOS efficiently abolished the ISO induced rise in cGMP levels (see figure 42).

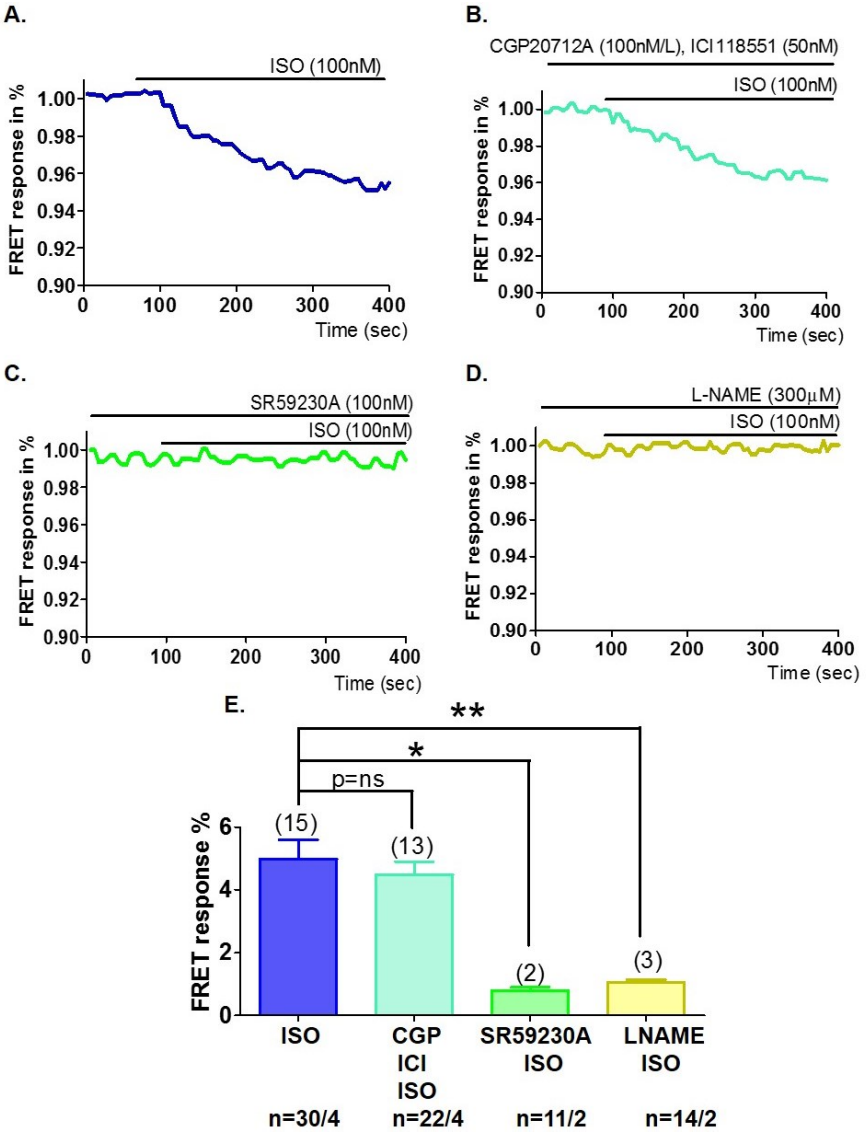

Figure 42 β_3AR dependent cGMP FRET response investigation. cGMP FRET response curves to the application of (A.) ISO, (B.) β_1AR and β_2AR blockage (with ICI118551 and CGP 20712A) followed by ISO, (C.) β_3AR blockage (with SR59230A) followed by ISO and (D.) eNOS blockage (with L-NAME) followed by ISO onto Red cGES DE5 transduced cardiomyocytes. (E.) cGMP FRET response to ISO after no blockage, β_1AR and β_2AR blockage, β_3AR blockage and eNOS blockage. Bars represent mean values ± standard error of the mean. Numbers above bars = number of single cells tested / number of animals utilized. Statistical one way ANOVA test followed by Bonferroni correction post-hoc testing, $^{**}p < 0.001$, $^{*}p < 0.05$, p = ns; not significant.

5.3.6. β_3AR dependent cGMP levels decrease in HF

To see if β_3AR-dependent cGMP levels significantly alter in HF cardiomyocytes age matched control cardiomyocytes and cardiomyocytes 16 weeks post-MI expressing the cytosolic FRET sensor Red cGES DE5 were stimulated with ISO. Despite reported increases in β_3AR expression in HF (Zaugg et al. 2008; Moniotte et al. 2001; Niu et al. 2012) in our rat MI model β_3AR-dependent cGMP levels in failing cardiomyocytes were decreased by ~50% (see figure 43). Interestingly only about half of all cells react to catecholamine stimulation via a measureable FRET response in cGMP levels in both control and HF cardiomyocytes.

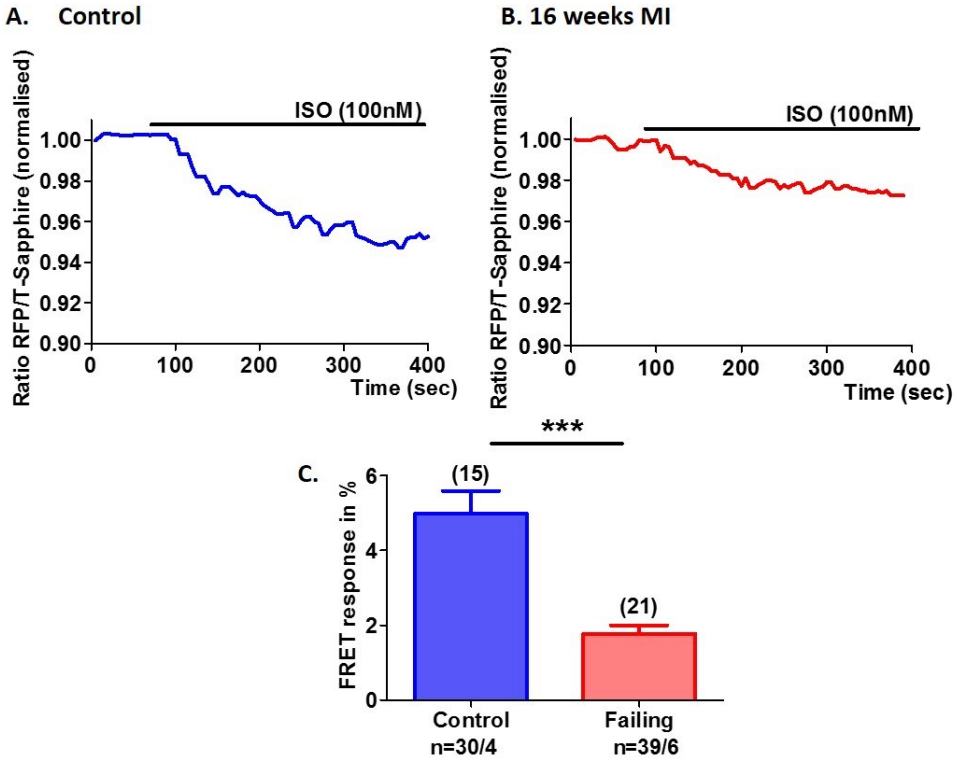

Figure 43 Whole cell cGMP response to ISO in control and HF cardiomyocytes expressing Red cGES DE5 FRET sensor. Representative cGMP FRET curves to ISO application onto (A.) sham-operated control cardiomyocytes or (B.) cardiomyocytes 16 weeks post-MI. (C.) cGMP FRET response to ISO applciation in sham-operated control cardiomyocytes and cells 16 weeks post-MI. Bars represent mean values ± standard error of the mean. Numbers above bars = number of single cells tested / number of animals utilized. Statistical Student's two-sided T-test, **p < 0.001.

5.3.7. β_3AR dependent cGMP degraded by PDEs 2 and 5

To determine which PDEs are responsible for hydrolysing β_3AR-dependent cGMP pools age matched control cells and cells 16 weeks post-MI expressing the cGMP FRET sensor Red cGES DE5 were stimulated with ISO followed by PDEs 1, 2, 3 and 5 inhibition with the respective blockers (Vinpocetine, EHNA, Cilostamide, Tadalafil) followed by total, non-selective PDE inhibition (with IBMX). The results indicate that it is PDE2 and PDE5 which decrease β_3AR-dependent cGMP levels as cGMP increases the most after their inhibition by around 2% each (see figure 43). To see if basal cGMP levels which stem from constitutive sGC activity are regulated by PDE5, cells were furthermore treated with Tadalafil followed by IBMX. Interestingly this approach lead to no detectable increase in cGMP levels in this study (data not shown). In cardiomyocytes 16 weeks post-MI it was also PDE2 and PDE5 inhibition which lead to the highest accumulation of β_3AR-dependent cGMP after ISO stimulation (see figure 44). Also a significant increase in cGMP levels after ISO stimulation and PDE2 inhibition or non-selective PDE inhibition via IBMX treatment was noticed, indicating that PDE2 activity increases during HF (see figure 45). The bar graphs in figures 43 to 45 show the additional FRET response after PDE inhibition on top of ISO stimulation in the respective cells.

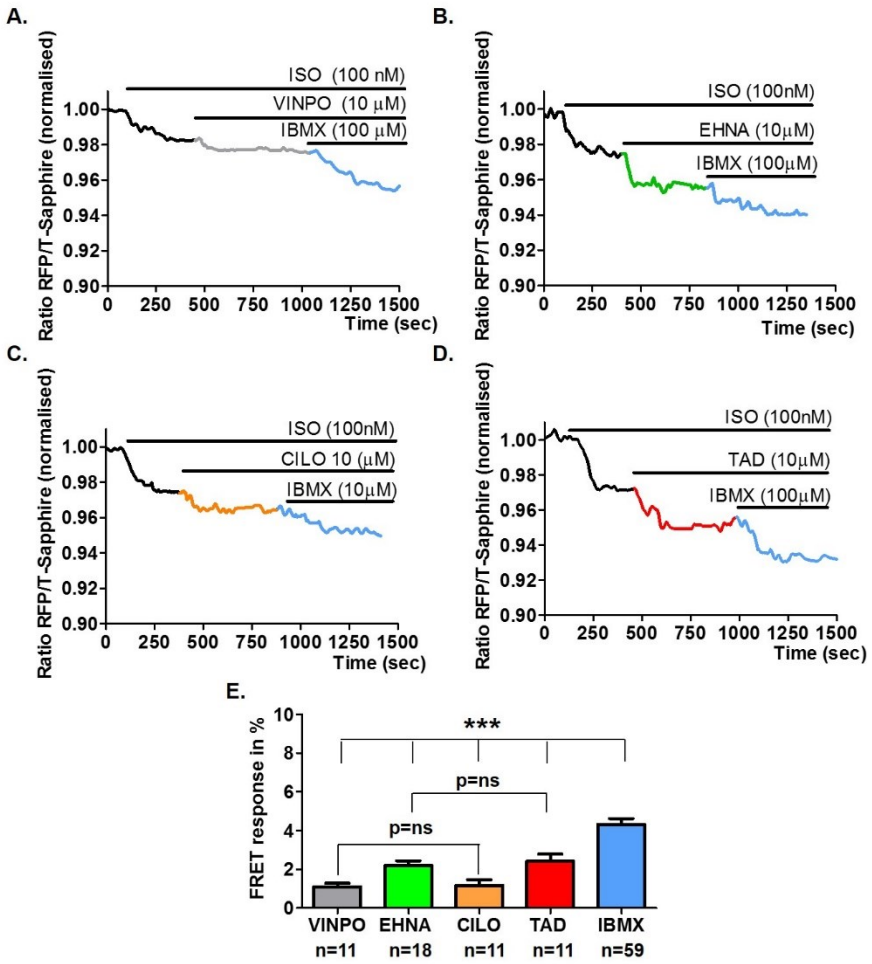

Figure 44 Whole cell cGMP response to ISO and PDE blockers in control cardiomyocytes expressing Red cGES DE5 FRET sensor. Representative cGMP FRET curves to ISO application onto control cardiomyocytes followed by (A.) PDE1 inhibition (with Vinpocetine), (B.) PDE2 inhibition (with EHNA), (C.) PDE3 inhibition with Cilostamide (D.) PDE5 inhibition (with Tadalafil) and inhibition of all PDEs (with IBMX). Colors correlate to cGMP response of cells on top of ISO shown in (E.). n= number of single cells measured. Animals utilised n≥4. Bars represent mean values ± standard error of the mean. Statistical one-way ANOVA test followed by Bonferroni correction post-hoc testing, ***p < 0.001.

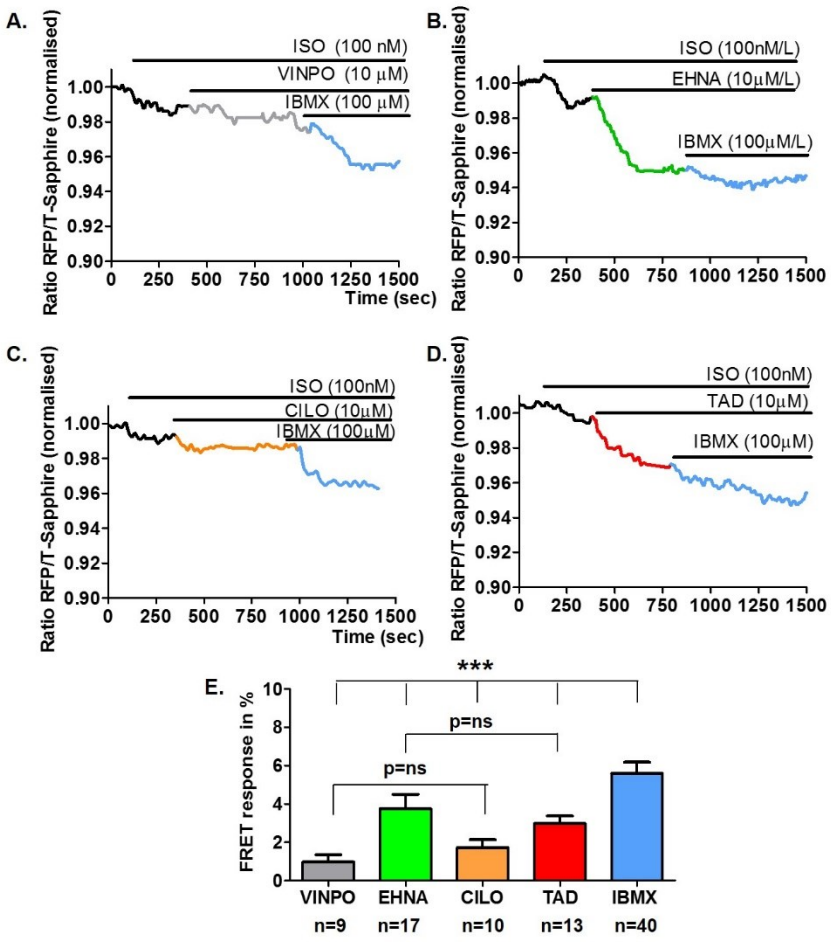

Figure 45 Whole cell cGMP response to ISO and PDE blockers in cardiomyocytes 16 weeks post-MI expressing the Red cGES DE5 FRET sensor. Representative cGMP FRET curves to ISO application onto control cardiomyocytes followed by (A.) PDE1 inhibition (with Vinpocetine), (B.) PDE2 inhibition (with EHNA), (C.) PDE3 inhibition with Cilostamide (D.) PDE5 inhibition (with Tadalafil) and inhibition of all PDEs (with IBMX). Colors correlate to cGMP response of cells on top of ISO shown in (E.). n= number of single cells measured. Animals utilised n≥3. Bars represent mean values ± standard error of the mean. Statistical one-way ANOVA test followed by Bonferroni correction post-hoc testing, ***p < 0.001.

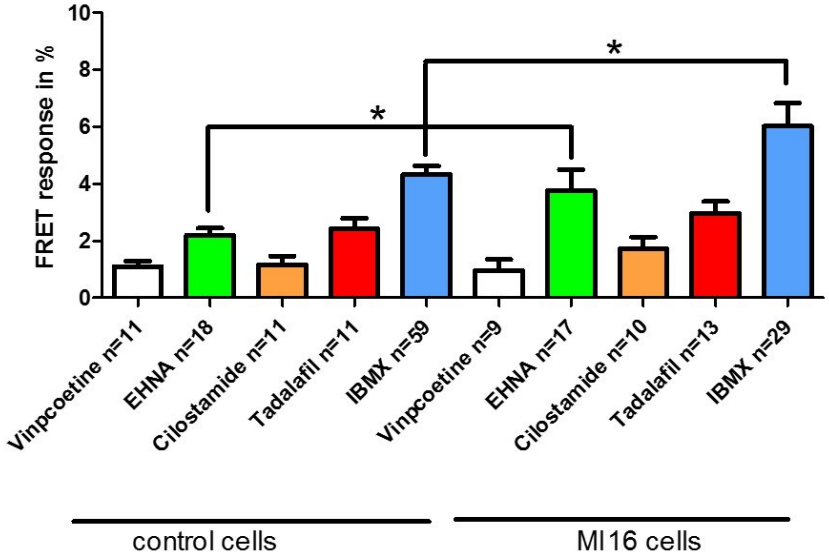

Figure 46 cGMP FRET response in age matched control cardiomyocytes and in cardiomyocytes at 16 weeks post-MI expressing the cGMP FRET sensor Red cGES DE5. PDE1 inhibition (with Vinpocetine), PDE2 inhibition (with EHNA), PDE3 inhibition with Cilostamide and PDE5 inhibition (with Tadalafil) and inhibition of all PDEs (with IBMX). n= number of single cells measured. Animals utilised n≥3. Bars represent mean values ± standard error of the mean. Statistical one-way ANOVA test followed by Bonferroni correction post-hoc testing, *p < 0.05.

5.3.8. Functional β_3AR localisation in T-tubule openings and on cell crests in control and HF cardiomyocytes

To determine the localisation of functional β_3AR on the surface of cardiomyocytes combined FRET and SICM studies were performed. β_1AR and β_2ARs were blocked specifically and β_3ARs were stimulated via ISO application either into the T-tubule openings or onto crest areas of age matched control cardiomyocytes and cardiomyocytes at 16 weeks post-MI. The results show that β_3AR-dependent cGMP signalling in control cells of around 1% is localised almost exclusively inside T-tubules while in end stage HF β_3AR-dependent cGMP signals of around 0.5% are equally elicitable in both T-tubules and crests (see figure 46).

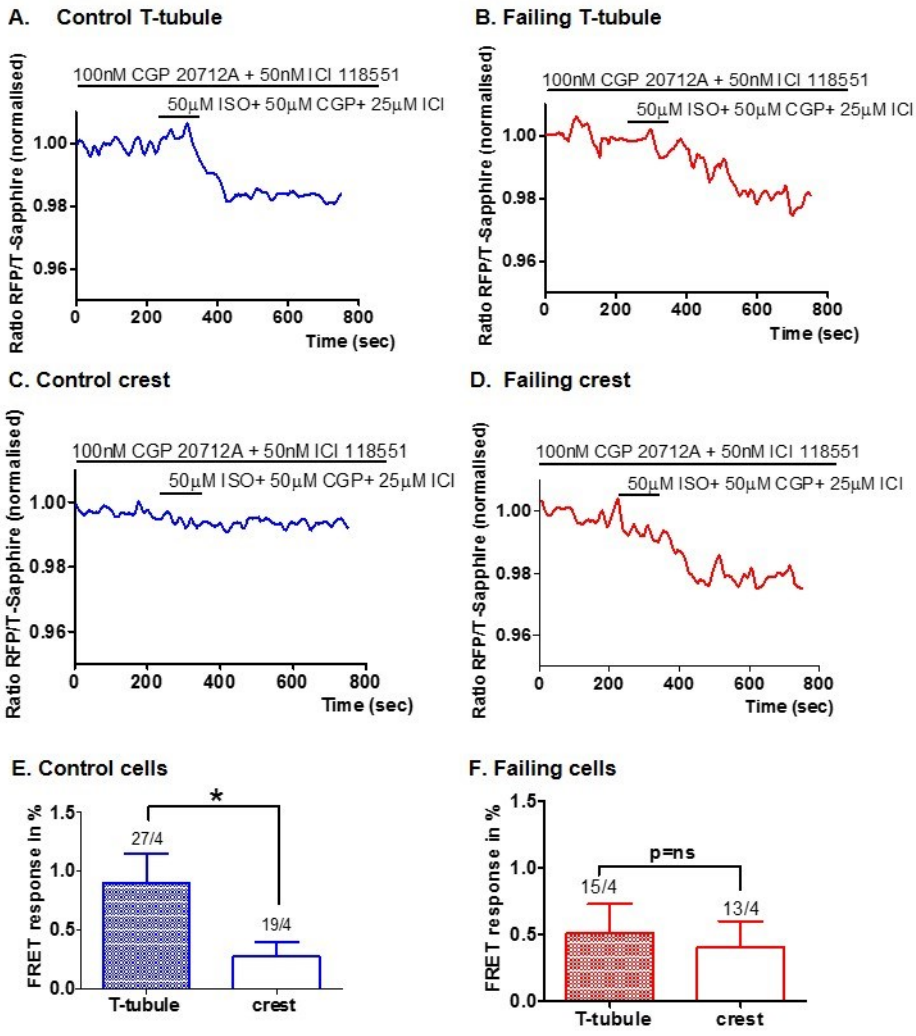

Figure 47 FRET based localisation of functional β_3ARs via their localised cGMP response. (A.) Representative β_3ARs-cGMP FRET response curves after local β_3ARs stimulation either in T-tubule openings or on crest areas of (A.) sham-operated control cardiomyocytes and (B.) cardiomyocytes 16 weeks post-MI. Local β_3ARs-cGMP FRET response after agonist application into T-tubule or crest in (C.) control cardiomyocytes and (D.) cardiomyoctes at 16 weeks post MI. n= number of single cells measured. Animals utilised n=4 each. Bars represent mean values ± standard error of the mean. Number above bars indicates responsive cells. Statistical Student's two-sided T-test, *p < 0.05, p=ns; not significant.

5.3.9. The subcellular location of Cav3, sGC and eNOS in control cardiomyocytes

To investigate the presence and location of proteins involved in β_3AR-dependent cGMP signalling in adult rat cardiomyocytes from age matched control hearts cells were fixed on the day of their isolation and single stained with an antibody selective for Cav3 and sGC. Confocal images of the immunocytochemical single-staining of the respective cardiomyocytes shows that Cav3 localises over the whole cardiomyocyte sarcolemma including the T-tubule membranes sGC appears to follow a Z-line localisation, which might colocalise with T-tubules, but not the whole cardiomyocyte sarcolemma (see figure 4).

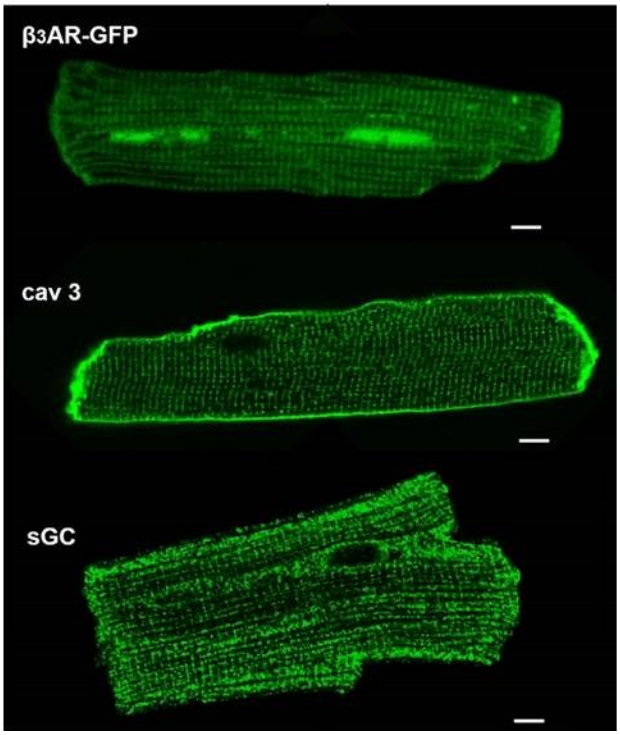

Figure 48 Subcelllular location of the artificially expressed β_3AR-GFP fusion protein and immunocytochemically stained Cav3 and sGC in cardiomyocytes. Representative confocal images of β3AR-GFP fusion protein expression and immunocytochemical single staining of Cav3 and sGC in age matched control cardiomyocytes. Scale bars equal 10 µm.

5.3.10. Cav3 and sGC colocalise in control cardiomyocytes but this colocalisation is lost in HF cardiomyocytes

To obtain insight into the subcellular co-localisation of proteins involved in the β_3AR dependent signalling cascade age matched, control cardiomyocytes and cardiomyocytes at 16 weeks post-MI were fixed on the day of their isolation and double-stained Cav3 and sGC. The analysis of the obtained confocal Z-stacks show that Cav3 and sGC colocalise to some degree with a Pearson's correlation coefficient (PCC) of over 0.20 around 0.24 while this colocalisation appears to be lost in failing cardiomyocytes whose PCC significantly decreases to less than 0.2 to around 0.17. From the confocal images it appears that this colocalisation is close to the sarcolemma and inside the T-tubules which are marked by Cav3 (see figure 48).

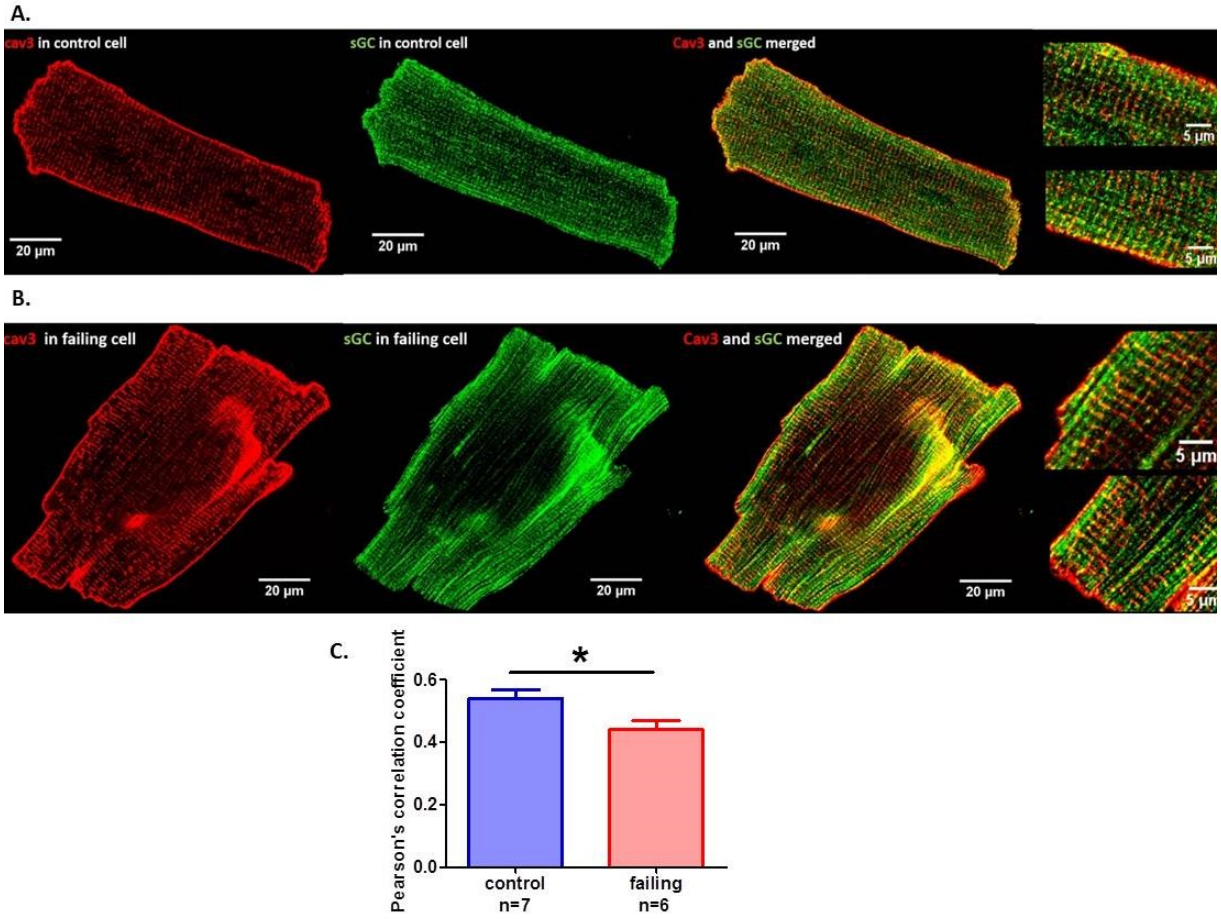

Figure 48 Subcellular colocalisation study of Cav3 and sGC. (A.) Representative immunocytochemical double staining of Cav3 and sGC in an age matched control cardiomyocyte and a failing cardiomyocyte at 16 weeks post-MI. Scale bars, 20 µm. Images provided by Dr. Claire Poulet (Imperial College London). Representative scatter plots from control and failing cardiomyocytes which are used to determine potential correlation of staining of Cav3 and sGC in (C.) the cytosol or (D.) the sarcolemma via Pearson correlation coefficient (PCC) analysis. The averaged PCC of subcellular colocalisation of Cav3 with sGC in control cardiomyocytes and failing cardiomyocytes in (D.) the cytosol (F.) the sarcolemma.

5.4. Discussion

5.4.1. The novel cGMP FRET sensor Red cGES DE5 enables NO, NP and β_3AR-dependent cGMP FRET measurements

The affinity and efficiency of the FRET sensor Red cGES DE5 for cGMP (=40nmol) is higher than that of any prior cGMP specific FRET construct and hence allows the measurement of even very low levels of the second messenger cGMP. A recent study (Götz et al. 2014) showed that it effectively detects cGMP levels after a combination of catecholaminergic with NO stimulation or pure NP stimulation of cardiomyocytes. The same study showed that the CNP represents the stimulus for the highest cytosolic cGMP production followed by a three times lower cGMP production after stimulation with the NO donor SNAP and an almost six times lower cGMP production after stimulation via the ANP. In the study presented in this thesis CNP also revealed to be the most effective stimulant of the highest cGMP levels, while the NO donor GSNO and the NP ANP elicited similar levels of cGMP which were around 3 times lower in comparison to CNP elicited cGMP levels. However only a relatively low number of cells actually responded to CNP stimulation. The reason for this low response rate to CNP is unknown. We do not expect it to stem from variable levels of basal cGMP levels, which if excessively high might lead to the saturation of the FRET sensor, else the other 2 donors would have shown a similar response rate, which they didn't. Also the measurements of basal, sGC dependent cGMP levels via ODQ showed that the basal cGMP levels are relatively stable and are not excessively high. It is possible that the cardiomyocytes with responsiveness to CNP belong to a subpopulation of cardiomoycytes while almost all cardiomyocytes appear to be responsive to ANP and NO. Prior work has investigated the presence and functionality of β_3AR-dependent cGMP signalling in human (Gauthier et al. 1998; Pott et al. 2006) and neonatal rodent cardiomyocytes (Mongillo et al. 2006). FRET measurements of β_3AR-dependent cGMP in isolated, adult cardiomyocytes were however impeded by the far lower levels of cGMP being produced in comparison to neonatal cells. Also no cGMP FRET sensors with high enough affinity and specifity were available. This limitation was only recently overcome by the generation of the cGMP FRET sensor Red cGES DE5 (Niino et al. 2009). This sensor was succesfully used for cGMP FRET measurements in transgenic mice (Götz et al. 2014) which have very low β_3AR expression levels, so that β_3AR overexpression has to be introduced before mice cardiomyocytes can generate a measureable β_3AR-dependent cGMP FRET response (Belge et al. 2014). But the Red cGES DE5 sensor was not yet used for the transduction of adult rat cardiomyocytes. Hence as far as the writer of this thesis is aware the

β_3AR-dependent cGMP FRET measurements in intact control and end stage HF cardiomyocytes described herein are the very first, published measurements of β_3AR-dependent cGMP signalling in adult, rat ventricular cardiomyocytes.

5.4.2. DMSO elicits a detectable cGMP FRET signal in cardiomyocytes

During pretesting of the novel cGMP FRET sensor Red cGES DE5 the solvent DMSO elicited low but clear levels of cGMP. How DMSO potentially leads to increased cGMP levels is not quite clear and was not investigated further. A general literature review of DMSO on Pubmed (http://www.ncbi.nlm.nih.gov/pubmed) reveals multiple possibilities for how DMSO might excert effects on cells. Among other chemical properties of DMSO are its reactivity with water molecules and its potential to affect cellular constituents (Szmant 1975). When limiting the literature search to "DMSO" in combination with "cardiomyocytes" Pubmed yields 132 publications of which only 3 actually studied the effect of DMSO on primary adult cardiomyocyte structure and function. These papers ascribe DMSO's effects on cells to its mitochondria improving function by scavenging hydroxyl radicals which form at the mitochondria during ischemia and to an associated decreased submitochondrial ATPase activity (Jacob and Herschler 1986). Interestingly DMSO also appears to have effects on the Ca^{2+} handling of cardiomyocytes and might lead to increased permeability of the sarcolemmal membrane (Jacob and Herschler 1986). DMSO was furthermore shown to induce increased heme oxygenase 1 (HO-1) enzyme expression. As its name indicates the enzyme HO-1 catabolizes heme groups and as a byproduct produces carbon monoxide (Man et al. 2014). This carbon monoxide could potentially lead to or be the cause of consecutive cGMP generation via binding to sGC (Derbyshire and Marletta 2009). Therefore experimentalists should be aware of DMSO's potential effects on cardiomyocyte function and cyclic nucleotide signalling.

5.4.3. Whole cell and localised β_3AR-dependent cGMP signalling

Stimulation of cardiomyocytes expressing the FRET sensor Red cGES DE5 lead to a clear cGMP response in adult rat cardiomyocytes. Specific blocking of the β_1AR and β_2AR subtypes and alternative blocking of β_3ARs or NO production via NOS showed that this signal with all likelihood stems from β_3ARs, which have been shown to be present at a functional level in rat cardiomoyctes in the past (Mongillo et al. 2006; Watts et al. 2013). The localisation of these functional β_3ARs in adult rat cardiomoyctes has however not been determined before. Studies in mouse specified the putative position of β_3ARs inside the T-tubular membrane as

determined via proximity ligation assays which showed colocalisation of artificially overexpressed β_3ARs with eNOS and Cav3 (Belge et al. 2014). Emulating the successful compartmentation study of β_2AR-dependent cAMP conducted by our group in the past (Nikolaev et al. 2010) the localisation of functional β_3AR on the surface of cardiomyocytes was studied by combining SICM with FRET measurements. The results confirmed functional β_3AR are primarily located inside T-tubules in control cardiomoyctes but like β_2AR (Nikolaev et al. 2010) they change their position at the end stage of HF to the whole sarcolemma.

5.4.3. β_3AR dependent cGMP levels decrease in HF

Despite reports of increased β_3AR expression in senescence and HF (Birenbaum et al. 2008; Niu et al. 2012; Niu et al. 2014) during the FRET measurements described in this thesis β_3AR-dependent cGMP levels were significantly decreased at the end stage of HF. The reasons for this reduction in cGMP generation will have to be established in future work and could be due to a combination of causes. Speculatively, decreased β_3AR-dependent cGMP levels could be due to significantly increased PDE activity, uncoupling/ decrease of downstream targets like the sGC and eNOS or even a switch between the NOS subtypes a phenomenon, which has been described before (Niu et al. 2012). According to the FRET experiments using the cytosolic sensor Red cGES DE5 described in this thesis the major PDE to degrade β_3AR-dependent cGMP levels are PDE2 and PDE5. At 16 weeks post-MI PDE2 activity appeared to be significantly increased in the FRET experiments. This increase of PDE2 activity is at least partly accountable for the decreased cGMP levels which were observed in end stage HF. β_3ARs have been shown to signal over eNOS and sGC (Mongillo et al. 2006). Immunocytochemical single staining of sGC shows that the molecule distributes along the Z-lines of cardiomyocytes and could potentially localise to the T-tubules or at least their vicinity. Consecutive double-staining with Cav3 and sGC showed partial colocalisation of cav3 and sGC in what is presumably the membrane of T-tubules. Additionally subcellular co-localisation studies of Cav3 with sGC showed significant differences between age matched control cardiomyocytes and end stage HF cardiomyocytes which could be indicative of either relocation or decrease of sGC levels in HF cardiomyocytes. Studies of potentially occuring activity changes of both sGC and eNOS remain to be conducted in the future.

5.4.4. β_3AR dependent cGMP degradation via PDEs 2 and 5

The pretreatment of cardiomyocytes with specific PDE blockers and consecutive FRET measurements of β_3AR-dependent cGMP identified PDE2 and PDE5 as major β_3AR-

dependent cGMP degradors. PDE2 dependent regulation of β_3AR-dependent cGMP and retrospectively β_1AR and β_2AR dependent cAMP levels is corroborated by findings in neonatal rat cardiomyocytes, which revealed a NO and cGMP dependent decrease of cAMP levels close to the membrane through PDE2A hydrolysis (Mongillo et al. 2006). PDE5 acts solely on cGMP derived from sGC and is strongly influenced by the presence of its substrate cGMP which increases its hydrolytic capability by binding to the respective GAF binding domains (Kass 2012). It is therefore possible that PDE5 is generally active on constitutively produced cGMP levels by eNOS. In the investigation described in this thesis however no accumulation of cGMP was revealed after treating cardiomyocytes with the specific PDE5 blocker Tadalafil or with an unselective PDE blocker without prior βAR stimulation. Despite its low expression in cardiomyocytes under physiological conditions PDE5's activity appears to increase during HF in humans. This is accompanied by a drop in cardiac cGMP levels. As cGMP is widely regarded to counter act excessive cAMP dependent signalling and to decrease cardiac hypertrophy it was concluded that PDE5 inhibition might ameliorate the pathological phenotype of the diseased myocardium (Kass 2012). Though PDE9 is also known to be expressed in cardiomyocytes and to degrade cGMP (Stangherlin and Zaccolo 2012) its role in regulating β_3AR-dependent cGMP levels has not been assessed in this work for lack of a specific PDE9 inhibitor. However a recent study ascribing PDE9A a prominent role in natriuretic peptide pathways concluded that PDE9 primarily acts on NOS independent cGMP pools (Lee et al. 2015).

5.4.5. Conclusion regarding cGMP signalling in cardiomyocytes

The novel cGMP FRET sensor Red cGES DE5 is can be used for cGMP FRET measurements after cardiomoycyte stimulation with NO donors or NPs. Also β_3AR-dependent cGMP production occurs in adult, rat cardiomoyctes at levels which are measureable with this cGMP FRET sensor. In HF cardiomyocytes this β_3AR-dependent cGMP production is significantly decreased together with alterations in signalling molecules like sGC which are important members of the β_3AR-dependent cGMP signalling pathway. In control cardiomyocytes β_3ARs are situated inside the T-tubules but their location changes at the end stage of HF when they are also found on crest areas. In both control and HF cardiomyocytes the β_3AR-dependent cGMP response to catecholaminergic stimulation is regulated by PDEs 2 and 5. In HF PDE2 activity appears to be significantly increased, which might explain the overall decrease in cGMP levels in HF. All the aforementioned observations show that rat cardiomyocytes should be considered as a useful tool for further studying the β_3AR ad its role in physiology as well as pathophysiology.

Chapter 6: Modelling of localised ISO application onto cardiomyocyte structures via electrical potential switch

6.1. Introduction

In the general Introduction and Material and Methods section (see chapters 1 and 2) it was mentioned, that the mode of agonist application using the SICM nanopipette was changed from pressure-driven (Nikolaev et al. 2010) to voltage-driven (Babakinejad et al. 2013). The fact that the agonist used in this case, namely ISO, has a slightly positive net electrical charge (of +1e) in solutions makes its dynamics during application much more complicated, particularly due to the fact that the cells have a complex surface topography. Thus we developed a mathematical model to simulate its application onto the cell surface and hence understand the spreading process. During the conduction of SICM experiments using voltage-driven application a few electrochemical phenomena emerge: Firstly, when the surface of the nanopipette and the cell surface come into contact with the freely diffusible, electrolytic solution this generates a charged diffusive layer between the electrolyte solution and the surfaces (Babakinejad et al. 2013). This layer is called the electrical double layer (EDL). It possesses a specific electrical potential, the ζ potential, at the space where the liquid slips along the solid surfaces. However the ζ potential cannot be determined experimentally. Instead it is common practice to determine the electrophoretic mobility of molecules, which is the experimentally observable rate of movement of a charged particle in the electrolyte solution. As both the application outlet (the nanopipette) and the structures, which are dealt within this investigation, are on the nanoscale level, this will lead to the exertion of forces which will repel or attract a small, charged and dissolved molecule like ISO. Additional repelling and attracting forces arise in colloidal fluids like the physiological buffer used for FRET experiments described in this thesis (Hunter 1981). Together with the scale of the nanopipette and of the ISO molecule itself all the aforementioned forces will determine how fast ISO diffuses out of the nanopipette and how much of the underlying cardiomyocyte structures it will reach.

The objective of chapter 6 is therefore to determine an appropriate experimental setup to collect sufficient experimental data to validate or improve the precision of our voltrage-driven SICM application mode via mathematical modelling. Hence the electrophoretic mobility of ISO in physiological buffer in a glass capillary and the averaged structural scale of the nanopipette and the cardiomyocyte structures as well as the optimal setup for voltage-driven application were determined. The parameters obtained were fed into the finite element model describing the problem through partial differential equations to find an approximate solution of which experimental settings to use for the precise application of ISO onto the cardiomyocyte surface.

6.2. Methods and Materials

6.2.1. Determination of averaged cardiomyocyte surface and nanopipette structures and their translation into mathematical geometries

Using the SICM imaging software (Ionoscope) the average size (height, width, length) and number of T-tubule openings, the amount of Z-grooves and of crests on control cardiomyocytes and cardiomyocytes during the progression towards HF were determined from SICM surface scans after 48 hours of cell transduction. The averaged scale of the nano-pipette was taken from Babakinejad et al. 2013 who use the same nano-pipette make and puller (see chapter 2, paragraph 2.5.1.).

6.2.2. Determination of the electrophoretic mobility of ISO

As the attracting and repelling forces determine the direction and the velocity of freely diffusible particles in solution it was imperative to determine the electrophoretic mobility of ISO. Therefore a sample of 50µM of ISO diluted in physiological buffer (ddH_2O containing NaCl 144 mM, KCl 5mM, HEPES 10mM and $MgCl_2$ 1mM, pH 7.4) was sent to the company Brookhaven Instruments for measurements of the electrophoretic mobility of the agonist. Measurements were conducted by Dr. Dan Clarke. For the measurements the sample was analysed in 5 consecutive runs at 25°C through a glass capillary using a NanoBrook ZetaPALS machine (model: NanoBrook Omni, Brookhaven Instruments Corporation, UK) and phase analysis light scattering (PALS). The correlation-function of the phase shift from which the electrophoretic mobility was determined via the Smoluchowski drift-diffusion equation is shown below (see figure 49).

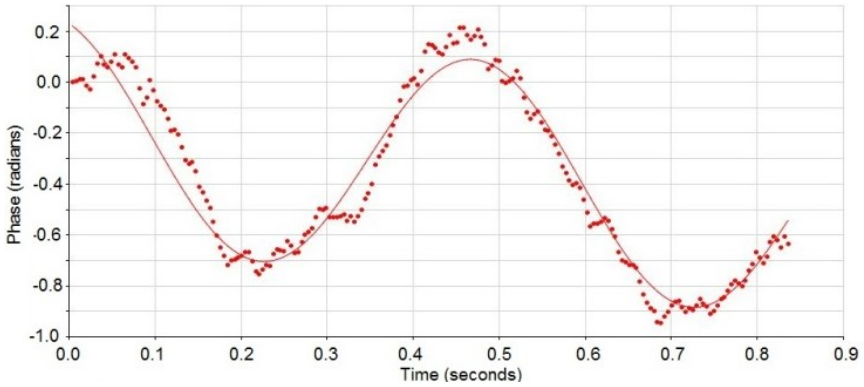

Figure 49 Determination of the electrophoretic mobility of the agonist ISO. Shown is a graph of the correlation-function (red line) used to determine the electrophoretic mobility of ISO in physiological buffer and the correlating measurements (red dots) taken with a phase analysis light scattering technique. Here the phase (given in radians corresponding to an angle of ~ 57.3°) defines the position of a particle at a specific point in time during a waveform cycle of 360°.

6.2.3. Numerical simulations of ISO application onto cardiomyocyte structures

The following steps and finite element simulations were performed together with Dr. Peter Jönsson (University Lund, Sweden):

The program COMSOL Multiphysics® 4.4 (COMSOL AB, Stockholm, Sweden) was used to solve for the concentration of ISO delivered from the nano-pipette due to a voltage drop ($\Delta\Psi$) applied over the pipette. The time the concentration takes to reach steady state via voltage-application is much faster than the time scales normally used for the delivery via pressure-displacement and stationary equations can therefore be used. The following three sets of equations were solved:

(Electrostatics) $$\nabla^2\Psi = 0 \quad (1)$$

(Creeping flow) $$-\nabla p + \eta\nabla^2 \boldsymbol{u} = 0 \quad (2a)$$

$$\nabla \cdot \boldsymbol{u} = 0 \quad (2b)$$

(Transport of diluted species) $$\nabla \cdot \boldsymbol{J} = 0 \quad (3a)$$

$$\boldsymbol{J} = -D\nabla c + c\left(\boldsymbol{u} - \mu_{ep}\nabla\Psi\right) \quad (3b)$$

where Ψ is the electric potential, p the hydrostatic pressure, $\boldsymbol{u}$ the liquid flow vector, η the viscosity of the liquid and $\boldsymbol{J}$ the molecular flux of ISO. Equation 1 gives the electric field in the pipette, and is solved for first. Next, Equation 2 is solved to determine the electroosmotic flow in the system, where the determined electric field $\boldsymbol{E} = -\nabla\Psi$ is used as input value. The concentration of ISO is finally determined by solving Equation 3 with the already simulated values of $\boldsymbol{u}$ and Ψ as input values to determine the amount of ISO delivered.

The boundary conditions used in the simulations of ISO application via a nano-pipette are given in Table 6 and the assumed parameter values in Table 7. It is noteworthy that the electrophoretic and electroosmotic mobility has the opposite sign, and that the latter dominates the delivery in this situation. When applying into a T-tubule opening the point on the surface below the pipette is (x,y,z) = (0,0,0), and each side of the simulation geometry is 10 µm (width and depth are equal to 9 µm for the crest application simulations, where the point on the surface below the pipette corresponds to (x,y,z) = (1,1,1) µm.

Table 6 Boundary conditions of ISO application via the SICM nanopipette.

	Boundary condition
Electrostatics	
Top (inside) of the pipette at z = 10 µm[1]	$\Psi = \Delta\Psi\times(1-R_0/R_{top})$
x = 10 µm	$\Psi = 0$
y = 10 µm	- ‘’ -
z = 10 µm (outside the pipette)	- ‘’ -
All other boundaries[2]	$\boldsymbol{n}\cdot\nabla\Psi = 0$
Creeping flow	
Top (inside) of the pipette at z = 10 µm	$p = 0$, $(\nabla\mathbf{u}+(\nabla\boldsymbol{u})^T)\boldsymbol{n} = \mathbf{0}$
x = 10 µm	- ‘’ -
y = 10 µm	- ‘’ -
z = 10 µm (outside the pipette)	- ‘’ -
Pipette walls (inside the pipette)	$\boldsymbol{u} = -\mu_{eo}\nabla\Psi$
x = 0	$\boldsymbol{u}\cdot\boldsymbol{n} = 0$, $(\nabla\mathbf{u}+(\nabla\boldsymbol{u})^T)\boldsymbol{n} - ((\nabla\mathbf{u}+(\nabla\boldsymbol{u})^T)\boldsymbol{n}\cdot\boldsymbol{n})\boldsymbol{n} = \boldsymbol{0}$
y = 0	- ‘’ -
All other boundaries	$\boldsymbol{u} = \mathbf{0}$
Transport of diluted species	
Top (inside) of the pipette at z = 10 µm	$c = c_0$
x = 10 µm[3]	$c = c_{flat}$
y = 10 µm	- ‘’ -
z = 10 µm (outside the pipette)	- ‘’ -
All other boundaries	$\boldsymbol{J}\cdot\boldsymbol{n} = \boldsymbol{0}$

[1] R_{top} = 0.50 µm, inner radius at the top, inside of the pipette.

[2] $\boldsymbol{n}$ = unit vector to the surface boundaries.

[3] c_{flat} is the analytical expression for the concentration on a flat surface using Eqs. 1 and 2.

Table 7 Parameters and values for modelling the delivery of ISO.

Name	**Description**	**Value**

R_0	Inner pipette tip radius	40 nm to 60nm
R_1	Outer pipette tip radius	90- 110 nm
θ	Inner pipette half-cone angle	3°
h	Pipette-cardiomyocyte surface distance	500 nm
D	Diffusivity of ISO (Venter 1978)	6.7×10^{-10} m^2/s
μ_{ep}	Electrophoretic mobility of ISO	-7×10^{-9} m^2/V s
μ_{eo}	Electroosmotic mobility of ISO in the pipette (Babakinejad et al. 2013)	1.4×10^{-8} m^2/V s
c_0	ISO concentration inside the pipette at time point 0	50 µM
$\Delta\Psi$	Applied voltage over the pipette	400 mV-600 mV

Approximate expressions have been used to calculate the boundary conditions for the concentration far from the pipette in order to reduce the simulation volume, similar to what has previously been done (Babakinejad et al. 2013). As the features on the surface far from the pipette will have less influence on the concentration profile, they will approach the values for a flat surface. The concentration at those distances can thus be set to the values for a flat surface. Equations 1 to 3 were solved using linear MUltifrontal Massively Parallel sparse direct Solver (MUMPS), with a sufficiently fine mesh size to not produce any significant changes in the outcome of the simulations when further refining the mesh.

6.2.4. Simulating ISO application onto cardiomyocyte structures

In order to quantify the applied concentration and the diffusion of the applied agonist ISO, once it is unloaded from the nanopipette, it was necessary to generate a mathematical model and to simulate the application conditions onto the 3 dimensional structure of cardiomyocytes. Our collaborator Dr. Peter Jönsson (Lund University, Sweden) previously modelled and compared the application of molecules onto flat surface structures via pressure and voltage-driven application (Babakinejad B. et al. 2013). Here he generated a mathematical description of ISO application onto differential cardiomyocyte structures according to my requirements and instructoins. The following description was kindly provided by him. The total flux Q_{tot} of studied molecules out of the tip of the pipette is approximately given by equation 1 (Babakinejad et al. 2013):

$$Q_{\mathrm{tot}} = c_0\left(\mu_{\mathrm{ep}} + \mu_{\mathrm{eo}}\right)\pi R_0 \tan(\theta)\Delta\Psi \qquad (1)$$

taken from (Babakinejad et al. 2013), where c_0 is the concentration of molecules in the bulk of the pipette, R_0 is the inner tip radius of the pipette, θ the inner half cone angle and $\Delta\Psi$ the

voltage drop over the pipette. When the molecules leave the pipette they will be rapidly diluted due to diffusion. For a flat surface the concentration varies with the distance (*x*,*y*) from a point on the surface just below the pipette (0,0) according to the expression in equation 2 (Babakinejad et al. 2013):

$$c(x,y) = 2c_0\left(1 - \exp\left(-Q_{\text{tot}} \Big/ 4\pi c_0 D\sqrt{x^2 + y^2 + h^2}\right)\right) \quad (2)$$

where C_0 is the concentration inside the pipette at time point 0, D is the diffusivity of the molecules and h is the distance between the tip of the pipette and the surface. When $c << c_0$ then equation 2 simplifies to:

$$c(x,y) \approx c_0 \frac{(\mu_{\text{ep}} + \mu_{\text{eo}})R_0 \tan(\theta)\Delta\Psi}{D\sqrt{x^2 + y^2 + h^2}} \quad (3)$$

The concentration thus scales approximately inversely with the distance to the point (0,0) and increases linearly with the radius of the pipette and the applied voltage.

6.2.5. Experimentally testing application precision

10x 10 µM SICM surface scans of control cardiomyocytes were generated before lowering down the nanopipette to 500 nm above the respective structure onto which ISO was to be applied. To apply ISO, the SICM mode of application was changed from pressure to voltage-driven using the settings, that had been mathematically determined through finite element modelling. A detailed description of the SICM and the β_2ARs dependent second messenger signal measurements are given in the general material and methods section (see chapters 2, paragraphs 2.8.1. and 2.8.2.). It is important to note that the bath solution was continuously exchanged via a perfusion system in under 5 seconds.

6.3. Results

6.3.1. Averaged, experimental structures for the simulation of ISO application

The diameter of the T-tubule opening at the primary application site (*x*,*y*,*z*) = (0,0,0) was determined to be approximately 400 nm for both control cardiomyocytes and cardiomyocytes at 4, 8 and 16 weeks post-MI. This is explained by a bias on the part of the experimentalist during the procedure of application, where the agonist is applied preferentially into the most clearly visible T-tubule opening on the corresponding SICM surface scan. The nanopipette scale was taken from (Babakinejad et al. 2013).

Based on the afore-mentioned values, a representative model of healthy cardiomyocytes was constructed from the SICM images (see Figure 50). The geometry consists of a 10 μm^3 cube with parts subtracted to construct:

(i) 0.4 μm wide and 1 μm high grooves along the y-direction, spaced 2 μm apart.

(ii) 0.4 μm wide and 0.25 μm high grooves in the x-direction, spaced 2 μm apart.

(iii) A pipette with an inner tip radius of 50 nm, an outer radius of 100 nm and an inner half cone angle of 3°.

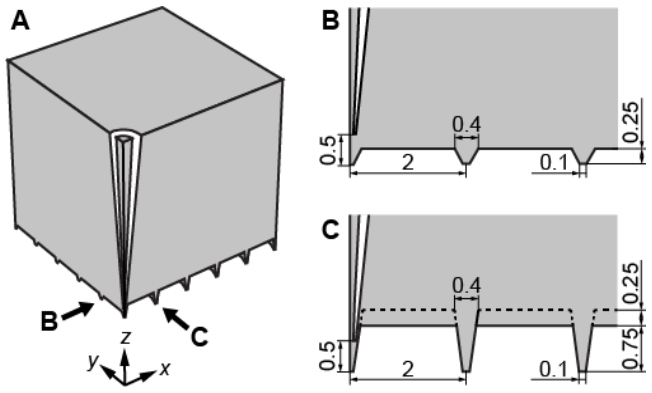

Figure 50 The geometry used in the numerical simulations for a healthy cardiomyocyte. (A) The simulation geometry consists of a cube with the side lengths 10 μm, in which parts have been subtracted to make up the Z-grooves and T-tubule openings as well as the pipette. (B) A zoom-in of the yz-plane at x = 0 together with some of the dimensions of the simulation geometry. (C) A zoom-in of the xz-plane at y = 0 together with some dimensions of the simulation geometry. The pipette has an inner tip radius of 50 nm, an outer tip radius of 100 nm and an inner half cone angle of 3º. All distances are given in μm.

6.3.2. The electrophoretic mobility of ISO

According to the measurements performed for this study (by the company Brookhaven Instruments, UK), the agonist ISO possesses an electrophoretic mobility (μ_{ep}) of -7×10^{-9} m^2/V s and an electroosmotic mobility (μ_{eo}) of 1.4×10^{-8} m^2/V s in the physiological buffer with high ion concentrations used for the experiments described herein. Hence this value was used to solve the finite element model of ISO application onto the cardiomyocyte surface.

6.3.3. Parameters for ISO application onto cardiomyocyte surface structures

Using the finite element model, we were able to simulate ISO application with variable nanopipette openings or application voltages and to predict the resulting concentration and the diffusion distance of ISO after its application onto the T-tubule openings or surface crest structures of cardiomyocytes. The concentration profile will change for different values of $\Delta\Psi$ and R_0, but will roughly scale according to the expression in equation. 3 (data not shown):

$$c(x,y) \approx c_0 \frac{(\mu_{ep} + \mu_{eo}) R_0 \tan(\theta) \Delta\Psi}{D\sqrt{x^2 + y^2 + h^2}}$$

This means that for a pipette with a 20% larger radius the concentration will be 20% larger if all other parameters are kept constant. Similarly, the concentration will scale roughly linearly with the applied voltage under the condition that c << c0. Therefore the experimentalist should strife to use pipettes of a constant size.

The set of parameters that should be used for precise and reproducible experimentation is shown in table 8.

Table 8 Parameters and values predicted for the precise delivery of ISO.

Name	Description	Value
R_0	Inner pipette tip radius	50 nm
R_1	Outer pipette tip radius	100 nm
θ	Inner pipette half-cone angle	3°
h	Pipette-cardiomyocyte surface distance	500 nm
D	Diffusivity of ISO (Venter 1978)	6.7×10^{-10} m^2/s
μ_{ep}	Electrophoretic mobility of ISO	-7×10^{-9} m^2/V s
μ_{eo}	Electroosmotic mobility of ISO in the pipette (Babakinejad et al. 2013)	1.4×10^{-8} m^2/V s

c_0	ISO concentration inside the pipette at time point 0	50 µM
$\Delta\Psi$	Applied voltage over the pipette	400 mV

6.3.4. Simulation of ISO application onto cardiomyocyte surface structures

In the simulation of ISO concentration that results from using an electrical potential of 400mV in the pipette, we found that 7×10^5 molecules/s of ISO per second leave the nanopipette. ISO application was also modelled seperately in the T-tubule (see figure 51) openings and crest areas (see figure 52). In the case of T-tubule openings, the flux of ISO is initially guided along the Z-groove at x = 0 in the y-direction. The concentration along the lower edge at x = 0 and the lower edge at y = 0 is shown where the concentration is also compared to the corresponding value for a flat surface, h = 500 nm above the surface. The distance is given as the value of y for the edge at x = 0 (see Figure 54D) and as the value of x for the edge at y = 0. The simulated concentration over the T-tubule opening at (x, y, z) = (0, 0, 0) is ~3.5 µM, which is approximately 6.5 times higher than the concentration for a theoretical, flat surface at the same distance to the pipette. The reason for this behaviour is that the molecules are initially limited to diffuse along the length of the Z-groove, which results in a slower decrease of the concentration in this direction. At larger distances the molecules start to diffuse in all directions again and the concentration approaches that of a flat surface. In fact, the concentration at the T-tubule opening in the second groove at (x, y, z) = (2 µm, 0, 0) is only ~10% different from the value for a flat surface. This value is approximately 30 times lower than the concentration at the T tubule opening at (x, y, z) = (0, 0, 0). The concentration for the second T-tubule opening in the groove at (x, y, z) = (0, 2 µm, 0) is higher due to the guiding effect of the groove, but is still ~15 times lower compared to the concentration over the first opening (at x = y = 0), indicating that the delivery is mainly limited to the T-tubule opening beneath the pipette. When instead delivering to the crest (see figure 52) in between the Z-grooves (x = y = 1 µm) with h = 500 nm above the surface, the concentration in the nearest T-tubule is approximately 6.5 times lower compared to when delivering directly to the T-tubule (see Figure 51 and 52).

In order to improve the visualisation of the concentration profile of ISO outside the pipette, the colour scale shown in the following figures ranges between 0 and 5 µM, while the concentration in the bulk of the pipette is 50 µM.

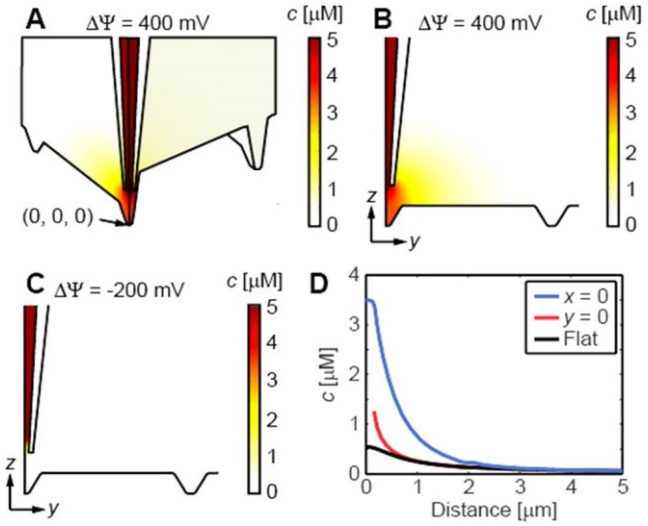

Figure 51 Delivery of ISO to a T-tubule opening. (A) 3D image showing the simulated concentration of ISO when deliver-ing with ΔΨ = 400 mV. The concentration in the bulk of the pipette is 50 µM. (B and C) 2D zoom-in at the plane *x* = 0 showing the concentration distribution at ΔΨ = 400 mV and -200 mV, respectively. (D) Line profiles of the concentration at ΔΨ = 400 mV along the lower edge at x = 0 (blue) and y = 0 (red) as a function of the distance y and x, respectively, from the point (x, y, z) = (0, 0, 0). The black line is the corresponding value for a flat surface using Eqs. 1 and 2.

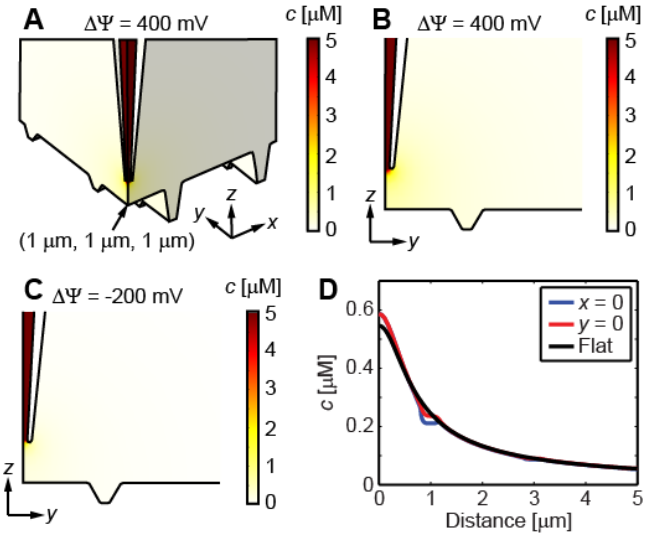

Figure 52 Delivery of ISO to the crest between T-tubule openings. (A) 3D image showing the concentration of ISO when delivering with ΔΨ = 400 mV. The concentration in the bulk of the pipette is 50 µM. (B and C) 2D zoom-in at the plane x = 1 µm showing the concentration distribution at ΔΨ= 400 mV and -200 mV, respectively. (D) Line profiles of the concentration along the lower edge at x = 1 µm (blue) and y = 1 µm (red) as a function of the distance y and x, respectively, from the point (x, y, z) = (1, 1, 1) µm. The black line is the corresponding value for a flat surface using Eqs. 1 and 2 (relative to the point (1, 1, 1) µm).

6.3.5. ISO application via voltage is precise

Under experimental conditions using control cardiomyocytes the β_2ARs dependent second messenger signal of cardiomyocytes only changed when ISO was applied into the T-tubule opening on the cell surface and not on the crest area in between the Z-grooves (see Figure 52). This was in accordance to prior work conducted in our group which elicited the same

results with a pressure-driven approach (Nikolaev et al. 2010). Hence the precision of local agonist application was assured both mathematically and experimentally.

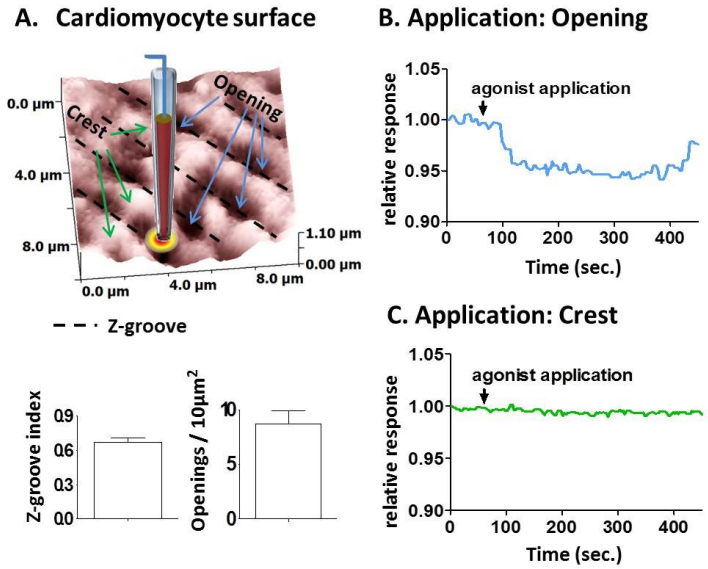

Figure 53 A 10×10 µm SICM surface scan, showing ISO application into an opening on the surface of a cardiomyocyte. Z-grooves are indicated by black dotted lines, openings by blue arrows and crests by green arrows. The respective Z-groove index as well as the number of openings on the 10×10 µm area are summarised in the bottom panel. (B and C) Graphs showing cell internal β_2AR dependent second messenger response to agonist application into (B) the T-tubule opening and (C) onto the crest of the cell surface, obtained by moving the pipette to the respective coordinates on the computer-generated SICM scan and unloading ISO locally via a voltage switch from -200mV to +400mV.

6.4. Discussion

In chapter 6 a mathematical model of ISO application onto variable surface structures was generated and finite element simulations were performed to establish the approximate amount of the molecule ISO being delivered from a nanopipette onto either T-tubule openings or crest structures. To obtain the required parameters for these simulations a representative model of the cell surface and the pipette dimensions was established and the ligands electrophoretic mobility was measured.Though the above described finite element model is highly specific for the SICM microscope this does not diminish its usefulness for further simulations to find out the approximate precision and molecule concentration for any molecule one might wish to apply onto the cardiomyocyte surface via the SICM nanopipette. An increasing number of investigations highlight the importance of compartment-specific signaling of this cell type and the investigation and manipulation of single compartments will become crucial for fully understanding their physiological and pathophysiological regulation. So far SICM is the only method that enables us to perform non-invasive experiments that are as localized as a single T-tubule opening. The analytical verification of this application method presented here encourages a range of further local application experiments. The technique allows delivering essentially any compound to multiple structured cell types with a precision determined by the pipette dimensions and the potential compound charge.

Chapter 7: General discussion

7.1. Study limitations:

7.1.1. Human versus rodent cardiomyocytes:

When working with model organisms such as the rat model of chronic MI used in this thesis it is of paramount importance to realise that not all of this study can be implemented in humans as there are strong species-dependent differences in the structure and in the signalling cascades of cardiomyocytes. These differences are visible in chapter 3 where actual human preparations were available for structural investigations (see chapter 3, paragraph 3.5). As can be seen the rodent cardiomyocytes of intact hearts and at different stages of HF exhibit more regular and more numerous T-tubule structures than human cardiomyocytes from MV surgery patients and hearts obtained from transplantation procedures. Partly the discrepancies between humans and rodent cyclic nucleotide signalling are discussed in chapter 1 when the cardiac PDEs are introduced (see chapter 1, paragraph 1.8.16). Therefore the findings in animal models cannot be translated readily into treatments for human conditions and great care has to be taken when drawing overarching conclusions without due regard to species differences.

7.1.2. FRET measurements after 48h of cardiomyocyte culture

It is well known, that primary cells in culture undergo dedifferentiation and structural loss (Mitcheson et al. 1998). The cardiomyocytes which were utilized for β_2AR and β_3AR dependent cyclic nucleotide signalling studies via FRET measurements were kept in culture and transduced with virus for 48h. The consequence of this loss of structural integrity of cells during prolonged culture might become visible in the FRET measurements themselves, when looking at second messenger diffusion after local agonist application through the SICM nanopipette. Theoretically, based on the dimensions of the TAT network and the size of a single sarcomere, a highly compartmentalised cAMP response in control cells might be expected to spread no further than 2 microns each side. As β_2AR-dependent cAMP pools are regulated in great measure by PDEs in close association with the ACs, physiological cAMP diffusion might be expected to be even smaller. However, during our experiments local stimulation of the β_2ARs in the T-tubule opening via the nanopipette generates a cAMP response that even in control cardiomyocytes diffuses much further (~15 microns) into the cardiomyocyte's cytosol than would be expected in a physiological environment. This could potentially be due to the agonist extracellulary diffusing further inside the TAT network than expected or due to PDEs adhering to the vicinity of GPCRs like the β_2AR and β_3AR and acting like cyclic nucleotide "draining sinks" rather than physical barriers (Terrin et al. 2006). It could

also be due to the structural deterioration which primary cardiomyocytes experience in culture (Mitcheson et al. 1998).

7.1.3. PDE blockers do not distinguish specific splice variants of PDEs

In this thesis β_3AR-dependent cGMP in adult rat cardiomyocytes was shown to be degraded by PDEs 2 and 5. However due to the nature of the PDE blockers, which were used for experimentation, no distinction was made between different isoforms of PDE2 and PDE5. cGMP binding to the PDE2 GAF domain boosts the PDE's activity, which decreases both cAMP and cGMP at similar speed and efficiency. PDE2 possesses 3 splice variants, one of which is PDE2A (Omori and Kotera 2007). Based on published findings in neonatal rat cardiomyocytes showing that β_3AR appears to be regulated via PDE2A (Mongillo et al. 2006) we assume that perhaps this splice variant might primarily fulfil the same function in adult, rat cardiomyocytes. Despite the identification of 3 isoforms of PDE5 with variable tissue specificity (namely PDE5 A1, A2 and A3) no functional variability was found between these isoforms (Kass 2012).

7.1.4. Specificity of available inhibitory compounds

Some of the compounds used for PDE inhibition in chapters 5 are known to provide only partial blockage for the respective PDEs, for which they were said to be specific. These compounds could potentially induce a rise in cAMP and/or cGMP response levels which could skew the data obtained and its respective interpretation. The first of these compounds is the PDE1 blocker Vinpocetine. Even though Vinpocetine is widely used it does not exhibit high PDE1 specificity (Bender and Beavo 2006; Kass 2007; Richter et al. 2011). Indeed, according to literature there is currently no cell permeable, PDE1 blocker, which is specific enough to use without off target effects (Bender and Beavo 2006). Furthermore EHNA, the PDE2 blocker used in this study, has shown to lead to side effects by inhibiting the enzyme adenosine deamidase, which catalyses adenosine into inosine (Miller and Yan 2010). This should however have no direct consequence on the cGMP measurements conducted here. Similarly Tadalafil, the blocker used for PDE5 inhibition, has shown some capacity to bind and block members of the PDE11 family (Omori and Kotera 2007). The PDE11 family appears to have no role in cardiomyocytes though (Miller and Yan 2010). Unlike the PDE inhibitors mentioned above the NOS blocker L-NAME is blocks all three types of NOS: eNOS, iNOS and nNOS. It can therefore not distinguish alterations in eNOS, iNOS and nNOS activity, which have been

reported to take place in HF (Sarker et al. 2001) and in sepsis in connection to β_3ARs (Niu et al. 2014).

7.1.5. Responsiveness of cells to cGMP eliciting reagents

During the FRET investigation of cGMP levels in control and failing cardiomyocytes it was found that not all of the isolated cardiomyocytes responded to stimulation. Indeed only about 50% of cells used for measurements exhibited a clear cGMP induced FRET response. This could be due to cell external reasons, like the solvability or shelf life of the used reagents in solution or to cellular reasons like potentially occurring cell subpopulations which of which some may not react to cGMP triggering stimuli.

7.2. Study summary and future work

7.2.1. Summary: Cardiomyocyte β_2AR-dependent cAMP signalling and structure are altered progressively during the development of HF

MI obliterates a great number of cardiomyocytes and results in the loss of crucial cardiac output as a result of decreased functionality of the remaining myocardium. This loss can only be transiently compensated by the remaining myocardium through the execution of multiple adaptive alterations in both cardiomyocyte structure and contractile function and, without clinical interference, this will progressively lead to end stage HF (Laflamme and Murry 2005) (this reference was in the reference list). The βARs are crucial in transducing the extracellular stimuli of the SNS into intracellular changes in cell contractility (Zipes, Jalife 2009). Signalling via cAMP has been shown to be gravely altered at the end stage of HF (Bristow et al. 1982; Nikolaev et al. 2010; Kishi 2012). Most strikingly, β_2AR relocate from the cardiomyocyte T-tubules to the sarcolemma at the end stage of HF (Nikolaev et al. 2010). The purpose of T-tubules is to synchronize responses to the external stimuli and to serve as conduit from the sarcolemma into the cardiomyocyte body which creates a regulated environment of ions and ligands close to ion channels and receptors. Multiple studies including previous work of our own group have shown that T-Tubules are severely disrupted in both humans and animals at the end stage of HF (Lyon et al. 2009; Wei et al. 2010; Nikolaev et al. 2010; Wagner et al. 2012). However an integrative study was lacking of alterations in cardiomyocyte structure and associated β_2AR dependent cAMP signalling occurring progressively over time during HF development even though it could yield a vital insight into new treatment strategies of HF. Hence chapter 3 focused on the structural alterations of the TAT network and the surface membrane of cardiomyocytes during the progression of HF while chapter 4 dealt with the

FRET based investigation of β_2AR-dependent cAMP signalling during the progression of HF. In healthy cardiomyocytes, where the external surface structure (Z-grooves and crests) and internal TAT network are intact, β_2AR are exclusively situated inside the T-tubules (Nikolaev et al. 2010). At the same time JPH2 efficiently connects T-tubules with the SR (Han et al. 2013). Furthermore in intact cardiomyocytes cAMP is efficiently contained close to the site of β_2AR activation in specific functional compartments. Such cAMP signalling compartments have both physical components as well as virtual components. On the one hand the physical components comprise the TAT network with the β_2ARs positioned inside of it and on the other hand JPH2 bridging of the T-tubule and SR. We now know that both of these are severely altered at the end stage of HF. The components are generally assumed to be additional factors such as the distribution of cAMP downstream targets and cAMP degradation via various PDEs, in particular PDE4 (Terrin et al. 2006; Nikolaev et al. 2010), as well as efficient β_2AR coupling to Gi, as was shown in this thesis. In the experiments described in this thesis the TAT network is already disrupted during early hypertrophy as is visible by a severe loss of tubules (about 50%) in the transverse orientation. These findings are in agreement with observations that have been reported before by other groups (Wei et al. 2010; Wagner et al. 2012). This loss might be partially compensated with a transient increase in longitudinal elements during the early, compensatory phase of HF. This increase might occur due to decreased levels of JPH2, which is important for TAT network tubule orientation (Bennett et al. 2013; Pinali et al. 2013). The increase in longitudinal elements could also be due to alterations in BIN1 which could lead to deformations of the plasma membrane (Hong et al. 2010) or due to a general return to the expression of early developmental genes (Wagner et al. 2012). Also at the early stage of HF the β_2AR-dependent cAMP signal levels in T-tubules decrease significantly in comparison to control cells. At the same time the cAMP signal itself is no longer confined to a small intracellular area but diffuses throughout the whole cell cytosol. At the later, decompensated stage of HF, β_2ARs partially leave their exclusive T-tubular position and probably also uncouple from Gi proteins. Finally at the end stage of HF, the overall TAT network structure and AC activity is disrupted and as a consequence so is the β_2AR cAMP signal. In summary chapters 3 and 4 reveal a build up of time-dependent alterations in the composition of cardiomyocytes after the introduction of chronic MI, each of which might pose a leverage point for improved, differential treatment of HF thus slowing disease progression. The changes in both cardiomyocyte structure and β_2AR-dependent cAMP signalling are summarised and reiterated in the schematic below (see figure 53).

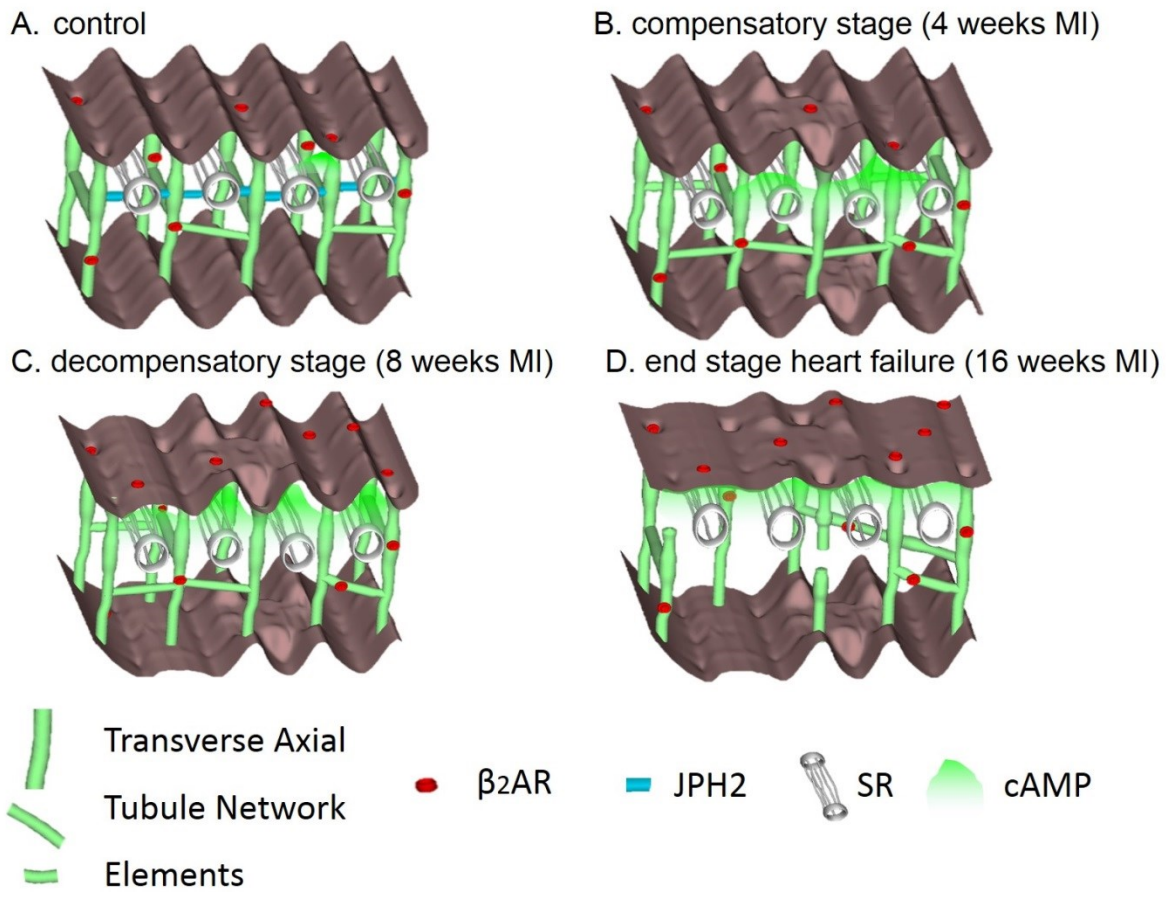

Figure 54 Summary schematic of major changes occuring at the level of local β_2AR dependent cAMP signalling and cardiomyocyte structure at consecutive time points during the progression of HF. In HF the surface structure deteriorates progressively; T-tubule regularity and density is perturbed after only 4 weeks of MI, with the loss of most of JPH2; the number of longitudinal elements increases at 4 and 8 weeks after MI, perhaps as a compensatory mechanism; β_2ARs start to migrate to the crest at 8 weeks of MI, with consequent higher diffusion of cAMP. The schematic was generated by Mr. Andrey Buzuk (Imperial College London) according to my instructions.

7.2.2. Future work: Investigations of the whole heart in terms of cardiomyocyte structure and β_2AR-dependent cAMP signalling investigations of the whole heart

Chapter 3 sets out to elucidate left ventricular cardiomyocyte structure after chemical treatment and most importantly during HF progression. In parallel chapter 4 focussed on the elucidation of β_2AR-dependent cAMP signalling changes in left ventricular cardiomyocytes during HF progression. Still there are many aspects which could be addressed in the future. Depending on their anatomical location in the heart, cardiomyoctes can exhibit structural differences that can range from striking (i.e. atrial versus ventricular cells) to very subtle (i.e. right versus left ventricular cells) in regard to the presence and arrangement of their structure as well as their reactivity to βAR stimulation. For example, the degree of the TAT network presence and function in the atrial cardiomyocytes is much more variable and less defined than in left ventricular cardiomyocytes. Three atrial cell types have been described with either

orderly, disorderly or no TAT systems (Frisk et al. 2014). This structural variability indicates strong differences in the function of atrial versus ventricular cardiomyocytes. Furthermore endocardial and epicardial differences in cardiomyocyte structures such as variations in size (Gerdes et al., 1986) and function (Haynes et al. 2014; Zygmunt et al. 2001; Cordeiro et al. 2004) were observed transmurally. Hence the first evident gap of this doctoral study is that the cardiomyocytes studied herein were primarily from the left ventricle, with no regard to transmural and position-dependent cell differences. Similarly, during the examination of cardiomyocyte structures in their progression towards HF no distinction has been made between cardiomyocytes isolated close or remote from the infarcted area, as cells from all over the remaining ventricular myocardial tissue were isolated together. However it might be difficult to ascertain that the quality of cell isolations remains the same for all anatomical portions, were they to be separated. Perhaps it would be more feasible to investigate cardiomyocyte structure as well as βAR dependent signalling in the entire heart or tissue context. In mouse such structural combined with functional βAR investigations were already performed in the epicardium of intact, Langendorff-perfused hearts through laser confocal *in situ* imaging combined with βARs inhibition (Wei et al. 2010; Chen et al. 2012). This showed that cardiomyocytes remote from the infarct zone experienced only moderate structural alterations while cardiomyocytes close to the infarct zone experienced more severe changes. These changes were in part reversible through βAR-dependent signal blocking. However such studies do not allow the localised stimulation of βARs, which was crucial for the investigations performed in this thesis. A further limitation of the studies described within this thesis regards cardiomyocyte motility. As cardiomyocytes are naturally contracting cells it must be determined what role motion might play in relation to receptor-dependent cyclic nucleotide signalling as well as in receptor localisation and in remodelling of cardiomyocytes. Cell motion is oftentimes conceived as introducing artefacts into live cell and tissue measurements (Tai et al. 2004). As a consequence many techniques consider forcing cells into artificially-induced mechanical arrest to cease unwanted cell movement. This can be achieved by withdrawal of molecules necessary for continuous motion, such as Ca^{2+} (O'Neill et al. 1990), or the F-actin polymerisation inhibitor cytochalasin D (Biermann et al. 1998). The deliberate quenching of motion may be justifiable in relatively static cell types, however, in highly motile cells such as contracting cardiomyocytes making all measurements under static conditions could lead to distorted understanding of GPCR-dependent cell signalling and pharmacology. Mechano-sensitivity of GPRCs and conformational changes of these receptors as a result of shear stress have been shown in a range of cell types and pathways, including endothelial cells (Chachisvilis et al. 2006) and the angiotensin II pathway in cardiac cells (Yasuda et al. 2008). Therefore the induction of mechanical arrest should be considered an investigative limitation,

as motion itself in combination with sub-cellular structures might have an as of yet unappreciated role in helping to form sub-cellular microdomains.

7.2.3. Summary: Rat cardiomyocytes possess functional β_3AR which signal via cGMP

Despite multiple publications from separate groups about the presence and function of β_3AR in human and rodent cardiomyocytes (Gauthier et al. 1996; Mongillo et al. 2006; Amour et al. 2007; Belge et al. 2014) scientists are still sceptical about the physiological importance and actual function of β_3ARs in the heart (Kulandavelu and Hare 2012). This scepticism could in part be due to the low expression levels of β_3ARs. For example only about 0.02% of all βARs present in neonatal rat cardiomyocytes appear to be β_3ARs (Mongillo et al. 2006). However, jumping to the conclusion that something is unimportant just because something is hard to find is a conjecture which should be avoided. To illustrate this point one might cite as an example that, in a specific type of breast cancer, it only takes a single base mutation for the cancerous remodelling of a whole cell (Hart et al. 2015). The fact that there is a disagreement amongst published reports on whether β_3ARs couple to Gs or to Gi further adds to the controversy surrounding this βAR subtype. Endogenous β_3ARs in human heart tissue preparations (Gauthier et al. 1996) and in whole guinea pig hearts (Kitamura et al. 2000) showed negative inotropic effects on contractility, which indicates Gi-dependent signalling. When human β_3ARs were however overexpressed relatively little response to catecholamines has been reported and the receptors appeared to signal via both Gs and Gi (Kohout et al. 2001). The discrepancies in the aforementioned studies could have arisen due to species differences or differences in the stimulatory drugs which were used. Studies conducted in our group in adult rat cardiomyocytes detected no differences in cAMP levels when specifically blocking β_3ARs before whole cell stimulation with ISO (Nikolaev et al. 2010). Therefore β_3AR does not appear to signal via Gs in adult rat cardiomyocytes. This finding is corroborated by a study in neonatal rat cardiomyocytes (Mongillo et al. 2006) which ascribes β_3ARs cAMP lowering effects by inducing increased PDE2 activity as a result of cGMP binding to the PDE's GAF domain. The presence of functional β_3ARs in adult, rat cardiomyocytes has been shown in this thesis after recording the β_3AR-dependent cGMP signal using the novel cGMP FRET sensor Red cGES DE5. This sensor possesses high enough affinity and an EC_{50} around ~50nM for cGMP to measure the cyclic nucleotide reliably in cardiomyocytes (Niino et al. 2009; Götz et al. 2014). Also in this thesis the PDEs responsible for β_3AR-dependent cGMP signalling were identified; PDE2 and PDE5. Increased β_3AR expression levels in the heart have been reported in various disease states including diabetes, sepsis and HF (Moniotte et al. 2001; Moniotte et al. 2007; Niu et al. 2012; Kulandavelu and Hare 2012) as well as in senescence (Birenbaum et al. 2008). Surprisingly despite these reports the cGMP-FRET

measurements in end stage HF cardiomyocytes described in this thesis showed a significantly decrease in the amount of cGMP signalling via β_3AR in comparison to control cardiomyocytes. One of the reasons for this decrease has been shown to be the upregulation of PDE2 activity in end stage HF. Due to this low expression as well as the receptors membrane bound position it is difficult to determine its localisation in the intact cardiomyocyte via immunocytochemcial approaches. A recent study in transgenic mice overexpressing β_3AR in cardiomyocytes used cell fractionation and Western blotting to deduce the putative localisation of β_3ARs. Colocalisation with eNOS and Cav3 showed that the β_3AR are most likely to be situated inside the T-tubules (Belge et al. 2014). The same study showed that β_3ARs fused to the GFP, which were artificially introduced through adenovirus construct transduction, localise to the sarcolemma of neonatal cardiomyocyes (Belge et al. 2014). In this thesis the same fusion β_3AR-GFP proteins were artificially overexpressed in adult rat control cardiomyocytes. The introduced receptor appeared to localise along the Z-lines and this once more indicates that the endogenous receptor might be situated inside the cardiomyocyte T-tubules. To additionally verify this potential localisation combined SICM/FRET studies were applied and indeed showed that β_3AR in control cardiomyocytes sits primarily inside the T-tubules. Given this T-tubular location of the endogenous β_3ARs, one might deduce that their associated cGMP signals may produce an effect only onto confined signalling compartments similar to those displayed by β_2ARs (Nikolaev et al. 2010). The physiological consequences of β_3AR-dependent cGMP production were not studied in this thesis. However prior reports of studies performed in neonatal rat cardiomyocytes suggested that β_3ARs serve as negative inotropic counterbalance to the positive inotropic effects of β_1AR and β_2AR-dependent signalling through Gs. In this study we mainly found that β_3ARs functions by eliciting a cGMP response which is able to trigger an increase in PDE2 activity which in turn probably impacts cAMP level (Mongillo et al. 2006). A similar function is ascribed by others to β_3ARs in the human myocardium where stimulating β_3ARs via a specific agonist BRL37344 as well as NOR while blocking the other two βAR subtypes leads to a significant decrease in contractility. This effect was reversible via the application of the NOS blocker L-NAME (Gauthier et al. 1998). Hence in intact control cardiomyocytes and hearts the function of β_3ARs is assumed to be of an accessory, mitigating nature. The β_3AR may potentially protect the heart from cardiomyocyte remodelling and damage induced via excessive β_1ARs stimulation (Pott et al. 2006). However it has been shown recently that in the human atria the specific β_3AR agonist, BRL37344 elicited both β_1AR and β_2AR-dependent positive inotropic effects as well as β_3AR-dependent negative effects, which might dispute the specificity and hence the effects of this agonist (Pott et al. 2003). A more recent study of the long term effects (≥ 10 days) of activating β_3AR-dependent cGMP signalling in control mice and a transverse aortic constriction (TAC) model of mice furthermore revealed a capacity of β_3ARs to prevent chronic hypertrophic remodelling

arising due to excessive, neurohormonal stimulation the β_1AR and β_2AR subtypes (Belge et al. 2014). In another β_3AR study in mice where MI was induced following LAD aorta ligation β_3AR-dependent cGMP signalling over both the eNOS as well as nNOS furthermore protected cardiac tissue against fibrotic scarring and cardiomyocyte apoptosis (Niu et al. 2014). By generating a nNOS knockout mouse model in combination with TAC the same group established that β_3AR signalling which primarily occurs via eNOS in the intact myocardium redirects its downstream signalling cascade to occur via nNOS in the failing myocardium (Niu et al. 2012). In MI nNOS has been shown to leave the vicinity of RyRs and to colocalise with Cav3 (Kulandavelu and Hare 2012). This switch between NOS isoforms and their localisation might be associated with β_3AR relocalisation, which was observed in this thesis and might further explain the decrease in β_3AR-dependent cGMP signalling which was observed in cardiomyocytes at the end stage of HF also described in this thesis.

In summary chapter 5 has revealed the novel finding that β_3AR-dependent cGMP signalling does occur in adult cardiomyocytes at a level measureable via a cytosolic cGMP FRET sensor. This signal which is generated via sGC is indeed regulated via PDE2 and PDE5 as was previously reported (Mongillo et al. 2006; Takimoto et al. 2007). Also SICM/FRET measurements showed that the β_3ARs are situated inside the T-tubule domain of cardiomyocytes in health but alter their location at the end stage of HF to all over the cardiomyocyte sarcolemma just like β_2ARs (Nikolaev et al. 2010).

7.2.4. Future work: β_3AR-dependent cGMP signalling in adult rat cardiomyocytes

As the suitability of Red cGES DE5 to measure β_3AR-dependent cGMP signalling in adult, rat cardiomyocytes is an entirely, novel finding a lot of research avenues are open for future investigation. Though the rat has hereby proven to be a valid model for the study of endogenous β_3ARs it might be recommendable to see if similar measurements can be made in other animal models. In this thesis the β adrenergic stimulator ISO combined with specific blockage of the β_1ARs and β_2ARs was used to elucidate β_3AR-dependent cGMP signalling in healthy and failing adult rat cardiomyocytes. The study described herein has not investigated any measureable influence of β_3AR-dependent signalling on cardiomyocyte function. This could be the first future step of investigation. Some preliminary experiments might combine contractility studies of cardiomyocytes with the specific inhibition or stimulation of β_3ARs in control cardiomyocytes. In consecutive work it will furthermore be interesting to test and measure the differences in β_3AR-dependent cGMP signalling in intact and failing cardiomyocytes in more detail. For this it would also be desirable to test the specificity of the β_3AR specific agonist BRL37344 to elicit β_3AR-dependent cGMP pools and to obtain subtype

specific NOS inhibitors. If beneficial, functional effects of the β_3ARs can be established in healthy and failing cardiomyocytes the β_3AR might become a promising new therapeutic target in the treatment of HF.

7.2.5 Summary: Mathematical modelling

Chapter 6 of this thesis described a finite element mathematical modelling (FEM) approach to determine the approximate concentration of the agonist ISO applied via the SICM nanopipette during local stimulation of βARs via voltage-dependent dispersion of the pipette solution onto cardiomyocyte surface structures. The model allowed us to simulate the influence of variable parameters on agonist application. It also allowed us to determine the optimal settings necessary for localised receptor stimulation. The described mathematical model is very specifically tailored to our SICM/FRET measurement method as it for example showed a high dependency of agonist application on the nanopipette size and also on the cardiomyocyte structure lying underneath the nanopipette i.e. the T-tubule opening acts as a reservoir for the applied agonist. However despite its specificity the described mathematical model also shows, that the SICM nanopipette delivery of agonists onto cardiomyocytes opens up the possibility of very precisely affecting the ionic or ligand content of only a single T-tubule. No other currently available technique is capable of such focussed manipulation of a structural domain that is as important to cellular function as the T-tubule is to the cardiomyocyte.

7.2.6. Future work: Modelling ISO diffusion through the TAT network

As was stated in the prior paragraph the mathematical model described in this thesis is highly specific to determining the approximate amount of ISO which diffuses out of the SICM nanopipette after a switch of the electrical potential inside the nanopipette from negative to positive. Despite its specificity the model has the potential for further application. In the case of cardiomyocytes, the modelling principle described in this thesis could be applied for delivering fluorescent dyes and investigating diffusion dynamics within a single T-tubule or the whole TAT network, delivering universal and specific agonists as well as ions, for example Ca^{2+} to monitor Ca^{2+} induced Ca^{2+} release. The concept could also be expanded to local application following membrane sealing by the nanopipette, which would allow to avoid diffusion of the agonist into the extracellular space and to achieve higher concentrations inside the TAT structure. Therefore, the model also presents a universal approach to quantify local application and to adjust such parameters as precision, speed and ultimate concentration through modulating the ionic current and pipette structure. Even though the simulations

presented in this thesis were for the specific case of ISO delivery to cardiomyocytes the simulations could also be applied and made useful for other cell types and agonist delivery applications, as it allows the quantification, and possible optimization, of application processes that deal with nanoscale structures that evade experimental determination.

7.3. Concluding statement:

I, Sophie Schobesberger, would like to conclude this thesis by stating that I accomplished the goals I set out for myself and thereby contributed the following to the body of scientific knowledge:

I elucidated progressive changes in the structure and β_2AR-dependent cyclic nucleotide signalling during heart failure progression which could both compensate (i.e. increase of longitudinal elements in the TAT network) or exacerbate the disease phenotype (i.e. β_2AR leaving their exclusive T-tubule position and unlimited cAMP diffusion throughout the cytosol due to a combination of factors).

Furthermore, with the help of the novel cGMP FRET sensor Red cGES DE5, I generated evidence supporting the position of β_3ARs as well as β_3AR-dependent cGMP signalling in intact and failing, adult cardiomyocytes. Additionally I elucidated the position of β_3AR downstream signalling partners like sGC and eNOS.

Lastly I generated a mathematical model to validate the precision of the improved, voltage-driven mode of agonist application via the SICM nanopipette.

References:

Abi-Gerges A, Richter W, Lefebvre F, Mateo P, Varin A, Hey- mes C, Samuel JL, Lugnier C, Conti M, Fischmeister R, Vandecasteele G. (2009) Decreased expression and activity of cAMP phosphodiesterases in cardiac hypertrophy and its impact on beta-adrenergic cAMP signals. *Circ Res*. 105(8):784–792.

Afzal F., Aronsen J.M., Moltzau L.R., Sjaastad I., Levy F.O., Skomedal T. Osnes J., Qvigstad E. (2011) Differential regulation of β2-adrenoceptor-mediated inotropic and lusitropic response by PDE3 and PDE4 in failing and non-failing rat cardiac ventricle. *Br J Pharmacol*. 162(1): 54–71

Agarwal S.R., MacDougall DA, Tyser R, Pugh SD, Calaghan SC, Harvey RD. (2011) Effects of cholesterol depletion on compartmentalized cAMP responses in adult cardiac myocytes. *J Mol Cell Cardiol.* 50 (3) 500-509

Ahmad F, Shen W, Vandeput F, Szabo-Fresnais N, Krall J, Degerman E, Goetz F, Klussmann E, Movsesian M, Manganiello V. (2015) Regulation of sarcoplasmic reticulum Ca2+ ATPase 2 (SERCA2) activity by phosphodiesterase 3A (PDE3A) in human myocardium: phosphorylation-dependent interaction of PDE3A1 with SERCA2. *J Biol Chem*. 290(11):6763-76

Amour J, Loyer X, Le Guen M, Mabrouk N, David JS, Camors E, Carusio N, Vivien B, Andriantsitohaina R, Heymes C, Riou B. (2007) Altered contractile response due to increased beta3-adrenoceptor stimulation in diabetic cardiomyopathy: the role of nitric oxide synthase 1-derived nitric oxide. *Anesthes*. 107(3):452-60.

Aragón JP1, Condit ME, Bhushan S, Predmore BL, Patel SS, Grinsfelder DB, Gundewar S, Jha S, Calvert JW, Barouch LA, Lavu M, Wright HM, Lefer DJ. (2011) Beta3-adrenoreceptor stimulation ameliorates myocardial ischemia-reperfusion injury via endothelial nitric oxide synthase and neuronal nitric oxide synthase activation. *J Am Coll Cardiol*. 58(25):2683-91.

Arai Y., Nagai T. Extensive use of FRET in biological imaging. *Microscopy.* 62(4):419-28.

Babakinejad B, Jönsson P, López Córdoba A, Actis P, Novak P, Takahashi Y, Shevchuk A, Anand U, Anand P, Drews A, Ferrer-Montiel A, Klenerman D, Korchev YE. (2013) Local delivery of molecules from a nanopipette for quantitative receptor mapping on live cells. *Anal. Chem*. 85 (19) 9333-42

Balijepalli R. C., Foell J. D., Hall D. D., Hell J. W., Kamp T. J. (2006) Localization of cardiac L-type Ca2+ channels to a caveolar macromolecular signaling complex is required for b2-adrenergic regulation. *Proc. Natl Acad*. *Sci*. USA 103, 7500–7505

Barouch LA, Harrison RW, Skaf MW, Rosas GO, Cappola TP, Kobeissi ZA, Hobai IA, Lemmon CA, Burnett AL, O'Rourke B, Rodriguez ER, Huang PL, Lima JA, Berkowitz DE, Hare JM. (2002) Nitric oxide regulates the heart by spatial confinement of nitric oxide synthase isoforms. *Nature*. 416(6878):337-9.

Beavo J., Brunton L. (2002) Cyclic nucleotide research -- still expanding after half a century. *Nature reviews. Mol. Cell. Biol*. 3 (9) 710-8

Belge C., Hammond J, Dubois-Deruy E, Manoury B, Hamelet J, Beauloye C, Markl A, Pouleur AC, Bertrand L, Esfahani H, Jnaoui K, Götz KR, Nikolaev VO, Vanderper A, Herijgers P, Lobysheva I, Iaccarino G, Hilfiker-Kleiner D, Tavernier G, Langin D, Dessy C, Balligand JL. (2014) Enhanced expression of β3-adrenoceptors in cardiac myocytes attenuates neurohormone-induced hypertrophic remodeling through nitric oxide synthase. *Circulation.* 129, 451-462

Bennet H.J., Davenport J.B., Collins R.F., Trafford A.W., Pinali C., Kitmitto A. (2013) Human junctophilin-2 undergoes a structural rearrangement upon binding PtdIns(3,4,5)P3 and the S101R mutation identified in hypertrophic cardiomyopathy obviates this response. *Biochem. J.* 456(2):205-17

Bers D. (2002) Excitation contraction coupling. *Nature*. 415, 198-205.

Berthouze-Duquesnes M, Lucas A, Saulière A, Sin YY, Laurent AC, Galés C, Baillie G, Lezoualc'h F. (2012) Specific interactions between Epac1, β-arrestin2 and PDE4D5 regulate β-adrenergic receptor subtype differential effects on cardiac hypertrophic signaling. *Cell Signal*. 25(4):970-80.

Biermann M, Rubart M, Moreno A, Wu J, Josiah-Durant A, Zipes DP. (1998) Differential effects of cytochalasin D and 2,3 butanedione monoxime on isometric twitch force and transmembrane action potential in isolated ventricular muscle: implications for optical measurements of cardiac repolarization. *J Cardiovasc Electrophysiol*. 9(12):1348-57.

Birenbaum A, Tesse A, Loyer X, Michelet P, Andriantsitohaina R, Heymes C, Riou B, Amour J. (2008) Involvement of beta 3-adrenoceptor in altered beta-adrenergic response in senescent heart: role of nitric oxide synthase 1-derived nitric oxide. *Anesthes*. 109,1045–53.

Börner S., Schwede F., Schlipp A., Berisha F., Calebiro D., Lohse M.J., Nikolaev V.O. (2011) FRET measurements of intracellular cAMP concentrations and cAMP analog permeability in intact cells. *Nat. Proto*. 6 (4) 427-38

Boerrigter G, Costello-Boerrigter LC, Burnett JC (2009) Natriuretic peptides in the diagnosis and management of chronic heart failure. *Heart Fail Clin*. 5 (4):501-14

Bossuyt J, Taylor BE, James-Kracke M, Hale CC. (2002) The cardiac sodium-calcium exchanger associates with caveolin-3. *Ann N Y Acad Sci*. 976:197–204

Brandes R., Bers D. (1997) Intracellular Ca2+ increases the mitochondrial NADH concentration during elevated work in intact cardiac muscle. *Circ. Res.* 80 (1) 82-7

Brenner S. & Scott R. (2000) The Mathematical Theory of Finite Element Methods. Springer-Verlag. Corr. 3rd edition. [Chapters 0: Secs. 0.1–0.6, Chapter 3: Secs. 3.1].

Brette F. Orchard C.H. (2003) T-tubule function in mammalian cardiac myocytes. *Circ. Res.* 92 (11) 1182-1192

Brette F., Despa S., Bers D.M., Orchard C.H. (2005) Spatiotemporal characteristics of SR Ca(2+) uptake and release in detubulated rat ventricular myocytes. *J. Mol. Cell. Cardiol*. 39 (5) 804-12

Brette F, Sallé L, Orchard CH. (2006) Quantification of calcium entry at the T-tubules and surface membrane in rat ventricular myocytes. *Biophys J*. 90(1):381-9

Bristow M.R., Ginsburg R., Minobe W., Cubicciotti R.S., Sageman W.S., Lurie K., Billingham M.E., Harrison D.C., Stinson E.B. (1982) Decreased catecholamine sensitivity and beta-adrenergic-receptor density in failing human hearts. *N. Engl. J. Med*. 307 (4) 205-211

Brodde O., Michel M. (1999) Adrenergic and muscarinic receptors in the human heart. *Pharmacol. Rev.* 51 (4) 651-690

Brown L.A., Harding S.E. (1992) The effect of pertussis toxin on beta-adrenoceptor responses in isolated cardiac myocytes from noradrenaline-treated guinea-pigs and patients with cardiac failure. *Br J Pharmacol*. 106(1):115-22

Brown G.C., Borutaite V. (2007) Nitric oxide and mitochondrial respiration in the heart. *Cardiovasc. Res*. 75 (2) 283-90

Brum P., Rolim N., Bacurau V.N., Medeiros A. (2006) Neurohumoral activation in heart failure: The role of adrenergic receptors. *Anais da Academia Brasileira de Ciencias* 78, 485-503

Buxton I., Brunton L. (1983) Compartments of cyclic AMP and protein kinase in mammalian cardiomyocytes *J. Biol. Chem*. 258 (17)10233-10239

Calaghan S., White. E. (2006) Caveolae modulate excitation-contraction coupling and beta2-adrenergic signalling in adult rat ventricular myocytes. *Cardiovasc. Res.* 69, 816–24.

Calebiro D, Nikolaev VO, Gagliani MC, de Filippis T, Dees C, Tacchetti C, Persani L, Lohse MJ. (2009) Persistent cAMP-signals triggered by internalized G-protein-coupled receptors. *PLoS Biol*. 7(8):e1000172.

Candelore MR, Deng L, Tota L, Guan XM, Amend A, Liu Y, Newbold R, Cascieri MA, and Weber AE (1999) Potent and selective human β3-adrenergic receptor antagonists. *J Pharmacol Exp Ther*. 290: 649–655.

Capriotti K., Capriotti J.A. (2012) Dimethyl sulfoxide: history, chemistry, and clinical utility in dermatology. *J Clin Aesthet Dermatol*. 5(9):24-6

Cary S.P., Winger J.A., Marletta M. A. (2005). Tonic and acute nitric oxide signaling through soluble guanylate cyclase is mediated by nonheme nitric oxide, ATP, and GTP. *Proc. Natl. Acad. Sci.* U S A 102,13064−13069.

Casteel DE, Zhang T, Zhuang S, Pilz RB. (2008) cGMP-dependent protein kinase anchoring by IRAG regulates its nuclear translocation and transcriptional activity. *Cell Signal* 20:1392–1399.

Castro L.R.V., Schittl J., Fischmeister R (2010) Feedback control through cGMP-dependent protein kinase contributes to differential regulation and compartmentation of cGMP in rat cardiac myocytes. *Circ. Res*. 107 (10) 1232-40

Chachisvilis M, Zhang YL, Frangos JA. (2006) G protein-coupled receptors sense fluid shear stress in endothelial cells. *Proc Natl Acad Sci*. 103(42):15463-8.

Chen B, Li Y, Jiang S, Xie YP, Guo A, Kutschke W, Zimmerman K, Weiss RM, Miller FJ, Anderson ME, Song LS. (2012) β-Adrenergic receptor antagonists ameliorate myocyte T-tubule remodeling following myocardial infarction. *FASEB J*. 26(6):2531-7

Chen B., Guo A, Zhang C, Chen R, Zhu Y, Hong J, Kutschke W, Zimmerman K, Weiss RM, Zingman L, Anderson ME, Wehrens XH, Song LS. (2013) Critical roles of junctophilin-2 in T-tubule and excitation-contraction coupling maturation during postnatal development. *Cardiovasc. Res*. 100(1):54-62

Clerfond G, Bière L, Mateus V, Grall S, Willoteaux S, Prunier F, Furber A. (2015) End-systolic wall stress predicts post-discharge heart failure after acute myocardial infarction. *Arch Cardiovasc Dis*. S1875-2136

Conti M, Beavo J. (2007) Biochemistry and physiology of cyclic nucleotide phosphodiesterases: essential components in cyclic nucleotide signaling. *Annu. Rev. Biochem*. 76:481-511.

Cordeiro J.M., Greene L., Heilmann C., Antzelevitch D., Antzelevitch C. (2004) Transmural heterogeneity of calcium activity and mechanical function in the canine left ventricle. *Am J Physiol Heart Circ Physiol*. 86 (4) 1471-9

Daaka Y, Luttrell LM, Lefkowitz RJ. (1997) Switching of the coupling of the beta2-adrenergic receptor to different G proteins by protein kinase A. *Nature*. 390(6655):88-91.

De L.A., Stadel J.M., Lefkowitz R.J. (1980) A ternary complex model explains the agonist-specific binding properties of the adenylate cyclase-coupled beta-adrenergic receptor. *J Biol Chem.* 255 (15) 7108-17

Derbyshire E.R., Marletta M. (2009) Biochemistry of Soluble Guanylate Cyclase. *Handbook of Experimental Pharmacology 191*, 17-31

Di Benedetto G, Zoccarato A, Lissandron V, Terrin A, Li X, Houslay MD, Baillie GS, Zaccolo M. (2008) Protein kinase A type I and type II define distinct intracellular signaling compartments. *Circ Res*. 103(8):836-44.

Dickstein K., Cohen-Solal A., Filippatos G., McMurray J., Ponikowski P., Poole-Wilson P.A., Strömberg A., Van Veldhuisen D., Atar D., Hoes A.W., Keren A., Mebazaa A., Nieminen M., Priori S.G., Swedberg K. (2008) ESC Guidelines for the diagnosis and treatment of acute and chronic heart failure. 29, 2388-2442

Dorri F., Niederer PF, Lunkenheimer PP, Anderson RH. (2010) The architecture of the left ventricular myocytes relative to left ventricular systolic function. *Eur. J. Card. Thor. Surg.* 37 (2) 384-92

Dunlay S., Pereira N., Kushwaha S. (2014) Contemporary Strategies in the Diagnosis and Management of Heart Failure. *Mayo Clin. Proc.* 89 (5) 662-676

El-Armouche A, Zolk O, Rau T, Eschenhagen T. (2003) Inhibitory G-proteins and their role in desensitization of the adenylyl cyclase pathway in heart failure. *Cardiovasc. Res.* 60:478–87.

Espinasse I., Iourgenko V., Richer C., Heimburger M., Defer N., Bourin M.C., Samson F., Pussard E., Giudicelli J.F., Michel J.B., Hanoune J., Mercadier J.J. (1999) Decreased type VI adenylyl cyclase mRNA concentration and Mg(2+)-dependent adenylyl cyclase activities and unchanged type V adenylyl cyclase mRNA concentration and Mn(2+)-dependent adenylyl cyclase activities in the left ventricle of rats with myocardial infarction and longstanding heart failure. *Cardiovasc Res*. 42(1):87-98.

Feil R., Kemp-Harper B. (2006) cGMP signalling: from bench to bedside. Conference on cGMP generators, effectors and therapeutic implications. *EMBO Rep*. 7 (2):149-53.

Fink MA, Zakhary DR, Mackey JA, Desnoyer RW, Apperson-Hansen C, Damron DS, Bond M. (2011) AKAP-mediated targeting of protein kinase a regulates contractility in cardiac myocytes. *Circ. Res*. 88:291–297.

Sartiani L, Bochet P, Cerbai E, Mugelli A, Fischmeister R. (2002) Functional expression of the hyperpolarization-activated, non-selective cation current I(f) in immortalized HL-1 cardiomyocytes. *J. Physiol*. 545(1):81-92.

Fischmeister R., Castro L.R.V., Abi-Gerges A., Rochais F., Jurevicius J., Leroy J., Vandecasteele G. (2006) Compartmentation of cyclic nucleotide signaling in the heart: the role of cyclic nucleotide phosphodiesterases. *Circ Res*. 99(8):816-28.

Francis SH, Blount MA, Corbin JD. (2011) Mammalian cyclic nucleotide phosphodiesterases: molecular mechanisms and physiological functions. *Physiol Rev*. 91(2):651-90.

Franzini-Armstrong C, Protasi F, Ramesh V. (1999) Shape, size, and distribution of Ca(2+) release units and couplons in skeletal and cardiac muscles. 77(3):1528-39

Frederiksson R., Lagerström M.C., Lundin L.G., Schiöth H.B. (2003) The G-protein-coupled receptors in the human genome form five main families. Phylogenetic analysis, paralogon groups, and fingerprints. *Mol. Pharmacol*. 63 (6) 1256-72

Frisk M., Koivumäki J.T., Norseng P.A., Maleckar M.M., Sejersted O.M., Louch W.E. (2014) Variable t-tubule organization and Ca2+ homeostasis across the atria. *Am J Physiol Heart Circ. Physiol*. 307 (4) 609-20

Frueh J, Maimari N, Homma T, Bovens SM, Pedrigi RM, Towhidi L, Krams R. (2013) Systems biology of the functional and dysfunctional endothelium. *Cardiovasc Res*. 99(2):334-41

Gamanuma M, Yuasa K, Sasaki T, Sakurai N, Kotera J, Omori K. (2003) Comparison of enzymatic characterization and gene organization of cyclic nucleotide phosphodiesterase 8 family in humans. *Cell Signal*.15:565–574.

Ganguly PK, Dhalla KS, Shao Q, Beamish RE, Dhalla NS. (1997) Differential changes in sympathetic activity in left and right ventricles in congestive heart failure after myocardial infarction. *Am. Heart J*. 133 (3) 340-345

Gauthier C, Tavernier G, Charpentier F, Langin D, Le Marec H. (1996) Functional beta3-adrenoceptor in the human heart. *J Clin Invest*. 98(2):556-62

Giveritz M.M. (2011) Ventricular Assist Devices: Important Information for Patients and Families. *Circulation.* 124: e305-e311

Granneman JG, Lahner KN. (1994) Analysis of human and rodent beta 3-adrenergic receptor messenger ribonucleic acids. *Endocrinology*. 135(3):1025-31.

Götz KR, Sprenger JU, Perera RK, Steinbrecher JH, Lehnart SE, Kuhn M, Gorelik J, Balligand JL, Nikolaev VO. (2014) Transgenic mice for real-time visualization of cGMP in intact adult cardiomyocytes. *Circ Res*. 114(8):1235-45.

Goldstein D. (2011) Catecholamines 101. *Clin. Auton. Res.* 20 (6) 331-352

Goodenough D.A., Paul D.L. (2009) Gap junctions. *Cold Spring Harb. Perspect. Biol.* 1 (1) a002576

Gorelik J, Wright PT, Lyon AR, Harding SE. (2013) Spatial control of the βAR system in heart failure: the transverse tubule and beyond. *Cardiovasc Res*. 1;98(2):216-24.

Gorelik J., Yang L.Q., Zhang Y., Lab M., Korchev Y.E., Harding, S.E. (2006) A novel Z-groove index characterizing myocardial surface structure. *Cardiovasc. Res.*. 72, 422-429

Grandi E., Herren A. (2014) CaMKII-dependent regulation of cardiac Na(+) homeostasis. *Front Pharmacol.* 5:41

Guo A, Zhang X, Iyer VR, Chen B, Zhang C, Kutschke WJ, Weiss RM, Franzini-Armstrong C, Song LS. (2014) Overexpression of junctophilin-2 does not enhance baseline function but attenuates heart failure development after cardiac stress. Proc Natl Acad Sci U S A. 111(33):12240-5.

Han J., Wu H, Wang Q, Wang S. (2013) Morphogenesis of T-tubules in heart cells: The role of junctophilin-2 *Science China Life Sciences*. 56, 647-652

Hansma P.K., Drake B., Marti O., Gould S.A., Prater C.B. (1989) The scanning ion-conductance microscope. *Science*. 243(4891):641-3.

Harvey R., Calaghan S. (2012) Caveolae create local signalling domains through their distinct protein content, lipid profile and morphology. *J. Mol. Cell. Card.* 52 (2) 366-375

Hart JR, Zhang Y, Liao L, Ueno L, Du L, Jonkers M, Yates JR 3rd, Vogt PK. The butterfly effect in cancer: a single base mutation can remodel the cell. *Proc Natl Acad Sci USA*. 112(4):1131-6.

Hatano A., Okada J, Hisada T, Sugiura S. (2012) Critical role of cardiac t-tubule system for the maintenance of contractile function revealed by a 3D integrated model of cardiomyocytes. *J Biomech*. 45(5):815-23

Hayes JS, Brunton LL, Mayer SE. (1980) Selective activation of particulate cAMP-dependent protein kinase by isoproterenol and prostaglandin E1. *J Biol Chem*. 255: 5113–5119.

Haynes P. Nava K., Lawson B., Chung C.S., Mitov M.I., Campbell S.G., Stromberg A.J., Sadayappan S., Bonnell M.R., Hoopes C.W., Campbell K.S. (2014) Transmural heterogeneity of cellular level power output is reduced in human heart failure. *J. Mol. Cell. Card.* 72, 1-8

Heijman J, Volders PG, Westra RL, Rudy Y. (2011) Local control of beta-adrenergic stimulation: effects on ventricular myocyte electrophysiology and Ca(2+)-transient. *J Mol Cell Cardiol* 50:863–71

Hein S., Kostin S., Heling A., Maeno Y., Schaper J. (2000) The role of the cytoskeleton in heart failure. *Cardiovasc. Res*. 45, 273-278

Hill S. (2006) G-protein-coupled receptors: past, present and future. *Brit. J. Pharmac.* 147 S27-37

Hoffman F., Feil R, Kleppisch T, Schlossmann J. (2006) Function of cGMP-dependent protein kinases as revealed by gene deletion. *Physiol. Rev*. 86(1):1-23.

Hoffmann C. Leitz MR, Oberdorf-Maass S, Lohse MJ, Klotz KN. (2004) Comparative pharmacology of human β-adrenergic receptor subtypes - Characterization of stably transfected receptors in CHO cells. *Naunyn Schmiedebergs Arch Pharmacol*. 369, 151-159

Hong T.T., Smyth J.W., Gao D., Chu K.Y., Vogan J.M., Fong T.S., Jensen B.C., Colecraft H.M., Shaw R.M. (2010) BIN1 localizes the L-type calcium channel to cardiac T-tubules. *PLoS Biol.* 8(2):e1000312

Hunter R.J. (1981) Zeta Potential in Colloids. *Science.* 10-11

Hussain R., Aronsen JM, Afzal F, Sjaastad I, Osnes JB, Skomedal T, Levy FO, Krobert KA. (2013) The functional activity of inhibitory G protein (G(i)) is not increased in failing heart ventricle. *J. Mol. Cell. Cardiol*. 56, 129-138

Iancu RV, Ramamurthy G, Warrier S, Nikolaev VO, Lohse MJ, Jones SW, Harvey RD (2008) Cytoplasmic cAMP concentrations in intact cardiac myocytes. *Am J Physiol Cell Physiol*. 295(2):C414-22.

Ibrahim M., Gorelik J., Yacoub M.H., Terracciano C.M. (2011) The structure and function of cardiac t-tubules in health and disease. *Proc. Biol. Sci*. 278(1719):2714-23

Ibrahim M, Navaratnarajah M, Siedlecka U, Rao C, Dias P, Moshkov AV, Gorelik J, Yacoub MH, Terracciano CM. (2012) Mechanical unloading reverses transverse tubule remodelling and normalizes local Ca(2+)-induced Ca(2+)release in a rodent model of heart failure. *Eur J Heart Fail*. 14(6):571-80

Irannejad R, Tomshine JC, Tomshine JR, Chevalier M, Mahoney JP, Steyaert J, Rasmussen SG, Sunahara RK, El-Samad H, Huang B, von Zastrow M. (2013) Conformational biosensors reveal GPCR signalling from endosomes. Nature. 495(7442):534-8

Jacob SW, Herschler R. (1986) Pharmacology of DMSO. *Cryobiology*. 23(1):14-27.

January B, Seibold A, Whaley B, Hipkin RW, Lin D, Schonbrunn A, Barber R, Clark RB. (1997) beta2-adrenergic receptor desensitization, internalization, and phosphorylation in response to full and partial agonists. *J Biol Chem*. 272(38):23871-9.

Johnson WB, Katugampola S, Able S, Napier C, Harding SE. (2012) Profiling of cAMP and cGMP phosphodiesterases in isolated ventricular cardiomyocytes from human hearts: comparison with rat and guinea pig. *Life Sci*. 90(9-10):328-36.

Kadir S.H., Miragoli M., Abu-Hayyeh S., Moshkov A.V., Xie Q., Keitel V., Nikolaev V.O., Williamson C., Gorelik J. (2010) Bile Acid-Induced Arrhythmia Is Mediated by Muscarinic M2 Receptors in Neonatal Rat Cardiomyocytes. *PLoS One*. 5(3): e9689.

Kapiloff MS, Schillace RV, Westphal AM, Scott JD. mAKAP: an A-kinase anchoring protein targeted to the nuclear membrane of differentiated myocytes (1999) *J Cell Sci*. 112(16):2725-36.

.

Kass D. (2012) Cardiac Role of Cyclic-GMP Hydrolyzing Phosphodiesterase Type 5: From Experimental Models to Clinical Trials. *Curr Heart Fail Rep.* 9(3): 192–199

Kaya, Onaran HO., Özcan G., Ambrosio C., Costa T., Balli S., Ugur Ö. Cell contact-dependent functional selectivity of β2-adrenergic receptor ligands in stimulating cAMP accumulation and extracellular signal-regulated kinase phosphorylation. (2012) *J Biol Chem*. 287(9):6362-74

Keef KD, Hume JR, Zhong J. (2001) Regulation of cardiac and smooth muscle Ca2+ channels (CaV 1.2a,b) by protein kinases. *Am J Physiol Cell Physiol*. 281:C1743–C1756.

Kishi T. (2012) Heart failure as an autonomic nervous system dysfunction. *J. Cardiol.* 59 (2) 117-22

Kitamura T, Onishi K, Dohi K, Okinaka T, Isaka N, Nakano T. (2000) The negative inotropic effect of beta3-adrenoceptor stimulation in the beating guinea pig heart. *J Cardiovasc Pharmacol*. 35(5):786-90.

Klauck TM, Faux MC, Labudda K, Langeberg LK, Jaken S, Scott JD. (1996) Coordination of Three Signaling Enzymes by AKAP79, a Mammalian Scaffold Protein. *Science*. 271(5255):1589-1592

Knoll R., Hoshijima M. F., Hoffman HM., Person V. F., Lorenzen-Schmidt I. F., Bang ML., Hayashi T. F., Shiga N. F., Yasukawa H. F., Schaper W. F. (2002) The cardiac mechanical stretch sensor machinery involves a Z disc complex that is defective in a subset of human dilated cardiomyopathy. *Cell*. 67: 1481–93

Kohout TA, Takaoka H, McDonald PH, Perry SJ, Mao L, Lefkowitz RJ, Rockman HA. (2001) Augmentation of cardiac contractility mediated by the human beta(3)-adrenergic receptor overexpressed in the hearts of transgenic mice. *Circ*. 104(20):2485-91.

Kohout T.A., Lefkowitz R.J. (2003) Regulation of G protein-coupled receptor kinases and arrestins during receptor desensitization. *Mol Pharmacol*. 63(1):9-18

Kompa AR and Summers RJ (1999) Desensitization and resensitization of β1- and putative β4-adrenoceptor mediated responses occur in parallel in a rat model of cardiac failure. *Br. J. Pharmacol*. 128:1399–1406.

Krishnamoorthi S., Perotti L.E., Borgstrom N.P., Ajijola O.A., Frid A., Ponnaluri A.V., Weiss J.N., Qu Z., Klug W.S., Ennis D.B., Garfinkel A. (2014) Simulation Methods and Validation Criteria for Modeling Cardiac Ventricular Electrophysiology. *PlosONE.* 9 (12) 114494

Kulandavelu S, Hare JM. (2012) Alterations in β3-adrenergic cardiac innervation and nitric oxide signaling in heart failure. *J Am Coll Cardiol*. 59 (22):1988-90.

Kuznetsova T, Citterio L, Zagato L, Delli Carpini S, Thijs L, Casamassima N, D'hooge J, Bianchi G, Manunta P, Staessen JA. (2013) Left ventricular radial function associated with genetic variation in the cGMP-dependent protein kinase. *Hypertension*. 62(6):1034-9.

Land S, Niederer A., Louch WE, Sejersted OM, Smith NP. (2013) Integrating multi-scale data to create a virtual physiological mouse heart. *Interface Focus*. 3(2): 20120076.

Lee DI, Vahebi S, Tocchetti CG, Barouch LA, Solaro RJ, Takimoto E, Kass DA. (2010) PDE5A suppression of acute beta-adrenergic activation requires modulation of myocyte beta-3 signaling coupled to PKG-mediated troponin I phosphorylation. *Basic Res Cardiol*. 105(3):337-47.

Lee D.I., Zhu G., Sasaki T., Cho G.S., Hamdani N., Holewinski R., Jo S.H., Danner T., Zhang M., Rainer P.P., Bedja D., Kirk J.A., Ranek M.J., Dostmann W.R., Kwon C., Margulies K.B.,

Van Eyk J.E., Paulus W.J., Takimoto E., Kass D.A. (2015) Phosphodiesterase 9A controls nitric-oxide-independent cGMP and hypertrophic heart disease. *Nature*. 519 (7544) 472-476

Lefkowitz R.J., Roth J., Pastan I. (1970) Radioreceptor assay of adrenocorticotropic hormone: new approach to assay of polypeptide hormones in plasma. *Science.* 170(3958):633-5

Laflamme M., Murry C. (2005) Regenerating the heart. *Nat. Biotech*. 23 (7) 845-56

LeGrice I.J., Smaill B.H., Chai L.Z., Edgar S.G., Gavin J.B., Hunter P.J. (1995) Laminar structure of the heart: ventricular myocyte arrangement and connective tissue architecture in the dog. *Am J Physiol.* 269 (2) 571-82

Lichter JG, Carruth E, Mitchell C, Barth AS, Aiba T, Kass DA, Tomaselli GF, Bridge JH, Sachse FB. (2014) Remodeling of the sarcomeric cytoskeleton in cardiac ventricular myocytes during heart failure and after cardiac resynchronization therapy. *J Mol Cell Cardiol*. 72:186-95.

Ligget S., Freedman N., Schwinn D., Lefkowitz R. (1993) Structural basis for receptor subtype-specific regulation revealed by a chimeric beta 3/beta 2-adrenergic receptor. 90, 3665-3669

Litwin SE, Katz SE, Litwin CM, Morgan JP, Douglas PS. (1999) Gender differences in postinfarction left ventricular remodeling. Cardiology. 91(3):173-83.

Lohse M., Egelhardt S. Eschenhagen T. (2003) What Is the Role of β-Adrenergic Signaling in Heart Failure? *Circ. Res.* 93, 896-906

Lukowski R, Krieg T, Rybalkin SD, Beavo J, Hofmann F. (2014) Turning on cGMP-dependent pathways to treat cardiac dysfunctions: boom, bust, and beyond. *Trends Pharmacol Sci*. 35(8):404-13.

Lynch M.J., Baillie G.S., Houslay M.D. (2007) cAMP-specific phosphodiesterase-4D5 (PDE4D5) provides a paradigm for understanding the unique non-redundant roles that PDE4 isoforms play in shaping compartmentalized cAMP cell signalling. *Biochem. Soc. Trans.* 35(5):938-41

Lymperopoulos A., Rengo G., Koch W.J. (2007) Adrenal adrenoceptors in heart failure: fine-tuning cardiac stimulation. *Trends in molecular medicine.* 13 (12) 503-11

Lyon A., MacLeod K., Zhang Y., Garcia E., Kanda G., Lab M., Korchev Y.E., Harding S.E., Gorelik J. (2009). Loss of T-tubules and other changes to surface topography in ventricular myocytes from failing human and rat heart. *Proc. Natl. Acad. of Sci. USA.* 106 (16), 6854–9.

Lyon A, Nikolaev VO, Miragoli M, Sikkel MB, Paur H, Benard L, Hulot JS, Kohlbrenner E, Hajjar RJ, Peters NS, Korchev YE, Macleod KT, Harding SE, Gorelik J. (2012) Plasticity of surface structures and β(2)-adrenergic receptor localization in failing ventricular cardiomyocytes during recovery from heart failure. *Circ Heart Fail*. 5(3):357-65

Madamanchi (2007) Beta-adrenergic receptor signaling in cardiac function and heart failure. *MJM*. 10(2):99-104

Man W, Ming D, Fang D, Chao L, Jing C. (2014) Dimethyl sulfoxide attenuates hydrogen peroxide-induced injury in cardiomyocytes via heme oxygenase-1. *J Cell Biochem*. 115(6):1159-65.

Martinez SE, Beavo JA, Hol WG. (2002) Gaf domains: Two-billion-year-old molecular switches that bind cyclic nucleotides. *Mol Intervent*. 2: 317–323.

Mauban JR, O'Donnell M, Warrier S, Manni S, Bond M. (2009) Akap- scaffolding proteins and regulation of cardiac physiology. *Physiology (Bethesda)*. 24:78–87.

Massion PB, Dessy C, Desjardins F, Pelat M, Havaux X, Belge C, Moulin P, Guiot Y, Feron O, Janssens S, Balligand JL. (2004) Cardiomyocyte-restricted overexpression of endothelial nitric oxide synthase (NOS3) attenuates beta-adrenergic stimulation and reinforces vagal inhibition of cardiac contraction. *Circ.* 110(17):2666-72.

Matkovich SJ, Van Booven DJ, Youker KA, Torre-Amione G, Diwan A, Eschenbacher WH, Dorn LE, Watson MA, Margulies KB, Dorn GW (2009) Reciprocal regulation of myocardial microRNAs and messenger RNA in human cardiomyopathy and reversal of the microRNA signature by biomechanical support. *Circ.* 119(9):1263-71.

McMurray J., Stewart S. (2000) Epidemiology, aetiology, and prognosis of heart failure. *Heart (British Cardiac Society)* 83 (5):596-602

Miller CL, Oikawa M, Cai Y, Wojtovich AP, Nagel DJ, Xu X, Xu H, Florio V, Rybalkin SD, Beavo JA, Chen YF, Li JD, Blaxall BC, Abe J, Yan C (2009) Role of Ca2+/calmodulin-stimulated cyclic nucleotide phosphodiesterase 1 in mediating cardiomyocyte hypertrophy. *Circ Res*. 105(10):956-64.

Miller CL, Yan C. (2010) Targeting cyclic nucleotide phosphodiesterase in the heart: therapeutic implications. *J Cardiovasc Transl Res*. 3(5):507-15.

Minamisawa S., Oshikawaa J., Takeshimab H., Hoshijimac M., Wangd Y., Chienc K.R., Ishikawaa Y., Matsuoka R. (2004) Junctophilin type 2 is associated with caveolin-3 and is down-regulated in the hypertrophic and dilated cardiomyopathies. Biochem Biophys Res Comm. 325 (2004) 852–856

Mitcheson J.S., Hancox J.C., Levi A.J. (1998) Cultured adult cardiac myocytes: future applications, culture methods, morphological and electrophysiological properties. *Cardiovasc. Res*. 39(2):280-300

Moltzau LR, Aronsen JM, Meier S, Nguyen CH, Hougen K, Ørstavik Ø, Sjaastad I, Christensen G, Skomedal T, Osnes JB, Levy FO, Qvigstad E. (2013) SERCA2 activity is involved in the CNP-mediated functional responses in failing rat myocardium. Br J Pharmacol. 170(2):366-79.

Moltzau LR, Aronsen JM, Meier S, Skogestad J, Ørstavik Ø, Lothe GB, Sjaastad I, Skomedal T, Osnes JB, Levy FO, Qvigstad E. (2014) Different compartmentation of responses to brain natriuretic peptide and C-type natriuretic peptide in failing rat ventricle. *J Pharmacol Exp Ther*. 350(3):681-90.

Mongillo M., Tocchetti C.G., Terrin A., Lissandron V., Cheung Y.F., Dostmann W.R., Pozzan T., Kass D., Paolocci N., Houslay M.D., Zaccolo M. (2006) Compartmentalized phosphodiesterase-2 activity blunts beta-adrenergic cardiac inotropy via an NO/cGMP-dependent pathway. 98 (2) 226-34

Monnet E., Chachques J. (2005) Animal models of heart failure: what is new? *The Annals of thoracic surgery*. 79 (4) 1445-53

Moniotte S, Kobzik L, Feron O, Trochu JN, Gauthier C, Balligand JL. (2001) Upregulation of beta(3)-adrenoceptors and altered contractile response to inotropic amines in human failing myocardium. *Circulation*. 27;103(12):1649-55.

Moniotte S, Belge C, Sekkali B, Massion PB, Rozec B, Dessy C, Balligand JL. (2007) Sepsis is associated with an upregulation of functional beta3 adrenoceptors in the myocardium. *Eur J Heart Fail*. 9(12):1163-71.

Mudd J., Kass D. (2008) Tackling heart failure in the twenty-first century. *Nature.* 451 (7181) 919-28

Mukoyama, M., Nakao, K., Hosoda, K., Suga, S., Saito, Y., Ogawa, Y., Shirakami G, Jougasaki M, Obata K, Yasue H (1991). Brain natriuretic peptide as a novel cardiac hormone in humans. Evidence for an exquisite dual natriuretic peptide system, atrial natriuretic peptide and brain natriuretic peptide*. J. Clin. Invest*. 87, 1402–1412.

Nagai T., Komuro I. (2012) Gene and cytokine therapy for heart failure: molecular mechanisms in the improvement of cardiac function. *AJP: Heart and Circulatory Physiology.* 303, 501-512

Nahrendorf M, Wiesmann F, Hiller KH, Hu K, Waller C, Ruff J, Lanz TE, Neubauer S, Haase A, Ertl G, Bauer WR. (2001) Serial cine-magnetic resonance imaging of left ventricular remodeling after myocardial infarction in rats. *J Magn Reson Imaging*.14(5):547-55.

Nantel F, Bonin H, Emorine LJ, Zilberfarb V, Strosberg AD, Bouvier M, Marullo S. (1993) The human beta 3-adrenergic receptor is resistant to short term agonist-promoted desensitization. *Mol Pharmacol*. 43:548–555.

Napp A, Brixius K, Pott C, Ziskoven C, Boelck B, Mehlhorn U, Schwinger RH, Bloch W. (2009) Effects of the beta3-adrenergic agonist BRL 37344 on endothelial nitric oxide synthase phosphorylation and force of contraction in human failing myocardium. *J Card Fail*. 15(1):57-67.

Nerbonne J.M., Kass R. (2005) Molecular physiology of cardiac repolarization. *Physiol Rev*. 85 (4) 1205-53

Niino Y., Hotta K., Oka K. (2009) Simultaneous live cell imaging using dual FRET sensors with a single excitation light. *PLoS One*. 4(6):e6036

Nikolaev V.O., Bünemann M., Hein L., Hannawacker A., Lohse M.J. (2004) Novel single chain cAMP sensors for receptor-induced signal propagation. *J Biol Chem*. 279(36):37215-8

Nikolaev V.O., Lohse M. (2006) Monitoring of cAMP synthesis and degradation in living cells. *Physiology.* 21, 86-92

Nikolaev V.O., Moshkov A., Lyon A.R., Miragoli M., Novak P., Paur H., Lohse M.J., Korchev Y.E., Harding S.E., Gorelik J. (2010) Beta2-adrenergic receptor redistribution in heart failure changes cAMP compartmentation. *Science*. 327 (5973) 1653-7.

Nishimura S, Nagai S, Katoh M, Yamashita H, Saeki Y, Okada J, Hisada T, Nagai R, Sugiura S. (2005) Microtubules modulate the stiffness of cardiomyocytes against shear stress. *Circ Res*. 98(1):81-7.

Niu X., Zhao L., Li X., Xue Y., Wang B., Lv Z., Chen J., Sun D., Zheng Q. (2012) Cardioprotective Effect of Beta-3 Adrenergic Receptor Agonism. *JACCS*. 59(22):1979-1987

Niu X., Lianyou Z., Xue L., Yusheng X., Bin W. Zongqiang L., Jianghong C., Dongdong S., Zheng Q. (2014) β3-Adrenoreceptor Stimulation Protects against Myocardial Infarction Injury via eNOS and nNOS Activation. *PLoS One*. 9(6): e98713.

Novak P, Li C, Shevchuk AI, Stepanyan R, Caldwell M, Hughes S, Smart TG, Gorelik J, Ostanin VP, Lab MJ, Moss GW, Frolenkov GI, Klenerman D, Korchev YE. (2009) Nanoscale live-cell imaging using hopping probe ion conductance microscopy. *Nat Methods*. (4):279-81.

O'Hara T, Virág L, Varró A, Rudy Y. (2011) Simulation of the undiseased human cardiac ventricular action potential: model formulation and experimental validation. *PLoS Comput Biol*. 7 (5):e1002061

Okada T., Takeda K., Kouyama T. (1998) Highly selective separation of rhodopsin from bovine rod outer segment membranes using combination of divalent cation and alkyl(thio)glucoside. *Photochem. Photobiol*. 67(5):495-9

Omori K., Kotera J. (2007) Overview of PDEs and their regulation. *Circ. Res*. 100 (3): 309-327

O'Neill SC, Mill JG, Eisner DA. (1990) Local activation of contraction in isolated rat ventricular myocytes. *Am J Physiol*. 258(6 Pt 1):C1165-8.

Pandey K.N. (2014) Guanylyl cyclase/natriuretic peptide receptor-A signaling antagonizes phosphoinositide hydrolysis, Ca2+ release, and activation of protein kinase C. *Frontiers in Molecular Neuroscience*. 7, 1-14

Pasek M., Simurda J, Christé G, Orchard CH. (2008) Modelling the cardiac transverse-axial tubular system. *Prog Biophys Mol Biol*. 96(1-3):226-43.

Pasek M, Simurda J, Orchard CH. (2012) Role of t-tubules in the control of trans-sarcolemmal ion flux and intracellular Ca2+ in a model of the rat cardiac ventricular myocyte. *Eur Biophys J*. 41:491–503

Petroff MG, Kim SH, Pepe S, Dessy C, Marbán E, Balligand JL, Sollott SJ. (2001) Endogenous nitric oxide mechanisms mediate the stretch dependence of Ca2+ release in cardiomyocytes. *Nat Cell Biol*. 3(10):867-73

Pinali C., Bennett H., Davenport J.B., Trafford A.W., Kitmitto A. (2013) Three-dimensional reconstruction of cardiac sarcoplasmic reticulum reveals a continuous network linking transverse-tubules: this organization is perturbed in heart failure. *Circ. Res.* 113(11):1219-30

Pott C, Brixius K, Bundkirchen A, Bolck B, Bloch W, Steinritz D, Mehl- horn U, Schwinger RH (2003) The preferential beta3-adrenoceptor agonist BRL 37344 increases force via beta1-/beta2-adrenoceptors and induces endothelial nitric oxide synthase via beta3-adrenoceptors in human atrial myocardium. *Br J Pharmacol.* 138: 521–529.

Pott C, Brixius K, Bloch W, Ziskoven C, Napp A, Schwinger RH. (2003) Beta3-adrenergic stimulation in the human heart: signal transduction, functional implications and therapeutic perspectives. *Die Pharmazie.* 61(4):255-60.

Potter LR, Abbey-Hosch S, Dickey DM. (2006) Natriuretic peptides, their receptors and cGMP-dependent signaling functions. *Endocr Rev*. 27:47–72.

Polakova E, Sobie EA. (2013) Alterations in T-tubule and dyad structure in heart disease: challenges and opportunities for computational analyses. *Cardiovasc. Res*. 98, 233–239

Pullan A.J., Cheng L.K., Buist M.L. (2005) Mathematically Modelling the Electrical Activity of the Heart: From Cell to Body Surface and back again. Copyright World Scientific Publishing Co. Pte. Ltd. USA. Pages 5-6.

Pyriochou A, Papapetropoulos A. (2005) Soluble guanylyl cyclase: more secrets revealed. *Cell Signal.* 17:407–443.

Rasmussen, S. G., Choi, H. J., Rosenbaum, D. M., Kobilka, T. S., Thian, F. S., Edwards, P. C., Kobilka, B. K. (2007). Crystal structure of the human beta-2 adrenergic G-protein-coupled receptor. *Nature*. 450(7168), 383-387.

Richards M.A., Clarke J.D., Saravanan P., Voigt N., Dobrev D., Eisner D.A., Trafford A.W., Dibb K.M. (2011) Transverse tubules are a common feature in large mammalian atrial myocytes including human. *Am. J. Physiol. Heart Circ. Physiol*. 301 (5) 1996-2005

Richter, W., Xie, M., Scheitrum, C., Krall, J., Movsesian, M.A. & Conti, M. (2011) Conserved expression and functions of PDE4 in rodent and human heart. *Basic Res. Cardiol*. 106, 249–262.

Ryter SW, Alam J, Choi AM. (2006) Heme oxygenase-1/carbon monoxide: from basic science to therapeutic applications. *Physiol Rev*. 86(2):583-650.

Sacconi L. Ferrantini C., Lotti J., Coppini R., Yan P., Loew L.M., Tesi C., Cerbai E., Poggesi C., Pavone F.S. (2012) Action potential propagation in transverse-axial tubular system is impaired in heart failure. *PNAS, USA.* 109 (15) 5815-9

Saji K., Fukumoto Y., Suzuki J., Fukui S., Nawata J., Shimokawa H. (2007) Colchicine, a microtubule depolymerizing agent, inhibits myocardial apoptosis in rats. *Tohoku J Exp Med*. 213(2):139-48.

Sanchez-Quintana D., Garcia-Martinez V., Hurle J.M. (1990) Myocardial fibre architecture in the human heart. *Acta. Anat.* 138:352–358.

Sarkar D, Vallance P, Harding SE. (2001) Nitric oxide: not just a negative inotrope. *Eur J Heart Fail*. 3(5):527-34.

Schindelin (2012) Arganda-Carreras I, Frise E, Kaynig V, Longair M, Pietzsch T, Preibisch S, Rueden C, Saalfeld S, Schmid B, Tinevez JY, White DJ, Hartenstein V, Eliceiri K, Tomancak P, Cardona A. Fiji: an open-source platform for biological-image analysis. *Nat. Meth.* 9(7):676-82

Scriven D.R.L., Dan P., Moore E.D.W. (2000) Distribution of Proteins Implicated in Excitation-Contraction Coupling in Rat Ventricular Myocytes. *Biophysical J*. 79, 2682–2691

Seki S., Nagashima M., Yamada Y., Tsutsuura M., Kobayashi T., Namiki A., Tohse N. (2003) Fetal and postnatal development of Ca2+ transients and Ca2+ sparks in rat cardiomyocytes. *Cardiovasc. Res*. 58(3):535-48.

Severs N. (2000) The cardiac muscle cell. *BioEssays.* 22, 188-199

Shaffer F., Mccraty R., Zerr C.L., Dorn V. (2014) A healthy heart is not a metronome: an integrative review of the heart's anatomy and heart rate variability. *Front. Psych.* 5 (1) 1-19

Shah M.R., Califf RM, Nohria A, Bhapkar M, Bowers M, Mancini DM, Fiuzat M, Stevenson LW, O'Connor CM. (2011) The STARBRITE trial: a randomized, pilot study of B-type natriuretic peptide-guided therapy in patients with advanced heart failure. *J Card Fail*. 17(8):613-21

Shimizu H., Okabe M. (2007) Evolutionary origin of autonomic regulation of physiological activities in vertebrate phyla. J. Comp. *Physiol. A. Neuroethol. Sens. Neural. Behav. Physiol*. 193 (10) 1013-9

Shakur Y, Holst LS, Landstrom TR, Movsesian M, Degerman E, Manganiello V. (2001) Regulation and function of the cyclic nucleotide phosphodiesterase (PDE3) gene family. *Prog Nucleic Acid Res Mol Biol*. 66:241–277.

Soeller C., Crossman D., Gilbert R., Cannell MB. (2007) Analysis of ryanodine receptor clusters in rat and human cardiac myocytes. *Nat. Acad. Scien. USA* 104 (38) 14958–14963

Solaro J.R., Stull J.T. (2011) Thematic minireview series on signaling in cardiac sarcomeres in health and disease. *J. Biol. Chem*. 286, 9895

Song K.S., Scherer P.E., Tang Z., Okamoto T., Li S., Chafel M., Chu C., Kohtz D.S., Lisanti M.P. (1996) Expression of caveolin-3 in skeletal, cardiac, and smooth muscle cells. Caveolin-3 is a component of the sarcolemma and co-fractionates with dystrophin and dystrophin-associated glycoproteins. *J. Biol. Chem*. 271 (25) 15160-5

Song LS, Sobie EA, McCulle S, Lederer WJ, Balke CW, Cheng H. (2006) Orphaned ryanodine receptors in the failing heart. Proc Natl Acad Sci U S A. 103(11):4305-4310.

Soni S., Scholten A., Vos M.A., Van Veen T.A.B. (2014) Anchored protein kinase A signalling in cardiac cellular electrophysiology. *J. Cell. Mol. Med*. 18(11):2135-2146

Sperelakis N., Rubio R. (1971) An orderly lattice of axial tubules which interconnect adjacent transverse tubules in guinea-pig ventricular myocardium. *J. Mol. Cell. Card.* 2(3):211-220

Sprenger J, Nikoolaev V.O. (2013) Biophysical Techniques for Detection of cAMP and cGMP in Living Cells. *Int J Mol Sci*. 14(4):8025-46

Stangherlin A, Gesellchen F, Zoccarato A, Terrin A, Fields LA, Berrera M, Surdo NC, Craig MA, Smith G, Hamilton G, Zaccolo M. (2011) cGMP signals modulate cAMP levels in a

compartment-specific manner to regulate catecholamine-dependent signaling in cardiac myocytes. *Circ. Res*. 108(8):929-39.

Stangherlin A, Zaccolo M. (2012) Phosphodiesterases and subcellular compartmentalized cAMP signaling in the cardiovascular system. A*merican journal of physiology. Heart and circulatory physiology.* 302 (2) H379-90

Sugden PH, Fuller SJ, Weiss SC, Clerk A. (2008) Glycogen synthase kinase 3 (GSK3) in the heart: a point of integration in hypertrophic signalling and a therapeutic target? A critical analysis. *Br J Pharmacol*. 1:S137-53.

Szmant HH. (1975) Physical properties of dimethyl sulfoxide and its function in biological systems. *Ann N Y Acad Sci*. 27;243:20-3

Takimoto E, Belardi D, Tocchetti CG, Vahebi S, Cormaci G, Ketner EA, Moens AL, Champion HC, Kass DA. (2007) Compartmentalization of cardiac beta-adrenergic inotropy modulation by phosphodiesterase type 5. *Circ*. 115:2159–2167.

Tai DC, Caldwell BJ, LeGrice IJ, Hooks DA, Pullan AJ, Smaill BH. (2004) Correction of motion artifact in transmembrane voltage-sensitive fluorescent dye emission in hearts. *Am J Physiol Heart Circ Physiol*. 287(3):H985-93

Terrin A, Di Benedetto G, Pertegato V, Cheung YF, Baillie G, Lynch MJ, Elvassore N, Prinz A, Herberg FW, Houslay MD, Zaccolo M. (2006) PGE(1) stimulation of HEK293 cells generates multiple contiguous domains with different [cAMP]: role of compartmentalized phosphodiesterases. J Cell Biol. 175(3): 441–451.

Tian Q., Pahlavan S, Oleinikow K, Jung J, Ruppenthal S, Scholz A, Schumann C, Kraegeloh A, Oberhofer M, Lipp P, Kaestner L. (2012) Functional and morphological preservation of adult ventricular myocytes in culture by sub-micromolar cytochalasin D supplement. *J Mol Cell Cardiol.* 52(1):113-24

Timofeyev V, Myers RE, Kim HJ, Woltz RL, Sirish P, Heiserman JP, Li N, Singapuri A, Tang T, Yarov-Yarovoy V, Yamoah EN, Hammond HK, Chiamvimonvat N. (2013) Adenylyl cyclase subtype-specific compartmentalization: differential regulation of L-type Ca2+ current in ventricular myocytes. *Circ. Res*. 112(12):1567-76.

Tobisse K., Ishikawa Y, Holmer SR, Im MJ, Newell JB, Yoshie H, Fujita M, Susannie EE, Homcy CJ. (1994) Changes in type VI adenylyl cyclase isoform expression correlate with a decreased capacity for cAMP generation in the aging ventricle. C*irc. Res.* 74(4):596-603.

Tomita H. Nazmy M., Kajimoto K., Yehia G., Molina C., Sadoshima J., (2003) Inducible cAMP early repressor (ICER) is a negative-feedback regulator of cardiac hypertrophy and an important mediator of cardiac myocyte apoptosis in response to β-adrenergic receptor stimulation. *Circ. Res.* 93, 12-22

Torrent-Guasp F., Kocica M.J., Corno A., Komeda M., Cox J., Flotats A., Ballester-Rodes M., Carreras-Costa F. (2004) Systolic ventricular filling. *Eur. J. Card. Thor. Surg*. 25, 376-386

Tranter M.H., Wright P.T., Sikkel M.B., Lyon A.R. (2013) Takotsubo Cardiomyopathy: The Pathophysiology. *Heart Fail. Clin*. 9 (2) 187–196

Ungerer M. Böhm M., Elce J.S., Erdmann E., Lohse M.J. (1993) Altered expression of beta-adrenergic receptor kinase and beta 1- adrenergic receptors in the failing human heart. *Circ*. 87(2) 454-463

Vandeput F, Wolda SL, Krall J, Hambleton R, Uher L, McCaw KN, Radwanski PB, Florio V, Movsesian MA. (2007) Cyclic Nucleotide Phosphodiesterase PDE1C1 in Human Cardiac Myocytes. *J. Biol. Chem.,* 282, 32749-32757.

Venter J.C. (1978) Cardiac sites of catecholamine action: diffusion models for soluble and immobilized catecholamine action on isolated cat papillary muscles. *Mol. Pharmacol*. (4):562-74.

Verde I, Vandecasteele G, Lezoualc'h F, Fischmeister R. (1999) Characterization of the cyclic nucleotide phosphodiesterase subtypes involved in the regulation of the L-type Ca2+ current in rat ventricular myocytes. *Br J Pharmacol*. 127(1):65-74.

Vlahovich N., Kee AJ, Van der Poel C, Kettle E, Hernandez-Deviez D, Lucas C, Lynch GS, Parton RG, Gunning PW, Hardeman EC. (2009) Cytoskeletal tropomyosin Tm5NM1 is required for normal excitation– contraction coupling in skeletal muscle. *Mol. Biol. Cell*. 20, 400– 409.

Wagner E, Lauterbach MA, Kohl T, Westphal V, Williams GS, Steinbrecher JH, Streich JH, Korff B, Tuan HT, Hagen B, Luther S, Hasenfuss G, Parlitz U, Jafri MS, Hell SW, Lederer WJ, Lehnart SE. (2012) Stimulated emission depletion live-cell super-resolution imaging shows proliferative remodeling of T-tubule membrane structures after myocardial infarction. *Circ. Res*. 111(4):402-414

Wallukat G. (2002) The β-adrenergic receptors. *Herz.* 27 (7) 683-690

Wan X., Bryant S.M., Hart G. (2003) A topographical study of mechanical and electrical properties of single myocytes isolated from normal guinea-pig ventricular muscle. *J Anat.* 202 (6) 525-36.

Wang Y., De Archangelis V., Gao X., Ramani B., Jung Y.S., Xiang, Y. (2008) Norepinephrine- and Epinephrine-induced Distinct β2-Adrenoceptor Signaling Is Dictated by GRK2 Phosphorylation in Cardiomyocytes. *J. Biol. Chem. 283*, 1799-1807.

Watts VL, Sepulveda FM, Cingolani OH, Ho AS, Niu X, Kim R, Miller KL, Vandegaer K, Bedja D, Gabrielson KL, Rameau G, O'Rourke B, Kass DA, Barouch LA. (2013) Anti-hypertrophic and anti-oxidant effect of beta3-adrenergic stimulation in myocytes requires differential neuronal NOS phosphorylation. *J Mol Cell Cardiol*. 62, 8-17

Weber K. (1989) Cardiac interstitium in health and disease: the fibrillar collagen network. *J. A.C.C.* 13 (7) 1637-1652

Wei S, Guo A, Chen B, Kutschke W, Xie YP, Zimmerman K, Weiss RM, Anderson ME, Cheng H, Song LS. (2010) T-tubule remodeling during transition from hypertrophy to heart failure. *Circ. Res*. 107(4):520-31

Wong J., Baddeley D., Bushong E.A., Yu Z., Ellisman M.H., Hoshijima M., Soeller C. (2013) Nanoscale distribution of ryanodine receptors and caveolin-3 in mouse ventricular myocytes: dilation of t-tubules near junctions*. Biophys J*. 104 (11) 22-4

Woodman S.E, Park D.S., Cohen A.W., Cheung M.W., Chandra M., Shirani J., Tang B., Jelicks L.A., Kitsis R.N., Christ G.J., Factor S.M., Tanowitz H.B., Lisanti M.P. (2002) Caveolin-3 knock-out mice develop a progressive cardiomyopathy and show hyperactivation of the p42/44 MAPK cascade. *J. Biol. Chem*. 277 (41) 38988-97

Wright P.T., Nikolaev V.O., O'Hara T., Diakonov I., Bhargava A., Tokar S., Schobesberger S., Shevchuk A.I., Sikkel M.B., Wilkinson R., Trayanova N.A., Lyon A.R., Harding S.E., Gorelik J. (2014) Caveolin-3 regulates compartmentation of cardiomyocyte beta2-adrenergic receptor-mediated cAMP signalling. *J. Mol. Cell. Card.* 67, 38-48

Xiang Y., Rybin V.O., Steinberg S.F., Kobilka B. (2002) Caveolar localization dictates physiologic signaling of beta 2-adrenoceptors in neonatal cardiac myocytes. *J Biol Chem*. 277 (37) 34280-6

Xiang, Y. (2011). Compartmentalization of beta-adrenergic signals in cardiomyocytes. *Circ. Res*. 109(2), 231–44.

Xiao R. (2001) Beta-adrenergic signaling in the heart: dual coupling of the beta2-adrenergic receptor to G(s) and G(i) proteins. *Science*. (104) re15

Xiao R, Cheng H, Zhou YY, Kuschel M, Lakatta EG. (1999) Recent advances in cardiac beta(2)-adrenergic signal transduction. *Circ Res.* 26;85(11):1092-100.

Xiao R., Ji X., Lakatta E.G. (1995) Functional coupling of the beta2-adrenoceptor to a pertussis toxin-sensitive G protein in cardiac myocytes. *Mol. Pharmacol*. 47, 322–329

Xiao RP, Zhang SJ, Chakir K, Avdonin P, Zhu W, Bond RA, Balke CW, Lakatta EG, Cheng H. (2003) Enhanced G(i) signaling selectively negates beta2-adrenergic receptor (AR)--but not beta1-AR-mediated positive inotropic effect in myocytes from failing rat hearts. *Circulation*. 108(13):1633-9.

Yan AT, Yan RT, Spinale FG, Afzal R, Gunasinghe HR, Stroud RE, McKelvie RS, Liu PP. (2008) Relationships between plasma levels of matrix metalloproteinases and neurohormonal profile in patients with heart failure. *Eur J Heart Fail*. 10(2):125-8

Yasuda N, Miura S, Akazawa H, Tanaka T, Qin Y, Kiya Y, Imaizumi S, Fujino M, Ito K, Zou Y, Fukuhara S, Kunimoto S, Fukuzaki K, Sato T, Ge J, Mochizuki N, Nakaya H, Saku K, Komuro I. (2008) Conformational switch of angiotensin II type 1 receptor underlying mechanical stress-induced activation. *EMBO Rep*. 9(2):179-86

Yuan SM, Jing H. (2010) Cardiac pathologies in relation to Smad-dependent pathways. *Interact Cardiovasc Thorac Surg*. 11(4):455-60.

Yue T.L., Gu J.L., Wang C., Reith A.D., Lee J.C., Mirabile R.C., Kreutz R., Wang Y., Maleeff B., Parsons AA., Ohlstein EH. (2000) Extracellular signal-regulated kinase plays an essential role in hypertrophic agonists, endothelin-1 and phenylephrine-induced cardiomyocyte hypertrophy. *J Biol Chem*, 37895–37901

Zaccolo M., Movsesian M. (2007) cAMP and cGMP signaling cross-talk: role of phosphodiesterases and implications for cardiac pathophysiology. *Circ. Res*. 100(11):1569-78

Zakhary D.R., Moravec C.S., Stewart R.W., Bond M. (1999) Protein kinase A (PKA)-dependent troponin-I phosphorylation and PKA regulatory subunits are decreased in human dilated cardiomyopathy. *Circulation.* 99(4):505-10

Zakhary D.R., Moravec C.S., Bond M. (2000) Regulation of PKA Binding to AKAPs in the Heart Alterations in Human Heart Failure. *Circulation.* 1459-1465

Zamah AM, Delahunty M, Luttrell LM, Lefkowitz RJ. (2002) Protein kinase A-mediated phosphorylation of the beta 2-adrenergic receptor regulates its coupling to Gs and Gi. Demonstration in a reconstituted system. *J Biol Chem*. 277: 31249–56.

Zarain-Herzberg Afzal N, Elimban V, Dhalla NS. (1996) Decreased expression of cardiac sarcoplasmic reticulum Ca(2+)-pump ATPase in congestive heart failure due to myocardial infarction. *Mol Cell Biochem*. 163-164:285-90.

Zaugg M. (2008) β3-Adrenergic Receptor Subtype Signaling in Senescent Heart. *Anesthesiol*. 109,956–9

Zhang T., Brown J. (2004) Role of Ca2+/calmodulin-dependent protein kinase II in cardiac hypertrophy and heart failure. *Cardiovasc. Res*. 63, 476-486

Zhang C, Chen B, Guo A, Zhu Y, Miller JD, Gao S, Yuan C, Kutschke W, Zimmerman K, Weiss RM, Wehrens XH, Hong J, Johnson FL, Santana LF, Anderson ME, Song LS. (2014) Microtubule-mediated defects in junctophilin-2 trafficking contribute to myocyte transverse-tubule remodeling and Ca2+ handling dysfunction in heart failure. *Circ*. 129(17):1742-50

Zhang, R., Yang, J., Zhu, J. & Xu, X. (2009) Depletion of zebrafish Tcap leads to muscular dystrophy via disrupting sarcomere– membrane interaction, not sarcomere assembly. *Hum. Mol. Genet*. 18, 4130– 4140.

Zhu W.Z., Wang S.Q., Chakir K., Yang D., Zhang T., Brown J.H. (2003) Linkage of beta1-adrenergic stimulation to apoptotic heart cell death through protein kinase A-independent activation of Ca2+/calmodulin kinase II. *J. Clin. Invest*. 111 (5) 617–625.

Zhu W. Z., Zheng, M., Koch, W. J., Lefkowitz, R. J., Kobilka, B. K. & Xiao, R. P. (2001) Dual modulation of cell survival and cell death by β2-adrenergic signaling in adult mouse cardiac myocytes. *Proc. Natl. Acad. Sci. U.S.A.* 98, 1607-1612.

Ziman A., Gómez-Viquez NL, Bloch RJ, Lederer WJ. (2010) Excitation-contraction coupling changes during postnatal cardiac development. *J Mol Cell Cardiol*. 48 (2) 379-86

Zipes D.P., Jalife J. (2009) Cardiac Electrophysiology: From Cell to Bedside. *Card. Electrophys.* 1392

Ziskoven C, Grafweg S, Bolck B, Wiesner RJ, Jimenez M, Giacobino JP, Bloch W, Schwinger RH, Brixius K. (2007) Increased Ca2+ sensitivity and protein expression of SERCA 2a in situations of chronic beta3-adrenoceptor deficiency. *Pflugers Arch*. 453:443–53

Zygmunt A.C., Eddlestone G.T., Thomas G.P., Nesterenko V.V., Antzelevitch C. (2001) Larger late sodium conductance in M cells contributes to electrical heterogeneity in canine ventricle. *Am J Physiol Heart Circ Physiol*. 81 (2) 689-97